

**Geochemical signatures of black shales deposited during Oceanic
Anoxic Event 2 (Cenomanian/Turonian) in the tropical Atlantic
(Demerara Rise, ODP Leg 207) and in northern Germany (Wunstorf)**

Geochemische Signaturen von Schwarzschiefer-Ablagerungen des
Ozeanischen Anoxischen Ereignisses 2 (Cenoman/Turon) im tropischen
Atlantik (Demerara Rise, ODP Leg 207) und Norddeutschland (Wunstorf)

Dissertation

zur Erlangung des Grades eines Doktors der Naturwissenschaften

– Dr. rer. nat. –

angenommen bei der Fakultät für Mathematik und Naturwissenschaften
der Carl von Ossietzky Universität Oldenburg

von

Almut Bunte

geb. Hetzel

geboren am 23.12.1978 in Marl (Westf.)

Erstreferent: Prof. Dr. H.-J. Brumsack

Koreferent: Prof. Dr. M. E. Böttcher

Eingereicht am: 02.07.2009

Disputation am: 28.08.2009

Abstract

In the mid-Cretaceous, several distinct periods of organic-rich black shale deposition appear. The enhanced burial of organic carbon in marine sediments during these so called Oceanic Anoxic Events (OAEs) is thought to arise either from enhanced bio-productivity or from intensified preservation of organic matter during anoxic conditions. The Cenomanian-Turonian Boundary Event (CTBE = OAE 2; ca. 93.5 Ma) is one of the most prominent manifestations of a global oceanic anoxic event. Under severe oxygen-depleted conditions, several redox-sensitive or sulfide forming trace elements are enriched within the sediments. Therefore the CTBE is characterized by a specific distribution pattern of diagnostic trace metals. Studies of modern analogues of organic carbon-rich sedimentation typically reveal quite different enrichment patterns to those at the C/T boundary. It is therefore suggested, that trace metals provide useful information when reconstructing paleoenvironmental conditions.

This study presents inorganic geochemical analyses of two OAE 2 sequences located in different paleogeographical settings resulting in different lithological expressions regarding black shale deposition. During Ocean Drilling Program ODP Leg 207 expanded, shallowly buried Cretaceous sediments were recovered from Demerara Rise off Suriname, South America. The almost continuous bottom water anoxia at Demerara Rise during the Cenomanian/Turonian transition resulted in perfectly preserved primary signals, without overprinting by changes in bottom water oxygenation. These sediments are thus uniquely suited for paleoenvironmental reconstructions using trace metal (TM) distribution patterns. At Wunstorf (northern Germany) a continuous core spanning 76 m of middle Cenomanian to middle Turonian sediments was drilled in 2006. The Wunstorf area represents the basinal part of an intrashelf basin that was formed during the Cenomanian transgression as a part of an extended epicontinental shelf. The CTBE is represented by a 26.5 m thick sedimentary succession consisting of rhythmically bedded laminated black shales, dark organic-rich marls and marly limestones.

To analyze the sedimentation history of Demerara Rise bulk sediment geochemical data from squeeze cakes (pore water squeezing residues) were used to characterize the five lithologic units describing the Cretaceous to Paleogene sequence recovered

during ODP Leg 207. Sediments consist of different mixtures between biogenous carbonate and detrital material. Lithologic Units II-IV show high carbonate contents, whereas Unit I and V are dominated by terrigenous detritus. The Cretaceous black shales of Unit IV are clearly enriched in redox-sensitive and stable sulfide-forming elements indicating high paleoproductivity and severe oxygen depletion in the water column. The analysis of iron and sulfur speciation indicates euxinic conditions during Cretaceous black shale deposition. High amounts of organically bound sulfur show that organic matter acted as an important sulfur trap during early diagenesis in addition to fixation of sulfide by iron.

High-resolution major and minor element data for black shale sequences of ODP Leg 207 Sites 1258 and 1260 were generated to identify changes in redox-conditions of the depositional environment during OAE 2 by using distribution patterns of trace element enrichment as well as iron and sulfur speciation and stable sulfur isotope data. The existence of an expanded oxygen-minimum-zone (OMZ) is demonstrated by extremely low Mn/Al ratios. Elevated Fe/Al and Co/Al values within the Cenomanian/Turonian interval document euxinic conditions but, at the same time, require a zone where reducing but non-sulfidic conditions prevail, allowing reductive Fe and Co mobilization in oxygen-depleted nearshore sediments. High ratios of reactive to total iron indicate pyrite formation both in the water column and within the sediment confirming at least temporarily free dissolved sulfide in the water column. These results are in line with organic-geochemical studies. Extremely high concentrations of derivatives of isorenieratene and chlorobactene, fossil pigments derived from green sulfur bacteria, indicate at least occasionally truly euxinic conditions in the photic zone during OAE 2.

Although the C/T black shales of Demerara Rise are clearly enriched in redox-sensitive and sulfide forming TM, a decline in seawater derived TM enrichment (e.g. for Mo, V, and Zn) is noticeable at OAE 2. Because suboxic or even euxinic environments form a significant sink for TM, the global enlargement of oxygen-depleted depositional areas at the onset of black shale deposition during OAE 2 has likely led to a drawdown of the seawater TM reservoir. TM/TOC ratios in sediments deposited during OAE 2 are much lower than in sediments deposited before and thereafter, where values are similar to TM/TOC found in other C/T black shales. This may indicate a decoupling of TM enrichment and TOC deposition during OAE 2, due to lower TM concentration in seawater.

On-going diagenesis in Cretaceous black shales of Demerara Rise is indicated by pore water data. Ba enrichments in sediments above the black shale sequences show former diagenetic mobilization from barite in underlying sediment layers. A reaction-transport model was used to infer the long-term evolution of anaerobic organic matter degradation in Cretaceous black shales of Demerara Rise based on present-day porewater and authigenic barite profiles.

High resolution investigations of major and minor elements were carried out on the Cenomanian-Turonian sedimentary succession at Wunstorf. Seven black shale packages, each containing several black shale layers, were defined by TOC values. Distribution patterns of sulfur, iron and redox-sensitive and sulfide-forming trace metals hint to suboxic to anoxic conditions at the sediment-water interface. Because variations in element/Al ratios follow the cyclic patterns defined by Voigt et al. (2008), we postulate climatically induced changes in sediment supply. Reduced vertical mixing has led to the stabilisation of water column stratification, thus causing black shale deposition.

Kurzfassung

Während der mittleren Kreidezeit kommt es zu bestimmten Zeiten mehrfach zur Ablagerung Organik-reicher Schwarzschiefer. Man geht davon aus, dass die vermehrte Einlagerung von organischem Kohlenstoff (C_{org}) in Meeressedimenten während der so genannten Ozeanischen Anoxischen Ereignisse (OAEs) entweder aus erhöhter Primärproduktion oder aus verstärkter Erhaltung organischem Materials unter anoxischen Bedingungen resultiert. Das Cenoman-Turon-Grenzereignis (CTBE = OAE 2; ca. 93,5 Ma) ist eines der ausgeprägtesten Beispiele eines globalen ozeanischen anoxischen Ereignisses. Unter sauerstoffarmen Bedingungen werden redoxsensitive oder stabile Sulfide bildende Spurenelemente im Sediment angereichert. Deshalb ist das CTBE durch ein spezifisches Verteilungsmuster von diagnostischen Spuremetallen charakterisiert. Untersuchungen an rezenten Analogbeispielen C_{org} -reicher Sedimentation zeigen unterschiedliche Verteilungsmuster im Vergleich zur C/T-Grenze. Es wird deshalb angenommen, dass Spuremetalle nützliche Informationen zur Rekonstruktion von Paläoumweltbedingungen liefern.

Diese Studie präsentiert eine anorganisch-geochemische Untersuchung von OAE 2-Sedimentabfolgen zweier unterschiedlicher paläogeografischer Standorte, an denen sich daher auch die Schwarzschiefer-Ablagerung lithologisch unterschiedlich ausdrückt. Im Rahmen von ODP Leg 207 wurden auf dem Demerara Rise vor Surinam, Südamerika, mächtige Sedimentabfolgen der Kreidezeit aus geringer Tiefe erbohrt. Anhaltende Bodenwasser-Anoxia während des Cenoman/Turon Übergangs führten hier zur idealen Erhaltung primärer Signale ohne Überprägung durch Bodenwasserbelüftung. Daher sind diese Sedimente hervorragend geeignet, Verteilungsmuster von Spuremetallen für Paläoumwelt-Rekonstruktionen anzuwenden. Nahe Wunstorf (Norddeutschland) wurde 2006 ein durchgehender, 76 m langer Kern erbohrt, der Sedimente des mittleren Cenoman bis mittleren Turon umfasst. Das Gebiet um Wunstorf bildet das Becken eines Randmeeres, das während der Cenoman-Transgression als Teil des erweiterten epikontinentalen Schelfs gebildet wurde. Das CTBE drückt sich in einer 26,5 m mächtigen zyklischen Wechsellagerung von laminierten Schwarzschiefern, dunklen C_{org} -reichen Mergeln und mergeligen Kalken aus.

Zur Untersuchung der Sedimentationsentwicklung des Demerara Rise wurden zunächst geochemische Daten von Sediment-Presslingen (Rückstände der Porenwassergewinnung) verwendet, um die fünf lithologischen Einheiten der während ODP Leg 207 erbohrten Sedimentabfolge von der Kreide bis zum Paläogen geochemisch zu charakterisieren.

Sedimente bestehen aus variablen Mischungen von biogenem Karbonat und terrigenem Detritus. Die lithologischen Einheiten II-IV zeigen hohe Karbonat-Gehalte, wohingegen die Einheiten I und V durch terrigenen Detritus dominiert werden. Die Kreide-Schwarzschiefer der Einheit IV sind klar an redoxsensitiven und stabile Sulfide bildenden Elementen angereichert, wodurch hohe Paläoproduktivität und ein deutliches Sauerstoff-Defizit in der Wassersäule angezeigt werden. Die Analyse von Eisen- und Schwefel-Spezies deutet auf euxinische Bedingungen während der Schwarzschieferablagerung hin. Hohe Gehalte von organisch gebundenem Schwefel zeigen, dass das organische Material - zusätzlich zur Fixierung des Sulfids mit Eisen - als bedeutende Schwefel-Senke während der frühen Diagenese wirkte.

Hochaufgelöste Profile von Haupt- und Spurenelementen wurden für die Schwarzschieferfolgen von ODP Leg 207 an den Bohrlokationen 1258 und 1260 gewonnen. Verteilungsmuster von Spurenelement-Anreicherungen sowie Eisen- und Schwefelspezifikationen und stabile Schwefel-Isotopen-Daten wurden genutzt, um Änderungen der Redox-Bedingungen des Ablagerungsmilieus während OAE 2 anzuzeigen. Die Existenz einer ausgedehnten Sauerstoff-Minimum-Zone (OMZ) wird durch äußerst niedrige Mn/Al-Verhältnisse dokumentiert. Erhöhte Fe/Al- und Co/Al-Werte während des Cenoman/Turon zeigen euxinische Bedingungen an, erfordern aber zur gleichen Zeit das Vorhandensein einer Zone, in der reduzierende, jedoch nicht sulfidische Bedingungen herrschen, um eine reduktive Mobilisierung von Fe und Co in sauerstoffarmen, küstennahen Sedimenten zu ermöglichen. Hohe Verhältnisse von reaktivem Eisen zu Gesamteisen zeigen Pyrit-Bildung sowohl in der Wassersäule als auch innerhalb des Sedimentes an, wodurch zumindest zeitweise das Vorhandensein von freiem gelöstem Sulfid in der Wassersäule bestätigt wird. Diese Ergebnisse stimmen mit organisch-geochemischen Untersuchungen überein. Äußerst hohe Konzentrationen von Derivaten von Isorenieraten und Chlorobacten, fossile Pigmente Grüner Schwefel-Bakterien, zeigen an, dass während OAE 2 zumindest gelegentlich euxinische Bedingungen in der photischen Zone herrschten.

Obwohl die C/T-Schwarzschiefer des Demerara Rise deutlich an redoxsensitiven und Sulfide bildenden Spurenmetallen angereichert sind, ist während des OAE 2 ein Rückgang der Anreicherung von aus dem Meerwasser stammenden Elementen, wie Mo, V und Zn, sichtbar. Da suboxische oder sogar euxinische Paläo-Umweltbedingungen signifikante Spurenmetall-Senken darstellen, hat die Ausdehnung euxinischer Ablagerungsgebiete mit dem globalen Einsetzen der Ablagerung von Schwarzschiefern während OAE 2 höchstwahrscheinlich zu einer Absenkung des Metall-Vorrats im Meerwasser geführt. Metall/TOC Verhältnisse in Sedimenten des OAE 2 sind viel niedriger als in Sedimenten, die zuvor oder danach abgelagert wurden und deren Werte anderer C/T-Schwarzschiefer ähneln. Dies weist auf eine Entkopplung von Spurenmetall-Anreicherung und TOC-Ablagerung aufgrund verringerter Metall-Konzentrationen im Meerwasser hin.

Auch heute andauernde Diagenese in Kreide-Schwarzschiefern des Demerara Rise wird durch Porenwasserdaten angezeigt. Barium Anreicherungen in Sedimenten oberhalb der Schwarzschieferlagen zeigen eine frühere diagenetische Mobilisierung von Baryt aus tieferen Sedimentschichten. Ein Reaktions-Transport-Modell wurde verwendet, um die langzeitige Entwicklung des anaeroben Abbaus des organischen Materials in den Kreide-Schwarzschiefern des Demerara Rise abzuleiten, basierend auf heutigen Porenwasser- und authigenen Baryt-Profilen.

Hochaufgelöste Untersuchungen der Haupt- und Spurenelemente wurden an der Cenoman-Turon-Sedimentationsabfolge von Wunstorf durchgeführt. Sieben Schwarzschiefer-Pakete mit jeweils mehreren einzelnen Schwarzschiefer-Lagen wurden anhand der TOC-Werte definiert. Verteilungsmuster von Schwefel, Eisen und redoxsensitiven und Sulfide bildenden Spurenmetallen zeigen suboxische bis anoxische Bedingungen an der Sediment-Wasser-Grenzschicht. Da Schwankungen in den Element/Al-Verhältnissen den von Voigt et al. (2008) ermittelten zyklischen Mustern folgen, werden klimatisch induzierte Veränderungen im Sedimenteintrag postuliert. Verringerte vertikale Durchmischung führte zu einer Stabilisierung der Wassersäulenschichtung, wodurch die Ablagerung von Schwarzschiefern verursacht wurde.

Table of Contents

Abstract	I
Kurzfassung.....	IV
Table of Contents	1
1. Introduction.....	6
Motivation.....	6
OAE 2 and geological settings investigated	8
Demerara Rise	9
Wunstorf	10
OM burial and geochemical characteristics.....	10
Objectives and Outline of the author's contribution.....	13
References.....	16
2. Inorganic geochemical characterization of lithologic units recovered during ODP Leg 207 (Demerara Rise).	19
Introduction	21
Material and Methods.....	22
Site description	22
Carbon and Sulfur	23
Major and Trace Elements	23
Rare Earth Elements (REEs).....	23
Results and Discussion.....	24
Conclusions	40
Acknowledgements.....	41
References.....	41
Appendix.....	44
3. Sulfur-iron-carbon geochemistry in sediments of the Demerara Rise.....	56

Introduction	57
Material and Methods.....	59
Results and Discussion.....	63
Lithologic Units, Pore Waters, Sulfate Reduction, and Anaerobic Methane Oxidation	63
Sedimentary Iron and Sulfur Species	64
Reactive Iron Phases and Pyrite Formation	64
Organic Sulfur Formation	68
Conclusions	70
Acknowledgements	70
References.....	71
4. Paleo-redox conditions during OAE 2 reflected in Demerara Rise sediment geochemistry (ODP Leg 207)	75
Introduction	77
Material and Methods.....	78
Site description.....	78
Analytical methods	83
Results and discussion	84
Preliminary remarks.....	84
Bulk parameters	85
Iron	90
Sulfur and sulfur isotopes	92
Redox-sensitive and sulfide forming trace metals	97
Productivity proxies	107
Paleoenvironmental implications and comparison with other paleoproxies.....	110
Summary and Conclusions	113
Acknowledgements	114
References.....	114

Appendix	121
5. Reconstruction of water column anoxia in the equatorial Atlantic during the Cenomanian-Turonian oceanic anoxic event using biomarker and trace metal proxies	124
Introduction	125
Geological setting and Stratigraphy	129
Methods	130
Results	132
Biomarkers	132
Trace metals and major elements	134
Discussion.....	136
Anoxia and water column stratification at Site 1260	136
Trace metal drawdown during OAE-2.....	141
Water column anoxia in the North Atlantic during OAE-2	141
OM accumulation rates in the North Atlantic	143
Conclusions	144
Acknowledgements	144
References.....	144
6. Evolution of organic matter degradation in Cretaceous black shales inferred from authigenic barite: A reaction-transport model	150
Introduction	152
Materials and Methods.....	154
Site description.....	154
Previous work and modeling strategy.....	156
Sampling methods	160
Model Description	161
Transport	161
Reaction network.....	161

Numerical Solution	165
External forcing and initial conditions	165
Inverse modeling	169
Results and Discussion.....	170
Distribution of barite.....	170
Inverse modeling	171
Evolution of biogeochemical dynamics at Demerara Rise.....	173
Reactivity and preservation of black shale organic matter at Demerara Rise..	178
Implications for black shale deposition at Demerara Rise	182
Uncertainties and Model Limitations	185
Conclusions	187
Acknowledgements.....	188
References.....	189
7. Geochemical environment of Cenomanian – Turonian black shale deposition at Wunstorf (northern Germany) – a new reference section for Oceanic Anoxic Event 2	195
Introduction	196
Material and Methods.....	197
Site description	197
Analytical methods	199
Results and Discussion.....	199
Bulk parameters and major components	203
Terrigenous material and cyclostratigraphy.....	206
Manganese.....	209
Productivity proxies	210
Carbon-Sulphur-Iron systematics and redox-sensitive and sulphide-forming trace metals.....	211
Comparison to other C/T black shale sections	216

Summary and palaeoenvironmental implications for black shale deposition.....	220
Acknowledgements	221
References.....	221
Appendix	225
8. Conclusions and Perspectives.....	226
Curriculum vitae.....	VII
Conference abstracts	VIII
Acknowledgements / Danksagung	XI
Erklärung	XIII

1. Introduction

Motivation

Extreme changes in Earth's climate and massive perturbations of the global carbon cycle, so-called Oceanic Anoxic Events, are recognized in the mid Cretaceous (~124 - 90 Ma). They represent short-lived episodes of organic carbon burial that are distinguished by their widespread distribution as discrete black beds and are characterized by pronounced carbon isotopic excursions. Despite decades of research, the underlying causes and effects of these critical events in earth history are still under debate.

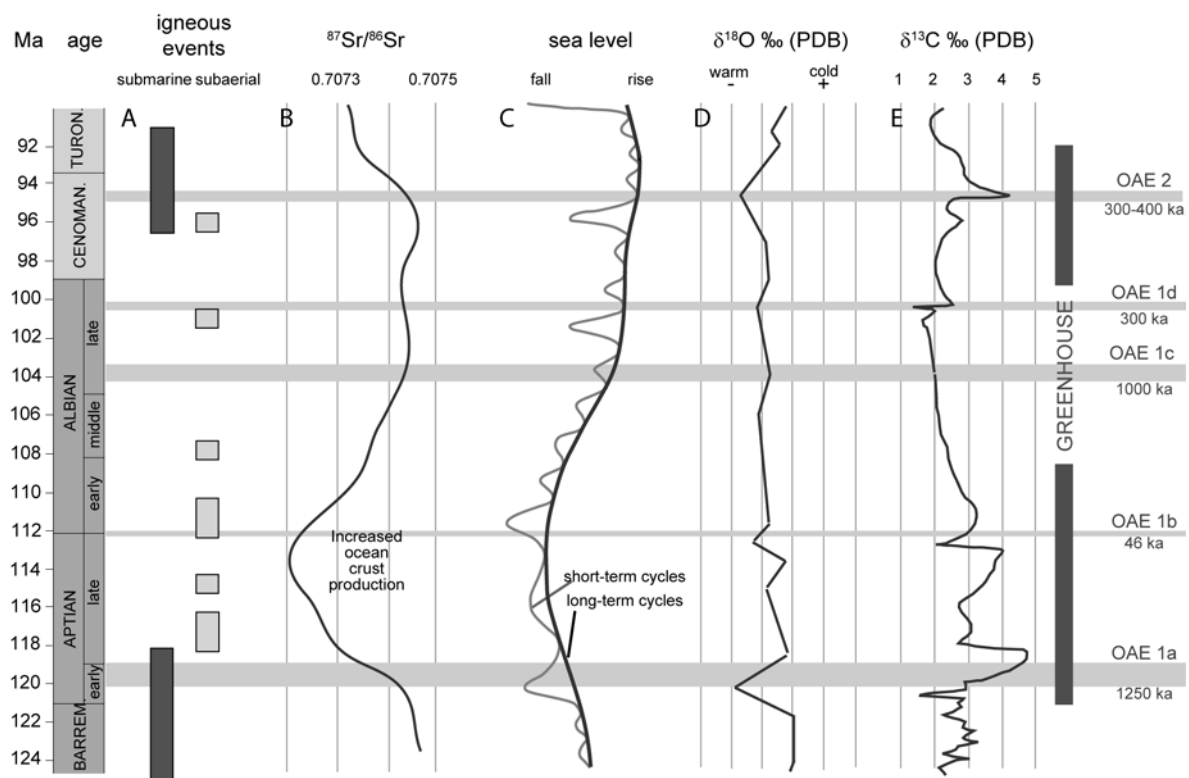


Figure 1.1 Major tectonic events, sea level changes and geochemical signatures in the mid-Cretaceous (modified from Erba, 2004, and Leckie et al., 2002).

Figure 1.1 summarizes the major tectonic, sea level and geochemical records during the mid-Cretaceous that contributed to global greenhouse conditions. During this time interval the tectonic and volcanic activity was enhanced. Several large submarine and subaerial igneous events occurred (Fig. 1.1A; Larson, 1991a, 1991b). An increased ocean crust production rate is constrained by less radiogenic strontium

isotopic data (Fig. 1.1B; Bralower et al., 1997; Jones and Jenkyns, 2001). $^{87}\text{Sr}/^{86}\text{Sr}$ ratios in seawater decreased during submarine volcanic events, and increased during times of enhanced continental weathering. The excess of volcanogenic exhalations in the atmosphere was promoting the Greenhouse mode (e.g. Bice and Norris, 2002). Accelerated continental weathering and river run-off increased the nutrient supply to the ocean. In the same way submarine igneous events are thought to enhance ocean paleoproductivity by introducing bio-limiting metals (Snow et al., 2005) and led to higher sea level (Fig. 1.1C; Haq et al., 1988) causing continental flooding and formation of shallow shelf seas.

The oxygen isotopic data (Fig. 1.1D) suggest that globally averaged sea surface temperatures in the mid-Cretaceous were more than 10°C higher than today (Norris et al., 2002). Ocean circulation was probably driven in part by the sinking of warm, saline waters from shelves to deep ocean basins in subtropical regions during the mid-Cretaceous (Hay et al., 2006). Ocean circulation model experiments show that high-latitude sources of deep water, particularly in the Northern Hemisphere, diminished and thus subtropical convection was restricted to isolated basins (Poulsen et al., 2001).

Temporal variations in $\delta^{13}\text{C}$ values of carbonates and organic matter document changes in the global carbon cycle (Fig. 1.1E). Positive shifts indicate burial of large amounts of organic carbon, which is depleted in ^{13}C . The remaining C-source is therefore isotopically heavier and marine carbonates show elevated $\delta^{13}\text{C}$ values (Arthur et al., 1985, 1988; Schlanger et al., 1987; Hayes et al., 1989).

Mid-Cretaceous sediments rich in organic carbon, so-called black shales, were synchronously deposited globally - not only in shallow seas, but also in deep ocean basins. The time intervals of black shale deposition are called Oceanic Anoxic Events (OAEs; Schlanger and Jenkyns, 1976; Jenkyns, 1980). OAEs are hypothesized to have played a major role in the evolution of Earth's climatic and biotic history. The mechanisms causing the extensive burial of TOC-rich sediments are still under debate. Studying OAEs and their formation mechanism should lead to a deeper understanding of the global carbon budget and the climatic conditions in an extreme greenhouse situation. Geochemical studies of black shale successions will provide important information on the causes and consequences of enhanced organic matter burial.

OAE 2 and geological settings investigated

OAE 2 occurred at the Cenomanian-Turonian transition, about 93.5 Ma ago, and is also known as the Cenomanian-Turonian Boundary Event (CTBE). It forms a short-termed, global and synchronous phenomenon.

During the OAE 2 the flood basalt province of the Caribbean Plateau was built, and both sea level (ca 250 m higher than present; Haq et al. 1987) and temperature were extremely high (sea surface temperature for equatorial Atlantic ocean ~35 - 36 °C at the onset of OAE 2 in comparison to ~27 - 29 °C for today; Forster et al., 2007). The $\delta^{13}\text{C}$ values show a pronounced positive shift in marine carbonate and marine and terrestrial organic matter (Schlanger and Jenkyns, 1976; Tsikos et al., 2004). As such, OAE 2 constitutes an ideal candidate for detailed investigations of the changing environmental conditions responsible for the establishment of widespread marine anoxia during the mid-Cretaceous. Suboxic, anoxic or even euxinic conditions developed in oxygen minimum zones along continental margins of the tropical Tethys, in restricted epicontinental seas, and in the widening North and South Atlantic Ocean basins. These conditions led to deposition of rhythmically bedded sedimentary sequences including organic-rich black shale (Leckie et al., 2002).

Although OAE 2 is thought to be a global event as concluded from positive carbon isotopic excursions, organic carbon burial differs in its geographic expression. For example, the Eastbourne (United Kingdom) sediment succession, which serves as a reference section, is an extensive limestone (Tsikos et al., 2004). The name "Cretaceous" (145 - 65 million years ago) is derived from the Latin word for chalk ("creta") and was first applied to these deposits forming the white cliffs along the English Channel between Great Britain and France. Another type locality is situated in the Marche–Umbrian Apennines of central Italy. Here OAE 2 is called the Bonarelli Event after the Livello Bonarelli (Tsikos et al., 2004), the characteristic discrete black shale level within the calcareous sequence.

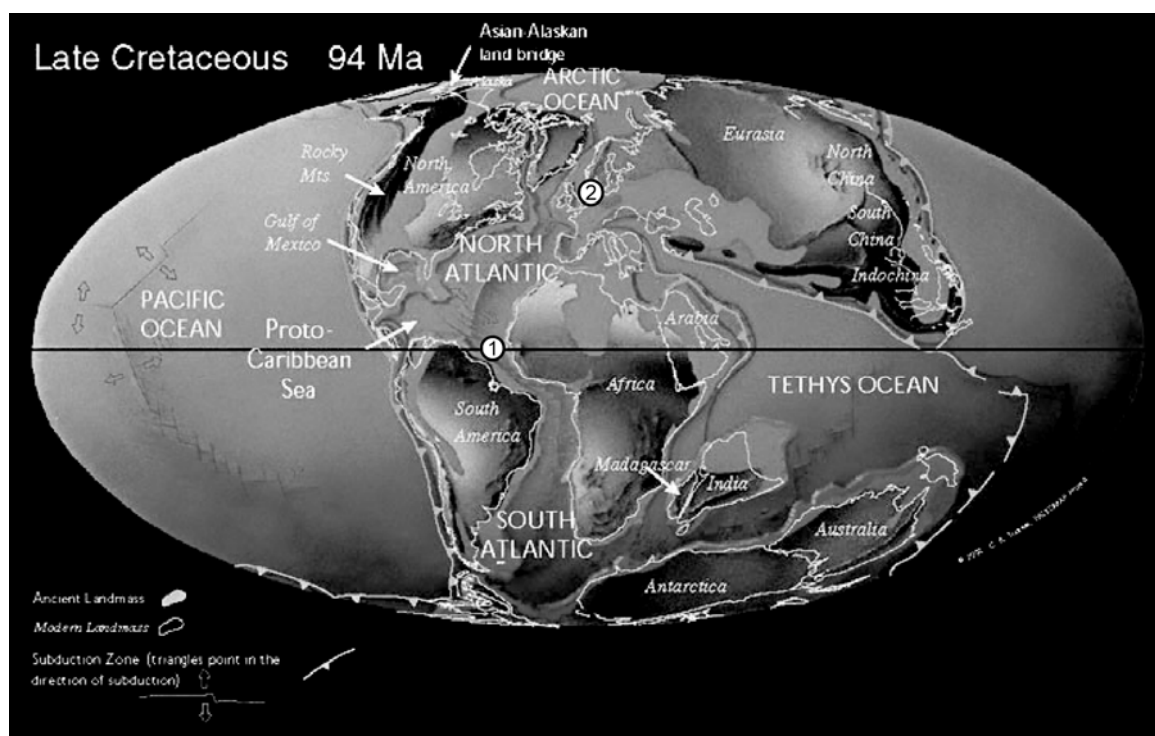


Figure 1.2 Plate tectonic reconstruction of the Late Cretaceous (from <http://www.scotese.com/cretaceo.htm>) with the study sites (1) Demerara Rise and (2) Wunstorf.

This study presents inorganic geochemical data from two OAE 2 successions located in different paleogeographic settings, resulting in different lithological expressions regarding black shale deposition.

Demerara Rise

During Ocean Drilling Program (ODP) Leg 207, an expanded succession of shallow-buried Cretaceous sediments was recovered from Demerara Rise off Suriname, South America (Fig. 1.2). CTBE black shales on Demerara Rise form part of a thick black shale interval (thickness up to 90 m) encompassing the Albian to Santonian (Erbacher et al., 2004). This may be the result of both the paleogeographic setting of Demerara Rise, lacking significant ventilation of bottom-waters prior to the opening of the equatorial Atlantic gateway (Friedrich and Erbacher, 2006), and/or enhanced nutrient influx evoked by terrestrial runoff and/or upwelling. The OAE 2 sedimentary successions studied here exhibit 1.4 m and 4 m in thickness, based on distinctive positive carbon isotope excursions of $\sim 6.5\%$ (Erbacher et al., 2005).

Wunstorf

At Wunstorf (northern Germany) a continuous core of 76 m comprising middle Cenomanian to middle Turonian sediments was drilled in 2006. The Wunstorf area represents the basinal part of an intra-shelf basin that was formed during the Cenomanian transgression as a part of the extended epicontinental shelf (Figure 1.2). The CTBE is represented by a 26.5 m thick sedimentary succession consisting of rhythmically bedded laminated black shales, dark organic-rich marls and marly limestones (Erbacher et al., 2007). A high-resolution carbonate $\delta^{13}\text{C}$ curve resolves all known features of the positive $\delta^{13}\text{C}$ anomaly of OAE 2 with high accuracy (Voigt et al, 2008).

OM burial and geochemical characteristics

Organic matter (OM) burial is mainly controlled by three factors: organic matter production, microbial decomposition, and bulk sedimentation rate or dilution (Sageman et al., 2003). As shown in Figure 1.3 these factors are influenced by several processes interfering with each other, e.g. enhanced production may enhance biogenous skeletal material flux and thus dilution of the detrital component.

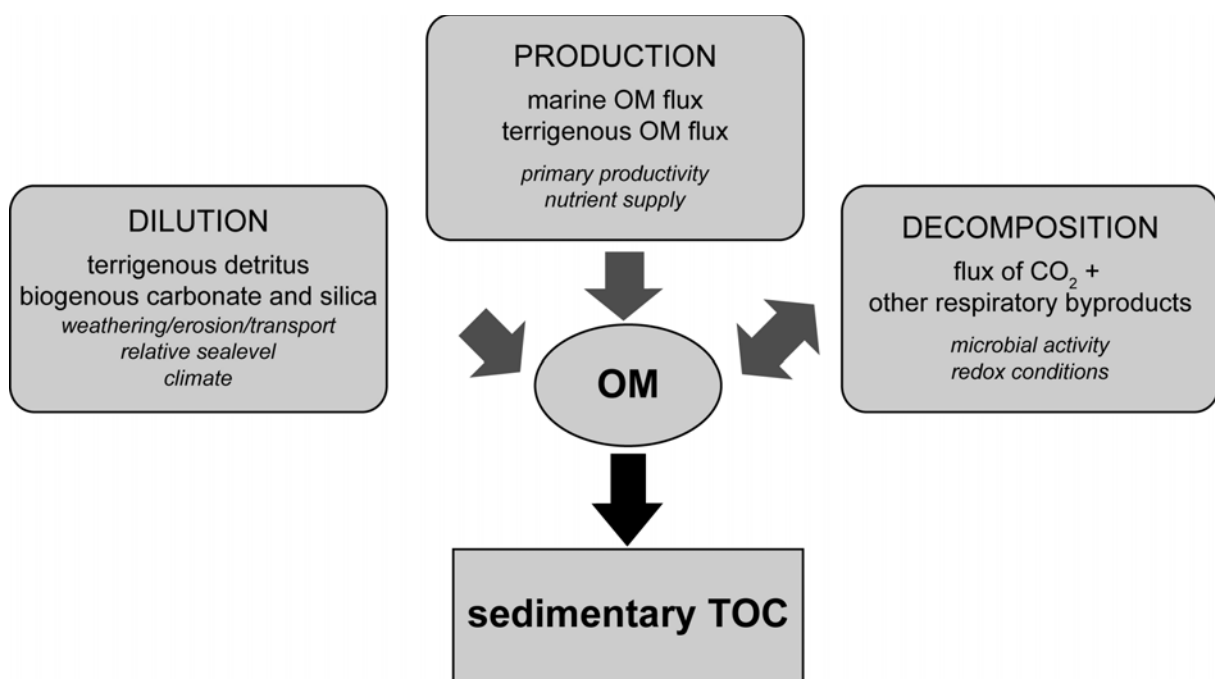


Figure 1.3 Factors controlling organic matter (OM) burial (modified from Sageman et al., 2003).

One important factor is the rate at which OM is remineralized both in the water column and sediments. This strongly depends on the dominant biogeochemical regime. Oxidic respiration is the favored way of decomposition as it gains the highest energy yield for the microbes. Following the order of energy yield there is an idealized sequence of OM decomposition pathways as listed in Table 1.1.

Table 1.1 Pathways and stoichiometries of OM (CH_2O) decomposition in the order of decreasing energy yields (modified from Jørgensen, 2006).

Oxidic respiration	$\text{CH}_2\text{O} + \text{O}_2 \rightarrow \text{CO}_2 + \text{H}_2\text{O}$
Denitrification	$5 \text{CH}_2\text{O} + 4 \text{NO}_3^- \rightarrow 2 \text{N}_2 + 4 \text{HCO}_3^- + \text{CO}_2 + 3 \text{H}_2\text{O}$
Mn(IV) reduction	$\text{CH}_2\text{O} + 3 \text{CO}_2 + \text{H}_2\text{O} + 2 \text{MnO}_2 \rightarrow 2 \text{Mn}^{2+} + 4 \text{HCO}_3^-$
Fe(III) reduction	$\text{CH}_2\text{O} + 7 \text{CO}_2 + 4 \text{Fe}(\text{OH})_3 \rightarrow 4 \text{Fe}^{2+} + 8 \text{HCO}_3^- + 3 \text{H}_2\text{O}$
Sulfate reduction	$2 \text{CH}_2\text{O} + \text{SO}_4^{2-} \rightarrow \text{H}_2\text{S} + 2 \text{HCO}_3^-$
	$4 \text{H}_2 + \text{SO}_4^{2-} + \text{H}^+ \rightarrow \text{HS}^- + 4 \text{H}_2\text{O}$
	$\text{CH}_3\text{COO}^- + \text{SO}_4^{2-} + 2 \text{H}^+ \rightarrow 2 \text{CO}_2 + \text{HS}^- + 2 \text{H}_2\text{O}$
Methane production	$4 \text{H}_2 + \text{HCO}_3^- + \text{H}^+ \rightarrow \text{CH}_4 + 3 \text{H}_2\text{O}$
	$\text{CH}_3\text{COO}^- + \text{H}^+ \rightarrow \text{CH}_4 + \text{CO}_2$
Acetogenesis	$4 \text{H}_2 + 2 \text{CO}_3^{2-} + \text{H}^+ \rightarrow \text{CH}_3\text{COO}^- + 4 \text{H}_2\text{O}$
Fermentation	$\text{CH}_3\text{CH}_2\text{OH} + \text{H}_2\text{O} \rightarrow \text{CH}_3\text{COO}^- + 2 \text{H}_2 + \text{H}^+$
	$\text{CH}_3\text{CH}_2\text{COO}^- + 3 \text{H}_2\text{O} \rightarrow \text{CH}_3\text{COO}^- + \text{HCO}_3^- + 3 \text{H}_2 + \text{H}^+$

Following the availability of free oxygen for decomposition of OM different redox conditions are considered for depositional environments. Under oxidic conditions OM is remineralized by oxidic respiration. Suboxic, also called dysoxic, conditions prevail under oxygen deficiency where denitrification and Mn and Fe reduction occur. If no free oxygen is present conditions are called anoxic. Hydrogen sulfide is released during sulfate reduction, which forms iron sulfides, ultimately pyrite, with Fe^{2+} formed during reduction of Fe (hydr)oxides. If sulfate reduction rates are high and sulfide-reactive metals are less available, free hydrogen sulfide may be present in the pore water and/or the water column. These conditions are called euxinic or sulfidic.

For formation of ancient TOC-rich sediments, two major mechanisms are discussed: high flux of organic matter to the seafloor due to increased primary productivity (Pedersen and Calvert, 1990; Wilson and Norris, 2001) and/or enhanced preservation of organic matter (Brumsack, 1980; Bralower and Thierstein, 1984;

Herbin et al., 1986; Erbacher et al., 2001) due to oxygen depletion in the water column and/or high sedimentation rates.

Modern analogues of such organic-rich sediments are deposited below areas of high primary productivity that are found in coastal upwelling areas at continental margins. Sediments underlying an anoxic to euxinic water column are found in the modern oceans only in restricted basins like the Black Sea (Brumsack, 2006, and references therein). Figure 1.4 summarized the geochemical water column characteristics and chemical processes for these two environments. In a coastal upwelling area primary productivity is enhanced due to upwelling of nutrient-rich intermediate water. During decomposition of the organic material oxygen is consumed and an oxygen minimum zone (OMZ) is formed. Within the OMZ, suboxic conditions lead to reduction of Mn (hydr)oxides and dissolved Mn^{2+} can convey into the open ocean. In restricted anoxic basins the situation is different. Due to stagnation no oxygen-rich water can flush deeper parts of the water column. Even low productivity may lead to anoxic conditions in deep water masses. Due to Mn cycling at the redox boundary and restriction of the anoxic basins Mn is trapped and accumulated. Trace metals (TM) are transported to the basin by seawater and fluvial input. If these metals are forming stable sulfides they are trapped in the H_2S -bearing water column.

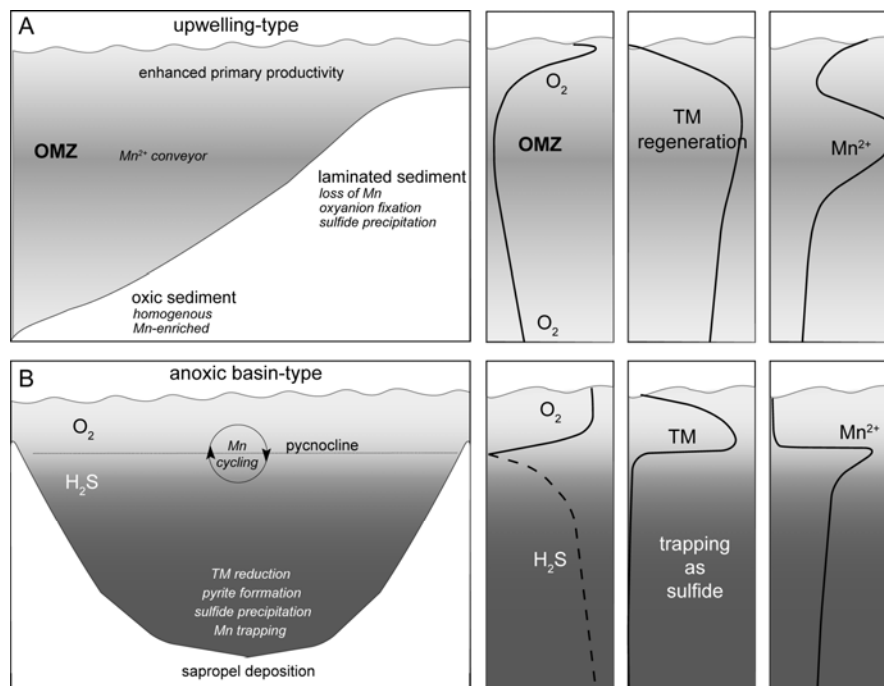


Figure 1.4 Chemical processes and geochemical water column characteristics of (A) coastal upwelling areas and (B) restricted anoxic basins (modified from Brumsack, 2006).

Under severe oxygen-depleted conditions, several redox-sensitive or sulfide-forming elements are enriched within the sediments. From studying modern analogues of TOC-rich sediments it seems evident that several TMs are very sensitive to changes in redox conditions. Thus, depletions or enrichments of certain TMs are characteristic for depositional environments and may document specific redox conditions (Brumsack, 2006; Tribovillard et al., 2006). Therefore, the distribution patterns of diagnostic metals in black shales like those deposited during OAE 2 may help to reconstruct paleoenvironmental conditions.

Objectives and Outline of the author's contribution

In this thesis major and minor element data are used to address the following goals:

- provenance of terrigenous detritus
- paleoenvironmental/paleoceanographic reconstruction based on high-resolution accumulation patterns of specific TMs (degree of anoxia, bioproductivity)
- evaluation of the importance of black shale deposition for global TM cycles and consideration of the origin of metal enrichments
- post-depositional element migration.

The thesis comprises six manuscripts already published or submitted for publication in international journals as individual chapters, with individual reference section each. My contribution to each of the manuscripts is detailed below. Publications are or will be published under my maiden name Almut Hetzel.

Chapter 2: Inorganic geochemical characterization of lithologic units recovered during ODP Leg 207 (Demerara Rise)

Almut Hetzel, Hans-Jürgen Brumsack, Bernhard Schnetger, Michael E. Böttcher

For geochemical characterization squeeze cakes (pore water squeezing residues) sampled during the cruise by Hans-Jürgen Brumsack and the Shipboard Scientific Party of ODP Leg 207 from Sites 1257 to 1261 on Demerara Rise were analyzed by XRF and standard bulk parameter techniques (C, S). Squeezed cakes from Site 1258 were additionally analyzed by ICP-AES and HR-ICP-MS. All sediment data presented in the manuscript were analyzed by me, supported by Bernhard Schnetger for method evaluation. The concept of the manuscript and interpretation of the results

were developed by me. As first-author I also did the writing and editorial handling of the publication, supported by suggestions from Michael E. Böttcher and Hans-Jürgen Brumsack.

This chapter was published 2006 in Proceedings of the Ocean Drilling Program, Scientific Results, 207. Mosher, D.C., Erbacher, J., Malone, M.J. (Eds.), College Station, TX (Ocean Drilling Program), 1-37.

Chapter 3: Sulfur-iron-carbon geochemistry in sediments of the Demerara Rise

Michael E. Böttcher, Almut Hetzel, Hans-Jürgen Brumsack, Andrea Schipper

In this study Fe-species, S-species as well as total organic carbon (TOC) and total inorganic carbon from Cretaceous black shales of Demerara Rise are presented giving information about the redox state both in the water column and the sediment. Bulk element concentrations (Fe_T, S_T, TOC and TIC) were contributed by me. I also participated in the interpretation of the results.

This chapter was published 2006 in Proceedings of the Ocean Drilling Program, Scientific Results, 207. Mosher, D.C., Erbacher, J., Malone, M.J. (Eds.), College Station, TX (Ocean Drilling Program), 1-23.

Chapter 4: Paleo-redox conditions during OAE 2 reflected in Demerara Rise sediment geochemistry (ODP Leg 207)

Almut Hetzel, Michael E. Böttcher, Ulrich G. Wortmann, Hans-Jürgen Brumsack

To address the high-resolution paleoenvironmental/paleoceanographic reconstruction of Demerara Rise during the late Cretaceous by accumulation patterns of specific trace metals, extended sequences of Cretaceous black shales (in particular OAE 2) were sampled from Site 1258 and Site 1260. Samples were taken by me at the ODP Core Repository in Bremen. Bulk parameters and major/trace elements were determined by me, supported by lab assistants. Fe-species, S-species and S-isotope data were elaborated by Michael E. Böttcher, O-isotope data by Ulrich G. Wortmann. As first-author, I developed the concept of the publication and wrote all sections on major and trace elements. Regarding Fe-C-S and isotope data the interpretation of the results and writing was done by me and Michael E. Böttcher, supported by comments from Hans-Jürgen Brumsack.

This chapter was published 2009 in Palaeogeography, Palaeoceanography, Palaeoecology 273(3-4), 302-328.

Chapter 5: Reconstruction of water column anoxia in the equatorial Atlantic during the Cenomanian-Turonian oceanic anoxic event using biomarker and trace metal proxies

Elisabeth van Bentum, Almut Hetzel, Hans-J. Brumsack, Astrid Forster, Gert-Jan Reichart, Jaap S. Sinninghe Damsté

The depositional environment during OAE 2 at Demerara Rise is addressed by this publication using biomarkers as well as TM distribution. Samples were taken by Astrid Forster and me. I was responsible for XRF measurements carried out at the ICBM and the TM data evaluation. I further supported Elisabeth van Bentum in interpreting inorganic geochemical data and in writing of the manuscript.

This chapter has been re-submitted to *Palaeogeography*, *Palaeoceanography*, *Palaeoecology*.

Chapter 6: Evolution of organic matter degradation in Cretaceous black shales inferred from authigenic barite: A reaction-transport model

Sandra Arndt, Almut Hetzel, Hans-Jürgen Brumsack

A reaction-transport model was used to infer the long-term evolution of anaerobic organic matter degradation in Cretaceous black shales of Demerara Rise based on present-day porewater and authigenic barite profiles. TOC values as well as Ba excess data were contributed by me, as well as comments during writing by Sandra Arndt.

This chapter was published 2009 in *Geochimica et Cosmochimica Acta* 73(7), 2000-2022.

Chapter 7: Geochemical environment of Cenomanian – Turonian black shale deposition at Wunstorf (northern Germany) – a new reference section for Oceanic Anoxic Event 2

Almut Hetzel, Hans-Jürgen Brumsack

High-resolution major and minor element data were generated to provide information on the depositional environment causing black shale deposition at the Wunstorf Cenomanian-Turonian succession. The concept of the study was established by me and I also did the sampling. Bulk parameters and major/trace elements were determined by me supported by lab assistants. All data were evaluated and

interpreted by me. The concept of the publication was developed by me. I also wrote the manuscript, supported by suggestions from Hans-Jürgen Brumsack, and I am responsible for editorial handling.

This chapter has been submitted for publication to *Cretaceous Research*.

References

- Arthur, M.A., Dean, W.E., Pratt, L.M., 1988. Geochemical and climatic effects of increased marine organic carbon burial at the Cenomanian/Turonian boundary. *Nature* 335(6192), 714-717.
- Arthur, M.A., Dean, W.E., Schlanger, S.O., 1985. Variations in the global carbon cycle during the Cretaceous related to climate, volcanism and changes in atmospheric CO₂. In: Sundquist, E.T., Broecker, W.S. (Eds.), *The carbon cycle and atmospheric CO₂: Natural variations archaic to present*. AGU Geophysical Monograph 32, 504-529.
- Bice, K.L., Norris, R.D., 2002. Possible atmospheric CO₂ extremes of the Middle Cretaceous (late Albian–Turonian). *Paleoceanography* 17(4), 1070.
- Bralower, T.J., Thierstein, H.R., 1984. Low productivity and slow deep-water circulation in mid-Cretaceous oceans. *Geology* 12(10), 614-618.
- Brumsack, H.-J., 1980. Geochemistry of Cretaceous black shales from the Atlantic Ocean (DSDP Legs 11, 14, 36, and 41). *Chemical Geology* 31, 1-25.
- Brumsack, H.-J., 2006. The trace metal content of recent organic carbon-rich sediments: implications for Cretaceous black shale formation. *Palaeogeography, Palaeoceanography, Palaeoecology* 232(2-4), 344-361.
- Erba, E., 2004. Calcareous nannofossils and Mesozoic oceanic anoxic events. *Marine Micropaleontology* 52(1-4), 85-106.
- Erbacher, J., Huber, B.T., Norris, R.D., Markey, M., 2001. Increased thermohaline stratification as a possible cause for an oceanic anoxic event in the Cretaceous period. *Nature* 409(6818), 325-327.
- Erbacher, J., Mosher, D.C., Malone, M.J., Shipboard Scientific Party, 2004. *Proceedings of the Ocean Drilling Program, Initial Reports*, 207. College Station, TX (Ocean Drilling Program), pp. 89.
- Erbacher, J., Mutterlose, J., Wilmsen, M., Wonik, T., Wunstorff Drilling Scientific Party, 2007. The Wunstorff Drilling Project: Coring a global stratigraphic reference section of the Oceanic Anoxic Event 2. *Scientific Drilling* 4, 19-21.
- Erbacher, J., Friedrich, O., Wilson, P.A., Birch, H., Mutterlose, J., 2005. Stable organic carbon isotope stratigraphy across Oceanic Anoxic Event 2 of Demerara Rise, Western Tropical Atlantic. *Geochemistry, Geophysics, Geosystems* 6, Q06010.
- Forster, A., Schouten, S., Moriya, K., Wilson, P.A., Sinninghe Damsté, J.S., 2007. Tropical warming and intermittent cooling during the Cenomanian/Turonian oceanic anoxic event 2: sea surface temperature records from the equatorial Atlantic. *Paleoceanography* 22, PA1219.
- Friedrich, O., Erbacher, J., 2006. Benthic foraminiferal assemblages from Demerara Rise (ODP Leg 207, western tropical Atlantic): possible evidence for a progressive opening of the equatorial Atlantic gateway. *Cretaceous Research* 27(3), 377-397.

- Haq, B.U., Hardenbol, J., Vail, P.R., 1988. Mesozoic and Cenozoic chronostratigraphy and cycles of sea-level change In: Wilgus, C.K., Hastings, B.S., Kendall, C.G.St.C., et al. (Eds.), *Sea-Level Changes: An Integrated Approach*. Special Publication Society of Economic Paleontologists and Mineralogists 42, 71-108.
- Hayes, J.M., Popp, B.N., Takigiku, R., Johnson, M.W., 1989. An isotopic study of biogeochemical relationships between carbonates and organic matter in the Greenhorn Formation. *Geochimica Cosmochimica Acta* 53(11), 2961-2972.
- Herbin, J.P., Masure, E., Roucaché, J., 1987. Cretaceous formations from the lower continental rise off Cape Hatteras: organic geochemistry, dinoflagellate cysts, and the Cenomanian/Turonian boundary event at Sites 603 (Leg 93) and 105 (Leg 11). *Deep Sea Drilling Program, Initial Reports* 93, 1139-1162.
- Jenkyns, H. C., 1980. Cretaceous anoxic events: From continents to oceans. *Journal of the Geological Society* 137(3), 171-188.
- Jørgensen B.B., 2006. Bacteria and marine biogeochemistry. In: Schulz, H.D., Zabel, M. (Eds.), *Marine Geochemistry*. Springer Verlag, Berlin. 169-201.
- Larson, R.L., 1991a. Geological consequences of superplumes. *Geology* 19(10), 963-966.
- Larson, R.L., 1991b. Latest pulse of Earth: Evidence for a mid-Cretaceous superplume. *Geology* 19(6), 547-550.
- Leckie, R.M., Bralower, T.J., Cashman, R., 2002. Oceanic anoxic events and plankton evolution: Biotic response to tectonic forcing during the mid-Cretaceous. *Paleoceanography* 17(3), 1040.
- Norris, R.D., Bice, K.L., Magno, E.A., Wilson, P.A., 2002. Jiggling the tropical thermostat during the Cretaceous hot house. *Geology* 30(4), 299-302.
- Pederson, T.F., Calvert, S.E., 1990. Anoxia vs. productivity: What controls the formation of organic-carbon-rich sediments and sedimentary rocks? *AAPG Bulletin* 74(4), 454-466.
- Poulsen, C.J., Barron, E.J., Arthur, M.A., Peterson, W.H., 2001. Response of the mid-Cretaceous global oceanic circulation to tectonic and CO₂ forcings. *Paleoceanography* 16(6), 576-592.
- Sageman, B.B., Murphy, A.E., Werne, J.P., Ver Straeten, C.A., Hollander, D.J., Lyons, T.W., 2003. A tale of shales: the relative roles of production, decomposition, and dilution in the accumulation of organic-rich strata, Middle-Upper Devonian, Appalachian basin. *Chemical Geology* 195(1-4), 229-273.
- Schlanger, S.O., Arthur, M.A., Jenkyns, H.C., Scholle, P.A., 1987. The Cenomanian-Turonian Oceanic Anoxic Event, I. Stratigraphy and distribution of organic carbon-rich beds and the marine $\delta^{13}\text{C}$ excursion. In: Brooks, J., Fleet, A.J. (Eds.), *Marine Petroleum Source Rocks*. Geological Society, London. Special Publication 26, 371-399.
- Schlanger, S.O., Jenkyns, H.C., 1976. Cretaceous oceanic anoxic events: causes and consequences. *Geologie en Mijnbouw* 55, 179-184.
- Tribovillard, N., Algeo, T.J., Lyons, T., Riboulleau, A., 2006. Trace metals as paleoredox and paleoproductivity proxies: An update. *Chemical Geology* 232(1-2), 12-32.
- Tsikos, H., Jenkyns, H.C., Walsworth-Bell, B., Petrizzo, M.R., Forster, A., Kolonic, S., Erba, E., Premoli Silva, I., Baas, M., Wagner, T., Sinninghe Damsté, J.S., 2004. Carbon-isotope stratigraphy recorded by the Cenomanian-Turonian oceanic anoxic event; Correlation and implications based on three key localities: *Journal of the Geological Society* 161(4), 711-719.

- Voigt, S., Erbacher, J., Mutterlose, J., Weiss, W., Westerhold, T., Wiese, F., Wilmsen, M., Wonik, T., 2008. The Cenomanian – Turonian of the Wunstorf section – (North Germany): global stratigraphic reference section and new orbital time scale for Oceanic Anoxic Event 2. *Newsletters on Stratigraphy* 43(1), 65-89.
- Wilson, P.A., Norris, R.D., 2001. Warm tropical ocean surface and global anoxia during the mid-Cretaceous period. *Nature* 412(6845), 425-429.

2. Inorganic geochemical characterization of lithologic units recovered during ODP Leg 207 (Demerara Rise).

Almut Hetzel, Hans-Jürgen Brumsack, Bernhard Schnetger, Michael E. Böttcher

This chapter was published 2006 in Proceedings of the Ocean Drilling Program, Scientific Results, 207. Mosher, D.C., Erbacher, J., Malone, M.J. (Eds.), College Station, TX (Ocean Drilling Program), 1-37.

Abstract

The Cretaceous and Paleogene sediments recovered during Ocean Drilling Program (ODP) Leg 207 can be divided into three broad modes of deposition: synrift clastics (lithologic Unit V), organic matter-rich, laminated black shales (Unit IV), and open-marine chalk and calcareous claystones (Units III to I). The aim of this study is to provide a quantitative geochemical characterization of sediments representing these five lithologic units. For this work we used the residues (squeeze cakes) obtained from pore water sampling. Samples were analyzed for bulk parameters (total inorganic carbon, total organic carbon, and S) and by X-ray fluorescence for major (Si, Ti, Al, Fe, Mn, Mg, Ca, Na, K, and P) and selected minor (As, Ba, Co, Cr, Cu, Mo, Ni, Pb, Rb, Sr, U, V, Y, Zn, and Zr) elements. Inductively coupled plasma-mass spectrometry analyses for rare earth elements (REEs) were performed on acid digestions of the squeeze cake samples from Site 1258.

The major element composition is governed by the mixture of a terrigenous detrital component of roughly “average shale” composition with biogenous carbonate and silica. The composition of the terrigenous detritus is close to average shale in Units II–IV. For Unit I, a more weathered terrigenous source is suggested. Carbonate contents reach >60wt% on average in chalks and calcareous claystones of Units II–IV. The SiO₂ contribution in excess of the normal terrigenous-detrital background indicates the presence of biogenous silica, with highest amounts in Units II and III. The contents of coarse-grained material (quartz) are enhanced in Unit V, where Ti and Zr contents are also high. This indicates a high-energy depositional environment. REE patterns are generally similar to average shale. A more pronounced negative Ce anomaly in Unit IV may indicate low-oxygen conditions in the water column. The

Cretaceous black shales of Unit IV are clearly enriched in redox-sensitive and stable-sulfide forming elements (Mo, V, Zn, and As). High phosphate contents point toward enhanced nutrient supply and high bioproductivity. Ba/Al ratios are rather high throughout Unit IV despite the absence of sulfate in the pore waters. This indicates elevated primary production. Manganese contents are extremely low for most of the interval studied. Such an Mn depletion is only possible in an environment where Mn was mobilized and transported into an expanded oxygen-minimum-zone ("open system"). The sulfur contents show a complete sulfidation of the reactive iron of Unit IV and a significant excess of sulfur relative to that of iron that indicates that part of the sulfur was incorporated into organic matter. We suppose extreme paleoenvironmental conditions during black shale deposition: high bioproductivity like in recent coastal upwelling settings together with severe oxygen depletion if not presence of hydrogen sulfide in the water column.

Introduction

During Ocean Drilling Program (ODP) Leg 207 expanded, shallowly buried Cretaceous and Paleogene sediments from Demerara Rise off Suriname, South America, were recovered. This period of the Earth's history involved episodes of ocean anoxia, rapid climate change, mass extinction, and opening of the Equatorial Atlantic Gateway. Therefore, the Demerara Rise provides ideal conditions for long-term paleoceanographic studies of the tropical Atlantic (Erbacher, Mosher, Malone, et al., 2004).

Our approach is to use bulk sediment geochemical data to analyze the sedimentation history of Demerara Rise. Major element composition provides insight into the relative proportions of major components in marine sediment: terrigenous detritus, biogenous material, and diagenetic products. Elements and element ratios related to terrigenous material further also help to identify provenance characteristics and thus changes in climate and/or sediment supply. Cross-correlation analysis of elements gives information about different mineral phases suggesting different depositional environmental features. Changes in paleoproductivity are mirrored by elements related to biogenous processes, and the oxygenation state of the water column may be deduced from the abundance of redox-sensitive elements. Beside these paleoceanographic studies, element distribution patterns in pore waters reveal information about post-depositional and on-going diagenesis in the sediment. Study of the whole sediment column can therefore help to locate the depth of past and still-active biogeochemical processes.

The aim of this study is to provide a quantitative geochemical characterization of sediments representing the five lithologic units encountered during ODP Leg 207. For this work we used the cakes obtained from pore water squeezing. The advantage of this material is its suitability for later chemical analysis in on-shore laboratories. Another advantage is its lower content of pore water. Because the effects of precipitated dissolved seawater salts are reduced no otherwise essential salt correction is applied. We will show that the material is useful for providing a first overview of the lithologic units by applying standard geochemical analytical methods.

Material and Methods

Site description

During ODP Leg 207 sediments were recovered from five Sites (1257-1261) on Demerara Rise, located at $\sim 9^\circ\text{N}$ in the western tropical Atlantic (Figure 2.1). The rise stretches ~ 380 km along the coast of Suriname and reaches a width of ~ 220 km from the shelf break to the northeastern escarpment, where water depths increase sharply from 1000 to >4500 m. Whereas most of the plateau lies in shallow water (700 m), the northwestern margin forms a gentle ramp reaching water depths of 3000 to 4000 m. Nearly uniform, shallowly buried sections of Cretaceous and Paleogene age were drilled with good stratigraphic control. The five drill sites (Sites 1257-1261) constitute a depth transect with water depths ranging from 1900 to 3200 m. The sediments recovered can be divided into three broad styles of deposition: synrift clastics (lithologic Unit V), organic matter-rich, laminated black shales (Unit IV), and open - marine chalk and calcareous claystones (Units III to I) (Erbacher, Mosher, Malone, et al., 2004).

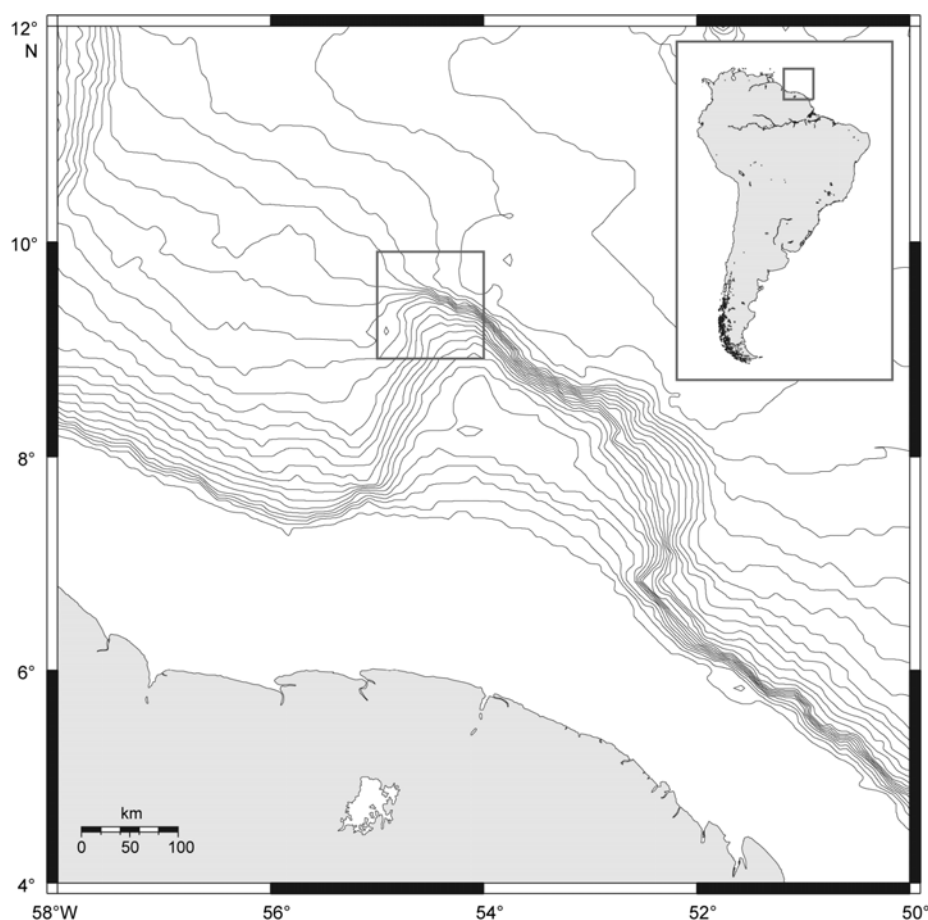


Figure 2.1 Demerara Rise (Online Map Creation www.aquarius.geomar.de).

On-board interstitial waters from 152 samples from Sites 1257-1261 and covering a depth range from the sediment/seawater interface to 648 mcd (meters composite depth) were collected and processed using standard ODP methods. Interstitial water samples were squeezed from sediment samples immediately after retrieval of the cores using titanium squeezers, modified after the standard ODP stainless steel squeezer (Manheim and Sayles, 1974). On-board splits of all squeeze cakes (pore water squeezing residues) were taken, freeze-dried, and stored in poly-ethylene bags. In the home laboratory the squeeze cake samples were ground and homogenized in an agate ball mill. The powdered samples were used for all subsequent geochemical analyses. The classification of lithologic units follows the scheme given by Erbacher, Mosher, Malone, et al. (2004).

Carbon and Sulfur

Total sulfur (TS) and total carbon (TC) were analyzed using a LECO SC-444 infrared analyzer. Total inorganic carbon (TIC) was determined coulometrically using a UIC CM 5012 CO₂ coulometer coupled to a CM 5130 acidification module. Total organic carbon (TOC) was calculated as the difference between TC and TIC. For detailed information on precision and accuracy of the methods applied see Prakash Babu et al. (1999).

Major and Trace Elements

For X-ray fluorescence (XRF) analysis, 600 mg of sample was mixed with 3600 mg of a 1:1 mixture of dilithiumtetraborate (Li₂B₂O₇) and lithiummetaborate (LiBO₂), preoxidized at 500°C with NH₄NO₃ and fused into glass-beads. The glass-beads were analyzed by XRF (Philips PW 2400) calibrated with 29 carefully selected geostandards. Analytical precision was better than 2% for major elements (Si, Ti, Al, Fe, Mn, Mg, Ca, Na, K, and P) and 6% for minor elements (As, Ba, Co, Cr, Cu, Mo, Ni, Rb, Sr, V, Y, Zn, and Zr), except for Pb and U (6%-10%).

Rare Earth Elements (REEs)

Samples from Site 1258 were also analyzed by inductively coupled-plasma mass spectrometry (ICP-MS). For acid digestion 50 mg of sample was pre-oxidized with 1 mL HNO₃ (65%) in polytetrafluoroethylene (PTFE) vessels overnight and heated with 3 mL HF (40%) and 3 mL HClO₄ (70%) in closed PTFE autoclaves (PDS-6) for 6 h at 180°C. The acids were then evaporated on hot plates at 180°C to incipient dryness. Afterwards, 3 mL 6-N HCl aliquots were added and evaporated at 180°C.

This step was repeated three times. The wet precipitate was dissolved in 1 mL HNO₃ (65%), diluted to ~10 mL and simmered at 60°C for 1 hr. The acid digestions were brought up to 50 mL final volume with deionized water. Only acids purified by sub-boiling distillation (HNO₃, HCl, and HClO₄) or of Suprapure (HF) quality were used. REE analyses were carried out using an Element (Finnigan MAT, Germany) HR-ICP-MS. Analytical precision as checked by multiple analysis of international reference materials (see Appendix A2.1) is better than 7%.

Results and Discussion

In a very simplistic way, Demerara Rise sediments consist of variable mixtures of terrigenous detritus (represented by Al₂O₃ and SiO₂) and biogenous material (represented by CaO and SiO₂). To compare the relative proportions of the major components, the relative proportions of CaO (mostly carbonate), SiO₂ (quartz/opal and aluminosilicates), and Al₂O₃ (aluminosilicates) are plotted in a triangle diagram (Figure 2.2) (Brumsack, 1989). For comparison, average shale (AS, Wedepohl, 1971), K-feldspar, and kaolinite are also plotted.

Sediments of Unit I (Fig. 2.2A) plot on a straight mixing line between carbonate and a clay component richer in Al than AS. This suggests that more intensely weathered clays (possibly a higher kaolinite proportion) are characteristic for Unit I sediments. Unit I samples show no additional enrichment in SiO₂, ruling out that significant amounts of biogenic silica are present. Given the present lack of quantitative mineral data, the presence of biogenic silica could be obscured if a higher proportion of kaolinite were present. Most sediments of Units II to IV (Fig. 2.2B) plot on a mixing line of AS and carbonate but show varying contents of biogenic silica. Unit II sediments are particularly rich in carbonate, whereas Unit III samples are generally lower in carbonate. The shift towards the SiO₂ edge indicates higher excess silica contents. Samples of Unit V (Fig. 2.2C) show a rather variable distribution. Excess silica contents are high in samples with low carbonate contents. This excess silica reflects the abundance of coarse-grained, quartz-rich sand in Unit V rather than to biogenous silica that typifies Units II to IV.

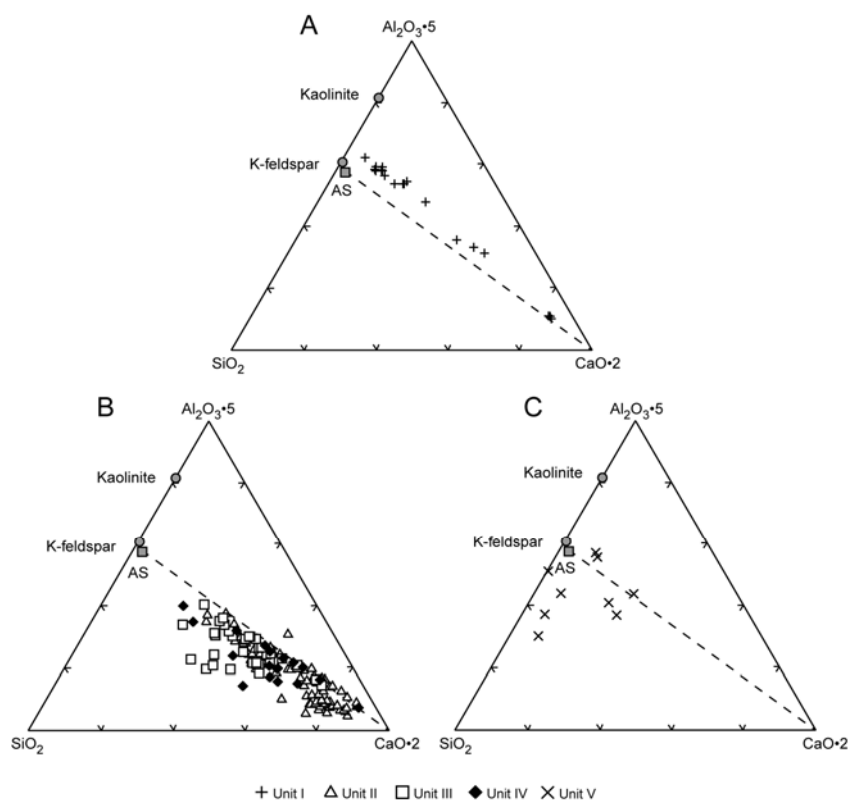


Figure 2.2 Major components of sediments from Demerara Rise in the system $\text{Al}_2\text{O}_3 \cdot 5$ – SiO_2 – $\text{CaO} \cdot 2$ (relative weight ratios). Data point for average shale (AS; Wedepohl, 1971) also shown for comparison. A. Unit I. B. Unit II-IV. C. Unit V.

In Figure 2.3 we present an overview of the changing proportion of major components of all lithologic units. The proportion of major components is calculated as follows:

carbonate contents are calculated from $\sum \text{CO}_2$ (TIC), assuming all TIC is present as pure CaCO_3 . Excess SiO_2 (biogenous opal and/or quartz) is estimated by subtracting the amount of SiO_2 present in aluminosilicates from total SiO_2 . We assume that the minimum $\text{SiO}_2/\text{Al}_2\text{O}_3$ ratio of each individual unit serves as terrigenous background, unless only $\text{SiO}_2/\text{Al}_2\text{O}_3$ ratios higher than AS are encountered. In this case the $\text{SiO}_2/\text{Al}_2\text{O}_3$ ratio of AS serves as the background value for calculating $\text{SiO}_{2\text{xs}}$. Organic matter (OM) contents are calculated by multiplying TOC by a factor of 1.34, a value given by Tissot and Welte (1984) for type II kerogen. Based on the Fe-to-S stoichiometry of pyrite, its contents can either be calculated from TS values assuming all TS is present as pyrite, or from Fe assuming all Fe is present as pyrite. Because the latter is unlikely, pyrite contents based on TS values are used unless they overnumbered the pyrite content based on Fe. In this case the excess sulfur fraction represents the “non pyritic S” component. The fraction we term “terrigenous detritus”

equals the difference between 100 wt% and the sum of major components calculated above (see also Table 2.1). Comparing our assumed “terrigenous detritus” with the sum of terrigenous elements analyzed exhibits a very good correlation ($R^2 = 0.997$) (Fig. 2.4).

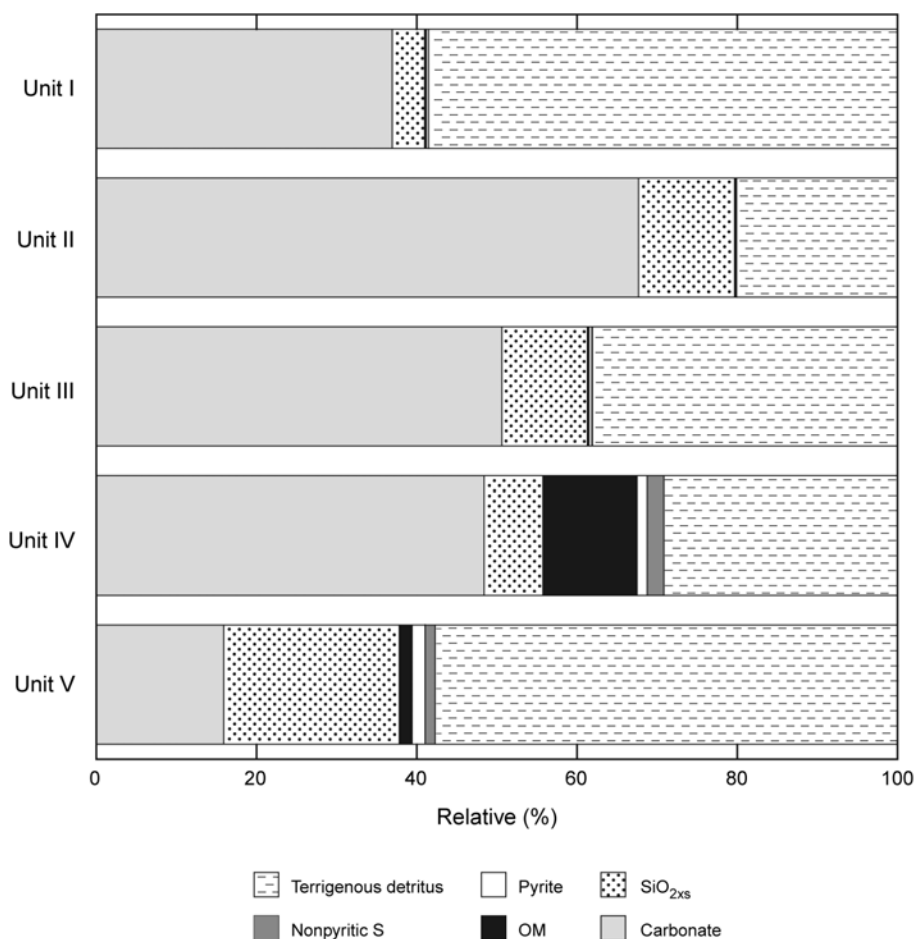


Figure 2.3 Proportion of major components of lithologic Units I-V.

Table 2.1 Calculation of proportions of major components presented in Figure 2.3.

carbonate	[%]	=	TIC [%] • 8.3331
SiO _{2xs}	[%]	=	SiO ₂ [%] - Al ₂ O ₃ [%] • (SiO ₂ /Al ₂ O ₃) _{min/Unit}
OM	[%]	=	TOC [%] • 1.34
pyrite	[%]	=	min (pyrite _{Fe} [%]; pyrite _{TS} [%])
if pyrite _{Fe} [%] < pyrite _{TS} [%]			
‘non pyritic’ S	[%]	=	TS [%] - S _{pyrite} [%]
terrigenous detritus	[%]	=	100% - Σ(carbonate; SiO _{2xs} ; OM; pyrite; ‘non pyritic’ S)

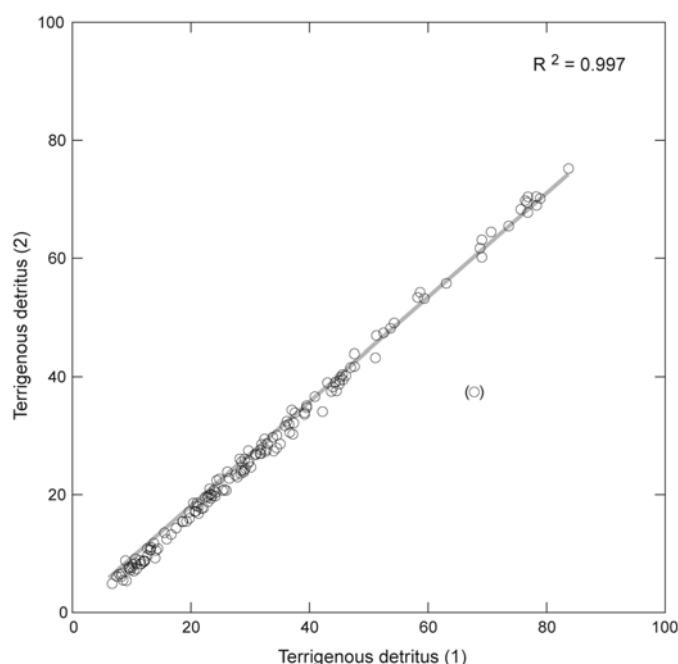


Figure 2.4 Correlation of two calculation methods for terrigenous detritus: (1) See Table 2.1 (2) Sum of measured concentrations.

Sediments from Demerara Rise are dominated either by carbonate or terrigenous detritus (Fig. 2.3). For Unit I the terrigenous detritus forms the major component (>58 wt%). The average carbonate content is 37.0 wt%. The $\text{SiO}_{2\text{xs}}$ content (4.0 wt%) is the lowest found in any lithologic unit. Concentrations of OM and pyrite are <0.3 wt% and non-pyritic sulfur is absent in Unit I.

In Units II to III carbonate (nannofossils, foraminifers, and partly diagenetic calcite) forms the major component, with concentrations that average 67.7 wt% in Unit II and 50.6 wt% in Unit III. $\text{SiO}_{2\text{xs}}$ contents (siliceous microfossils, radiolarians, and zeolites) are ~11 wt% in these sediments. According to low quantities of OM (<0.3 wt%), pyrite (<0.4 wt%) and non-pyritic sulfur (absent in Unit II, <0.1 wt% in Unit III), 20.1 wt% in Unit II and 38.1 wt% in Unit III of the sediment are terrigenous detritus.

The laminated black shales of Unit IV (of Cenomanian to Santonian age) are characterized by high OM contents (mean value >12 wt%, up to 24.9 wt% for individual samples). The content of pyrite is comparably low (0.7 wt%) in comparison to the amount of non-pyritic sulfur (2.1 wt%). This indicates a significant Fe limitation during pyrite formation and the sulfidation of OM. Beside the dilution effect of these components, the relative proportions of carbonate (48.4 wt%), terrigenous detritus (29.2 wt%) and $\text{SiO}_{2\text{xs}}$ (7.3 wt%) are similar to those found in overlaying sediments of Unit III.

Like Unit I, Unit V is dominated by terrigenous detritus (57 wt%). The average carbonate concentrations (15.9 wt%) are the lowest found in lithologic units of Demerara Rise. In sediments of Unit V siliceous microfossils are rare. Their former presence is indicated by zeolites. However, high amounts of $\text{SiO}_{2\text{xs}}$ (21.9 wt%) are mostly due to quartz, which is in accordance with the presumed shallow synrift deposit (Erbacher, Mosher, Malone, et al., 2004) (see discussion below). OM and pyrite contents are each 1.6 wt%. Thus, the pyrite content is highest in Unit V, whereas non-pyritic sulfur is present in smaller quantities (1.3 wt%) than in Unit IV.

The chemical index of alteration (CIA) (Taylor and McLennan, 1985) is a well-established parameter for determining the degree of weathering. During the degradation of feldspars, Ca, Na, and K are removed, and clay minerals with a higher fraction of Al are formed. The CIA is estimated from the proportion of Al_2O_3 vs. the weathering-prone oxides:

$$\text{CIA} = [\text{Al}_2\text{O}_3 / (\text{Al}_2\text{O}_3 + \text{CaO}^* + \text{Na}_2\text{O} + \text{K}_2\text{O})] \cdot 100,$$

where CaO^* represents the amount of CaO incorporated in the silicate fraction. A correction for carbonate and apatite content is therefore necessary. Unaltered feldspars have a CIA of 50, whereas kaolinite has a value of 100 (total removal of alkali elements). We understand that CIA values in carbonate-rich sediments may lead to compromised results. The correction required for carbonate often leads to negative CaO^* values due to the presence of additional carbonate phases like dolomite. In this case CaO^* contents were assumed to be zero. This may lead to an overestimation of CIA values due to an underestimation of CaO^* .

As described above and shown in Figure 2.3 and Table 2.1, we assumed that the terrigenous detritus round off the major components we calculated from the chemical analyses to 100 wt%. When dividing the terrigenous detritus component of each sample by the Al_2O_3 content, a factor f is obtained, which represents the relative abundance of Al_2O_3 in this component. The reciprocal value of this factor $1/f$ (= WF, weathering factor) should be a parameter for the degree of weathering, comparable to the CIA, but based on a broader range of chemical compounds.

In Figure 2.5 we compare WF with CIA values calculated for the lithologic units. Standard deviations (1σ) and results for AS (Wedepohl, 1971) are shown as well.

Both parameters require a number of simplifications and assumptions and therefore bear uncertainties. The values of the CIA as well as WF spread within the different

lithologic units. The standard deviations (<13rel%) overlap for both parameters. Only qualitative interpretations of the mean values for each unit are possible. Nevertheless, the weak correlation between both parameters ($R^2 = 0.55$) indicates that differences in weathering intensity did occur, since we can easily distinguish Units II to IV from Units I and V regarding their state of weathering.

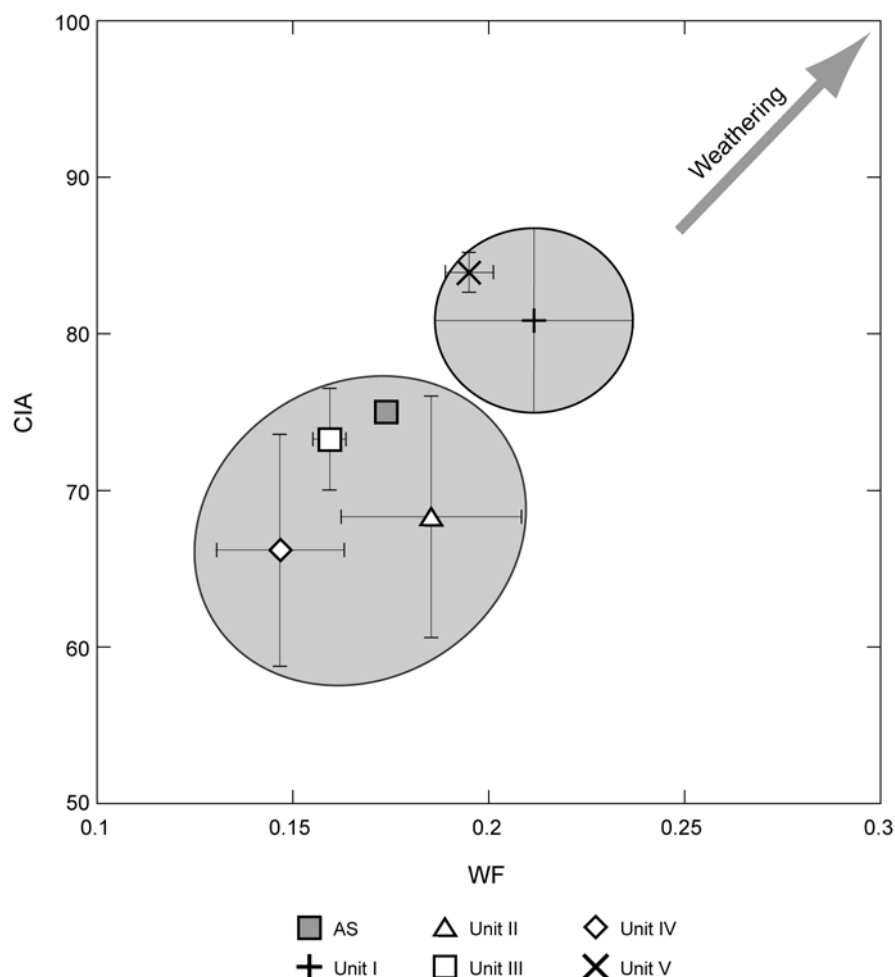


Figure 2.5 Comparison of values of weathering factor WF and chemical index of alteration (CIA) for Units I-V.

For Units II, III, and IV, values for both parameters, CIA as well as WF, are essentially the same as for AS (CIA = 70-75) (Taylor and McLennan, 1985) and thus support our interpretation of Figure 2.2, where a terrigenous component similar in composition to average shale is assumed.

The terrigenous material from Unit I is characterized by a CIA >80 indicating a high degree of weathering. Taylor and McLennan (1985) report CIA values between 80 and 90 for the Amazon mud cone. This is confirmed by the WF. Deposition of

lithologic Unit I began in the middle Miocene (Erbacher, Mosher, Malone, et al., 2004), which coincides with the initial uplift of the Andes. Resulting changes in provenance and/or drainage pathways (Potter, 1997) may have lead to different characteristics of the terrigenous detritus in Unit I, in agreement with our observations from Figure 2.2.

In Unit V, where only one sample was encountered with CaO^* contents >0 wt%, it is suggested that the CaO^* content is underestimated and therefore the high CIA value is incorrect. WF indicates more intense weathering, but a clear conclusion cannot be drawn for such quartz-rich sediments.

In Figure 2.6 the concentrations of TiO_2 (Fig. 2.6A) and Zr (Fig. 2.6B) are plotted vs. Al_2O_3 . To avoid simple dilution effects when cross-correlating element abundances, all samples were calculated on a “carbonate-free” basis. This calculation is based on the assumption that all TIC is present as pure CaCO_3 , which may lead to an underestimation for Ca and an overestimation for other carbonate-forming cations (mainly Mg and Sr, see discussion below). The resulting “carbonate-free” sediment still contains biogenous Si.

Data points from Units I to IV plot on a line ($R^2 = 0.93$ for TiO_2 and $R^2 = 0.65$ for Zr), indicating that TiO_2 and Zr are more or less uniformly incorporated into the clay component of these units. The observation that the AS data plot above the correlation line supports our interpretation that the terrigenous detrital component in Units I to IV is enriched in Al, possibly due to more intense weathering. Samples from Unit V plot above this line and show a negative correlation with Al_2O_3 ($R^2 = 0.74$ for TiO_2 and $R^2 = 0.86$ for Zr). We conclude that an additional TiO_2 and Zr bearing component other than clay minerals must be present in Unit V, most likely heavy minerals in the coarser-grained sands. In Figure 2.6C and 2.6D the concentrations of TiO_2 and Zr are plotted vs. $\text{SiO}_{2\text{xs}}$ (calculation as above but using carbonate-free data). Samples from Units I to IV again plot on a line ($R^2 = 0.53$ for TiO_2 and $R^2 = 0.33$ for Zr). The negative correlation shows that $\text{SiO}_{2\text{xs}}$ behaves independent of the terrigenous-detrital component and is generally higher in samples with lower clay content. The same is essentially true for $\text{SiO}_{2\text{xs}}$ and Zr. By contrast, for samples from Unit V a positive correlation is observed between $\text{SiO}_{2\text{xs}}$ and Zr ($R^2 = 0.86$) or TiO_2 ($R^2 = 0.82$). We assume that the $\text{SiO}_{2\text{xs}}$ from Units I to IV is derived from biogenous Si, which serves as a diluent for the terrigenous component in the carbonate-free

sediment, whereas TiO_2 and Zr contents are higher in the quartz-rich sands of Unit V. Elevated quartz and heavy mineral abundances signify high-energy environments (Dellwig et al., 2000), supporting the idea that Unit V sediments are of synrift origin as stated by Erbacher, Mosher, Malone, et al. (2004).

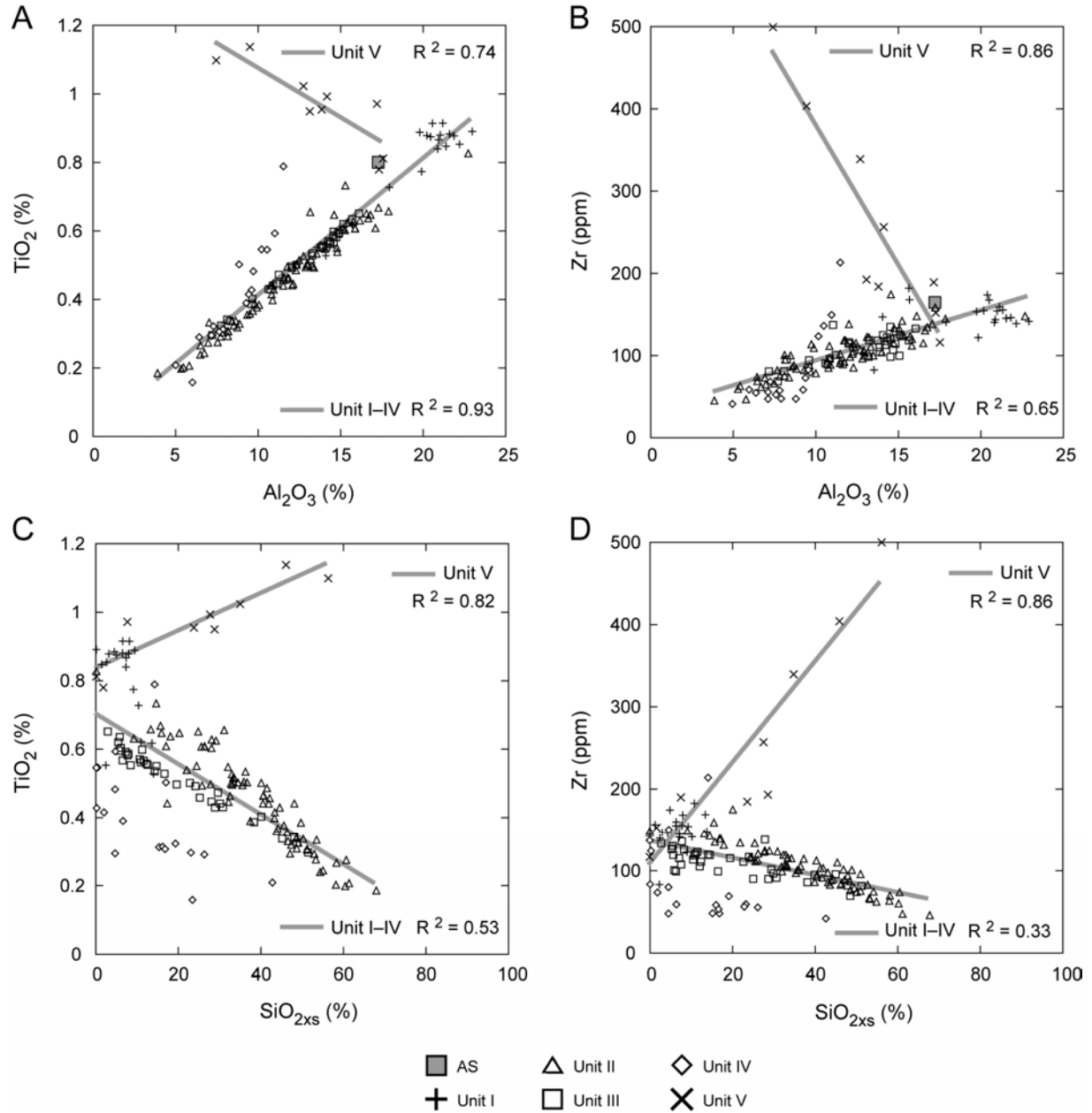


Figure 2.6 Scatter plots for heavy mineral indicating elements vs. major components. Samples are calculated "carbonate-free". A. TiO_2 vs. Al_2O_3 . B. Zr vs. Al_2O_3 . C. TiO_2 vs. $\text{SiO}_{2\text{xs}}$. D. Zr vs. $\text{SiO}_{2\text{xs}}$.

The REEs are regarded as being almost insoluble and are present in only very low concentrations in seawater and river water (McLennan, 1989). Thus, the REEs present in sediments are mainly transported as particulate matter. Because the effects of diagenesis are minor, REEs reflect the chemistry of their source areas and can be used for provenance studies. Sedimentary sorting can affect the concentrations of REE: clays show higher abundances than do coarser-grained sediments. The relative composition of REEs are generally similar for sandstones and shales. Quartz has only a diluting effect. The presence of heavy minerals may have an effect on the REE composition of an individual sample; however, a large heavy mineral contribution would be required to significantly change distribution patterns. The REE compositions of biogenous carbonates and chemical sediments in general reflect the REE composition of the surrounding seawater (McLennan, 1989). But again, high quantities are necessary to cause changes in the REE character of the sediment relative to the primary detrital flux. The REEs have generally similar chemical and physical properties. This arises from the fact that they all form stable 3+ ions of similar size. A small number of the REEs also exist in oxidation states other than 3+, but the only ions of geological importance are Ce^{4+} and Eu^{2+} . Changes in redox-conditions can therefore affect the chemistry and thus the solubility of these two elements and lead to enrichments or deficiencies relative to other REEs. In a normalized REE-distribution pattern a positive or negative 'anomaly' would result. The average REE distribution patterns for the individual units are shown in Figure 2.7. To avoid dilution due to high carbonate contents, element/Al ratios are used. Elemental ratios are normalized to element/Al ratios of upper continental crust (UCC from Taylor and McLennan, 1985). Values between 1 and 2 for sediments of Units I–IV indicate a weak REE enrichment, whereas sediments of Unit V show a small depletion in REEs (values between 0.7 and 1). A slightly more pronounced negative Ce anomaly is seen in Unit IV relative to the other units. This Ce anomaly may be quantified by comparing the measured concentration (Ce) with an expected concentration (Ce^*) obtained by interpolating between the values of the neighboring elements.

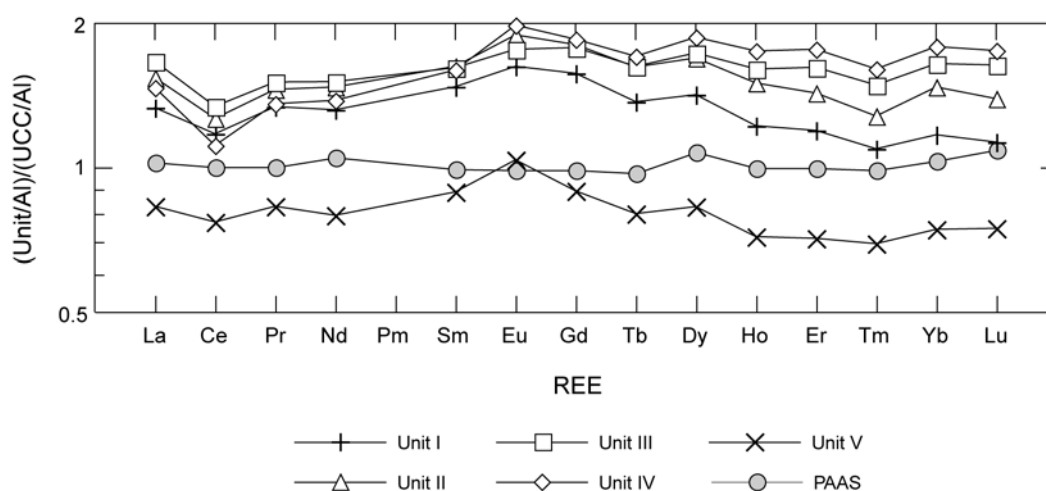


Figure 2.7 Average REE distribution patterns for Units I-V. Element/Al ratios are normalized to element/Al ratios of Upper Continental Crust (UCC; Taylor and McLennan, 1985). PAAS (Post Archean average Australian shale; Taylor and McLennan, 1985) also shown for comparison.

Wilde et al. (1996) linked Ce anomalies in shales of the anoxic facies to eustatic sea level changes. Similar to Mn, Ce^{4+} is less soluble under oxic conditions, whereas under anoxic conditions it will be mobilized, leading to a depletion in Ce in anoxic sediments relative to those deposited under oxic conditions. A negative Ce anomaly would result.

In Table 2.2 two different values are given for the Ce anomaly, which are based on different calculations. Taylor and McLennan (1985) recommended use of the geometric mean $\text{Ce}^* = \sqrt{(\text{La} \cdot \text{Pr})}$. The ratio Ce/Ce^* is then a measure of the anomaly, with values less than unity being termed negative. Wilde et al. (1996) support use of the arithmetic mean $\text{Ce}^* = (\text{La} + \text{Pr})/2$ and calculated the logarithm of the ratio Ce/Ce^* . Both calculations lead to essentially the same values for Ce^* , with the most negative anomaly in Unit IV.

Table 2.2 Ce anomaly for lithologic Units I – V. Two quantification approaches are given.

		Unit I	Unit II	Unit III	Unit IV	Unit V
Taylor and McLennan (1985)	$\text{Ce}^* = \sqrt{(\text{La} \cdot \text{Pr})}$	1.33	1.49	1.58	1.41	0.83
	Ce/Ce^*	0.88	0.85	0.85	0.79	0.93
Wilde et al. (1996)	$\text{Ce}^* = (\text{La} + \text{Pr})/2$	1.33	1.49	1.58	1.41	0.83
	$\log \text{Ce}/\text{Ce}^*$	-0.06	-0.07	-0.07	-0.10	-0.03

According to Wilde et al. (1996), the negative Ce anomaly for the black shales of Unit IV can be interpreted as a consequence of water column anoxia during sea level highstands in the Cretaceous. REE patterns in the sediments of Demerara Rise are complicated by the presence of biogenous and chemical compounds that record the surrounding seawater and pore waters (e.g., for phosphate). For example, carbonate tests of plankton living in the photic zone under oxic conditions would carry the surface seawater characteristics and would therefore display a negative Ce anomaly. However, this effect is not seen in the more carbonate-rich Units II and III.

The database is still too small for demonstrating that these REE characteristics hold true for Cenomanian/Turonian (C/T) black shales from Demerara Rise in general. Statistically, the REE patterns do not show any extraordinary characteristics and do not differ much from those of PAAS (Post-Archean average Australian; Taylor and McLennan, 1985).

Figure 2.8 illustrates the chemistry of the biogenous carbonates. In Figure 2.8A CaO concentration is plotted vs. the TIC contents. The good correlation shows that almost all CaO is present as CaCO_3 . Some samples from Unit IV contain additional CaO, which is present as apatite. The contents of CaO-bearing mineral phases other than carbonate are negligible. The positive correlation between Sr and TIC (Fig. 2.8B) indicates that a variable fraction of Sr is incorporated into carbonates (750 to 1300 ppm). The negative correlation of MgO and TIC (Fig. 2.8C) shows that Mg is mostly incorporated into clay components, even though a small contribution of Mg-rich calcite or dolomite cannot be excluded. MnO shows no correlation with TIC (Fig. 2.8D), but highest concentrations of MnO are found in the carbonate-rich Unit II. Figure 2.9 shows the average element/Al ratios of Ca, Sr, Mg, and Mn in Units I to V. Except for the strong Mn depletion in Unit IV (see discussion below), a similar distribution pattern is displayed.

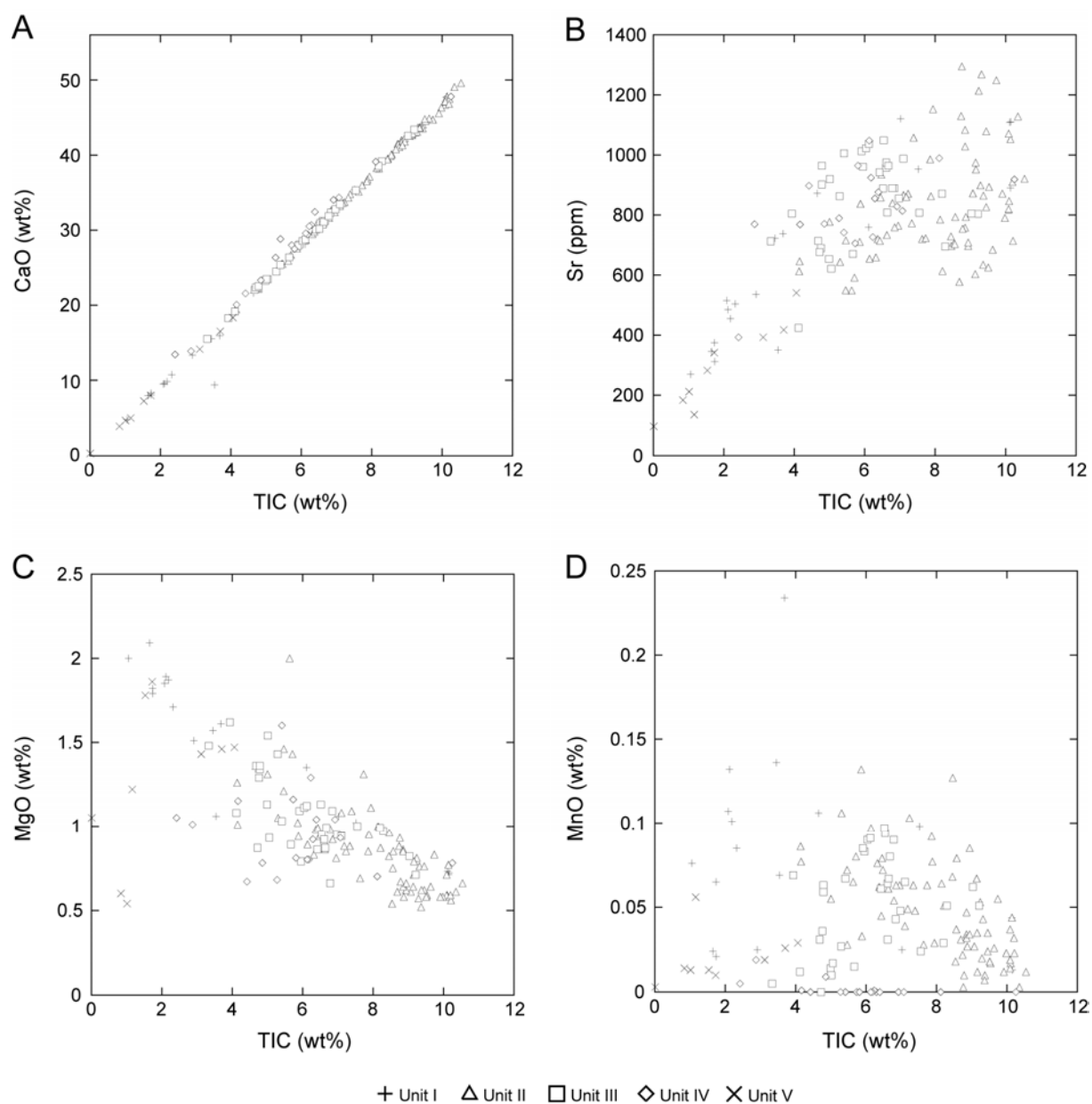


Figure 2.8 Scatter plots of carbonate chemistry. A. CaO vs. TIC. B. Sr vs. TIC. C. MgO vs. TIC. D. MnO vs. TIC.

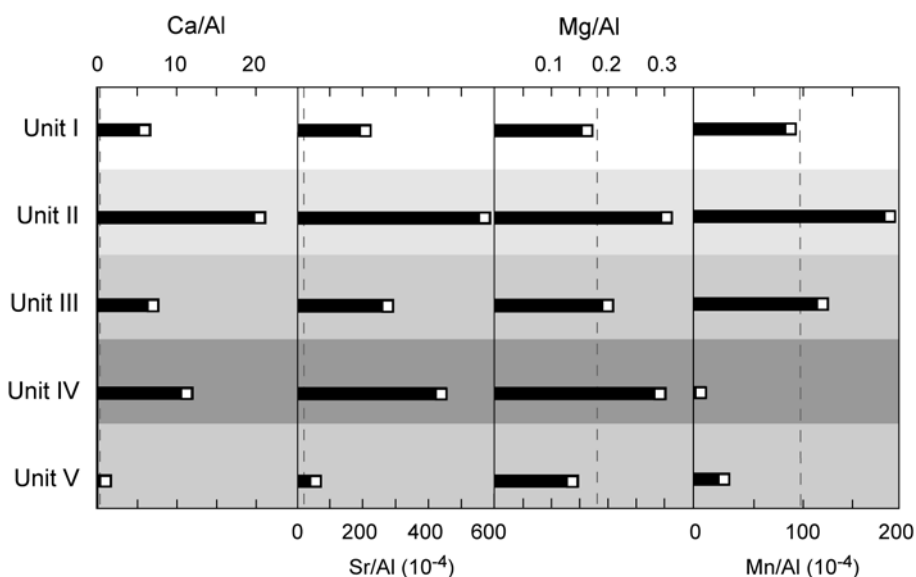


Figure 2.9. Mean values of element/Al ratios of Ca, Sr, Mg and Mn in Units I-V. Element/Al ratios in AS are indicated by dashed line.

The oxygenation state of the seawater and the redox state of the surface sediment form a crucial variable for the preservation of organic material and the formation of pyrite. Therefore, the contents of pyrite, reactive Fe, and TOC allow us to draw conclusions about the paleoenvironment during deposition of the sediment. The degree of pyritization based on bulk sediment analysis is visualized in a ternary Fe_x -TOC-S diagram (Fig. 2.10) (Brumsack et al., 1995). The content of reactive Fe (Fe_x) was estimated empirically ($Fe_x = Fe - 0.25 \cdot Al$) assuming that a certain fraction of aluminosilicate-bound Fe is not available for pyrite formation (Canfield et al., 1992). Results of a detailed analysis of reactive iron in the investigated samples is discussed in an accompanying publication (Böttcher et al., 2006). Data points that plot close to the pyrite saturation line (PSL) are assumed to represent samples that are completely pyritized.

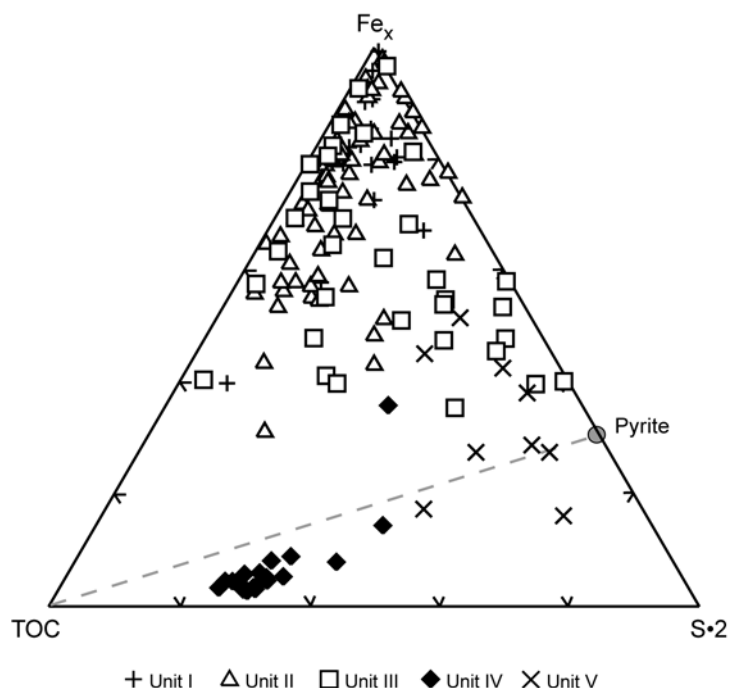


Figure 2.10 Degree of Pyritization of sediments from Demerara Rise in the Fe_x - TOC - $\text{S}\cdot 2$ (following stoichiometry of pyrite - FeS_2) system (relative weight ratios). Reactive Fe (Fe_x) is calculated with $\text{Fe}_x = \text{Fe} - 0.25 \cdot \text{Al}$. Data point for pyrite is also shown.

Most of the samples of Unit IV plot below the PSL, indicating the presence of an additional sulfur phase. Böttcher et al. (2006) found organic sulfur contents exceeding 3 wt% in Demerara Rise black shales. The presence of acid volatile sulfur points to the presence of metal sulfides other than pyrite, likely ZnS (Brumsack, 1980). Samples of Units I-III are positioned above the PSL, indicating that Fe_x was only partly used for pyrite formation, in agreement with direct measurements of sulfur and iron speciation (Böttcher et al., 2006).

Trace metal (TM) distribution patterns reveal information about the depositional environment. Due to TM participation in bio-cycling processes (Bruland, 1983), scavenging by particulate matter and dissolution and precipitation of redox-sensitive compounds TM enrichment as well as depletion in sediments are diagnostic for bio-productivity and redox-conditions during deposition. In combination with pore water data they allow indication of post-depositional element migration. Figure 2.11 shows the mean values of TM/Al ratios of diagnostic TM in the different lithologic units. TMs are shown in order of TM enrichment relative to AS (dashed line) in Unit IV.

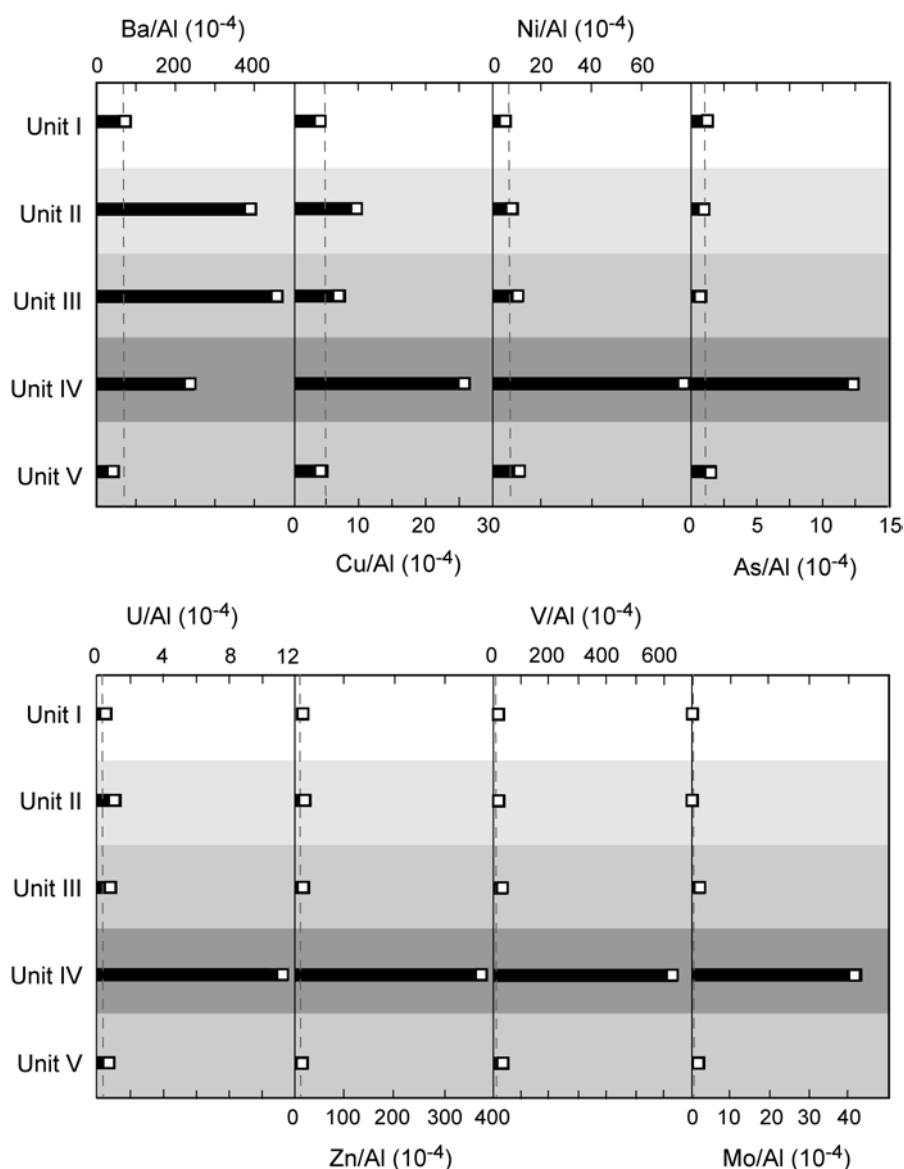


Figure 2.11 Mean values of TM/Al ratios of diagnostic TM in Units I-V. TM are presented in order of TM enrichment relative to AS (dashed line) in Unit IV.

The non-lithogenic excess Ba has been interpreted as a paleoproxy for bio-productivity (Schmitz, 1987; Dymond et al., 1992; Paytan et al., 1996). These biogenic barites (BaSO_4) (Bishop, 1988; Bertram and Cowen, 1997; Bernstein and Byrne, 2004) are only stable under seawater sulfate concentrations (Church and Wohlgemuth, 1972). Due to the microbial sulfate reduction in TOC-rich sediments, barite is dissolved, Ba is mobilized (Brumsack and Gieskes, 1983; McManus et al., 1998; Eagle et al., 2003), and authigenic barite precipitates at the top of the sulfate-

depletion zone forming diagenetic barite fronts within or above TOC-rich strata (Torres et al., 1996; Bréhéret and Brumsack, 2000).

Ba/Al ratios are highest in Units II and III. In the black shales of Unit IV Ba/Al ratios are still high despite the absence of sulfate in the pore waters (Erbacher, Mosher, Malone, et al., 2004). Arndt et al. (2006) show in a transport-reaction model that not only OM degradation but also anaerobic oxidation of methane (AOM) above the black shales of Demerara Rise influence sulfate availability and therefore the remobilization of biogenic barium. The authors further showed that temporal dynamics of degradation processes caused various shifts of the barite precipitation zone during burial, thus inhibiting the formation of an authigenic barite front or causing the dissolution of earlier formed fronts. In our view the Ba enrichment in Unit IV indicates elevated primary productivity during deposition. But a large fraction of former barite may remobilize and form diagenetic barites in Unit III. For this reason the use of Ba as a paleoproxy on a quantitative level (Dymond et al., 1992) for Cretaceous settings in such an environment is highly questionable.

The very high phosphate contents (>0.7 wt% P_2O_5 on average in Unit IV) are comparable to those in recent upwelling sediments and also points towards enhanced nutrient supply and resulting high bioproductivity (e.g., Böning et al., 2004).

The black shales of Unit IV are clearly enriched in redox-sensitive and stable sulfide-forming TMs. In today's ocean, TOC-rich sediments are deposited in coastal upwelling areas and euxinic basins. Brumsack (2006) attempted to distinguish both environments by their specific TM patterns. Thereby, the author discussed TM sources and fixation mechanisms. Cu and Ni are discussed to be involved in bio-cycling. The enrichment found in recent upwelling sediments (Böning et al., 2004) indicates deposition via bio-detritus. In contrast, oxyanions (As, U, V, and Mo) are primarily derived from seawater. The enrichments of Mo, U, and As indicate a sulfidic environment (Brumsack, 2006). High concentrations of sulfide-forming TM (Cu and Zn) and sulfur phases other than pyrite indicate Fe limitation and thus support the idea of an euxinic environment (Böttcher et al., 2006).

The strong depletion in Mn (Fig. 2.9) requires the presence of at least suboxic conditions in parts of the water column (Quinby-Hunt and Wilde, 1994). Dissolved Mn is conveyed away in an expanded oxygen-minimum-zone (OMZ) like in recent coastal upwelling areas. Thurow et al. (1992) describe such an Mn mobilization at the

northwest Australian margin during the Cenomanian/Turonian Boundary Event. The authors found Mn-poor sediments within the OMZ and Mn-rich sediments below the OMZ, indicating oxic deep waters during the C/T interval at this location. Mn enrichment under anoxic/euxinic conditions is only possible in a closed (silled-basin like) system, where dissolved Mn cannot be conveyed away and alkalinity is high enough to form Mn(II)carbonate. Lyons et al. (pers. communication) find these Mn-enrichments in euxinic Unit 1 in the modern Black Sea. Mn depletion in all samples of Unit IV shows that the investigated sites (1257-1261) must be located within the OMZ during deposition. In this case the re-oxidation and reduction of Mn oxides (Mn cycling) at the redox boundary may have induced TM scavenging by Mn-(oxy)hydroxides (Cu, Mo, and V) comparable to the Black Sea. But the Mn most likely was deposited in other parts of the Proto-Atlantic, where deep waters still might have contained oxygen.

However, one should mention that the elemental pattern of black shales from Demerara Rise is very similar to the one known from other C/T settings, particularly with respect to the extraordinarily high V and Zn contents (Brumsack, 2006).

Conclusions

Sediments recovered during Leg 207 from the Demerara Rise consist of different mixtures between biogenous carbonate and detrital material. Lithologic Units II-IV show high carbonate contents, whereas Unit I and V are dominated by terrigenous detritus. Major element analysis indicates a common origin of the terrigenous detritus similar to average shale, whereas the clay-dominated Unit I reveals a more weathered terrigenous component. Heavy minerals phases and quartz-bearing sands display a high-energy synrift deposit in Unit V.

The Cretaceous black shales of Unit IV are clearly enriched in redox-sensitive and stable sulfide-forming elements. This indicates high paleoproductivity and severe oxygen depletion in the water column. The complete sulfidation of the black shales and significant excess sulfur report a sulfidic environment, leading to sulfur incorporation into organic matter.

Ba enrichments in sediments above the black shale sequences show former diagenetic mobilization of barite in underlying sediment layers. Pore water data evidence that sulfate reduction due to anaerobic methane oxidation is still driving barite diagenesis.

Acknowledgements

We would like to thank the crew and scientific party of ODP Leg 207 for their kind support. This research used samples and / or data provided by the Ocean Drilling Program (ODP). ODP is sponsored by the U.S. National Science Foundation (NSF) and participating countries under management of Joint Oceanographic Institutions (JOI), Inc. Lori Peters of IODP edited the text in detail. Pat Wilde and Tim Lyons are thanked for their constructive reviews of the manuscript. This study was funded by Deutsche Forschungsgemeinschaft (grants BR 775/16, BR 775/17 and BO 1584/2) and Max Planck Society, Germany.

References

- Arndt, S., Brumsack, H.-J., Wirtz, K.W., 2006. Cretaceous black shales as active bioreactors: A biogeochemical model for the deep biosphere encountered during ODP Leg 207 (Demerara Rise). *Geochimica et Cosmochimica Acta* 70(2), 408-425.
- Bernstein R.E., Byrne R.H., 2004. Acantharions and marine barite. *Marine Chemistry* 86(1-2), 45-50.
- Bertram, M.A., Cowen, J.P., 1997. Morphological and compositional evidence for biotic precipitation of marine barite. *Journal of Marine Research* 55(3), 577-593.
- Bishop, J.K.B., 1988. The barite-opal-organic carbon association in oceanic particulate matter. *Nature* 332(6162), 341-343.
- Böning, P., Brumsack, H.-J., Böttcher, M.E., Schnetger, B., Kriete, C., Kallmeyer, J., Borchers, S.L., 2004. Geochemistry of Peruvian near-surface sediments. *Geochimica et Cosmochimica Acta* 68(21), 4429-4451.
- Böttcher, M.E., Hetzel, A., Brumsack, H.-J., Schipper, A., 2006. Sulfur-iron-carbon geochemistry in sediments of the Demerara Rise. In: Mosher, D.C., Erbacher, J., Malone, M.J. (Eds.), *Proceedings of the Ocean Drilling Program, Scientific Results, 207*. College Station, TX (Ocean Drilling Program), 1-23.
- Bréhéret, J.G., Brumsack, H.-J., 2000. Barite concretions as evidence of pauses in sedimentation in the Marnes Bleues Formation of the Vocontian Basin (SE France). *Sedimentary Geology* 130(3-4), 205-228.
- Bruland, K.W., 1983. Trace elements in seawater. In: Riley, J.P., Chester, R. (Eds.), *Chemical Oceanography* (Vol. 8). Academic Press, London, 157-220.
- Brumsack, H.-J., 1980. Geochemistry of Cretaceous black shales from the Atlantic Ocean (DSDP Legs 11, 14, 36, and 41). *Chemical Geology* 31, 1-25.
- Brumsack, H.-J., 1989. Geochemistry of recent TOC-rich sediments from the Gulf of California and the Black Sea. *Geologische Rundschau* 78(3), 851-882.
- Brumsack, H.-J., 2006. The trace metal content of recent organic carbon-rich sediments: implications for Cretaceous black shale formation. *Palaeogeography, Palaeoceanography, Palaeoecology* 232(2-4), 344-361.
- Brumsack, H.-J., Gieskes, J.M., 1983. Interstitial water trace-metal chemistry of laminated sediments from the Gulf of California, Mexico. *Marine Chemistry* 14(1), 89-106.
- Brumsack, H.-J., Heydemann, A., Kühn, V., Rachold, V., Usdowski, E., 1995. Geochemistry and mineralogy of Middle Aptian sediments from the Lower

- Saxony Basin, NW Germany. *Neues Jahrbuch für Geologie und Paläontologie, Abhandlungen* 196(2), 235-255.
- Canfield, D.E., Raiswell, R., Bottrell, S., 1992. The reactivity of sedimentary iron minerals toward sulfide. *American Journal of Science* 292, 659-683.
- Church, T.M., Wohlgemuth, K., 1972. Marine Barite Saturation. *Earth and Planetary Science Letters* 15(1), 35-44.
- Dellwig, O., Hinrichs, J., Hild, A., Brumsack, H.-J., 2000. Changing sedimentation in tidal flat sediments of the southern North Sea from the Holocene to the present: a geochemical approach. *Journal of Sea Research* 44(3-4), 163-181.
- Dymond, J., Suess, E., Lyle, M., 1992. Barium in deep-sea sediments: A geochemical proxy for paleoproductivity. *Paleoceanography* 7(2), 163-181.
- Eagle, M., Paytan, A., Arrigo, K.R., van Dijken, G., Murray, R.W., 2003. A comparison between excess barium and barite as indicators of carbon export. *Paleoceanography* 18(1), 1021.
- Erbacher, J., Mosher, D.C., Malone, M.J., Shipboard Scientific Party, 2004. *Proceedings of the Ocean Drilling Program, Initial Reports*, 207. College Station, TX (Ocean Drilling Program), pp. 89.
- Erbacher, J., Mutterlose, J., Wilmsen, M., Wonik, T., Wunstorff Drilling Scientific Party, 2007. The Wunstorff Drilling Project: Coring a global stratigraphic reference section of the Oceanic Anoxic Event 2. *Scientific Drilling* 4, 19-21.
- Manheim, F.T., Sayles, F.L., 1974. Composition and origin of interstitial waters of marine sediments, based on deep sea drill cores. In: Goldberg, E.D. (Ed.), *The Sea (Vol. 5): Marine Chemistry: The Sedimentary Cycle*. Wiley, New York, 527-568.
- McLennan, S.M., 1989. Rare earth elements in sedimentary rocks: influence of provenance and sedimentary processes. In: Lipin, B.R., McKay, G.A. (Eds.), *Geochemistry and Mineralogy of the Rare Earth Elements. Reviews in Mineralogy* 21, 169-200.
- McManus, J., Berelson, W.M., Klinkhammer, G.P., Johnson, K.S., Coale, K.H., Anderson, R.F., Kumar, N., Burdige, D.J., Hammond, D.E., Brumsack, H.-J., McCorkle, D.C., Rushdi, A., 1998. Geochemistry of barium in marine sediments: implications for its use as a paleoproxy. *Geochimica et Cosmochimica Acta* 62(21-22), 3453-3473.
- Paytan, A., Kastner, M., Chavez, F.P., 1996. Glacial to interglacial fluctuations in productivity in the equatorial Pacific as indicated by marine barite. *Science* 274(5291), 1355-1357.
- Potter, P.E., 1997. The Mesozoic and Cenozoic paleodrainage of South America: a natural history. *Journal of South American Earth Sciences* 10(5-6), 331-344.
- Prakash Babu, C., Brumsack, H.-J., Schnetger, B., 1999. Distribution of organic carbon in surface sediments along the eastern Arabian Sea: a revisit. *Marine Geology* 162(1), 91-103.
- Quinby-Hunt, M.S., Wilde, P., 1994. Thermodynamic zonation in the black shale facies based on iron-manganese-vanadium content. *Chemical Geology* 113(3-4), 297-317.
- Schmitz, B., 1987. Barium, equatorial high productivity, and the northward wandering of the Indian continent. *Paleoceanography* 2(1), 63-77.
- Taylor, S.R., McLennan, S.M., 1985. *The Continental Crust: Its Composition and Evolution*. Blackwell Scientific, Oxford.
- Thurrow, J., Brumsack, H.-J., Rullkötter, J., Littke, R., Meyers, P., 1992. The Cenomanian/Turonian boundary event in the Indian Ocean - a key to understand the global picture. In: Duncan, R.A., Rea, D.K., Kidd, R.B., von Rad, C.

- U., Weissel, J.K. (Eds.), The Indian Ocean: A Synthesis of Results from the Ocean Drilling Program. American Geophysical Union, Geophysical Monograph 70, 253-273.
- Wedepohl, K.H., 1971. Environmental influences on the chemical composition of shales and clays. In: Ahrens, L.H., Press, F., Runcorn, S.K., Urey, H.C. (Eds.), Physics and Chemistry of the Earth 8. Pergamon, Oxford, 305-333.
- Wedepohl, K.H., 1991. The composition of the upper earth's crust and the natural cycles of selected metals. Metals in natural raw materials. Natural Resources. In: Merian, E. (Ed.), Metals and Their Compounds in the Environment. VCH, Weinheim, 3-17.
- Wehausen, R., Schnetger, B., Brumsack, H.-J., Lange, G.D., 1999. Determination of major and minor ions in brines by X-ray fluorescence spectrometry: comparison with other common analytical methods. X-ray Spectrometry 28, 168-172.
- Werne, J.P., Hollander, D.J., Lyons, T.W., Sinninghe Damsté, J.S., 2004. Organic sulfur biogeochemistry: recent advances and future research directions. In: Amend, J., Edwards, K., Lyons, T. (Eds.), Sulfur Biogeochemistry: Past and Present. Geological Society of America. Special Paper 379, 135-150.
- Wijsman, J.W.M., Middelburg, J.J., Heip, C.H.R., 2001. Reactive iron in Black Sea sediments: implications for iron cycling. Marine Geology 172(3-4), 167-180.
- Wijsman, J.W.M., Middelburg, J.J., Herrmann, P.M., Böttcher, M.E., Heip, C.H.R., 2001. Sulfur and iron speciation in surface sediments along the northwestern margin of the Black Sea. Marine Chemistry 74(4), 261-278.
- Wilde, P., Quinby-Hunt, M.S., Erdtmann, B.-D., 1996. The whole-rock cerium anomaly: a potential indicator of eustatic sea-level changes in shales of the anoxic facies. Sedimentary Geology 101(1-2), 43-53.

Appendix

Appendix A2.1 Precision and accuracy of analyzed elements.

Element	Method	Precision SD (1σ) (rel%)	Accuracy (rel%)
TS	IR-analyzer	2.7	102.6
TC	IR-analyzer	1.3	100.5
TIC	Coulometry	0.8	99.8
SiO ₂	XRF	0.4	99.7
TiO ₂	XRF	1.0	102.8
Al ₂ O ₃	XRF	0.5	99.9
Fe ₂ O ₃	XRF	0.4	100.6
MnO	XRF	1.4	101.5
MgO	XRF	0.6	108.7
CaO	XRF	0.5	100.4
Na ₂ O	XRF	0.0	98.9
K ₂ O	XRF	1.4	92.7
P ₂ O ₅	XRF	0.7	103.4
As	XRF	2.7	93.8
Ba	XRF	3.0	104.7
Co	XRF	5.4	98.1
Cr	XRF	3.6	108.8
Cu	XRF	3.7	89.8
Mo	XRF	4.7	101.6
Ni	XRF	0.8	99.0
Pb	XRF	9.0	93.6
Rb	XRF	2.0	98.2
Sr	XRF	0.5	102.5
U	XRF	8.8	105.5
V	XRF	1.2	104.3
Y	XRF	3.0	100.7
Zn	XRF	1.7	97.8
Zr	XRF	2.8	103.0
REE	ICP-MS	6.8 ^a	95.9 - 102.6 ^b

Notes: Accuracy is defined as 100% times the mean of the repeat analyses divided by the expected value. Precision is defined as 100% times the best estimate standard deviation (1σ) divided by the mean of the repeats. SD = standard deviation.

^a maximum value

^b range

Appendix A2.2 Major element concentrations in sediments of Demerara Rise using pore water squeezing residues.

Hole, core, section, interval (cm)	Unit	Depth (mbsf)	Depth (mcd)	TS (%)	TIC (%)	TOC (%)	SiO ₂ (%)	TiO ₂ (%)	Al ₂ O ₃ (%)	Fe ₂ O ₃ (%)	MnO (%)	MgO (%)	CaO (%)	Na ₂ O (%)	K ₂ O (%)	P ₂ O ₅ (%)
207-																
1257A-1H-1, 145-150	I	1.45	1.45	0.03	1.65	0.06	46.47	0.669	17.11	6.36	0.024	2.09	7.97	1.29	2.41	0.069
1257A-2H-4, 145-150	II	8.55	8.55	0.06	7.94	0.08	18.63	0.187	4.98	2.06	0.029	1.11	37.13	0.93	0.81	0.099
1257A-3H-4, 145-150	II	18.05	18.05	0.03	8.85	0.18	14.52	0.131	3.47	1.34	0.034	0.86	41.98	0.94	0.65	0.086
1257A-4H-3, 145-150	II	26.05	26.05	0.08	8.85	0.00	14.04	0.130	3.50	1.44	0.032	0.85	41.97	0.83	0.64	0.137
1257A-5H-3, 145-150	II	35.55	35.55	0.02	7.39	0.18	21.85	0.234	5.78	2.31	0.048	1.09	34.79	0.87	0.68	0.100
1257A-6X-3, 145-150	II	45.05	45.05	0.04	9.07	0.04	16.82	0.060	1.63	0.66	0.027	0.61	42.53	0.60	0.15	0.060
1257A-7X-3, 145-150	II	49.35	49.35	0.03	9.45	0.01	14.63	0.059	1.59	0.62	0.024	0.62	44.05	0.66	0.21	0.065
1257B-3R-2, 145-150	II	52.75	56.12	0.01	9.15	0.22	15.62	0.095	2.57	0.92	0.035	0.71	42.66	0.56	0.25	0.057
1257A-8X-3, 145-150	II	58.55	58.55	0.05	7.63	0.02	26.69	0.076	2.10	1.04	0.028	0.69	35.12	0.69	0.18	0.061
1257B-4R-3, 143-150	II	63.82	70.93	0.02	8.46	0.24	16.89	0.132	3.56	1.64	0.127	0.96	39.55	0.94	0.84	0.108
1257B-5R-4, 42-49	II	73.65	76.70	0.02	7.88	0.16	20.47	0.172	4.44	1.73	0.077	0.95	36.74	1.01	0.88	0.102
1257B-7R-2, 143-150	III	91.23	95.60	0.04	6.61	0.19	29.92	0.194	4.81	1.63	0.064	0.91	31.21	1.03	0.77	0.080
1257B-8R-4, 142-150	III	103.79	107.22	0.05	5.95	0.21	33.34	0.232	5.86	1.51	0.083	0.79	28.09	1.31	1.24	0.082
1257B-9R-3, 140-150	III	112.02	113.79	0.02	6.54	0.21	27.90	0.253	6.30	2.15	0.094	0.95	30.92	1.28	1.21	0.085
1257A-14X-4, 140-150	III	117.70	117.70	0.02	5.91	0.17	30.98	0.284	7.03	2.62	0.085	1.09	27.92	1.32	1.28	0.080
1257B-10R-4, 140-150	III	123.10	125.68	0.01	6.04	0.25	29.52	0.290	7.29	2.74	0.090	1.11	28.56	1.28	1.20	0.077
1257A-15X-5, 140-150	III	128.90	128.49	0.02	6.12	0.18	29.14	0.291	7.26	2.58	0.091	1.12	28.76	1.33	1.18	0.078
1257B-11R-4, 140-150	III	132.70	135.28	0.02	3.93	0.12	39.76	0.407	10.13	4.40	0.063	1.62	18.27	1.67	1.45	0.082
1257B-12R-3, 140-150	III	140.60	143.27	1.52	4.79	0.04	34.66	0.342	8.73	4.55	0.069	1.34	22.19	1.58	1.38	0.087
1257B-13R-4, 140-150	III	151.70	154.90	0.38	6.84	0.14	26.16	0.231	5.69	2.14	0.043	1.09	32.34	1.22	0.99	0.063
1257C-8R-6, 90-100	III	157.50	159.95	0.06	6.61	0.20	30.65	0.199	4.87	1.23	0.031	0.92	30.71	1.26	0.88	0.054
1257A-18X-4, 140-150	III	156.16	161.96	0.18	5.29	0.13	35.32	0.309	7.69	2.40	0.027	1.43	24.50	1.40	1.29	0.078
1257C-9R-6, 51-61	III	166.15	168.56	0.18	5.67	0.03	39.10	0.179	4.34	1.45	0.015	0.89	26.40	1.24	0.77	0.105
1257C-10R-1, 140-150	III	169.80	172.21	0.31	3.33	0.08	48.33	0.324	7.97	2.41	0.005	1.48	15.51	1.64	1.44	0.189
1257C-12R-2, 90-100	IV	190.10	192.65	2.01	5.41	3.51	24.26	0.088	3.27	6.52	0.000	1.60	28.82	0.90	1.53	2.713
1257C-13R-2, 140-150	IV	200.20	202.75	1.34	5.27	6.03	33.66	0.118	2.77	0.90	0.000	0.68	26.34	1.32	0.52	0.990
1257C-15R-3, 17-27	IV	218.98	221.53	1.44	6.29	7.71	23.09	0.139	3.03	1.20	0.000	0.92	30.68	1.06	0.49	0.945
1257B-27R-3, 0-7	V	225.30	228.94	1.50	3.12	0.41	47.12	0.708	10.20	4.88	0.019	1.43	14.15	0.88	1.12	0.150
1257C-16R-6, 20-30	V	233.87	235.03	1.08	3.70	0.40	46.08	0.658	9.04	4.37	0.026	1.46	16.53	0.84	1.04	0.147
1257A-31X-1, 71-81	V	275.81	281.61	0.93	4.06	1.04	37.93	0.644	11.34	5.49	0.029	1.47	18.35	0.85	1.32	0.120

Notes: *italic values below detection limit.*

Appendix A2.2 continued [part 2 of 5]

Hole, core, section, interval (cm)	Unit	Depth (mbsf)	Depth (mcd)	TS (%)	TIC (%)	TOC (%)	SiO ₂ (%)	TiO ₂ (%)	Al ₂ O ₃ (%)	Fe ₂ O ₃ (%)	MnO (%)	MgO (%)	CaO (%)	Na ₂ O (%)	K ₂ O (%)	P ₂ O ₅ (%)
207-																
1258A-1R-1, 145-150	I	1.45	1.45	0.02	6.11	0.00	24.90	0.358	8.78	5.89	0.090	1.35	28.11	0.87	0.85	0.154
1258A-1R-2, 145-150	I	2.95	2.95	0.03	7.52	0.17	18.50	0.317	7.96	2.80	0.098	1.02	35.40	0.71	0.64	0.097
1258A-3R-4, 145-150	II	20.15	20.15	0.05	8.94	0.13	17.69	0.052	1.38	0.67	0.085	0.62	42.24	0.58	0.17	0.086
1258A-4R-4, 145-150	II	29.75	29.75	0.04	8.85	0.03	17.84	0.088	1.83	0.77	0.047	0.64	41.68	0.67	0.28	0.081
1258A-5R-3, 145-150	II	37.65	42.15	0.03	7.73	0.13	21.13	0.184	4.42	1.59	0.063	1.31	35.99	1.13	1.27	0.099
1258A-6R-4, 145-150	II	48.75	49.27	0.00	5.63	0.00	30.97	0.349	6.95	3.39	0.065	2.00	25.93	1.32	1.68	0.095
1258A-7R-4, 145-150	II	58.15	59.14	0.03	5.71	0.06	31.11	0.277	6.65	3.05	0.080	1.43	26.70	1.35	1.63	0.115
1258A-8R-4, 140-150	II	68.07	69.92	0.04	6.14	0.02	31.54	0.228	5.62	1.85	0.097	0.89	28.71	1.56	1.58	0.095
1258A-9R-6, 140-150	II	80.80	81.05	0.05	5.46	0.00	33.87	0.275	6.68	2.31	0.072	1.21	25.55	1.48	1.70	0.112
1258A-10R-3, 140-150	II	86.00	86.63	0.02	5.30	0.06	33.86	0.290	7.34	2.77	0.106	1.05	24.56	1.47	1.66	0.091
1258A-11R-5, 135-145	II	98.65	98.35	0.01	4.14	0.00	40.07	0.360	9.17	3.35	0.086	1.26	19.55	1.84	1.85	0.092
1258A-12R-5, 140-150	II	108.30	108.69	0.02	4.15	0.02	40.69	0.325	8.38	2.56	0.077	1.01	19.47	1.91	1.94	0.106
1258A-13R-4, 140-150	II	116.40	117.01	0.02	5.86	0.16	32.14	0.259	6.63	2.49	0.132	1.02	27.62	1.32	1.11	0.101
1258B-14R-4, 140-150	II	133.80	134.22	0.05	6.32	0.14	31.80	0.204	5.15	1.64	0.076	0.83	29.47	1.10	0.83	0.082
1258B-18R-3, 140-150	II	170.90	171.49	0.04	6.63	0.22	31.54	0.173	4.47	1.48	0.061	0.86	30.94	0.83	0.42	0.069
1258A-17R-4, 140-150	II	154.95	176.79	0.03	6.37	0.20	30.78	0.236	5.76	2.05	0.062	0.98	29.77	0.99	0.67	0.073
1258A-20R-2, 140-150	II	181.00	204.43	0.04	6.45	0.21	32.53	0.205	4.95	1.65	0.079	0.86	30.17	0.96	0.59	0.091
1258A-22R-3, 140-150	II	201.50	224.93	0.02	6.47	0.14	29.64	0.247	6.21	2.22	0.072	0.94	30.19	0.92	0.64	0.073
1258A-24R-3, 139-150	II	220.69	244.12	0.13	7.23	0.23	24.27	0.249	6.10	1.88	0.103	0.85	33.71	0.80	0.68	0.078
1258A-26R-2, 140-150	II	238.50	260.95	0.02	5.00	0.14	34.53	0.381	9.63	3.41	0.055	1.31	23.44	1.23	1.00	0.103
1258A-28R-5, 145-150	II	262.35	284.80	0.01	8.57	0.11	16.91	0.174	4.52	1.58	0.079	0.85	40.13	0.72	0.50	0.057
1258A-30R-2, 140-150	II	277.10	299.47	0.02	7.10	0.20	24.22	0.249	6.46	2.31	0.039	1.08	33.23	1.03	0.77	0.068
1258A-32R-5, 140-150	II	300.90	324.11	0.03	8.21	0.19	18.84	0.191	4.80	1.96	0.051	0.87	38.20	0.82	0.66	0.051
1258B-33R-4, 140-150	II	307.00	329.81	0.01	5.47	0.05	33.10	0.343	8.56	3.18	0.028	1.46	25.52	1.19	1.09	0.079
1258B-36R-3, 90-100	III	334.00	346.81	0.03	4.99	0.18	43.12	0.236	5.60	1.94	0.014	1.13	23.28	0.99	0.82	0.089
1258A-35R-3, 140-150	III	326.80	349.67	0.21	6.97	0.15	25.90	0.209	5.02	1.93	0.048	0.95	32.80	0.86	0.65	0.060
1258A-37R-2, 145-150	III	344.65	367.52	0.06	5.05	0.22	44.26	0.199	4.67	1.46	0.017	0.93	23.47	0.94	0.65	0.067
1258A-39R-1, 63-73	III	361.53	382.27	0.27	4.76	0.01	40.07	0.298	7.24	2.45	0.036	1.29	22.28	1.15	1.00	0.113
1258B-39R-5, 135-150	III	366.35	384.10	0.25	4.68	0.18	40.25	0.307	7.48	2.52	0.031	1.36	22.04	1.11	1.07	0.103
1258B-43R-2, 110-120	III	390.40	412.51	0.52	4.12	0.10	49.73	0.214	5.05	2.00	0.012	1.08	19.18	0.98	0.73	0.140
1258B-45R-2, 75-85	IV	399.25	420.08	3.41	4.17	15.14	25.34	0.256	6.02	2.10	0.007	1.15	20.08	1.56	1.10	0.188
1258B-46R-1, 31-44	IV	403.41	425.47	4.67	2.87	12.03	36.30	0.384	6.69	3.72	0.019	1.01	13.89	1.67	1.00	0.119
1258B-51R-2, 20-29	IV	427.92	452.24	1.86	6.23	9.17	18.46	0.233	4.64	1.91	0.007	1.29	30.52	0.86	0.80	0.909
1258B-52R-2, 70-80	IV	433.71	458.03	1.70	6.92	9.68	14.22	0.182	4.04	1.55	0.000	1.04	34.02	0.77	0.62	0.982
1258B-54R-3, 0-10	IV	444.38	468.86	1.95	5.73	8.57	22.48	0.311	5.72	2.12	0.000	1.16	28.01	0.70	0.79	0.951
1258B-55R-3, 58-68	IV	448.27	475.13	3.03	2.42	5.69	43.41	0.631	9.16	4.46	0.005	1.05	13.45	0.65	1.17	1.741
1258C-30R-1, 112-122	V	462.52	495.02	3.29	1.53	4.53	44.37	0.710	15.28	6.12	0.013	1.78	7.24	1.00	1.45	0.083
1258C-34R-2, 135-150	V	483.55	516.05	3.34	1.73	2.65	44.41	0.669	14.78	7.75	0.010	1.86	7.99	1.07	1.44	0.073

Notes: *italic values* below detection limit.

Appendix A2.2 continued [part 3 of 5]

Hole, core, section, interval (cm)	Unit	Depth (mbsf)	Depth (mcd)	TS (%)	TIC (%)	TOC (%)	SiO ₂ (%)	TiO ₂ (%)	Al ₂ O ₃ (%)	Fe ₂ O ₃ (%)	MnO (%)	MgO (%)	CaO (%)	Na ₂ O (%)	K ₂ O (%)	P ₂ O ₅ (%)
207-																
1259A-1R-2, 105-110	I	2.55	2.55	0.04	10.12	0.18	7.15	0.083	2.20	0.92	0.015	0.73	47.72	0.66	0.28	0.220
1259A-2R-2, 145-150	I	11.75	11.75	0.03	10.14	0.06	7.59	0.096	2.43	0.91	0.044	0.71	47.62	0.61	0.28	0.153
1259A-3R-4, 145-150	I	24.25	24.25	0.02	10.15	0.35	7.12	0.096	2.41	0.83	0.013	0.72	47.87	0.61	0.28	0.122
1259A-5R-2, 145-150	II	39.35	39.35	0.02	10.54	0.26	5.20	0.077	1.96	0.97	0.012	0.66	49.58	0.63	0.24	0.071
1259A-6R-2, 145-150	II	48.45	48.45	0.04	10.14	0.36	7.18	0.114	2.36	1.16	0.044	0.77	47.75	0.69	0.28	0.070
1259A-7R-4, 145-150	II	60.55	60.55	0.03	10.09	0.01	8.03	0.105	2.84	0.99	0.037	0.71	46.70	0.68	0.33	0.084
1259A-8R-4, 145-150	II	69.75	69.75	0.01	9.74	0.10	9.89	0.115	3.21	1.43	0.055	0.83	44.72	0.68	0.31	0.084
1259A-9R-5, 145-150	II	80.35	80.35	0.03	9.24	0.06	12.11	0.147	3.82	1.42	0.053	0.81	43.01	0.73	0.36	0.089
1259A-10R-5, 140-150	II	90.00	90.00	0.01	9.32	0.17	11.34	0.145	3.74	1.31	0.043	0.76	43.69	0.76	0.45	0.073
1259A-12R-5, 140-150	II	109.40	109.40	0.06	10.35	0.35	5.81	0.061	1.65	0.61	0.003	0.61	49.07	0.80	0.33	0.118
1259A-14R-3, 140-150	II	125.70	125.70	0.02	9.45	0.22	10.73	0.138	3.09	1.47	0.035	0.76	43.55	0.66	0.35	0.219
1259A-16R-1, 140-150	II	142.00	142.00	0.02	10.10	0.20	9.13	0.062	1.54	0.57	0.017	0.59	47.46	0.66	0.33	0.078
1259A-18R-1, 135-145	II	161.15	161.15	0.03	9.37	0.16	13.90	0.079	2.07	0.81	0.010	0.62	43.77	0.58	0.16	0.078
1259A-20R-4, 130-140	II	185.00	185.00	0.03	10.09	0.11	10.17	0.047	1.29	0.51	0.014	0.58	47.10	0.61	0.23	0.065
1259A-22R-3, 140-150	II	202.90	202.90	0.00	9.53	0.12	13.19	0.076	1.98	0.73	0.017	0.59	44.55	0.75	0.28	0.086
1259A-24R-1, 132-142	II	219.12	219.12	0.02	9.37	0.11	15.67	0.044	1.16	0.49	0.007	0.52	43.60	0.57	0.17	0.099
1259A-26R-5, 140-150	II	244.30	244.30	0.01	10.21	0.09	10.10	0.036	0.96	0.38	0.023	0.56	47.49	0.67	0.15	0.054
1259A-29R-4, 140-150	II	271.70	271.70	0.02	8.94	0.15	17.18	0.078	1.99	0.78	0.034	0.66	41.78	0.71	0.16	0.069
1259A-32R-1, 133-143	II	296.03	296.03	0.01	8.15	0.19	18.44	0.160	3.76	1.75	0.064	1.00	38.27	1.01	0.72	0.150
1259A-34R-2, 140-150	II	316.92	316.77	0.02	5.88	0.05	30.68	0.258	6.57	2.57	0.033	0.94	27.56	1.61	1.28	0.126
1259A-36R-1, 140-150	II	334.70	335.30	0.01	7.34	0.17	25.52	0.162	4.18	1.83	0.063	0.88	34.34	0.98	0.50	0.096
1259A-38R-1, 140-150	II	354.00	354.83	0.03	6.79	0.10	28.20	0.202	5.09	2.06	0.054	0.98	31.63	1.09	0.58	0.090
1259A-40R-3, 90-100	III	375.70	374.85	0.05	6.42	0.19	31.65	0.201	4.92	1.85	0.061	0.86	30.08	0.96	0.47	0.074
1259A-43R-1, 140-150	III	402.10	403.27	0.03	5.41	0.09	34.67	0.291	7.25	2.50	0.067	1.03	25.37	1.43	0.98	0.078
1259A-45R-2, 140-150	III	422.90	424.38	0.01	6.68	0.12	26.91	0.254	6.30	2.38	0.080	0.99	31.23	1.28	0.85	0.121
1259A-48R-3, 138-150	III	453.18	453.19	0.01	9.21	0.25	13.48	0.129	3.27	1.14	0.051	0.71	43.40	0.74	0.48	0.044
1259A-50R-5, 137-149	III	475.06	475.59	0.07	7.55	0.12	21.88	0.218	5.38	1.62	0.024	1.00	35.32	1.00	0.85	0.091
1259A-52R-1, 103-117	III	488.33	490.08	0.07	4.72	0.22	46.46	0.181	4.34	1.17	0.000	0.87	22.37	1.26	0.71	0.093
1259C-16R-5, 137-150	IV	525.65	529.18	1.29	7.07	7.63	18.30	0.133	2.97	0.99	0.000	0.93	34.36	1.08	0.56	0.384
1259C-17R-1, 136-146	IV	529.26	532.38	2.10	6.18	10.12	20.81	0.152	3.83	1.24	0.000	0.80	29.42	1.40	0.57	0.063
1259C-18R-4, 140-150	IV	543.40	547.73	4.52	4.86	18.55	17.55	0.176	4.23	2.49	0.009	0.78	23.33	1.23	0.72	0.185
1259C-19R-2, 78-88	V	549.22	551.57	1.50	0.01	0.54	68.50	0.994	14.10	3.61	0.003	1.05	0.34	0.75	1.97	0.080
1259B-25R-1, 89-100	V	554.09	555.18	0.44	1.16	0.26	64.80	0.926	11.46	3.87	0.056	1.22	4.99	0.67	1.47	0.072

Notes: *italic values* below detection limit.

Appendix A2.2 continued [part 4 of 5]

Hole, core, section, interval (cm)	Unit	Depth (mbsf)	Depth (mcd)	TS (%)	TIC (%)	TOC (%)	SiO ₂ (%)	TiO ₂ (%)	Al ₂ O ₃ (%)	Fe ₂ O ₃ (%)	MnO (%)	MgO (%)	CaO (%)	Na ₂ O (%)	K ₂ O (%)	P ₂ O ₅ (%)
207-																
1260A-1R-1, 58-63	I	0.58	0.58	0.07	1.74	0.34	46.13	0.761	16.87	6.23	0.021	1.79	8.29	1.37	2.37	0.086
1260A-2R-1, 145-150	II	2.45	2.45	0.02	7.86	0.00	16.33	0.286	7.82	3.23	0.092	0.85	36.48	0.62	0.67	0.085
1260A-3R-1, 145-150	II	11.75	11.75	0.00	8.74	0.08	14.00	0.182	4.68	1.87	0.022	0.88	41.47	0.61	0.45	0.206
1260A-4R-3, 145-150	II	23.95	23.95	0.01	8.76	0.31	14.23	0.146	3.98	1.58	0.003	0.93	41.45	0.81	0.60	0.073
1260A-6R-5, 90-100	II	45.10	45.10	0.01	8.78	0.00	17.62	0.096	2.49	0.79	0.010	0.67	41.04	0.84	0.55	0.085
1260A-7R-5, 145-150	II	54.95	55.05	0.03	10.09	0.00	10.40	0.051	1.38	0.49	0.019	0.59	47.14	0.70	0.36	0.067
1260A-8R-5, 142-150	II	64.62	64.72	0.02	10.20	0.10	10.00	0.049	1.27	0.49	0.032	0.59	46.83	0.71	0.22	0.063
1260A-9R-5, 142-150	II	74.32	73.32	0.01	9.29	0.04	14.79	0.070	1.83	0.63	0.020	0.57	43.09	0.73	0.36	0.071
1260A-10R-5, 142-150	II	84.02	83.12	0.06	9.98	0.12	11.46	0.052	1.37	0.51	0.023	0.58	46.33	0.76	0.32	0.062
1260A-12R-4, 140-150	II	101.80	100.42	0.05	8.54	0.02	21.89	0.054	1.11	0.49	0.018	0.54	39.87	0.71	0.10	0.068
1260A-14R-6, 105-110	II	123.85	122.17	0.02	8.69	0.00	19.77	0.074	1.78	0.67	0.031	0.61	40.78	0.72	0.33	0.072
1260A-17R-1, 145-150	II	145.65	143.84	0.01	9.64	0.06	13.09	0.067	1.69	0.61	0.026	0.64	44.87	0.72	0.33	0.061
1260A-19R-5, 143-150	II	170.63	168.82	0.03	8.56	0.07	19.39	0.097	2.40	0.94	0.037	0.75	40.05	0.79	0.31	0.069
1260A-21R-1, 130-140	II	183.80	181.99	0.01	9.14	0.04	15.46	0.079	2.10	0.72	0.067	0.64	42.77	0.98	0.43	0.088
1260A-23R-2, 140-150	II	204.30	202.49	0.01	8.45	0.10	18.63	0.131	3.20	1.42	0.068	0.82	39.45	1.08	0.68	0.114
1260A-25R-2, 141-150	II	223.61	221.80	0.03	6.43	0.22	27.81	0.234	5.68	2.34	0.045	0.99	30.68	1.40	1.21	0.127
1260A-27R-4, 140-150	II	245.90	244.39	0.03	6.95	0.15	27.78	0.193	4.83	1.53	0.063	0.81	32.37	1.24	0.87	0.113
1260A-29R-3, 130-140	II	262.99	262.22	0.14	6.85	0.27	28.21	0.190	4.92	1.65	0.063	0.92	32.63	1.11	0.69	0.094
1260A-31R-4, 140-150	III	283.98	283.21	0.12	6.64	0.17	30.83	0.212	5.00	1.54	0.067	0.87	31.10	0.84	0.56	0.089
1260A-33R-3, 0-12	III	300.76	299.99	0.01	6.78	0.31	31.27	0.169	4.15	1.10	0.090	0.66	31.87	0.92	0.64	0.066
1260A-35R-1, 135-150	III	318.45	317.37	0.02	6.52	0.00	27.82	0.291	7.14	2.74	0.097	1.13	30.20	1.10	0.91	0.114
1260A-37R-3, 135-150	III	340.75	341.00	0.01	9.03	0.18	14.52	0.154	3.74	1.19	0.062	0.82	42.57	0.67	0.48	0.050
1260A-39R-4, 135-150	III	361.45	362.19	0.02	8.29	0.25	18.37	0.202	4.96	1.82	0.051	0.97	39.17	0.78	0.59	0.082
1260A-41R-1, 140-150	III	376.30	378.96	0.29	5.01	0.24	36.10	0.331	8.33	2.60	0.070	1.54	23.47	1.44	1.30	0.076
1260B-38R-5, 140-150	IV	451.36	455.43	0.80	10.25	2.85	5.24	0.080	1.48	0.87	0.000	0.78	47.80	0.35	0.24	0.440
1260B-40R-4, 140-150	IV	469.00	473.58	1.46	8.12	5.98	11.89	0.177	3.39	1.70	0.000	0.70	39.12	0.60	0.46	0.479
1260A-54R-2, 110-120	V	490.50	492.98	1.87	1.02	0.55	71.10	1.007	6.77	3.55	0.013	0.54	4.65	0.52	0.94	0.074
1260B-46R-3, 140-150	V	505.90	508.58	1.71	0.84	0.65	68.28	1.060	8.78	3.97	0.014	0.60	3.87	0.57	1.09	0.075

Notes: *italic values* below detection limit.

Appendix A2.2 continued [part 5 of 5]

Hole, core, section, interval (cm)	Unit	Depth (mbsf)	Depth (mcd)	TS (%)	TIC (%)	TOC (%)	SiO ₂ (%)	TiO ₂ (%)	Al ₂ O ₃ (%)	Fe ₂ O ₃ (%)	MnO (%)	MgO (%)	CaO (%)	Na ₂ O (%)	K ₂ O (%)	P ₂ O ₅ (%)
207-																
1261A-1R-2, 145-150	I	2.95	2.95	0.07	2.91	0.34	40.50	0.667	15.27	5.36	0.025	1.51	13.36	0.87	1.88	0.086
1261A-3R-1, 134-139	I	14.54	14.54	0.07	1.74	0.16	46.43	0.720	17.80	5.77	0.065	1.82	8.06	1.05	2.60	0.107
1261A-4R-1, 145-150	I	71.15	71.15	0.13	1.06	0.28	49.69	0.792	19.04	6.41	0.076	2.00	4.77	1.19	2.82	0.098
1261A-5R-4, 140-150	I	137.30	137.30	0.18	2.19	0.19	44.01	0.721	17.15	6.14	0.101	1.87	9.80	1.03	2.71	0.120
1261A-6R-5, 140-151	I	196.50	196.50	0.12	2.32	0.12	43.87	0.739	16.53	5.58	0.085	1.71	10.76	1.07	2.45	0.123
1261A-7R-3, 140-150	I	241.30	241.30	0.04	2.12	0.14	44.65	0.755	17.39	6.01	0.132	1.89	9.58	1.15	2.68	0.141
1261A-8R-3, 140-150	I	250.90	250.90	0.17	2.08	0.16	43.86	0.732	17.80	6.13	0.107	1.85	9.49	1.13	2.63	0.120
1261A-10R-3, 140-150	I	270.20	270.20	0.05	3.45	0.10	37.33	0.627	15.54	5.41	0.136	1.57	15.53	0.96	2.17	0.152
1261A-12R-5, 0-10	I	291.10	291.10	0.04	3.68	0.11	35.92	0.619	15.88	5.83	0.234	1.61	15.95	0.93	1.95	0.144
1261A-14R-6, 90-100	I	312.80	312.80	0.23	3.54	0.17	23.20	0.391	9.53	3.60	0.069	1.06	9.39	0.47	1.21	0.074
1261A-16R-3, 140-150	I	328.00	328.00	0.02	7.02	0.15	21.17	0.364	8.46	2.81	0.025	1.06	32.88	0.85	0.62	0.108
1261A-18R-5, 139-150	I	350.29	350.29	0.05	4.65	0.16	32.20	0.524	13.56	4.25	0.106	1.34	21.63	0.82	1.77	0.127
1261A-20R-6, 130-140	II	370.90	370.90	0.01	9.16	0.05	13.50	0.110	2.79	1.16	0.012	0.79	42.88	1.10	0.35	0.085
1261A-22R-3, 46-61	II	384.86	384.86	0.01	9.91	0.00	11.51	0.066	1.72	0.60	0.012	0.58	45.59	0.69	0.25	0.110
1261A-25R-4, 0-7	II	414.64	414.64	0.01	9.51	0.04	14.28	0.061	1.59	0.57	0.018	0.58	44.81	0.68	0.22	0.083
1261A-28R-3, 138-150	II	442.98	442.98	0.01	8.88	0.00	19.53	0.072	1.80	0.66	0.027	0.58	41.30	0.80	0.30	0.069
1261A-32R-5, 140-150	II	484.60	484.60	0.02	7.18	0.05	26.87	0.196	4.91	1.68	0.049	0.88	33.62	1.06	0.71	0.104
1261A-35R-5, 0-15	III	512.10	512.10	0.19	4.79	0.19	37.51	0.361	8.73	3.37	0.059	1.36	22.55	1.44	1.06	0.184
1261A-37R-1, 135-150	III	526.65	526.65	0.06	7.10	0.03	25.06	0.230	5.85	2.07	0.065	0.94	33.46	1.23	0.78	0.231
1261A-39R-1, 135-150	III	545.95	545.95	0.23	8.20	0.20	18.37	0.189	4.70	1.39	0.029	0.99	38.56	0.96	0.66	0.089
1261A-45R-3, 136-152	IV	606.34	606.31	2.00	6.13	9.37	21.26	0.154	3.82	1.16	0.000	0.80	29.59	1.31	0.61	0.548
1261B-11R-2, 147-157	IV	619.37	612.38	2.46	5.81	10.89	22.32	0.159	3.91	1.34	0.000	0.81	27.51	1.22	0.57	0.076
1261A-48R-5, 136-150	IV	638.31	635.37	3.26	4.42	11.98	30.24	0.188	4.49	2.19	0.000	0.67	21.57	1.48	0.71	0.348
1261B-14R-2, 130-140	IV	648.00	647.25	2.22	6.39	9.21	16.24	0.195	4.38	1.78	0.000	1.04	32.42	1.05	0.66	1.570

Notes: *italic values* below detection limit.

Appendix A2.3 Trace element concentrations in sediments of Demerara Rise using pore water squeezing residues.

Hole, core, section, interval (cm)	Unit	Depth		As (ppm)	Ba (ppm)	Co (ppm)	Cr (ppm)	Cu (ppm)	Mo (ppm)	Ni (ppm)	Pb (ppm)	Rb (ppm)	Sr (ppm)	U (ppm)	V (ppm)	Y (ppm)	Zn (ppm)	Zr (ppm)
		(mbsf)	(mcd)															
207-	I	1.45	1.45	5	298	9	71	24	1	27	19	129	345	3	131	18	101	105
1257A-1H-1, 145-150	II	8.55	8.55	2	577	5	28	17	0	22	2	28	1152	2	37	11	28	39
1257A-2H-4, 145-150	II	18.05	18.05	3	366	3	20	12	0	13	2	19	1028	1	25	10	31	32
1257A-3H-4, 145-150	II	26.05	26.05	3	377	5	17	22	0	16	1	21	1083	0	78	11	33	29
1257A-4H-3, 145-150	II	35.55	35.55	2	523	7	30	27	0	23	5	30	1057	1	78	12	45	51
1257A-5H-3, 145-150	II	45.05	45.05	1	466	1	11	6	0	2	0	8	872	1	15	6	28	15
1257A-6X-3, 145-150	II	49.35	49.35	1	405	2	14	7	0	4	0	10	826	2	12	6	16	14
1257A-7X-3, 145-150	II	52.75	56.12	1	499	2	14	13	0	8	1	14	974	0	18	10	26	23
1257B-3R-2, 145-150	II	58.55	58.55	1	740	2	13	16	0	5	0	11	720	2	18	7	23	17
1257B-4R-3, 143-150	II	63.82	70.93	1	1617	5	19	17	0	17	6	21	696	2	60	11	36	29
1257B-5R-4, 42-49	II	73.65	76.70	1	1165	4	27	13	0	18	4	27	862	1	55	12	49	36
1257B-7R-2, 143-150	III	91.23	95.60	1	1084	4	34	15	0	21	5	25	956	3	56	12	43	40
1257B-8R-4, 142-150	III	103.79	107.22	1	782	5	30	21	0	15	9	36	960	3	66	12	33	45
1257B-9R-3, 140-150	III	112.02	113.79	2	717	5	37	14	0	15	3	37	1048	2	71	14	46	50
1257A-14X-4, 140-150	III	117.70	117.70	2	1037	6	39	13	0	29	5	43	1012	2	65	13	59	53
1257B-10R-4, 140-150	III	123.10	125.68	1	822	4	39	13	0	19	5	43	1022	1	79	13	53	53
1257A-15X-5, 140-150	III	128.90	128.49	1	870	7	44	15	0	25	11	44	1036	2	88	12	67	56
1257B-11R-4, 140-150	III	132.70	135.28	2	960	9	56	27	0	37	8	60	804	1	104	15	91	67
1257B-12R-3, 140-150	III	140.60	143.27	1	863	6	45	30	0	33	8	47	964	1	77	16	69	59
1257B-13R-4, 140-150	III	151.70	154.90	1	969	5	35	17	0	18	3	39	889	2	35	13	42	51
1257C-8R-6, 90-100	III	157.50	159.95	1	2084	5	30	17	0	10	3	34	974	2	26	12	69	43
1257A-18X-4, 140-150	III	166.16	161.96	3	1413	10	49	43	0	32	7	53	862	2	48	15	68	66
1257C-9R-6, 51-61	III	166.15	168.56	1	294	4	35	23	0	11	4	33	670	3	30	17	25	50
1257C-10R-1, 140-150	III	169.80	172.21	2	535	5	65	23	0	17	8	59	712	2	55	24	61	99
1257C-12R-2, 90-100	IV	190.10	192.65	33	223	0	318	29	52	59	2	80	741	27	1075	45	494	32
1257C-13R-2, 140-150	IV	200.20	202.75	14	341	3	104	48	40	90	1	18	789	11	1015	16	1152	23
1257C-15R-3, 17-27	IV	218.98	221.53	23	169	5	134	54	48	103	5	22	855	19	1476	16	874	26
1257B-27R-3, 0-7	V	225.30	228.94	4	128	14	141	16	0	36	7	65	392	4	105	17	59	136
1257C-16R-6, 20-30	V	233.87	235.03	3	139	16	140	14	0	38	6	56	417	2	95	15	52	133
1257A-31X-1, 71-81	V	275.81	281.61	10	156	17	195	23	0	51	6	79	540	5	131	19	73	125

Notes: *italic values* below detection limit.

Appendix A2.3 continued [part 2 of 5]

Hole, core section, interval (cm)	Unit	Depth		As (ppm)	Ba (ppm)	Co (ppm)	Cr (ppm)	Cu (ppm)	Mo (ppm)	Ni (ppm)	Pb (ppm)	Rb (ppm)	Sr (ppm)	U (ppm)	V (ppm)	Y (ppm)	Zn (ppm)	Zr (ppm)
		(mbsf)	(mcd)															
207-																		
1258A-1R-1, 145-150	I	1.45	1.45	12	193	8	45	27	0	28	13	46	759	2	78	19	63	69
1258A-1R-2, 145-150	I	2.95	2.95	4	181	7	47	23	0	23	9	34	952	1	60	14	59	58
1258A-3R-4, 145-150	II	20.15	20.15	1	636	3	12	11	0	12	0	5	696	1	10	7	22	16
1258A-4R-4, 145-150	II	29.75	29.75	0	803	2	2	10	0	7	1	7	757	0	17	9	25	17
1258A-5R-3, 145-150	II	37.65	42.15	3	745	5	22	38	0	22	5	26	722	2	41	12	46	41
1258A-6R-4, 145-150	II	48.75	49.27	2	1068	11	34	29	1	38	8	42	548	3	60	14	71	65
1258A-7R-4, 145-150	II	58.15	59.14	3	1081	9	36	54	0	34	8	37	591	2	61	14	61	56
1258A-8R-4, 140-150	II	68.07	69.92	2	1123	4	24	21	0	34	7	28	654	2	78	15	40	46
1258A-9R-6, 140-150	II	80.80	81.05	2	1306	4	51	19	0	34	10	33	549	0	44	18	47	57
1258A-10R-3, 140-150	II	86.00	86.63	2	1159	7	36	28	0	28	8	35	643	1	84	17	58	58
1258A-11R-5, 135-145	II	98.65	98.35	2	1478	8	45	35	0	31	10	45	612	3	77	16	73	68
1258A-12R-5, 140-150	II	108.30	108.69	1	1259	5	37	21	1	23	10	40	645	3	59	17	52	63
1258A-13R-4, 140-150	II	116.40	117.01	2	1289	6	35	25	0	23	7	32	710	3	66	15	55	51
1258B-14R-4, 140-150	II	133.80	134.22	2	950	4	31	24	0	14	6	26	658	3	46	15	41	42
1258B-18R-3, 140-150	II	170.90	171.49	2	961	5	24	49	0	16	4	21	733	0	45	11	34	35
1258A-17R-4, 140-150	II	154.95	176.79	3	1061	3	36	21	0	18	3	26	720	1	63	12	44	40
1258A-20R-2, 140-150	II	181.00	204.43	1	1117	5	30	10	0	16	4	27	858	0	57	11	44	43
1258A-22R-3, 140-150	II	201.50	224.93	1	768	5	30	20	0	18	4	31	934	2	65	12	47	46
1258A-24R-3, 139-150	II	220.69	244.12	1	641	6	37	18	0	19	8	33	870	1	70	14	47	49
1258A-26R-2, 140-150	II	238.50	260.95	2	866	11	53	24	0	47	10	48	777	2	123	17	87	67
1258A-28R-5, 145-150	II	262.35	284.80	1	289	7	24	20	0	16	2	26	793	1	32	9	30	32
1258A-30R-2, 140-150	II	277.10	299.47	1	410	4	32	19	0	20	5	37	866	5	35	11	41	49
1258A-32R-5, 140-150	II	300.90	324.11	1	1580	2	27	29	0	16	3	33	613	1	32	12	34	39
1258B-33R-4, 140-150	II	307.00	329.81	1	168	6	48	25	0	33	6	59	715	3	51	15	59	67
1258B-36R-3, 90-100	III	334.00	346.81	2	148	5	42	11	0	14	3	44	653	2	37	15	31	55
1258A-35R-3, 140-150	III	326.80	349.67	1	11018	7	323	17	38	193	5	34	855	1	32	15	33	48
1258A-37R-2, 145-150	III	344.65	367.52	1	125	4	38	17	0	15	1	34	621	2	25	16	29	47
1258A-39R-1, 63-73	III	361.53	382.27	1	215	5	53	19	0	22	5	51	689	1	45	17	49	70
1258B-39R-5, 135-150	III	366.35	384.10	1	659	7	56	26	0	22	6	55	713	1	46	18	45	67
1258B-43R-2, 110-120	III	390.40	412.51	1	165	5	43	26	1	19	4	39	424	2	33	16	52	45
1258B-45R-2, 75-85	IV	399.25	420.08	24	477	8	127	93	149	211	9	37	768	16	211	13	1964	38
1258B-46R-1, 31-44	IV	403.41	425.47	31	701	15	78	84	23	108	7	29	769	7	319	14	99	36
1258B-51R-2, 20-29	IV	427.92	452.24	25	595	5	159	77	104	147	7	36	726	44	2039	22	705	38
1258B-52R-2, 70-80	IV	433.71	458.03	20	463	4	192	65	83	144	4	27	828	17	1778	16	532	35
1258B-54R-3, 0-10	IV	444.38	468.86	20	207	6	174	49	73	127	6	40	705	22	1584	22	405	78
1258B-55R-3, 58-68	IV	448.27	475.13	43	270	12	184	48	117	272	7	65	392	47	973	29	715	170
1258C-30R-1, 112-122	V	462.52	495.02	23	249	13	209	53	26	116	11	90	282	7	1101	13	608	101
1258C-34R-2, 135-150	V	483.55	516.05	7	247	16	186	37	0	60	11	88	341	2	169	17	151	130

Notes: *italic values below detection limit.*

Appendix A2.3 continued [part 3 of 5]

Hole, core, section, interval (cm)	Unit	Depth		As (ppm)	Ba (ppm)	Co (ppm)	Cr (ppm)	Cu (ppm)	Mo (ppm)	Ni (ppm)	Pb (ppm)	Rb (ppm)	Sr (ppm)	U (ppm)	V (ppm)	Y (ppm)	Zn (ppm)	Zr (ppm)
		(mbsf)	(mcd)															
207-																		
1259A-1R-2, 105-110	I	2.55	2.55	1	211	2	14	8	0	9	4	11	1108	0	12	9	23	23
1259A-2R-2, 145-150	I	11.75	11.75	1	218	3	15	22	0	12	1	11	890	1	19	10	26	26
1259A-3R-4, 145-150	I	24.25	24.25	1	343	2	16	12	0	8	1	13	1110	3	17	9	22	28
1259A-5R-2, 145-150	II	39.35	39.35	0	177	3	15	20	0	12	1	10	920	1	0	9	19	18
1259A-6R-2, 145-150	II	48.45	48.45	1	183	2	17	10	0	11	0	12	1052	3	28	9	23	22
1259A-7R-4, 145-150	II	60.55	60.55	0	256	2	14	17	0	10	4	14	1071	2	6	9	22	23
1259A-8R-4, 145-150	II	69.75	69.75	1	251	2	19	28	0	11	4	15	1248	2	20	8	19	26
1259A-9R-5, 145-150	II	80.35	80.35	1	369	6	21	11	0	13	3	21	1213	3	38	9	41	30
1259A-10R-5, 140-150	II	90.00	90.00	1	228	3	22	10	0	12	3	18	1268	3	33	9	30	30
1259A-12R-5, 140-150	II	109.40	109.40	1	216	2	13	17	0	6	1	11	1128	2	17	8	22	19
1259A-14R-3, 140-150	II	125.70	125.70	1	315	4	18	10	0	17	4	15	1078	0	26	14	31	37
1259A-16R-1, 140-150	II	142.00	142.00	1	245	1	17	6	0	7	1	10	846	1	15	6	16	18
1259A-18R-1, 135-145	II	161.15	161.15	1	366	3	14	6	0	7	0	10	864	1	17	7	13	18
1259A-20R-4, 130-140	II	185.00	185.00	1	459	2	8	13	0	4	1	7	818	1	14	6	58	16
1259A-22R-3, 140-150	II	202.90	202.90	1	472	2	10	12	0	10	1	9	893	0	12	8	18	18
1259A-24R-1, 132-142	II	219.12	219.12	1	361	0	8	7	0	4	0	8	634	2	5	8	14	13
1259A-26R-5, 140-150	II	244.30	244.30	1	369	1	7	5	0	2	0	4	713	2	3	7	14	11
1259A-29R-4, 140-150	II	271.70	271.70	1	715	4	11	8	0	12	2	7	708	1	13	8	19	19
1259A-32R-1, 133-143	II	296.03	296.03	0	677	3	16	12	0	17	7	19	784	2	25	15	38	38
1259A-34R-2, 140-150	II	316.92	316.77	2	1333	5	30	13	0	26	4	32	837	2	52	16	54	54
1259A-36R-1, 140-150	II	334.70	335.30	1	911	5	26	18	0	20	3	21	772	2	40	10	48	33
1259A-38R-1, 140-150	II	354.00	354.83	2	1115	7	29	13	0	28	3	26	839	1	47	11	52	40
1259A-40R-3, 90-100	III	375.70	374.85	9	1036	19	28	28	0	47	2	24	942	3	51	11	50	42
1259A-43R-1, 140-150	III	402.10	403.27	1	1018	21	40	28	0	52	4	40	1005	1	77	13	48	54
1259A-45R-2, 140-150	III	422.90	424.38	1	857	7	39	17	0	29	4	33	964	1	49	17	58	50
1259A-48R-3, 138-150	III	453.18	453.19	1	357	4	18	14	0	13	1	21	803	2	21	9	25	29
1259A-50R-5, 137-149	III	475.06	475.59	1	5268	6	26	16	0	20	3	38	807	1	34	13	34	50
1259A-52R-1, 103-117	III	488.33	490.08	1	168	0	34	20	0	11	2	34	676	4	34	14	45	49
1259C-16R-5, 137-150	IV	525.65	529.18	14	597	5	104	46	38	87	2	21	813	10	572	13	584	28
1259C-17R-1, 136-146	IV	529.26	532.38	19	832	3	58	34	87	155	3	21	924	11	942	6	294	23
1259C-18R-4, 140-150	IV	543.40	547.73	23	945	11	59	60	19	175	3	24	770	18	232	16	60	28
1259C-19R-2, 78-88	V	549.22	551.57	5	219	21	127	41	2	35	10	105	96	4	127	22	51	256
1259B-25R-1, 89-100	V	554.09	555.18	5	187	12	98	29	0	22	6	82	135	4	107	22	65	306

Notes: *italic values* below detection limit.

Appendix A2.3 continued [part 4 of 5]

Hole, core section, interval (cm)	Unit	Depth		As (ppm)	Ba (ppm)	Co (ppm)	Cr (ppm)	Cu (ppm)	Mo (ppm)	Ni (ppm)	Pb (ppm)	Rb (ppm)	Sr (ppm)	U (ppm)	V (ppm)	Y (ppm)	Zn (ppm)	Zr (ppm)
		(mbsf)	(mcd)															
207-	I	0.58	0.58	9	595	15	75	36	1	31	27	124	311	5	165	24	107	131
1260A-1R-1, 58-63	II	2.45	2.45	4	126	4	35	10	0	17	8	33	985	2	50	8	36	51
1260A-2R-1, 145-150	II	11.75	11.75	1	372	5	26	12	0	14	3	23	1129	3	37	13	33	43
1260A-3R-1, 145-150	II	23.95	23.95	2	281	2	25	14	0	15	2	24	1294	3	51	8	21	36
1260A-4R-3, 145-150	II	45.10	45.10	1	319	1	13	21	0	4	0	11	754	2	14	8	21	22
1260A-6R-5, 90-100	II	54.95	54.95	1	419	4	9	20	0	10	2	10	819	0	10	7	14	14
1260A-7R-5, 145-150	II	64.62	64.72	0	356	1	8	7	0	5	0	5	909	2	7	8	12	15
1260A-8R-5, 142-150	II	74.32	73.32	1	683	0	9	10	0	6	0	11	898	3	10	8	16	17
1260A-9R-5, 142-150	II	84.02	83.12	9	342	5	8	21	0	17	0	6	790	1	12	9	23	16
1260A-10R-5, 142-150	II	101.80	100.42	1	585	2	12	7	0	5	0	4	706	0	0	8	21	13
1260A-12R-4, 140-150	II	123.85	122.17	1	396	4	12	5	0	7	1	8	577	1	14	10	14	19
1260A-14R-6, 105-110	II	145.65	143.84	1	451	2	11	9	0	6	0	10	684	3	12	7	13	17
1260A-17R-1, 145-150	II	170.63	168.82	2	734	2	16	14	0	9	0	10	703	1	16	8	20	21
1260A-19R-5, 143-150	II	183.80	181.99	1	624	5	15	13	0	10	0	11	603	1	15	8	18	20
1260A-21R-1, 130-140	II	204.30	202.49	1	621	3	16	13	0	17	4	16	728	2	21	14	34	33
1260A-23R-2, 140-150	II	223.61	221.80	1	843	5	69	17	0	31	8	29	713	2	43	15	50	53
1260A-25R-2, 141-150	II	245.90	244.39	4	639	7	26	21	0	24	1	24	764	2	45	14	50	43
1260A-27R-4, 140-150	II	262.99	262.22	1	800	4	28	16	0	16	5	24	759	3	50	10	40	39
1260A-31R-4, 140-150	III	283.98	283.21	2	1288	3	27	14	0	17	3	28	808	2	50	14	38	45
1260A-29R-3, 130-140	III	300.76	299.99	2	93	1	26	52	0	4	1	21	889	2	39	11	18	37
1260A-33R-3, 0-12	III	318.45	317.37	1	2118	6	50	17	0	34	9	37	888	2	68	15	64	54
1260A-35R-1, 135-150	III	340.75	341.00	2	1479	3	19	21	0	12	1	23	804	3	26	9	24	31
1260A-39R-4, 135-150	III	361.45	362.19	1	123	3	26	12	2	17	2	29	695	1	33	13	66	41
1260A-41R-1, 140-150	III	376.30	378.96	3	82	6	53	17	0	25	5	59	919	2	41	14	54	71
1260B-38R-5, 140-150	IV	451.36	455.43	19	85	2	72	27	100	195	3	12	918	36	1081	13	743	18
1260B-40R-4, 140-150	IV	469.00	473.58	35	144	4	149	43	132	216	3	24	989	34	1758	16	798	44
1260A-54R-2, 110-120	V	490.50	492.98	8	200	8	148	14	1	20	4	51	211	3	81	20	32	457
1260B-46R-3, 140-150	V	505.90	508.58	9	209	14	358	15	28	152	8	60	183	3	105	22	39	375

Notes: *italic values* below detection limit.

Appendix A2.3 continued [part 5 of 5]

Hole, core, section, interval (cm)	Unit	Depth		As (ppm)	Ba (ppm)	Co (ppm)	Cr (ppm)	Cu (ppm)	Mo (ppm)	Ni (ppm)	Pb (ppm)	Rb (ppm)	Sr (ppm)	U (ppm)	V (ppm)	Y (ppm)	Zn (ppm)	Zr (ppm)
		(mbsf)	(mcd)															
207-																		
1261A-1R-2, 145-150	I	2.95	2.95	5	459	12	66	29	0	28	22	101	535	4	137	25	89	117
1261A-3R-1, 134-139	I	14.54	14.54	7	394	14	66	23	0	29	21	137	374	3	144	22	101	120
1261A-4R-1, 145-150	I	71.15	71.15	8	371	14	75	23	1	32	24	146	269	2	154	24	107	131
1261A-5R-4, 140-150	I	137.30	137.30	12	383	14	73	18	0	33	22	134	454	2	134	24	96	126
1261A-6R-5, 140-151	I	196.50	196.50	17	366	16	70	18	0	32	22	131	504	2	138	23	92	135
1261A-7R-3, 140-150	I	241.30	241.30	12	404	15	71	19	0	30	24	143	484	3	143	25	95	131
1261A-8R-3, 140-150	I	250.90	250.90	14	396	17	72	22	0	36	26	146	515	4	141	24	96	120
1261A-10R-3, 140-150	I	270.20	270.20	12	343	12	72	17	0	28	18	121	722	3	129	20	85	104
1261A-12R-5, 0-10	I	291.10	291.10	9	302	10	67	22	0	25	19	114	738	3	122	18	84	98
1261A-14R-6, 90-100	I	312.80	312.80	8	191	8	40	4	1	17	8	65	350	2	78	12	48	58
1261A-16R-3, 140-150	I	328.00	328.00	2	421	7	48	19	0	18	13	33	1120	2	57	15	55	72
1261A-18R-5, 139-150	I	350.29	350.29	6	316	11	61	20	0	26	17	95	872	2	106	18	67	85
1261A-20R-6, 130-140	II	370.90	370.90	0	491	3	19	9	0	7	2	14	951	4	17	8	18	28
1261A-22R-3, 46-61	II	384.86	384.86	0	449	2	11	8	0	4	2	9	871	2	12	8	15	19
1261A-25R-4, 0-7	II	414.64	414.64	0	503	2	8	8	0	9	0	7	625	0	9	7	16	17
1261A-28R-3, 138-150	II	442.98	442.98	1	962	2	11	14	0	6	2	9	793	1	11	9	20	19
1261A-32R-5, 140-150	II	484.60	484.60	1	1118	5	29	20	0	20	3	25	860	1	41	12	51	41
1261A-35R-5, 0-15	III	512.10	512.10	1	1158	7	44	30	0	34	8	47	901	3	80	23	94	72
1261A-37R-1, 135-150	III	526.65	526.65	1	1387	19	30	17	0	58	6	29	987	1	42	22	49	48
1261A-39R-1, 135-150	III	545.95	545.95	1	3776	5	31	18	0	15	4	28	871	1	26	10	26	41
1261A-45R-3, 136-152	IV	606.34	606.31	16	896	2	137	53	136	136	5	22	1047	15	1655	12	1037	28
1261B-11R-2, 147-157	IV	619.37	612.38	28	912	3	90	48	147	227	4	23	964	11	1355	4	937	27
1261A-48R-5, 136-150	IV	638.31	635.37	28	1178	9	51	51	55	190	4	25	897	18	559	19	165	35
1261B-14R-2, 130-140	IV	648.00	647.25	36	400	5	150	74	78	141	6	29	876	24	2054	15	1404	34

Notes: *italic values* below detection limit.

Appendix A2.4 Rare Earth Element (REE) concentrations in sediments of Demerara Rise (Site 1258) using pore water squeezing residues.

Hole, core, section, interval (cm)	Unit	Depth		La	Ce	Pr	Nd	Sm	Eu	Gd	Tb	Dv	Ho	Er	Tm	Yb	Lu
		(mbsf)	(mcd)	(ppm)	(ppm)	(ppm)	(ppm)	(ppm)	(ppm)	(ppm)	(ppm)	(ppm)	(ppm)	(ppm)	(ppm)	(ppm)	(ppm)
207-																	
1258A-1R-1, 145-150	I	1.45	1.45	24.63	45.35	5.86	21.34	4.18	0.92	3.90	0.57	3.20	0.63	1.76	0.24	1.60	0.24
1258A-1R-2, 145-150	I	2.95	2.95	19.46	37.48	4.62	16.54	3.15	0.66	2.71	0.40	2.29	0.45	1.28	0.16	1.24	0.16
1258A-3R-4, 145-150	II	20.15	20.15	7.28	7.87	1.53	5.94	1.18	0.31	1.22	0.19	1.04	0.21	0.56	0.06	0.55	0.07
1258A-4R-4, 145-150	II	29.75	29.75	8.31	10.40	1.76	7.28	1.43	0.36	1.36	0.21	1.22	0.25	0.67	0.07	0.71	0.09
1258A-5R-3, 145-150	II	37.65	42.15	16.26	25.97	3.61	13.33	2.64	0.61	2.56	0.38	2.15	0.44	1.22	0.17	1.19	0.17
1258A-6R-4, 145-150	II	48.75	49.27	19.58	37.08	4.44	15.83	3.02	0.66	2.75	0.42	2.39	0.48	1.33	0.18	1.29	0.18
1258A-7R-4, 145-150	II	58.15	59.14	20.23	38.82	4.55	16.45	3.07	0.69	2.82	0.44	2.44	0.49	1.36	0.18	1.33	0.18
1258A-8R-4, 140-150	II	68.07	69.92	17.70	32.18	3.93	14.66	2.79	0.61	2.57	0.39	2.30	0.46	1.28	0.17	1.21	0.17
1258A-9R-6, 140-150	II	80.80	81.05	21.43	43.23	5.06	17.71	3.39	0.77	3.29	0.49	2.80	0.56	1.52	0.21	1.50	0.22
1258A-10R-3, 140-150	II	86.00	86.63	20.82	41.10	4.81	17.97	3.36	0.72	3.12	0.47	2.74	0.56	1.63	0.21	1.59	0.22
1258A-11R-5, 135-145	II	98.65	98.35	24.50	50.31	5.58	20.23	3.72	0.82	3.38	0.50	2.98	0.58	1.64	0.22	1.56	0.23
1258A-12R-5, 140-150	II	108.30	108.69	21.58	43.68	4.91	17.85	3.35	0.74	3.20	0.48	2.76	0.54	1.55	0.21	1.48	0.21
1258A-13R-4, 140-150	II	116.40	117.01	18.57	35.46	4.26	15.19	2.96	0.67	2.74	0.41	2.31	0.47	1.27	0.17	1.23	0.17
1258B-14R-4, 140-150	II	133.80	134.22	15.59	27.49	3.37	12.56	2.42	0.53	2.23	0.35	1.93	0.41	1.16	0.15	1.10	0.15
1258B-18R-3, 140-150	II	170.90	171.49	14.40	25.99	3.21	12.11	2.21	0.49	2.05	0.30	1.73	0.35	0.95	0.12	0.94	0.13
1258A-17R-4, 140-150	II	154.95	176.79	12.53	21.28	2.74	10.15	1.98	0.45	1.88	0.27	1.55	0.32	0.85	0.11	0.83	0.11
1258A-20R-2, 140-150	II	181.00	204.43	12.33	22.07	2.76	10.86	2.16	0.48	1.98	0.30	1.79	0.37	1.05	0.12	1.08	0.14
1258A-22R-3, 140-150	II	201.50	224.93	14.67	26.77	3.37	12.16	2.31	0.52	2.21	0.33	1.90	0.40	1.07	0.15	1.09	0.15
1258A-24R-3, 139-150	II	220.69	244.12	16.14	29.98	3.57	13.42	2.57	0.57	2.37	0.37	2.16	0.45	1.23	0.17	1.25	0.18
1258A-26R-2, 140-150	II	238.50	260.95	24.97	46.44	6.28	22.37	4.32	0.97	4.03	0.59	3.25	0.64	1.74	0.23	1.60	0.23
1258A-28R-5, 145-150	II	262.35	284.80	13.09	23.05	2.80	10.35	1.99	0.44	1.81	0.27	1.55	0.31	0.84	0.11	0.84	0.12
1258A-30R-2, 140-150	II	277.10	299.47	17.14	30.76	3.88	14.10	2.55	0.57	2.34	0.34	1.97	0.39	1.05	0.14	1.00	0.13
1258A-32R-5, 140-150	II	300.90	324.11	15.86	29.79	3.53	12.35	2.32	0.51	2.08	0.33	1.92	0.39	1.04	0.14	1.06	0.15
1258B-33R-4, 140-150	II	307.00	329.81	22.90	45.20	5.35	19.33	3.52	0.76	3.09	0.46	2.57	0.51	1.38	0.19	1.30	0.19
1258B-36R-3, 90-100	III	334.00	346.81	18.46	32.35	3.94	14.84	2.73	0.58	2.48	0.38	2.17	0.46	1.29	0.18	1.32	0.20
1258A-35R-3, 140-150	III	326.80	349.67	16.73	29.39	3.53	12.60	2.39	0.43	2.16	0.34	1.97	0.41	1.14	0.15	1.12	0.17
1258A-37R-2, 145-150	III	344.65	367.52	17.56	30.22	3.69	13.27	2.35	0.54	2.32	0.36	2.13	0.46	1.31	0.18	1.31	0.19
1258A-39R-1, 63-73	III	361.53	382.27	20.10	34.78	4.51	16.24	3.14	0.67	2.86	0.44	2.61	0.55	1.65	0.21	1.61	0.22
1258B-39R-5, 135-150	III	366.35	384.10	21.36	37.30	4.66	16.49	3.06	0.68	2.82	0.44	2.55	0.53	1.55	0.21	1.43	0.21
1258B-43R-2, 110-120	III	390.40	412.51	18.47	30.07	3.91	15.25	2.80	0.62	2.62	0.39	2.30	0.49	1.48	0.18	1.39	0.19
1258B-45R-2, 75-85	IV	399.25	420.08	12.60	18.81	2.68	10.11	1.99	0.48	1.86	0.27	1.53	0.32	0.86	0.10	0.78	0.11
1258B-46R-1, 31-44	IV	403.41	425.47	11.11	18.02	2.89	10.81	2.43	0.64	2.47	0.38	2.21	0.44	1.17	0.15	1.05	0.14
1258B-51R-2, 20-29	IV	427.92	452.24	16.52	23.70	3.28	12.69	2.54	0.61	2.62	0.40	2.52	0.56	1.71	0.21	1.66	0.23
1258B-52R-2, 70-80	IV	433.71	458.03	13.26	19.50	2.70	10.20	2.03	0.50	1.96	0.30	1.79	0.40	1.14	0.15	1.14	0.17
1258B-54R-3, 0-10	IV	444.38	468.86	19.53	34.37	4.58	15.96	3.12	0.73	2.98	0.48	2.90	0.62	1.85	0.25	1.88	0.26
1258B-55R-3, 58-68	IV	448.27	475.13	30.68	57.54	6.86	25.52	4.96	1.18	4.79	0.77	4.58	0.96	2.82	0.40	2.70	0.41
1258C-50R-1, 112-122	V	462.52	495.02	19.24	40.08	4.95	17.46	3.58	0.83	2.98	0.48	2.46	0.48	1.36	0.18	1.34	0.19
1258C-34R-2, 135-150	V	483.55	516.05	29.74	56.82	6.65	23.21	4.30	0.97	3.71	0.56	3.25	0.65	1.86	0.27	1.88	0.28

3. Sulfur-iron-carbon geochemistry in sediments of the Demerara Rise

Michael E. Böttcher, Almut Hetzel, Hans-Jürgen Brumsack, Andrea Schipper

This chapter was published 2006 in Proceedings of the Ocean Drilling Program, Scientific Results, 207. Mosher, D.C., Erbacher, J., Malone, M.J. (Eds.), College Station, TX (Ocean Drilling Program), 1-23.

Abstract

The geochemical composition of sediments (squeeze cake samples) from five drill sites (Ocean Drilling Program Sites 1257 - 1261) on the Demerara Rise in the tropical Atlantic was determined, with special regard to a sequence of Cretaceous black shales. Sediments were analyzed for different iron (total, pyrite, Na dithionite, and HCl leachable) and sulfur (total, pyrite, acid volatile, and organic bound) fractions, in addition to total organic carbon (TOC) and total inorganic carbon. The relative abundance of highly reactive iron (FeHR/FeT) in the investigated black shale samples indicates that pyrite was formed both in the water column and the sediment. This corresponds to euxinic paleoenvironmental conditions, a situation similar to the modern deep Black Sea. This geochemical approach is independent of a possible minor contribution from ongoing sulfate reduction which is triggered by anaerobic methane oxidation above the black shale sequence. Pyrite sulfur in black shales makes up between 30% and 100% of total sulfur. In addition to fixation of sulfide with iron, organic matter (OM) acted as an important sulfur trap during early diagenesis, with organic sulfur composing between 5 and 10 atom% of TOC. The relative importance of OM sulfurization is increasing with its content.

Keywords: Ocean Drilling Program, JOIDES Resolution, Leg 207, Tropical Atlantic, microbial sulfate reduction, reactive iron, pyrite, organic sulfur, water column, sediment

Introduction

The paleo-environmental conditions during organic-matter rich black shale formation have been an important scientific issue in the field of global and regional biogeochemical element cycling for a considerable period of time (e.g., Gauthier, 1987; Arthur et al., 1988; Arthur and Sageman, 1994; Brumsack, 2006, and references therein) but still are far from being completely understood. A number of different geochemical approaches has been applied to approach these questions, including trace element, biomarker and stable isotope studies. As examples for more recent analogs for organic matter-rich sediment deposition the formation of sapropels in the Black Sea and the eastern Mediterranean has been investigated in detail (e.g., Brumsack, 1986; Calvert et al., 1996; Lyons, 1997; Arthur and Dean, 1998; Emeis et al., 2000; Rinna et al., 2002, Lourens et al., 2001; Brumsack and Wehausen, 1999; Böttcher et al., 2003).

Accumulation of organic matter in sediments is often associated with the enrichment of sulfur and iron. The systematics behind the combined (bio)geochemistry of sulfur, iron, and organic carbon have been evaluated for the modern Black Sea (e.g., Leventhal, 1983; Arthur and Dean, 1998; Canfield et al., 1996; Raiswell and Canfield, 1998; Anderson and Raiswell, 2004) and successfully applied by analogy to the ancient depositional environments of organic-matter-rich sediments (e.g., Dean and Arthur, 1989; Raiswell et al., 2001; Shen et al., 2003; Grice et al., 2005). Interpretation of ancient black shales is often complicated because of the modification by deeper burial and associated geochemical overprints. Close to the Earth's surface, modification of the geochemical composition of black shales can take place by weathering that may be induced by flow of rain and ground water (Petsch et al., 2000, 2001, 2005). Black shale sequences as well as corresponding pore water gradients obtained by deep sea drilling, on the other hand, have seldom been analyzed in a resolution sufficient for a detailed interpretation of past environmental change and possible diagenetic overprints. First analyses of pore waters associated with frequent sapropel layers from the Mediterranean gave no indication for a contribution of organic-matter-rich zones to the shapes of present pore water profiles (Böttcher et al., 1998, 2003). Widespread black shale formation took place during the global ocean anoxic events (OAEs) of the Cretaceous Period (e.g., Schlanger and Jenkyns, 1976; Jenkyns, 1980), the causes still being a matter of intense debate (e.g., Arthur and Sageman, 1994; Arthur et al., 1988; Brumsack, 1986; Sinninghe Damsté and Köster, 1998). In the present study, we carried out a detailed geochemical investigation on Cretaceous black shale samples from the southern North Atlantic not previously affected by surface weathering. Expanded, shallowly buried

Cretaceous sediments were recovered during Ocean Drilling Program (ODP) Leg 207 from the Demerara Rise off Surinam, South America, including multiple sequences of Cretaceous black shales. By means of a solid phase geochemical approach we aimed to characterize the sulfur-iron-carbon (S-Fe-C) systematics of these sediments and their use as indicators for the depositional paleo-environment. Results are compared to the composition of the overlying younger organic-poor sediments. This communication is accompanied by reports on the bulk inorganic geochemistry including trace element contents (Hetzel et al., 2006), a high-resolution geochemistry study of Cretaceous black shales (Hetzel et al., in prep.), and the biogeochemistry of stable sulfur and oxygen isotope fractionation in pore waters and authigenic sulfur phases (Böttcher et al., in prep.).

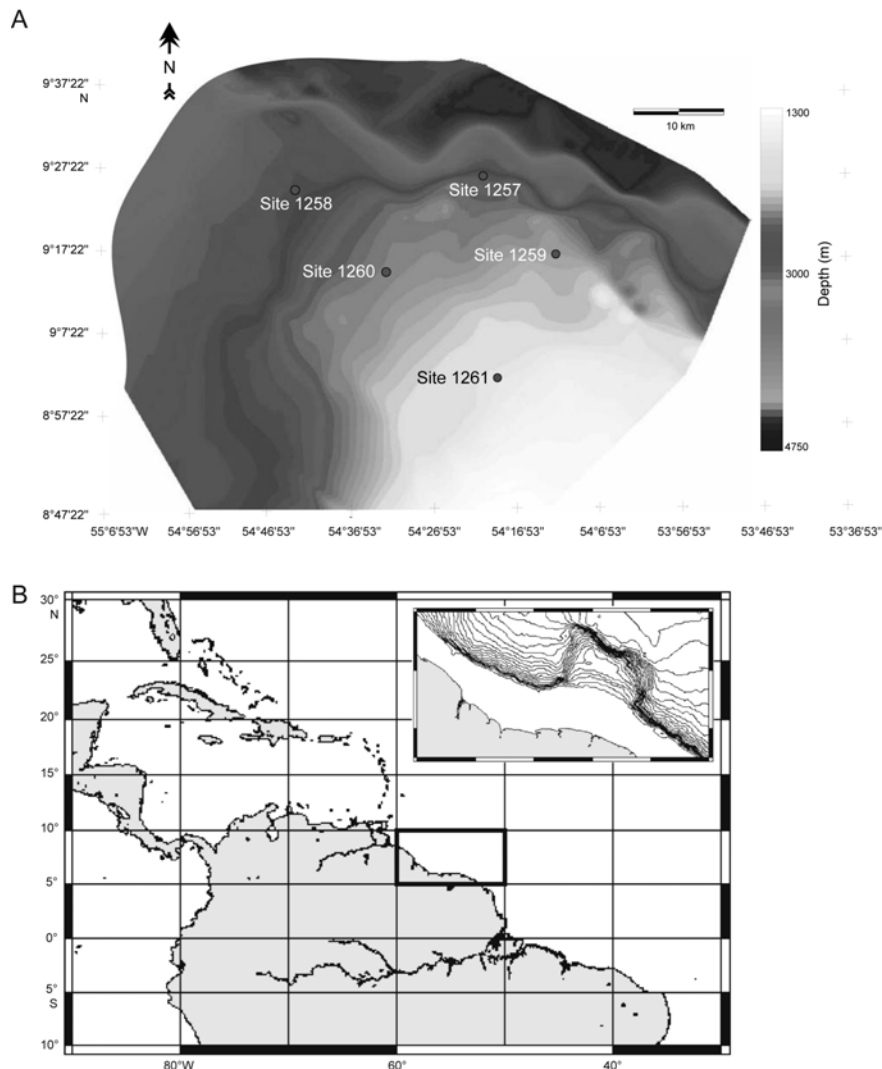


Figure 3.1 Positions of the investigated five sites cored during Leg 207 in the tropical Atlantic on the Demerara Rise, off Suriname. A. Map modified from Erbacher, Mosher, Malone, et al. (2004). B. Map was created using the Generic Mapping Tools (GMT) program (www.aquarius.geomar.de).

Material and Methods

During ODP Leg 207 sediments on the Demerara Rise were cored at ~9°N in the tropical Atlantic (Fig. 3.1; Table 3.1). The rise stretches ~380 km along the coast of Suriname and reaches a width of ~220 km from the shelf break to the northeastern escarpment, where water depths increase sharply from 1000 to >4500 m. Although most of the plateau lies in shallow water (700 m), the northwest margin is a gentle ramp that reaches water depths of 3000 to 4000 m. Nearly uniform, shallowly buried stratigraphically expanded sections of Cretaceous and Paleogene age exist with good stratigraphic control. Five drill sites (Sites 1257-1261) constitute a depth transect ranging in water depths from 1900 m to 3200 m (Fig. 3.1). The recovered sediments include multiple sequences of Cretaceous black shales (Erbacher, Mosher, Malone et al., 2004; Erbacher et al. 2005) pointing to varying levels of bottom water dysoxia and/or enhanced surface water productivity. Five units were identified: Unit I, consisting of modern, Pleistocene and Pliocene sediments; Unit II, of Oligocene and Eocene sediments; Unit III, of Late Paleocene to Campanian sediments; Unit IV, of Santonian to Cenomanian black shales; and Unit V, of Albian sediments.

Table 3.1 Drilling locations of ODP Leg 207 with geographical positions and water depths.

Site	Hole	Latitude	Longitude	Water depth (mbsl)
1257	A	9° 27.230'N	54° 20.518'W	2951.0
1257	B	9° 27.218'N	54° 20.508'W	2951.0
1257	C	9° 27.206'N	54° 20.495'W	2951.0
1258	A	9° 26.000'N	54° 43.999'W	3192.2
1258	B	9° 26.000'N	54° 43.982'W	3192.2
1258	C	9° 26.000'N	54° 43.966'W	3192.2
1259	A	9° 17.999'N	54° 11.998'W	2353.8
1259	B	9° 18.048'N	54° 11.945'W	2353.8
1259	C	9° 18.024'N	54° 11.969'W	2353.8
1260	A	9° 15.984'N	54° 32.633'W	2548.8
1260	B	9° 15.931'N	54° 32.652'W	2548.8
1261	A	9° 2.917'N	54° 19.038'W	1899.7
1261	B	9° 2.918'N	54° 19.049'W	1899.7

mbsl = meters below sealevel

Interstitial waters from 152 samples from Sites 1257 - 1261, covering a depth range from the sediment/seawater interface to 648 meters composite depth (mcd), were collected and processed using standard ODP methods. Interstitial water samples were squeezed from sediment samples immediately after retrieval of the cores using titanium squeezers, modified after the standard ODP stainless steel squeezer (Manheim and Sayles, 1974). Results for dissolved species relevant for the present study are summarized in Figure 3.2.

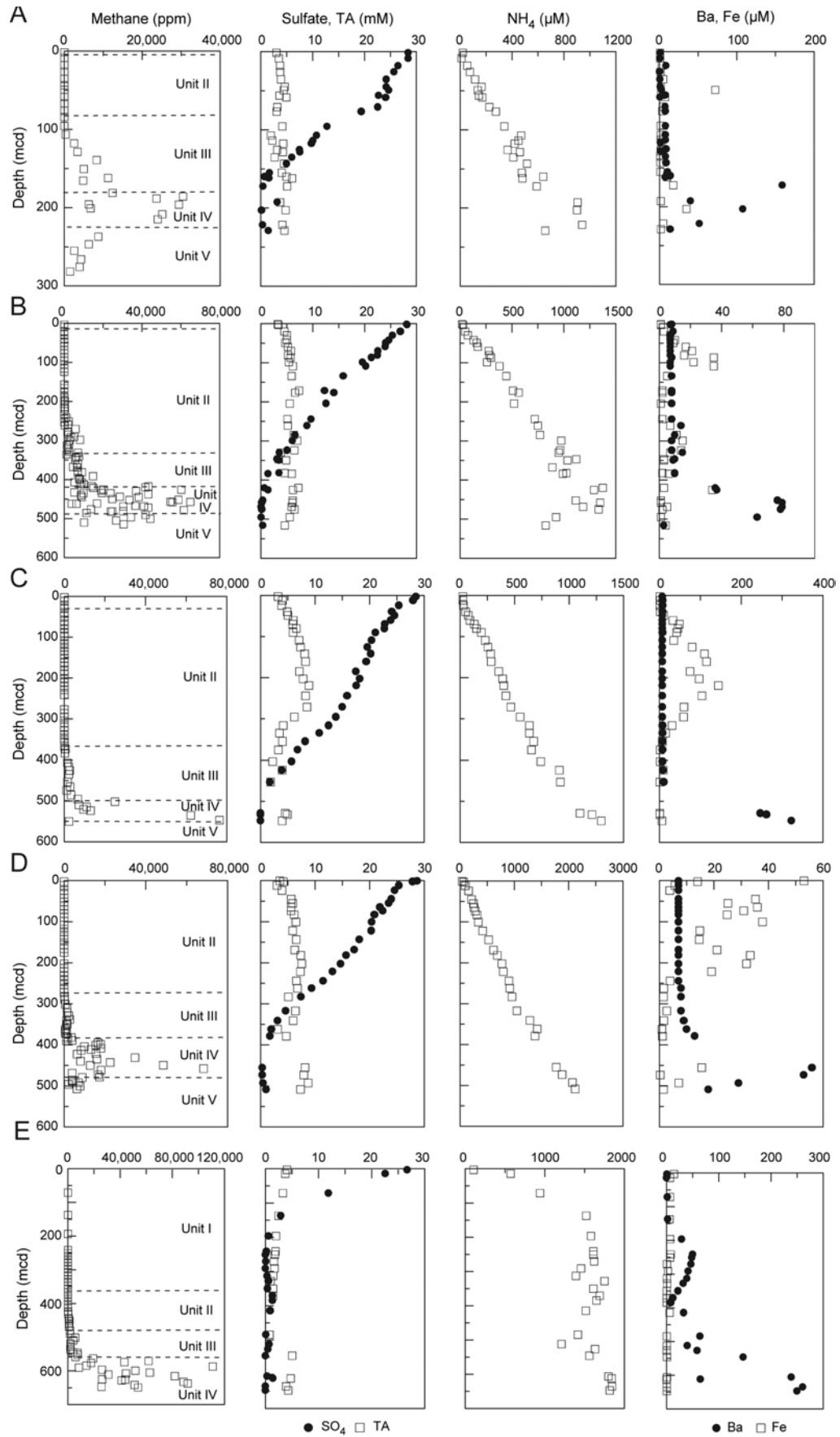


Figure 3.2 Onboard measurements of selected constituents in pore waters at Sites (A) 1257, (B) 1258, (C) 1259, (D) 1260, and (E) 1261 (from Erbacher, Mosher, Malone, et al. (2004) and ODP database). TA = total alkalinity.

On-board splits of all squeeze cakes were taken, freeze-dried and stored in poly-ethylene bags. In the shore-based laboratory the samples were ground and homogenized in an agate mill. X-ray fluorescence (XRF) analysis for main elements (Philips® PW 2400 X-ray spectrometer) using fused glass-beads were conducted as described by Schnetger et al. (2000). Detailed results are presented in Hetzel et al. (2006); the present communication only refers to the total iron (Fe_T) measurements. Total sulfur (S_T) and total carbon (TC) were analyzed using a LECO® SC-444 infrared-analyzer for squeeze cake-samples. Total inorganic carbon (TIC) was determined coulometrically using a UIC® CM 5012 CO_2 coulometer coupled to a CM 5130 acidification module. Total organic carbon (TOC) was calculated as the difference between TC and TIC (e.g., Prakash Babu et al., 1999). Different sedimentary sulfur fractions, acid volatile sulfur (S_{AVS}), chromium-reducible sulfur (S_P , essentially pyrite), organic matter (essentially kerogen)-bound organic sulfur (S_{ORG}), and residual sulfur (S_{RES}) were separated quantitatively on freeze-dried powdered samples. S_{AVS} was obtained via anaerobic distillation with 6M HCl (1 h). Because FeS is not expected to survive the diagenetic pyritization and laboratory-based freeze-drying process in the black shale samples, the S_{AVS} fraction is assumed to dominantly represent water-column derived ZnS and/or CuS (Brumsack, 1980). S_{AVS} contents (data not shown) in the investigated black shale samples are <270 mg/kg. These results will be discussed in the light of trace element enrichments in more detail in a latter contribution. Pyrite sulfur, S_P , was extracted via hot acidic $Cr(II)Cl_2$ (2 h) (Zhabina and Volkov, 1978; Canfield et al., 1986). Liberated H_2S was precipitated quantitatively in Zn acetate traps and measured spectrophotometrically (Cline, 1969). The residue was washed, dried and weighed and analyzed for the CNS contents via elemental analysis using a Fisons elemental analyzer. This fraction represents the sum of S_{ORG} and S_{RES} . The $Cr(II)$ residue was then tempered in a porcelain crucible for several hours at 550°C to remove organic matter, weighed and again analyzed for CNS (Böttcher and Schnetger, 2004). This fraction is considered to mainly represent residual barite sulfur. The S_{ORG-1} fraction was calculated from the difference of the two sulfur fractions. Additionally, the organic sulfur fraction was calculated from the difference of total sulfur and the sum of chromium-reducible sulfur and the sulfur content of the tempered Cr-residue according to $S_{ORG-2} = S_T - S_P - S_{RES}$. Organic sulfur results from both approaches agree well (Fig. 3.3).

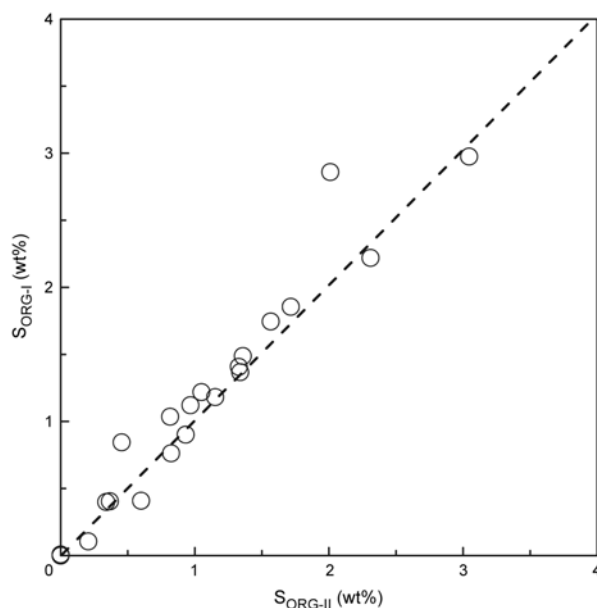


Figure 3.3 Comparison of the results of two analytical approaches to measure organic sulfur (S_{ORG}) contents in black shale samples (see "Materials and Methods").

Still-reactive iron (Fe_D) was extracted from sediment samples using a buffered solution of Na-dithionite (Canfield, 1989), which removes iron(oxyhydr)oxide phases (ferrihydrite, goethite, lepidocrocite, and hematite) but only small amounts of iron from silicates (Canfield, 1989; Haese, 2000). The iron concentration was determined spectrophotometrically (at 562 nm) with ferrozine in HEPES-buffer at pH 7 (Stookey, 1970). The amount of pyrite iron (Fe_P) was calculated from the content of pyrite sulfur, S_P . The highly reactive iron fraction Fe_{HR} is calculated as the sum of extractable and pyrite iron ($\text{Fe}_{\text{HR}} = \text{Fe}_D + \text{Fe}_P$). The range of geochemical results in the Fe-S-C system for Unit IV sediments is summarized in Table 3.2. Finally, the iron fraction extractable by cold 0.5M HCl (Fe_{HCl}) was determined in all samples (data not shown). Maximum dry weight contents of Fe_{HCl} are 140 mg/kg (Unit V, Site 1257), 70 mg/kg (Unit I, Site 1258), 199 mg/kg (Unit V, Site 1259), 83 mg/kg (Unit I, Site 1260), and 302 mg/kg (Unit I, Site 1261). Fe_{HCl} and Fe_D contents are positively correlated. Scanning electron microprobe analysis of gold-coated non-ground sediment samples was carried out using scanning electron microscopy (Hitachi S-3200N scanning electron microscope [SEM]).

Table 3.2 Range of geochemical parameters in the Fe-S-C system measured on squeeze cake samples of Unit IV sediments from ODP Leg 207.

Fe-S-C (wt%)	1257	1258	1259	1260	1261
TOC	3.5 - 7.7	5.7 - 15.1	7.6 - 18.6	2.7 - 6.0	9.2 - 12.0
TIC	5.3 - 6.3	2.4 - 6.9	4.9 - 7.1	8.1 - 10.4	4.4 - 6.4
Fe _T	0.6 - 4.6	1.1 - 3.1	0.7 - 1.7	0.6 - 1.2	0.8 - 1.5
Fe _P	0.4 - 1.4	0.5 - 2.3	0.4 - 1.2	0.4 - 0.9	0.6 - 1.3
Fe _{HR}	0.4 - 1.5	0.6 - 2.6	0.4 - 1.3	0.4 - 0.9	0.6 - 1.3
S _T	1.3 - 2.0	1.7 - 4.7	1.3 - 4.5	0.8 - 1.5	2.0 - 3.3
S _P	0.5 - 1.6	0.6 - 3.0	0.4 - 1.4	0.4 - 1.0	0.7 - 1.5
S _{ORG}	0.3 - 1.0	1.2 - 2.9	0.8 - 3.1	0.4 - 0.8	1.4 - 1.9

Fe_P was calculated from S_P measurements considering the stoichiometric composition of pyrite. Corresponding main, minor and trace elements are found in Hetzel et al. (2006). TOC = total organic carbon, TIC = total inorganic carbon, Fe_T = total iron, Fe_P = pyrite iron, Fe_{HR} = highly reactive iron, S_T = total sulfur, S_P = pyrite sulfur, S_{ORG} = organic matter (essentially kerogen)-bound organic sulfur.

Results and Discussion

Lithologic Units, Pore Waters, Sulfate Reduction, and Anaerobic Methane Oxidation

The depth profiles of the contents of different sedimentary carbon, sulfur, and iron fractions measured at all sites recovered during ODP Leg 207 are presented in Figure 3.4. The geochemical data demonstrate the occurrence of highly organic matter-rich (Cretaceous) black shales (Unit IV) with TOC contents up to 18 wt%. The black shales were deposited on synrift clastic sediments (Unit V). Units IV and V are overlain by organic-poor open-marine chalk and calcareous claystones (Units I - III) (Erbacher, Mosher, Malone, et al., 2004). Downcore variations of the pore water sulfate (Fig. 3.2) clearly indicate that deep-seated microbial sulfate reduction at slow rates is occurring in the sediments above Unit IV. Anaerobic oxidation of upward diffusing methane (AOM), which is derived from the black shale sequence, is the process associated with the microbial sulfate reduction process (Erbacher, Mosher, Malone, et al., 2004). AOM has been found to be carried out in marine sediments by a consortium of archaea and sulfate-reducing bacteria (Hoehler et al., 1994; Hinrichs et al., 1999; Boetius et al., 2000). The mechanistic, qualitative interpretations from the pore water profiles are additionally confirmed by quantitative modeling (Arndt et al., 2006). The reaction zone is currently positioned at Sites 1257 to 1260 above the black shale sequences and is triggered by a flux of biogenic methane from the organic-matter-rich shales, where it is produced by methanogenesis. At Site 1261, sulfate reduction already goes to completion within the upper 200 meters composite depth (mcd), indicating that organic matter degradation takes place in the rapidly deposited Pliocene nannofossil clay of

Unit I (Erbacher, Mosher, Malone, et al., 2004). Whereas, organic matter mineralization at depth is reflected by the continuous increase in ammonium concentrations, alkalinity data are partly superimposed by carbonate precipitation. Accumulation of dissolved barium concentrations in the pore waters (Fig.3.2) originates from the dissolution of biogenic barites and takes only place where pore water sulfate was completely exhausted. Enhanced dissolved iron concentrations, on the other hand, excludes significant sulfide concentrations.

Sedimentary Iron and Sulfur Species

The burial of organic matter in the black shale sequence is associated with an enrichment of all analyzed sulfur fractions: total, pyrite, and organic-bound sulfur (Fig. 3.4). This is due to the coupling of organic matter deposition to microbial sulfate reduction and the associated formation of sedimentary sulfur compounds. Dissimilatory sulfate reduction leads to the formation of hydrogen sulfide that may further react with reactive iron to precipitate iron sulfides (essentially pyrite, FeS_2) and with organic matter to form organic-sulfur compounds (e.g., Aizenshtat et al., 1983, 1995; Sinninghe Damsté and de Leeuw, 1990; Bein et al. 1990; Rullkötter, 2000; Werne et al., 2004). Other metal sulfides (e.g., ZnS) that may have been formed in a sulfidic paleo water-column (Brumsack, 1980), although found in investigated black shale samples (Hetzel, unpublished results), are quantitatively only of trace importance.

Reactive Iron Phases and Pyrite Formation

Pyrite typically occurs in marine sediments in framboidal and euhedral occurrence, depending on the physicochemical boundary conditions (Wilkin et al., 1996; Wang and Morse, 1996). As shown in Figure 3.5, framboidal pyrite was found in black shale samples from Site 1260. This occurrence is typical for pyrite that is formed in a euxinic water column or in the sediment closed to the sediment/water interface during early diagenesis (Wilkin et al., 1996). Besides sulfur, the iron contents are also enhanced in sediments of Unit IV (Fig. 3.4), in particular the Fe_P and Fe_D fractions. The only exception is Site 1261. The formation of pyrite is ultimately limited by the availability of iron minerals that are able to react with dissolved sulfide (Canfield, 1989). The amount of so-called highly reactive iron (Fe_HR) in marine sediments consists of the sum of the iron fraction that already reacted to pyrite (Fe_P) and sedimentary iron that is still able to react with sulfide. This still-reactive iron fraction (Fe_D) is extracted with buffered Na-dithionite solution (Canfield, 1989).

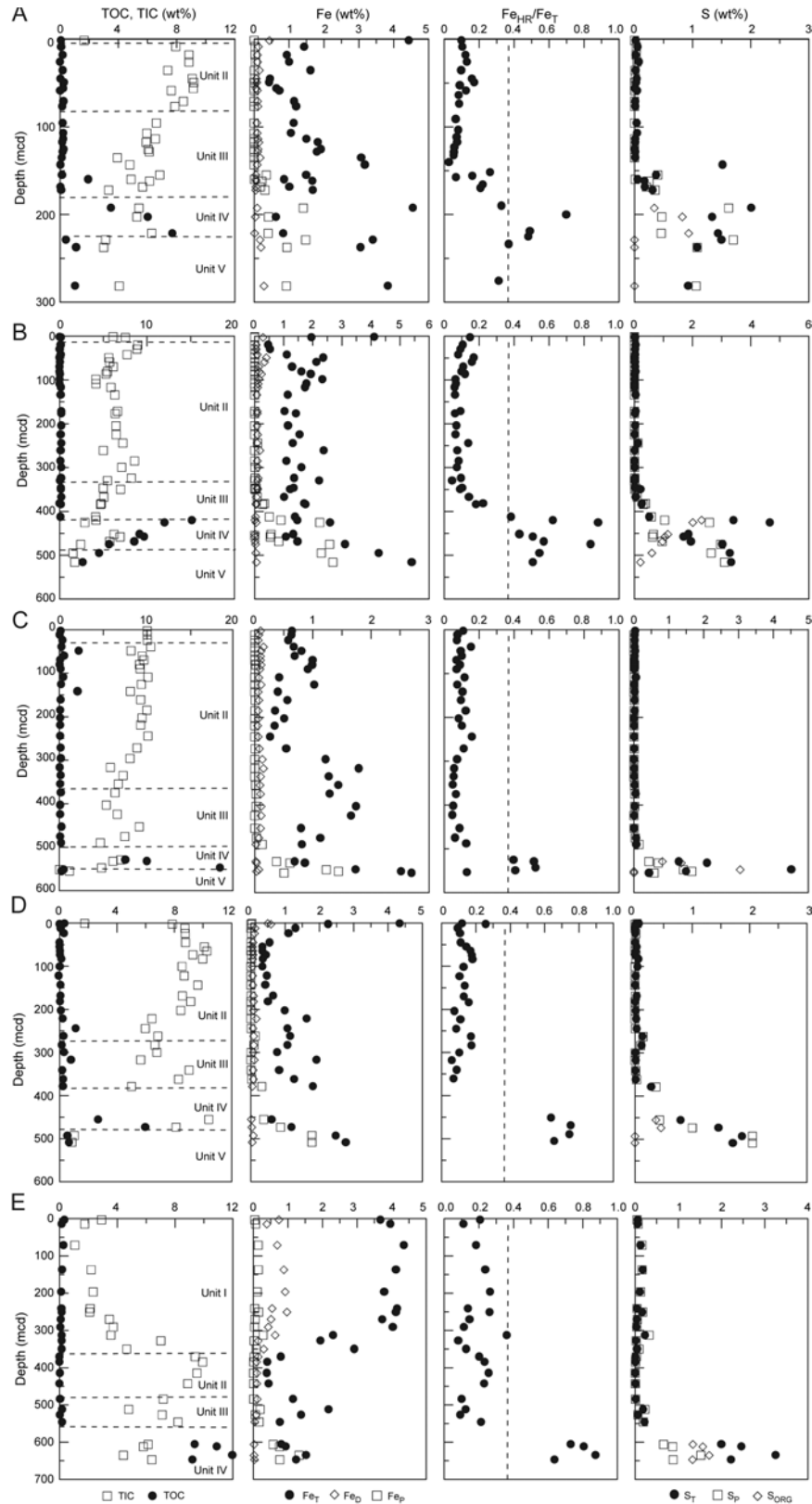


Figure 3.4 Downcore variations of selected geochemical parameters for Sites (A) 1257, (B) 1258, (C) 1259, (D) 1260, and (E) 1261. Definition of lithological units according to Erbacher, Mosher, Malone, et al. (2004). TOC = total organic carbon, TIC = total inorganic carbon, Fe_T = total iron, Fe_D = still-reactive iron, Fe_P = pyrite iron, S_T = total sulfur, S_P = pyrite sulfur, S_{ORG} = OM (essentially kerogen)-bound organic sulfur. Dashed line in the relative abundance of highly reactive iron (Fe_{HR}/Fe_T) plots indicates boundary to euxinic conditions (see "Reactive Iron Phases and Pyrite Formation").

The relationship between Fe_{HR} and total iron (Fe_{T}) has been shown to be indicative for the redox-conditions characterizing the sediment-forming environment, with $\text{Fe}_{\text{HR}}/\text{Fe}_{\text{T}}$ ratios below <0.38 in normal marine environments with oxic bottom waters (Raiswell and Canfield, 1998; Anderson and Raiswell, 2004). In euxinic systems, on the other hand, the clastic and reactive iron fluxes to the sediment may be decoupled, which may lead to $\text{Fe}_{\text{HR}}/\text{Fe}_{\text{T}}$ ratios >0.38 . This corresponds to an excess of reactive sedimentary sulfur in euxinic compared to oxic sediments. Below oxic bottom waters, pyrite formation takes place exclusively in the sediment. An additional fraction of iron sulfide may be formed in the water column of euxinic systems, as found in the modern Black Sea (Raiswell and Berner, 1985; Canfield et al., 1996). It has been shown for modern environments that the geochemical indicators in the iron-sulfur system, such as the $\text{Fe}_{\text{HR}}/\text{Fe}_{\text{T}}$ ratio and the degree of pyritization mostly lead to the same paleoredox-interpretations (e.g., Shen et al., 2003).

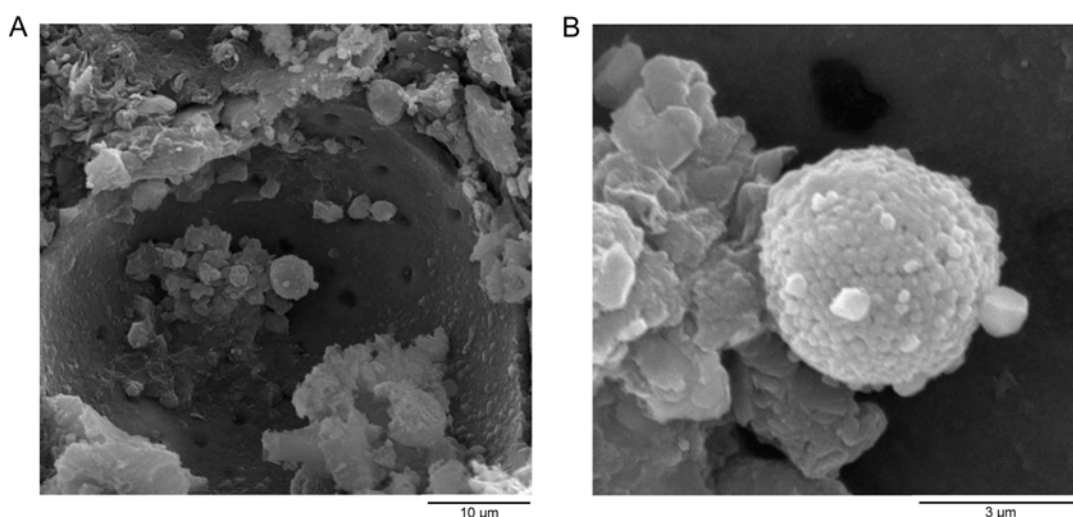


Figure 3.5 SEM photographs of framboidal pyrite found in a foraminifera shell in a black shale sample (Sample 207-1260B-40R-4, 140-150 cm). B is an extension from A.

The downcore variations of the relative fraction of highly reactive iron ($\text{Fe}_{\text{HR}}/\text{Fe}_{\text{T}}$) for the Leg 207 samples are presented in Figure 3.4. Reactive iron was enriched in virtually all black shale samples with $\text{Fe}_{\text{HR}}/\text{Fe}_{\text{T}}$ values >0.38 , indicating euxinic conditions during deposition of the organic-rich sediments of Unit IV (Fig. 3.4). Differences between the sites, as well as downcore variations of the relative enrichment of reactive iron indicate that environmental conditions and/or associated transport processes were not constant with time. Besides water column iron sulfide formation, the enrichment of reactive iron, requires also the presence of a paleo-shelf situation where an extended oxygen minimum zone led to the liberation of dissolved iron from shelf areas into a suboxic water column and, after further

transport, to the precipitation when reaching the sulfidic deeper waters (Canfield et al., 1996; Lyons, 1997; Wijsman et al., 2001; Anderson and Raiswell, 2004). Alternatively, such an enrichment may have been caused by a fluctuation of a chemocline on the shelf slope, leading to a pumping of dissolved iron into suboxic waters with subsequent fixation in areas of higher sulfide accumulation. The latter mechanism is similar to a model proposed by Lepland and Stevens (1998) for the formation of Mn(II)carbonates in an anoxic deep of the Baltic Sea. Additionally, an excess of Fe_{HR} is also found below the black shales in Unit V at Sites 1257, 1258 and 1260. In contrast, euxinic conditions were limited to Unit IV at Site 1259, based on the present sampling resolution. Besides an onset of euxinic conditions already occurring during clastic sediment deposition of Unit V, a later sulfidization of underlying sediments as described for sediments below sapropels of the Kau Basin (Middelburg, 1991), the Eastern Mediterranean (Passier and de Lange, 1998; Passier et al., 1996, 1997, 1999), the Baltic Sea (Böttcher and Lepland, 2000), or the Black Sea (Jørgensen et al., 2004) may also have caused this iron sulfide enrichment. A similar diagenetic sulfidization mechanism was identified in Mesoproterozoic marine sediments of the Belt Supergroup (Lyons et al., 2000).

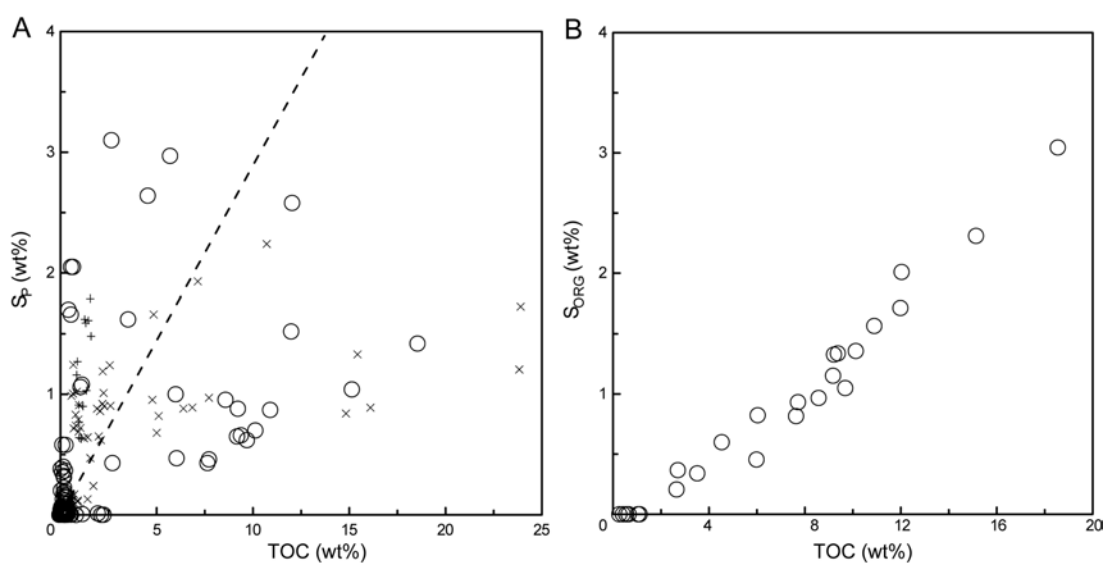


Figure 3.6 Covariation of (A) pyrite (S_P) and (B) organic sulfur (S_{ORG}) contents as a function of total organic carbon (TOC) contents. Dashed line marks the relationship derived for normal marine sediments as defined by Berner and Raiswell (1983). o = Leg 207, this study. x = data for Holocene and Pleistocene sediments from the Black Sea (Core BS4-14GC; Calvert et al., 1996; Core GeoB 7620-2, M. Böttcher and B. Jørgensen, unpubl. data). + = data for sapropelic sediments from the Mediterranean Sea (Böttcher et al., 2003).

$\text{Fe}_{\text{HR}}/\text{Fe}_{\text{T}}$ ratios in Units I to III are below the threshold value for euxinia indicating an essentially non-sulfidic water column during sediment formation. When the different sites are compared, however, it becomes obvious that reactive iron (Fe_{HR}) is relatively enriched in the sediments at Site 1261, which is positioned closest to the paleo-coastline and at the lowest paleo-water depth. An import of iron from shallower shelf sediments according to the (suboxic) oxygen minimum zone (OMZ) model is consistent with this observation.

The co-variation of pyrite sulfur, S_{P} , with TOC data is presented in a Berner-plot (Fig. 3.6) and compared to the relationship proposed for “normal marine sediments” (Berner and Raiswell, 1983). Only a few data points coincide with the relation found for clastic sediments below an oxic water column. A number of data points plot above the regression line, indicating an excess of sulfur that may coincide with a euxinic depositional environment (Leventhal, 1983; Raiswell and Berner, 1985). At highest TOC contents, however, most data show a relative excess of organic matter. This indicates a certain degree of iron limitation during black shale deposition (Leventhal, 1983) as also found for the Black Sea and Mediterranean sapropels (Fig. 3.6) or Albian black shales from the North Atlantic (Hofmann et al., 2000). Iron limitation upon black shale formation is also indicated from the sedimentary sulfur speciation (Fig. 3.4). Pyrite sulfur in the investigated black shale samples makes up between 30% and 100% of total sulfur, with a decrease of the relative importance with increasing organic matter content (Fig. 3.7). This indicates the importance of the balance between organic matter and the syngenetic metal flux to the surface sediments. Besides fixation of sulfide by the reaction with iron, organic matter (OM) acted as the second-important sulfur trap during early diagenesis.

Organic Sulfur Formation

Sulfur can react with organic matter via a number of different pathways, where sulfide and polysulfides are the most likely reaction partners (Aizenshtat et al., 1983, 1995). This requires a decreased availability of reactive iron and leads to a modification of reactivity of the remaining organic matter (Sinninghe Damsté and de Leeuw, 1990). Organic sulfur incorporation is found in the high-TOC black shale samples at all sites (Fig. 3.4). From the nearly linear variation of organic sulfur and organic carbon contents (Fig. 3.6), essentially constant atomic C/S ratios are obtained. Quantitatively, the samples with TOC contents exceeding ~2 wt% have up to 10 atom% organic sulfur. Most of the atomic S/C ratios fall in the range of 0.04 to 0.06. A similar linear relationship has been observed previously for Mediterranean sapropels by Passier et al. (1999). The fraction of S_{ORG} , however, is relatively more enriched in the Cretaceous black shale samples, probably due to a higher

abundance of reactive sulfur species or a higher reactivity of the organic matter towards sulfurization. From a comparison with literature data it is obvious that OM in the black shales is significantly enriched in sulfur when compared to marine planktonic material ($S/C \sim 0.008$) (Francois, 1987). This is due to the reaction of reduced sulfur species with organic matter upon early diagenesis (Aizenshtat et al., 1983, 1995; Bein et al., 1990; Raiswell et al., 1993; Sinnighe Damsté and de Leeuw, 1990; Passier et al., 1999; Werne et al., 2004). Stable sulfur isotope measurements have shown that the original seawater-derived sulfur in the organic matter was superimposed by the addition of diagenetic sulfur species (Bein et al., 1990; Passier et al., 1999). The relative importance of OM sulfurization compared to the bonding to pyrite increases with organic matter contents (Fig. 3.7). Deviations of atomic S/C ratios from the mean value of 0.056 ($TOC > 2$ wt%) may be caused by different extents of dissolved sulfur species availabilities and/or different sulfur sink capacities of organic matter. In Creaceous carbonates, Bein et al. (1990) observed maximum S/C ratios of up to 0.38. On the other hand, Jurassic black shales, anoxic Peru margin upwelling sediments, and Mediterranean sapropels had maximum S/C ratios of 0.019, 0.056, and 0.038, respectively (Raiswell et al., 1993; Mossmann et al., 1991; Passier et al., 1999).

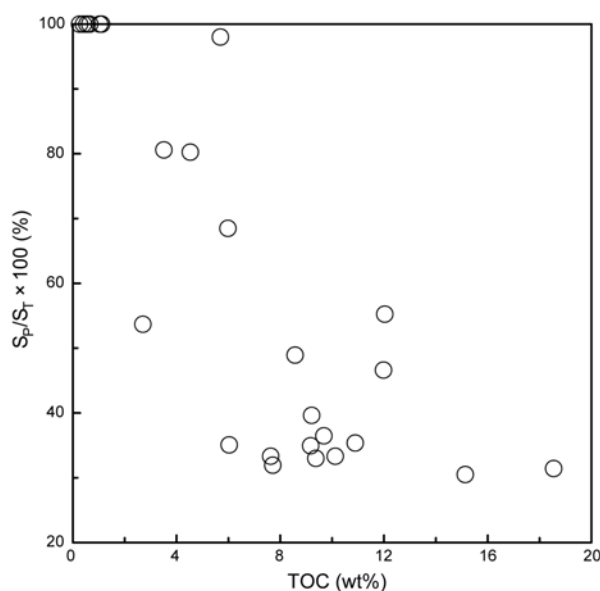


Figure 3.7 Covariation of the sulfur fraction in pyrite with total organic carbon (TOC) in black shale samples.

Conclusions

A detailed geochemical analysis of iron and sulfur speciation in sediments recovered during ODP Leg 207 on the Demerara Rise show that the paleo-environment was euxinic during Cretaceous black shale deposition with iron sulfides being formed in the sulfidic part of the water column and the sediment. This requires the transport of iron to the place of iron sulfide formation, for instance, via an intense but not sulfidic oxygen minimum zone. In addition, organic matter acted as an important early-diagenetic sink for dissolved reduced / intermediate sulfur species at (present) organic matter contents exceeding ~2 wt%. Results from the five different sites demonstrate that environmental redox conditions were not constant with time. A more detailed analysis of iron-sulfur speciation during black shale deposition at Sites 1258 and 1260 together with sulfur isotope partitioning between sulfur species is needed and is being currently being carried out to identify the frequency of changes in water column euxinia during black shale deposition with time in relation to the availability of iron.

Acknowledgements

We thank the scientific and technical crew of Leg 207 for support during onboard sampling, and R. Kort (ICBM Oldenburg) for technical support during SEM measurements. This research used samples and data provided by the Ocean Drilling Program (ODP). ODP is sponsored by the U.S. National Science Foundation (NSF) and participating countries under management of Joint Oceanographic Institutions (JOI), Inc. Research was funded by Deutsche Forschungsgemeinschaft (grants BO 1584/2-1,2 and BR 775/16-1,2 and 17-1,2), and Max Planck Society, Germany. Work on sediments from the Black Sea was funded by Deutsche Forschungsgemeinschaft to MEB and BBJ during DFG-SPP (RV METEOR cruise M51-4; grant JO 307/6-1). MEB wishes to thank E. Clapton, R. Gilbert, G. Harrison, and J. Lennon for their influence on the atmosphere during manuscript preparation. The manuscript is dedicated to E. Böttcher on the occasion of his 80th birthday. Constructive comments by editor M. Malone, reviewer T.J. Algeo, and an anonymous reviewer helped to improve the manuscript.

References

- Aizenshtat, Z., Krein, E., Vairavamurthy, M., Goldstein, T., 1995. Role of sulfur in the transformation of sedimentary organic matter: A mechanistic overview. *ACS Symposium Series* 612, 378-396.
- Aizenshtat, Z., Stoler, A., Cohen, Y., Nielsen, H., 1983. The geochemical sulphur enrichment of recent organic matter by polysulfides in the Solar Lake. In: Bjørøy, M., Albrecht, C., Cornford, C., de Groot, K., Eglinton, G., et al. (Eds.), *Advances in Organic Geochemistry*. Wiley, New York, 279-288.
- Anderson, T.F., Raiswell, R., 2004. Sources and mechanisms for the enrichment of highly reactive iron in euxinic Black Sea sediments. *American Journal of Science* 304, 203-233.
- Arndt, S., Brumsack, H.-J., Wirtz, K.W., 2006. Cretaceous black shales as active bioreactors: A biogeochemical model for the deep biosphere encountered during ODP Leg 207 (Demerara Rise). *Geochimica et Cosmochimica Acta* 70(2), 408-425.
- Arthur, M.A., Dean, W.E., 1998. Organic-matter production and preservation and evolution of anoxia in the Holocene Black Sea. *Paleoceanography* 13(4), 395-411.
- Arthur, M.A., Dean, W.E., Pratt, L.M., 1988. Geochemical and climatic effects of increased marine organic carbon burial at the Cenomanian/Turonian boundary. *Nature* 335(6192), 714-717.
- Arthur, M.A., Sageman, B.B., 1994. Marine black shales: Depositional mechanisms and environments of ancient deposits. *Annual Reviews of Earth and Planetary Sciences* 22, 499-551.
- Bein, A., Almogi-Labin, A., Sass, E., 1990. Sulfur sinks and organic carbon relationships in Cretaceous organic-rich carbonates: implications for evaluation of oxygen-poor depositional environments. *American Journal of Science* 290, 882-911.
- Berner, R.A., Raiswell, R., 1983. Burial of organic carbon and pyrite sulfur in sediments over Phanerozoic time: a new theory. *Geochimica et Cosmochimica Acta* 47(5), 855-862.
- Boetius, A., Ravensschlag, K., Schubert, C.J., Rickert, D., Widdel, F., Gieseke, A., Amann, R., Jørgensen, B.B., Witte, U., Pfannkuche, O., 2000. A marine microbial consortium apparently mediating the anaerobic oxidation of methane. *Nature* 407(7229), 623-625.
- Böning, P., Brumsack, H.-J., Böttcher, M.E., Schnetger, B., Kriete, C., Kallmeyer, J., Borchers, S.L., 2004. Geochemistry of Peruvian near-surface sediments. *Geochimica et Cosmochimica Acta* 68(21), 4429-4451.
- Böttcher, M.E., Brumsack, H.-J., de Lange, G.J., 1998. Sulfate reduction and related stable isotope (^{34}S , ^{18}O) variations in interstitial waters from the Eastern Mediterranean. In: Robertson, A.H.F., Emeis, K.-C., Richter, C., Camerlenghi, A. (Eds.), *Proceedings of the Ocean Drilling Program, Scientific Results*, 160. College Station, TX (Ocean Drilling Program), 365-373.
- Böttcher, M.E., Lepland, A., 2000. Biogeochemistry of sulfur in a sediment core from the West-Central Baltic Sea: Evidence from stable isotopes and pyrite textures. *Journal of Marine Systems* 25(3-4), 299-312.
- Böttcher, M.E., Rinna, J., Warning, B., Wehausen, R., Howell, M.W., Schnetger, B., Stein, R., Brumsack, H.-J., Rullkötter, J., 2003. Geochemistry of sediments from the connection between the western and eastern Mediterranean Sea (Strait of Sicily, ODP Site 963). *Palaeogeography, Palaeoclimatology, Palaeoecology* 190, 165-194.
- Böttcher, M.E., Schnetger, B., 2004. Direct measurement of the content and isotopic composition of sulfur in black shales by means of combustion-isotope-ratio-monitoring mass spectrometry (C-irmMS). In: de Groot, P. (Ed.), *Handbook of Stable Isotope Analytical Techniques*. Elsevier, Amsterdam, 597-603.

- Brumsack, H.-J., 1980. Geochemistry of Cretaceous black shales from the Atlantic Ocean (DSDP Legs 11, 14, 36, and 41). *Chemical Geology* 31, 1-25.
- Brumsack, H.-J., 1986. The inorganic geochemistry of Cretaceous black shales (DSDP Leg 41) in comparison to modern upwelling sediments from the Gulf of California. In: Summerhayes, C.P., Shackleton, N.J. (Eds.), *North Atlantic Paleocenography*. Geological Society, London. Special Publication 21, 447-462.
- Brumsack, H.-J., 2006. The trace metal content of recent organic carbon-rich sediments: implications for Cretaceous black shale formation. *Palaeogeography, Palaeoceanography, Palaeoecology* 232(2-4), 344-361.
- Brumsack, H.-J., Wehausen, R., 1999. A geochemical record of precession-induced cyclic eastern Mediterranean sedimentation: Implications for northern Sahara humidity during the Pliocene. *Naturwissenschaften* 86(6), 281-286.
- Calvert, S.E., Thode, H.G., Yeung, D., Karlin, R.E., 1996. A stable isotope study of pyrite formation in the Late Pleistocene and Holocene sediments of the Black Sea. *Geochimica et Cosmochimica Acta* 60(7), 1261-1270.
- Canfield, D.E., 1989. Reactive iron in marine sediments. *Geochimica et Cosmochimica Acta* 53(3), 619-632.
- Canfield, D.E., Lyons, T.W., Raiswell, R., 1996. A model for iron deposition to euxinic Black Sea sediments. *American Journal of Science* 296, 818-834.
- Canfield, D.E., Raiswell, R., Westrich, J.T., Reaves, C.M., Berner, R.A., 1986. The use of chromium reduction in the analysis of reduced inorganic sulfur in sediments and shale. *Chemical Geology* 54(1-2), 149-155.
- Dean, W.E., Arthur, M.A., 1989. Iron-sulfur-carbon-relationship in organic sequences, I. Cretaceous Western Interior Seaway. *American Journal of Science* 289, 708-743.
- Emeis, K.-C., Sakamoto, T., Wehausen, R., Brumsack, H.-J., 2000. The sapropel record of the Eastern Mediterranean Sea - Results of Ocean Drilling Program Leg 160. *Palaeogeography, Palaeoceanography, Palaeoecology* 158(3), 621-634.
- Erbacher, J., Friedrich, O., Wilson, P.A., Birch, H., Mutterlose, J., 2005. Stable organic carbon isotope stratigraphy across Oceanic Anoxic Event 2 of Demerara Rise, Western Tropical Atlantic. *Geochemistry, Geophysics, Geosystems* 6, Q06010.
- Francois, R., 1987. A study of sulfur enrichment in the humic fraction of marine sediments during early diagenesis. *Geochimica et Cosmochimica Acta* 51(1), 17-27.
- Gauthier, D.L., 1987. Isotopic composition of pyrite: relationship to organic matter type and iron availability in some North American Cretaceous shales. *Chemical Geology* 65, 293-303.
- Grice, K., Cao, C., Love, G.D., Böttcher, M.E., Twitchett, R.J., Grosjean, E., Summons, R.E., Turgeon, S.C., Dunning, W., Jin, Y., 2005. Photic zone euxinia during the Permian-Triassic superanoxic event. *Science* 307(5710), 706-709.
- Haese, R.R., 2000. The reactivity of iron. In: Schulz, H.D., Zabel, M. (Eds.), *Marine Geochemistry*. Springer, Berlin, 233-261.
- Hetzel, A., Brumsack, H.-J., Böttcher, M. E., Schmetger, B., 2006. Inorganic geochemical characterization of lithologic units recovered during ODP Leg 207 (Demerara Rise). In: Mosher, D.C., Erbacher, J., Malone, M.J. (Eds.), *Proceedings of the Ocean Drilling Program, Scientific Results, 207*. College Station, TX (Ocean Drilling Program), 1-37.
- Hinrichs, K.-U., Hayes, J.M., Sylva, S.P., Brewer, P.G., de Long, E.F., 1999. Methane consuming archaeobacteria in marine sediments. *Nature* 398(6730), 802-805.
- Hoehler, T.M., Alperin, M.J., Albert, D.B., Martens, C.S., 1994. Field and laboratory studies of methane oxidation in an anoxic sediment - evidence for methanogen-sulfate reducer consortium. *Global Biogeochemical Cycles* 8(4), 451-463.
- Hofmann, P., Ricken, W., Schwark, L., Leythäuser, D., 2000. Carbon-sulfur-iron relationships and $\delta^{13}\text{C}$ of organic matter for late Albian sedimentary rocks from the

- North Atlantic Ocean: paleoceanographic implications. *Palaeogeography, Palaeoceanography, Palaeoecology* 163(3), 97-113.
- Jenkyns, H. C., 1980. Cretaceous anoxic events: From continents to oceans. *Journal of the Geological Society* 137(3), 171-188.
- Lepland, A., Stevens, R.L., 1998. Manganese authigenesis in the Landsort Deep, Baltic Sea. *Marine Geology* 151(1), 1-15.
- Lourens, L.J., Wehausen, R., Brumsack, H.-J., 2001. Geological constraints on tidal dissipation and dynamical ellipticity of the Earth over the past three million years. *Nature* 409(6823), 1029-1033.
- Lyons, T.W., 1997. Sulfur isotopic trends and pathways of iron sulfide formation in upper Holocene sediments of the anoxic Black Sea. *Geochimica et Cosmochimica Acta* 61(16), 3367-3382.
- Lyons, T.W., Luepke, J.J., Schreiber, M.E., Zieg, G.A., 2000. Sulfur geochemical constraints on Mesoproterozoic restricted marine deposition: lower Belt Supergroup, northwestern United States. *Geochimica et Cosmochimica Acta* 64(3), 427-437.
- Manheim, F.T., Sayles, F.L., 1974. Composition and origin of interstitial waters of marine sediments, based on deep sea drill cores. In: Goldberg, E.D. (Ed.), *The Sea* (Vol. 5): *Marine Chemistry: The Sedimentary Cycle*. Wiley, New York, 527-568.
- Middelburg, J.J., 1991. Organic carbon, sulphur, and iron in recent semi-euxinic sediments of Kau Bay, Indonesia. *Geochimica et Cosmochimica Acta* 55(3), 815-828.
- Mossmann, J.R., Aplin, A.C., Curtis, C.D., Coleman, M.L., 1991. Geochemistry of inorganic and organic sulphur in organic-rich sediments from the Peru margin. *Geochimica et Cosmochimica Acta* 55(12), 3581-3595.
- Passier, H.F., Böttcher, M.E., de Lange, G.J., 1999. Sulfur enrichment in organic matter of eastern Mediterranean sapropels: a study of sulfur isotope partitioning. *Aquatic Geochemistry* 5(1), 99-118.
- Passier, H.F., de Lange, G.J., 1998. Sedimentary sulfur and iron chemistry in relation to the formation of Eastern Mediterranean sapropels. In: Robertson, A.H.F., Emeis, K.-C., Richter, C., Camerlenghi, A. (Eds.), *Proceedings of the Ocean Drilling Program, Scientific Results*, 160. College Station, TX (Ocean Drilling Program), 249-259.
- Passier, H.F., Middelburg, J.J., de Lange, G.J., Böttcher, M.E., 1997. Pyrite contents, microtextures and sulfur isotopes in relation to formation of the youngest Eastern Mediterranean sapropel. *Geology* 25(6), 519-522.
- Passier, H.F., Middelburg, J.J., van Os, B.J.H., de Lange, G.J., 1996. Diagenetic pyritization under eastern Mediterranean sapropels caused by downward sulphide diffusion. *Geochimica et Cosmochimica Acta* 60(1), 751-763.
- Petsch, S.T., Berner, R.A., Eglinton, T.I., 2000. A field study of the chemical weathering of ancient sedimentary organic matter. *Organic Geochemistry* 31(5), 475-487.
- Petsch, S.T., Edwards, K.J., Eglinton, T.I., 2005. Microbial transformations of organic matter in black shales and implications for global biogeochemical cycles. *Palaeogeography, Palaeoceanography, Palaeoecology* 219(1-2), 157-170.
- Petsch, S.T., Eglinton, T.I., Edwards, K.J., 2001. ^{14}C -dead living biomass: evidence for microbial assimilation of ancient organic carbon during shale weathering. *Science* 292(5519), 1127-1131.
- Prakash Babu, C., Brumsack, H.-J., Schnetger, B., 1999. Distribution of organic carbon in surface sediments along the eastern Arabian Sea: a revisit. *Marine Geology* 162(1), 91-103.
- Raiswell, R., Berner, R.A., 1985. Pyrite formation in euxinic and semi-euxinic sediments. *American Journal of Science* 285, 710-724.

- Raiswell, R., Bottrell, S.H., Al-Biatty, H.J., Tan, M.M., 1993. The influence of bottom water oxygenation and reactive iron content on sulfur incorporation into bitumens from Jurassic marine shales. *American Journal of Science* 293, 569-596.
- Raiswell, R., Canfield, D.E., 1998. Sources of iron for pyrite formation in marine sediments. *American Journal of Science* 298, 219-245.
- Raiswell, R., Newton R., Wignall, P.B., 2001. An indicator of water-column anoxia: resolution of biofacies variations in the Kimmeridge Clay (Upper Jurassic, UK). *Journal of Sedimentary Research* 71(2), 286-294.
- Rinna, J., Warning, B., Meyers, P.A., Brumsack, H.-J., Rullkötter, J., 2002. Combined organic and inorganic geochemical reconstruction of paleodepositional conditions of a Pliocene sapropel from the eastern Mediterranean Sea. *Geochimica et Cosmochimica Acta* 66(11), 1969-1986.
- Rullkötter, J., 2000. Organic matter: the driving force for early diagenesis. In Schulz, H.D., Zabel, M. (Eds.), *Marine Geochemistry*. Springer, Berlin, 129-172.
- Schlanger, S.O., Jenkyns, H.C., 1976. Cretaceous oceanic anoxic events: causes and consequences. *Geologie en Mijnbouw* 55, 179-184.
- Schnetger, B., Brumsack, H.-J., Schale, H., Hinrichs, J., Dittert, L., 2000. Geochemical characterization of deep-sea sediments from the Arabian Sea: a high-resolution study. *Deep Sea Research Part II: Topical Studies in Oceanography* 47(14), 2735-2768.
- Shen, Y., Knoll, A.H., Walter, M.R., 2003. Evidence for low sulphate and anoxia in a mid-Proterozoic marine basin. *Nature* 423(6940), 632-635.
- Shipboard Scientific Party, 2004. Leg 207 summary. In: Erbacher, J., Mosher, D.C., Malone, M.J., et al. (Eds.), *Proceedings of the Ocean Drilling Program, Initial Reports, 207*. College Station, TX (Ocean Drilling Program), 1-89.
- Sinninghe Damsté, J.S., de Leeuw, J.W., 1990. Analysis, structure and geochemical significance of organically-bound sulfur in the geosphere: State of the art and future research. *Organic Geochemistry* 16(4-6), 1077-1101.
- Sinninghe Damsté, J.S., Köster, J., 1998. A euxinic southern North Atlantic Ocean during the Cenomanian/Turonian oceanic anoxic event. *Earth and Planetary Science Letters* 158(3-4), 165-173.
- Stookey, L.L., 1970. Ferrozine - a new spectrophotometric reagent for iron. *Analytical Chemistry* 42(7), 779-781.
- Wang, Q., Morse, J.W., 1996. Pyrite formation under conditions approximating those in anoxic sediments - I. Pathways and morphology. *Marine Chemistry* 52(2), 99-121.
- Werne, J.P., Hollander, D.J., Lyons, T.W., Sinninghe Damsté, J.S., 2004. Organic sulfur biogeochemistry: recent advances and future research directions. In: Amend, J., Edwards, K., Lyons, T. (Eds.), *Sulfur Biogeochemistry: Past and Present*. Geological Society of America. Special Paper 379, 135-150.
- Wijsman, J.W.M., Middelburg, J.J., Heip, C.H.R., 2001. Reactive iron in Black Sea sediments: implications for iron cycling. *Marine Geology* 172(3-4), 167-180.
- Wilkin, R.T., Barnes, H.L., Brantley, S.L., 1996. The size distribution of framboidal pyrite in modern sediments: an indicator of redox conditions. *Geochimica et Cosmochimica Acta* 60(20), 3897-3912.
- Zhabina, N.N., Volkov, I.I., 1978. A method of determination of various sulfur compounds in sea sediments and rocks. In: Krumbein, W.E. (Ed.), *Environmental Biogeochemistry and Geomicrobiology (Vol. 3): Methods, Metals and Assessment*. Ann Arbor Science Publications, 735-745.

4. Paleo-redox conditions during OAE 2 reflected in Demerara Rise sediment geochemistry (ODP Leg 207)

Almut Hetzel, Michael E. Böttcher, Ulrich G. Wortmann, Hans-Jürgen Brumsack

This chapter was published 2009 in *Palaeogeography, Palaeoceanography, Palaeoecology* 273(3-4), 302-328.

Abstract

Cretaceous black shales deposited under severe oxygen-depletion are carriers of proxy signals for paleoenvironmental conditions. Using high-resolution patterns of iron and sulfur speciation, stable sulfur isotope discrimination, and trace element enrichment from black shale sequences of Sites 1258 and 1260 we identified alterations of the depositional environment during the Cenomanian/Turonian boundary Event (OAE 2) in the southern North-Atlantic (ODP Leg 207, Demerara Rise).

Changes in redox-conditions are suggested by high ratios of reactive to total iron which indicate that pyrite was formed both in the water column and within the sediment. This corresponds to euxinic paleoenvironmental conditions with at least temporarily free dissolved sulfide in the water column, a situation similar to the modern deep Black Sea. In addition, besides fixation of sulfide as iron sulfide, organic matter acted as an important sulfur trap during early diagenesis. Stable sulfur isotope fractionation went through a minimum within the OAE 2 interval indicating enhanced sulfur isotope discrimination during highest burial of organic matter (OM) potentially due to lower burial efficiency of reduced sulfur and/or a higher contributions from the oxidative part of the sulfur cycle (e.g., in the water column or the surface sediments). Elevated Fe/Al and Co/Al values within the Cenomanian/Turonian interval confirm euxinic conditions but, at the same time, require a zone where reducing but non-sulfidic conditions prevail, allowing reductive Fe and Co mobilization in oxygen-depleted nearshore sediments. The existence of an expanded oxygen-minimum-zone (OMZ) is demonstrated by extremely low Mn/Al ratios.

A change in the trace metal (TM) inventory of seawater is postulated from a decline in seawater derived TM enrichment. Because hypoxic or even euxinic environments form an important sink for TM, the enlargement of euxinic depositional areas at the global onset of

black shale deposition during OAE 2 have likely led to a drawdown of the seawater TM reservoir.

Keywords: Demerara Rise, Ocean Drilling Program, Leg 207, trace metals, Oceanic Anoxic Event 2, CTBE, paleoenvironment, pyrite, sulfur isotopes

Introduction

In the mid-Cretaceous, several distinct periods of organic-rich black shale deposition appear. The enhanced burial of organic carbon in marine sediments during these so called Oceanic Anoxic Events (OAEs; Schlanger and Jenkyns, 1976) is thought to arise either from enhanced bio-productivity or from intensified preservation of organic matter during anoxic conditions (e.g., Arthur et al., 1987, 1988; Schlanger et al., 1987). The Cenomanian-Turonian Boundary Event (CTBE = OAE 2; ca. 93.5 Ma) is one of the best studied global Oceanic Anoxic Events. It is characterized by a global organic carbon burial episode leading to a positive shift in $\delta^{13}\text{C}$ values of organic carbon and carbonate (e.g., Schlanger et al., 1987; Arthur et al., 1988; Gale et al., 1993; Erbacher et al., 2005). As the carbon cycle is tightly coupled to the sulfur cycle, perturbations in the global carbon cycle lead to changes in the seawater sulfur isotopic composition (e.g., Strauss, 1999; Paytan et al., 2004; Wortmann and Chernyavsky, 2007).

During Ocean Drilling Program (ODP) Leg 207, relatively expanded, shallowly buried Cretaceous sediments were recovered from Demerara Rise off Suriname, South America. CTBE black shales on Demerara Rise form part of a thick black shale succession encompassing the Albian to Santonian (Shipboard Scientific Party, 2004). This may be the result of both the paleogeographic setting of Demerara Rise (lacking significant ventilation of bottom-waters prior to the opening of the equatorial Atlantic gateway, which may have taken place in the Campanian; see Friedrich and Erbacher, 2006) and enhanced nutrient influx. The latter may have been evoked by terrestrial runoff and/or upwelling due to the proximal position of Demerara Rise to the South American landmass.

Cretaceous black shales deposited under severe oxygen-depletion are carriers of proxy signals for paleoenvironmental conditions like varying levels of bottom water dysoxia and/or enhanced surface water productivity. Changes in water column redox conditions lead to responses in the coupled biogeochemical sulfur-carbon-metal cycles and associated sedimentary signal formation. Therefore, distribution patterns of iron and sulfur speciation, sulfur isotope partitioning, and enrichments of redox-sensitive and sulfide forming trace metals provide important paleoenvironmental information on dynamics of biogeochemical element cycles and corresponding water column redox-conditions during black shale deposition. Excess iron contribution to selected Cretaceous Leg 207 black shales due to pyrite formation in a euxinic water column was shown by iron and sulfur speciation analyses, and enhanced organic matter sulfurization was shown to be caused by a limitation of reactive iron to form sulfide minerals (Böttcher et al., 2006).

High enrichments of redox-sensitive elements in organic carbon-rich sediments have been related to anoxic bottom waters. Under reducing conditions these metals may either be precipitated as sulfides, co-precipitated with iron sulfides or bound to organic matter (Brumsack, 1980; Jacobs et al., 1985, 1987; Brumsack, 1989; Breit and Wanty, 1991; Hatch and Leventhal, 1992; Calvert and Pedersen, 1993; Piper 1994; Nijenhuis et al., 1998). Based on the specific trace metal patterns of coastal upwelling areas and euxinic settings Brumsack (2006) discussed the enrichment of trace metals in Cretaceous black shales attempting to ascertain whether enhanced bio-productivity or widespread stagnation triggered black shale formation.

In the present study, we report on a high-resolution geochemical tracer record for black shale sequences of ODP Leg 207 Sites 1258 and 1260 using distribution patterns of trace element enrichment, iron and sulfur speciation, and stable sulfur isotope discrimination to identify changes in redox-conditions of the depositional environment during OAE 2.

Material and Methods

Site description

During ODP Leg 207, sediment cores were drilled on the Demerara Rise in the tropical North Atlantic (Fig. 4.1). The rise stretches ca. 380 km along the coast off Suriname and reaches a width of ca. 220 km from the shelf break to the northeastern escarpment, where water depths increase sharply from 1,000 to more than 4,500 m. While most of the plateau lies in shallow water (700 m), the northwest margin forms a gentle ramp reaching water depths of 3,000 to 4,000 m. The five drill sites (Sites 1257-1261) constitute a depth transect with water depths ranging from 1,900 to 3,200 m located within a tropical oxygen minimum zone that caused deposition of laminated organic-rich sediments of latest Albian to earliest Campanian age. Upper Cenomanian to Lower Turonian sediments on Demerara Rise are mainly expressed by distinctly laminated black shales with well-preserved fish debris and phosphatic nodules. Within this black shale sequence light-colored, laminated foraminiferal packstones and wackestones occur (Shipboard Scientific Party, 2004). A detailed sedimentological description is given by the Erbacher et al. (2004).

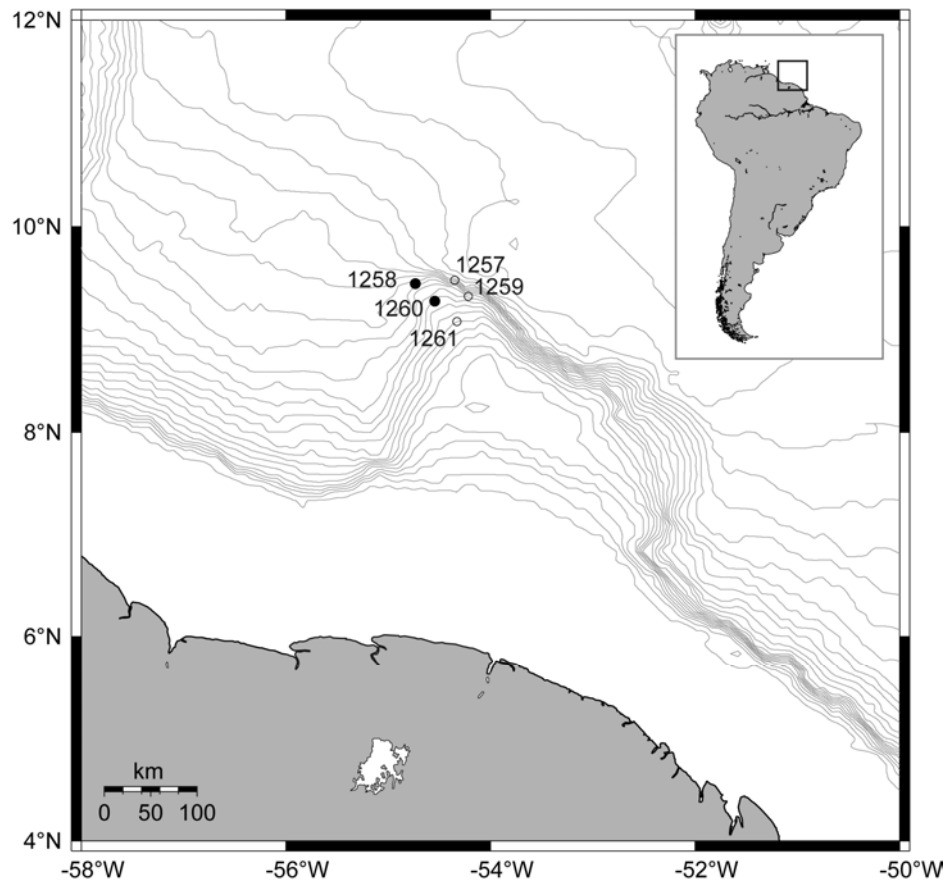


Figure 4.1 Geographic position of Sites 1257 - 1261 at Demerara Rise (ODP Leg 207). (Online Map Creation www.aquarius.geomar.de).

Linear sedimentation rates (LSRs) were estimated by the Shipboard Scientific Party (2004) from age-depth plots by fitting curves to available biostratigraphic and paleomagnetic data over certain depth intervals. Poor preservation or even absence of microfossils and the ambiguous interpretation of paleomagnetic data limit the bio- and magnetostratigraphic age assignment in most of the black shale sequences (Cenomanian–Santonian). Therefore, LSRs calculated for these intervals (0.3-0.5 cm/ka at Sites 1257, 1258, and 1259 and slightly higher values of ~0.85 cm/ka at Sites 1260 and 1261) should be considered as imprecise estimates.

Stable isotope stratigraphy provided by Erbacher et al. (2005) allows a detailed correlation of the investigated sites through the OAE 2 interval. At all studied sites, a distinctive positive carbon isotope excursion (~6.5 ‰) of the OAE 2 was identified (Fig. 4.2). The same authors were able to correlate a number of short-termed $\delta^{13}\text{C}_{\text{org}}$ peaks and troughs within and above the excursion interval between the investigated sites. The events of this record include: (1) The onset of the excursion labeled “A”. (2) A short-termed minimum “B” (not present at Site 1260). (3) An interval “C” with $\delta^{13}\text{C}_{\text{org}}$ values rising to -23 and -21 ‰. (4) The

final maximum value “D”. (5) A short positive peak “E” occurs during the general decrease in isotope values (not present at Site 1258). In addition, Erbacher et al. (2005) also correlated two peaks (“F” and “G”) located above the OAE 2 between the sites. Assuming a duration of ~400 ka for the interval between “A” (onset of excursion) and “D” (end of plateau) Erbacher et al. (2005) calculated average sedimentation rates between ~0.25 cm/ka (Site 1260) and ~1 cm/ka (Site 1258) for the OAE 2. There is no more detailed information available about sedimentation rates for the intervals above and below OAE 2 or variations within this interval.

In this study, two ODP sites along the Demerara Rise paleodepth-transect (Sites 1258 and 1260, see Table 4.1) were chosen to reconstruct paleoenvironmental changes during the late Cenomanian to earliest Turonian black shale deposition interval. Depths are expressed in meters composite depth (mcd), following the shipboard splice between the different holes drilled at each site (Shipboard Scientific Party, 2004).

Table 4.1 Drilling locations Site 1258 and 1260, ODP Leg 207.

Site	Hole	Latitude	Longitude	waterdepth (mbsl)	OAE 2 interval (mcd)	SR (cm/ka)
1258	A	9° 26.000'N	54° 43.999'W	3,192.2	425.95 - 422.18	~1
1258	B	9° 26.000'N	54° 43.982'W	3,192.2		
1258	C	9° 26.000'N	54° 43.966'W	3,192.2		
1260	A	9° 15.984'N	54° 32.633'W	2,548.8	426.34 - 424.94	~0.25
1260	B	9° 15.931'N	54° 32.652'W	2,548.8		

mbsl = meters below sealevel; mcd = meters composite depth; SR = sedimentation rate

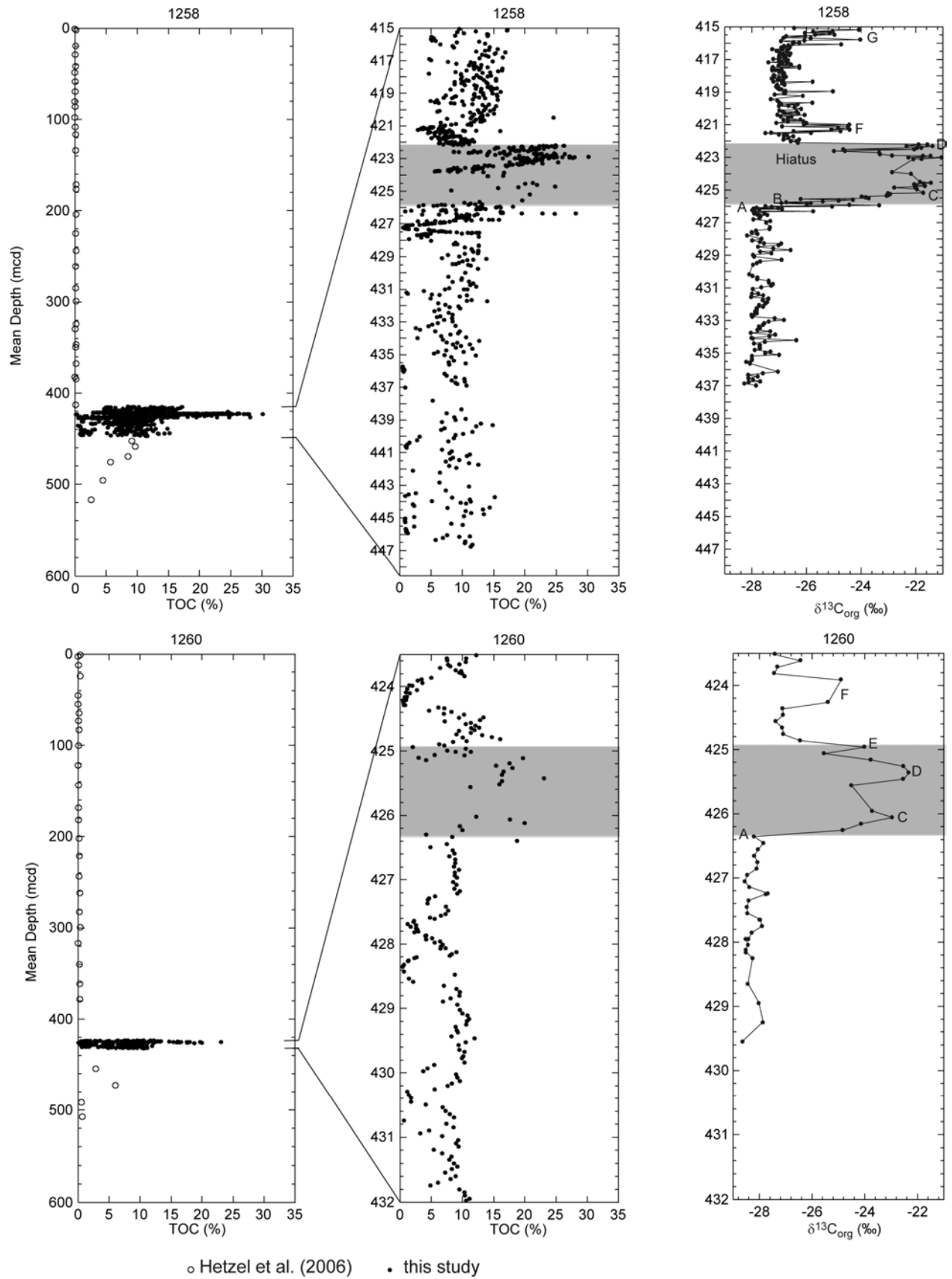


Figure 4.2 Depth-profiles for TOC contents for the whole sediment column investigated (open circles) (Hetzel et al., 2006) and for Cenomanian/Turonian black shales at Demerara Rise, ODP Sites 1258 and 1260. Grey: OAE 2; $\delta^{13}\text{C}_{\text{org}}$ -curve after Erbacher et al., 2005.

ODP Site 1258

Site 1258 is located in a water-depth of 3,192.2 m below modern sea level (mbsl) on the gently dipping western slope ($\sim 2^\circ$) of Demerara Rise. It is the deepest location in the SE–NW paleoceanographic depth transect across Demerara Rise (Shipboard Scientific Party, 2004). The 4 m-thick OAE 2, as defined by the pronounced $\delta^{13}\text{C}_{\text{org}}$ excursion, is located at a depth of 426 – 422 mcd (Erbacher et al., 2005). Based on $\delta^{13}\text{C}_{\text{org}}$ measurements, Erbacher et al. (2005) described a hiatus in the uppermost part of the OAE. The sediments of the investigated section comprise finely-laminated dark shales with occasional beds of phosphatic nodules, stringers of very dark homogeneous shales, and rare concretionary limestone nodules. Thirty-three and a half meters (415–448.5 mcd, see Table 4.2) of upper Cenomanian to lowermost Turonian laminated black shale sediments were investigated from a spliced interval of Holes 1258A, 1258B, and 1258C. 845 samples were taken at 1 cm resolution for the OAE 2 interval and at ~ 10 cm in underlying sediments. Assuming a sedimentation rate of ~ 1 cm/ka the studied interval covers a time span of ~ 3.35 Ma of deposition.

ODP Site 1260

Site 1260, in a water-depth of 2,548.8 mbsl, is positioned on the gently dipping ($\sim 1^\circ$) northwest-facing slope of Demerara Rise, at an intermediate depth in the SE–NW paleoceanographic depth transect. The 1.4 m thick OAE 2 is located between 426.4 and 425.0 mcd, being thus much thinner than at Site 1258. Lithologically, the interval is very similar to Site 1258, although phosphatic nodules are not as common as at the deeper site (Erbacher et al., 2005). About 8.5 m of upper Cenomanian to lowermost Turonian laminated black shale sediments were sampled every ~ 5 cm (219 samples in total, see Table 4.2) from a spliced interval of Holes 1260A and 1260B. Sedimentation rates of the OAE 2 interval are estimated to be on the order of approximately 0.25 cm/ka, thus leading to the same duration of ~ 3.4 Ma of deposition for the studied sequence.

Table 4.2 Sampling Site 1258 and 1260.

Site	Sampled interval (mcd)	Number of samples	Time of deposition (Ma)	Sampling resolution (cm)	Sampling resolution (ka)
1258	415.0 – 448.5	845	~ 3.35	~ 1 / ~ 10	~ 1 / ~ 10
1260	423.5 – 432.0	219	~ 3.40	~ 5	~ 20

mcd = meters composite depth

Analytical methods

Sediments splits were freeze-dried, ground and homogenized in an agate ball mill. For X-ray fluorescence (XRF) analysis (Philips® PW 2400 X-ray spectrometer), 600 mg of sample powder were mixed with 3600 mg of a 1:1 mixture of dilithiumtetraborate ($\text{Li}_2\text{B}_4\text{O}_7$) and lithiummetaborate (LiBO_2), or with 100% dilithiumtetraborate for carbonate-rich samples, preoxidized at 500°C with NH_4NO_3 (p.a.) and fused to glass beads. Total sulfur (S_T) and total carbon (TC) were analyzed using an ELTRA® CS-500 IR-analyzer. Total inorganic carbon (TIC) was determined coulometrically by a UIC® CM 5012 CO_2 coulometer coupled to a CM 5130 acidification module. Total organic carbon (TOC) was calculated as the difference between TC and TIC. Procedures and accuracy of the methods were checked with in-house reference materials (Prakash Babu et al., 1999; see Appendix A4.1). Different sedimentary sulfur fractions, chromium-reducible sulfur (S_P , essentially pyrite), organic matter (essentially kerogen-bound organic sulfur, S_ORG) and acid volatile sulfur (S_AVS) were separated quantitatively from powdered freeze-dried samples, as described by Böttcher et al. (2006). Chromium reducible sulfur, essentially pyrite sulfur, S_P , was extracted for 2 h via hot acidic Cr(II)Cl_2 (Zhabina and Volkov, 1978; Canfield et al., 1986; Fossing and Jørgensen, 1989). Liberated H_2S was precipitated quantitatively in Zn acetate traps and measured spectrophotometrically (Cline, 1969). The organic sulfur fraction, S_ORG , was calculated as the difference of total sulfur and the sum of chromium-reducible sulfur (Böttcher et al., 2006). S_AVS was extracted from selected samples from Site 1258 via anaerobic distillation with 6M HCl (1 h). Since FeS is not expected in the black shale samples to survive the diagenetic pyritization and lab-based freeze-drying process, the S_AVS fraction is assumed to correspond to acid-volatile metal monosulfides. ZnS , for instance, that might have been formed in a euxinic water column, has been found in C/T samples in the present study via SEM-EDX, and has also been reported in Createceous black shales previously (Brumsack, 1980). ZnS would have survived burial and later sample handling. The amount of pyrite iron (Fe_P) was calculated from the S_P content assuming ideal stoichiometry. This fraction essentially represents the total highly reactive iron fraction (Raiswell and Canfield, 1998; Poulton and Raiswell, 2002). To confirm this approach, iron-oxide bound iron was separately determined in selected black shale samples from Sites 1258 and 1260 and presented by Böttcher et al. (2006). As described in detail by these authors, iron(oxyhydr)oxide phases were extracted from sediment samples using a buffered solution of Na-dithionite and extracted iron was determined spectrophotometrically. It was found that this fraction is only present in very small amounts and that pyrite iron amounts to

96 - 99% of the total highly reactive iron pool. For samples from Site 1258 $^{34}\text{S}/^{32}\text{S}$ ratios of the S_P bound sulfur were determined by means of C-irmMS using a Eurovector 3000 elemental analyzer (EA) coupled to a Thermo Finnigan MAT253 and are given in the δ -notation versus the international V-CDT standard. Calibration of the mass spectrometer was carried using international IAEA and NBS reference materials. Sulfur isotope results for Site 1260 will be presented in a separate communication (Böttcher et al., in prep.).

Finally, selected non-ground carbon-coated (BAL-TEC sputter-coating device SCD 005) freeze-dried sediment samples were investigated by means of energy-dispersive X-ray analysis on an Oxford Link ISIS 300 EDX-System with Pentafet S ATW Si-detector installed on a Zeiss DSM 940 scanning electron microscope (SEM).

Results and discussion

Preliminary remarks

To account for dilution effects by varying carbonate or organic matter contents trace element contents were normalized to Al (TE/Al ratio). In cases of very low Al contents (see Fig. 4.3 and 4.4), normalization may lead to exaggerated peaks in TE/Al ratios, which has to be kept in mind when interpreting TE/Al profiles (van der Weijden, 2002). Some elements, like Al, Ti, K, Rb and Zr, are only present in the detrital component and are not influenced either by biogenic or diagenetic processes. Significant variations in TE/Al ratios of these elements therefore reveal changes in source area composition. While most of the investigated sediment intervals show TE/Al ratios similar to average shale (AS; Wedepohl 1971, 1991), several sediment layers of one centimeter to several decimeters thickness were identified by characteristic TE/Al ratios. At Site 1260 a 35 cm thick interval (425.61-425.96 mcd) within the OAE 2 is characterized by low K/Al (0.07, AS = 0.34), high Ti/Al ratios (0.102, AS = 0.053) and is depleted in Si (Si/Al 2.58, AS = 3.11; see Appendix A4.2). From macroscopic observation (Appendix A4.2b), this interval most likely is a diagenetically altered ash bed. At Site 1258, three sediment layers within OAE 2 (423.51-423.53 mcd, 423.87-424.04 mcd, and 425.22-425.50 mcd) correspond to this layer, identified by similar disturbances in TE/Al profiles. At both sites abrupt changes in carbonate, TOC and TS contents from extremely high concentrations to near zero values can be identified. Light $\delta^{13}\text{C}$ values of the carbonate in the discussed interval at Site 1260 (Friedrich, pers. communication) point towards the involvement of microbiological processes like anaerobic oxidation of methane (AOM) (e.g., Galimov, 2006). The production of bicarbonate by AOM could result in the precipitation of authigenic carbonates, and thus increase the degree of

carbonate diagenesis implying recrystallization of carbonates from foraminifera and nanofossils (Erbacher et al., 2004). With the geochemical methods applied (bulk element concentrations) the origin of the material can not be identified. To avoid misinterpretation of changes in element distribution patterns, samples from these intervals (7 samples from Site 1260 and 27 samples from Site 1258) were excluded from following discussion regarding changes of redox-conditions and trace metal availability. As the bulk geochemistry of sites is similar, analytical results of discussed intervals are given as average values listed in Appendix A4.2c.

Bulk parameters

Figure 4.2 shows the depth profiles of total organic carbon (TOC) for the whole sediment column (data from Hetzel et al., 2006) and the upper Cenomanian to lower Turonian black shale sequences (C/T back shales), which are in the focus of this study.

Sediments above these sequences are characterized by low TOC contents (<0.4 %). Below these intervals TOC contents decrease from ~10 % to ~1 % with increasing depth. The C/T black shales show varying TOC values: lowest contents (almost 0 %) in carbonate-rich layers and highest contents (30.2 % at Site 1258 and 23.1 % at Site 1260) within the OAE 2 interval, which is identified by correlation with the $\delta^{13}\text{C}_{\text{org}}$ curve from Erbacher et al. (2005) and marked in grey.

Figures 4.3 and 4.4 show the bulk chemistry of the C/T black shales: As mentioned above, highly variable TIC contents (<0.2 - 11.8 %) lead to dilution effects, which are shown by the inverse distribution pattern for TIC and Al, representing terrigenous detritus. The TIC profiles display the light-dark cycles described by the Shipboard Scientific Party. Whereas the profile of Site 1260 suggests a regular cyclicity possible modulated by orbital forcing, carbonate contents of Site 1258 show a less regular distribution pattern despite higher resolution (see Table 4.2). For both sites, time series analysis of our high-resolution TIC data does not evidence orbital cyclicity.

Nederbragt et al. (2007) analyzed the cyclicity during the Mid-Cretaceous at Demerara Rise. Due to the irregular spacing of the carbonate-rich and organic-rich cycles (lack of precise age control, variable sedimentation rates and/or degree of compaction and minor hiatuses), the authors concluded instead of establishing a continuous cyclostratigraphy for the entire organic-rich unit to perform time series analysis of sediment color data in selected intervals in combination with thin section analysis of representative lithologies. They found that cyclic variation in lithology at Demerara Rise is inferred to represent eccentricity and precession cycles with a weak obliquity component. For analysis of the cyclicity during OAE

2 the authors examined two cores from Site 1258 and 1260. Both, precession and eccentricity cycles were found.

To better compare TOC and S_T contents for Demerara C/T black shales with other C/T sections we calculated TOC_{cf} and $S_{T\ cf}$ for a carbonate-free sediment. Profiles are given in Figure 4.3 and 4.4 beside profiles of absolute concentrations. For Site 1258 most of the TOC values vary between ~0.5 and ~15 %. Adjusting for dilution by carbonate resulting TOC_{cf} values are quite higher (~10 - ~25 %). Some intervals of half a meter thickness are characterized by TOC contents >20 %. These peaks are distributed right below, within and above OAE 2. For Site 1260 the TOC contents vary between ~0.5 and ~12 % and on a carbonate free basis TOC_{cf} values fall between ~15 and ~22 %. Highest TOC contents (>15 %) are found within OAE 2.

Average contents below, within and above OAE 2 (Table 4.3) show higher TOC and lower TIC contents for Site 1258 in comparison to Site 1260. For both sites, average TOC values are in the same range (TOC: 6.9 - 10.1 %; TOC_{cf} : 17.6 - 19.3 %) below and above the OAE 2 and slightly higher during the OAE 2 with 17.8 % (TOC_{cf} 22.4 %) at Site 1258 and 12.1 % (TOC_{cf} 22.8 %) at Site 1260. The same is true for S_T values with 1.5 - 2.4 % ($S_{T\ cf}$ 3.8 - 4.7 %) below and above and 5.0 % ($S_{T\ cf}$ 6.3 %) within the OAE 2 at Site 1258 and 3.4 % ($S_{T\ cf}$ 6.5 %) within the OAE 2 at Site 1260.

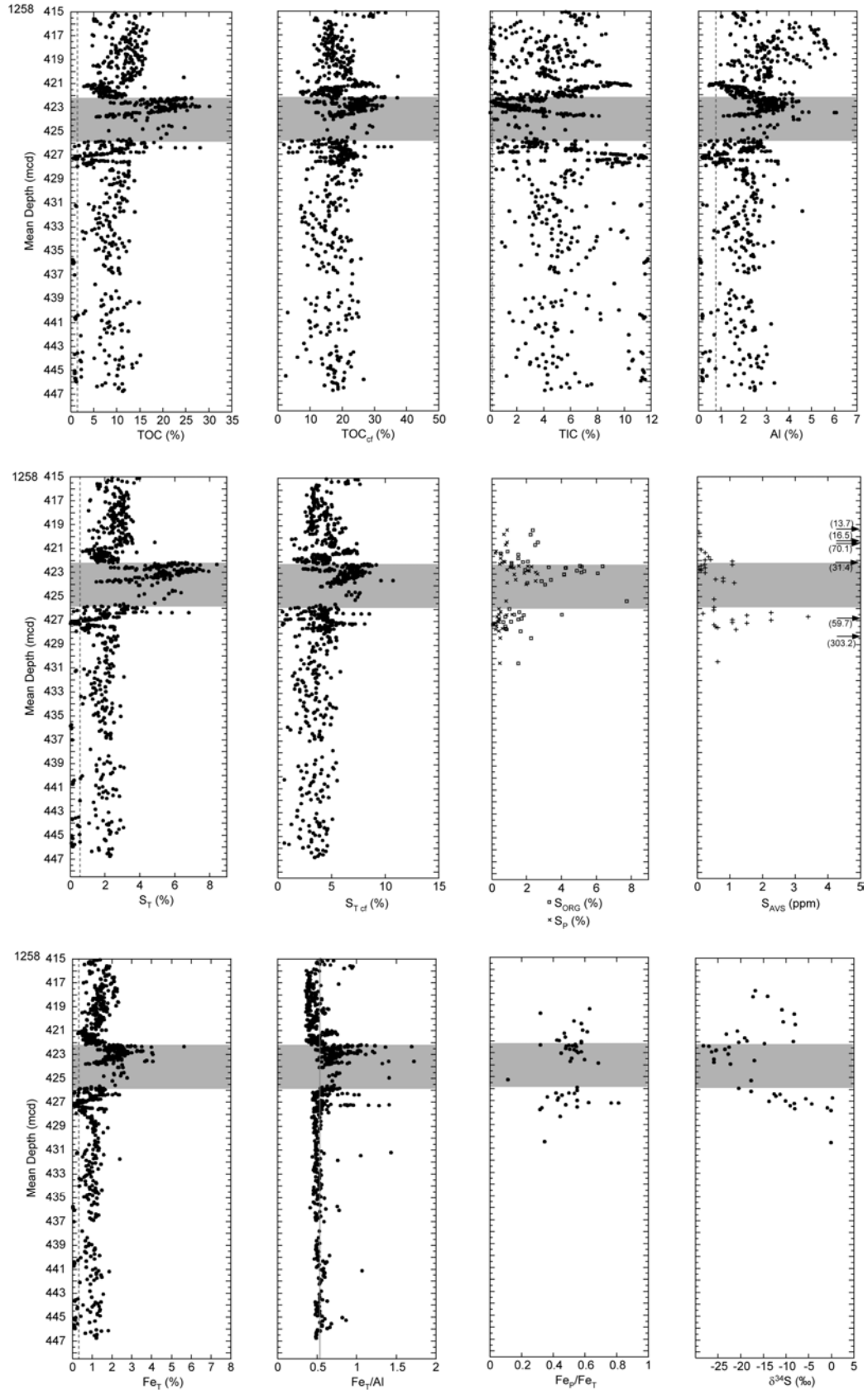


Figure 4.3 Depth-profiles for TOC, TIC, Al, S_T, S_{ORG}, S_P, S_{AVS} and Fe_T for Cenomanian/Turonian black shales at Site 1258. TOC_{cf} and S_{Tcf} are calculated for carbonate-free sediment. δ³⁴S of pyrite, Fe_T/Al ratios as well as Fe_P/Fe_T ratios are also shown. Grey: OAE 2; grey solid line: element/Al ratio of to 'average shale' (AS) (Wedepohl, 1971, 1991); dashed line: quantification limit (see Appendix A4.1).

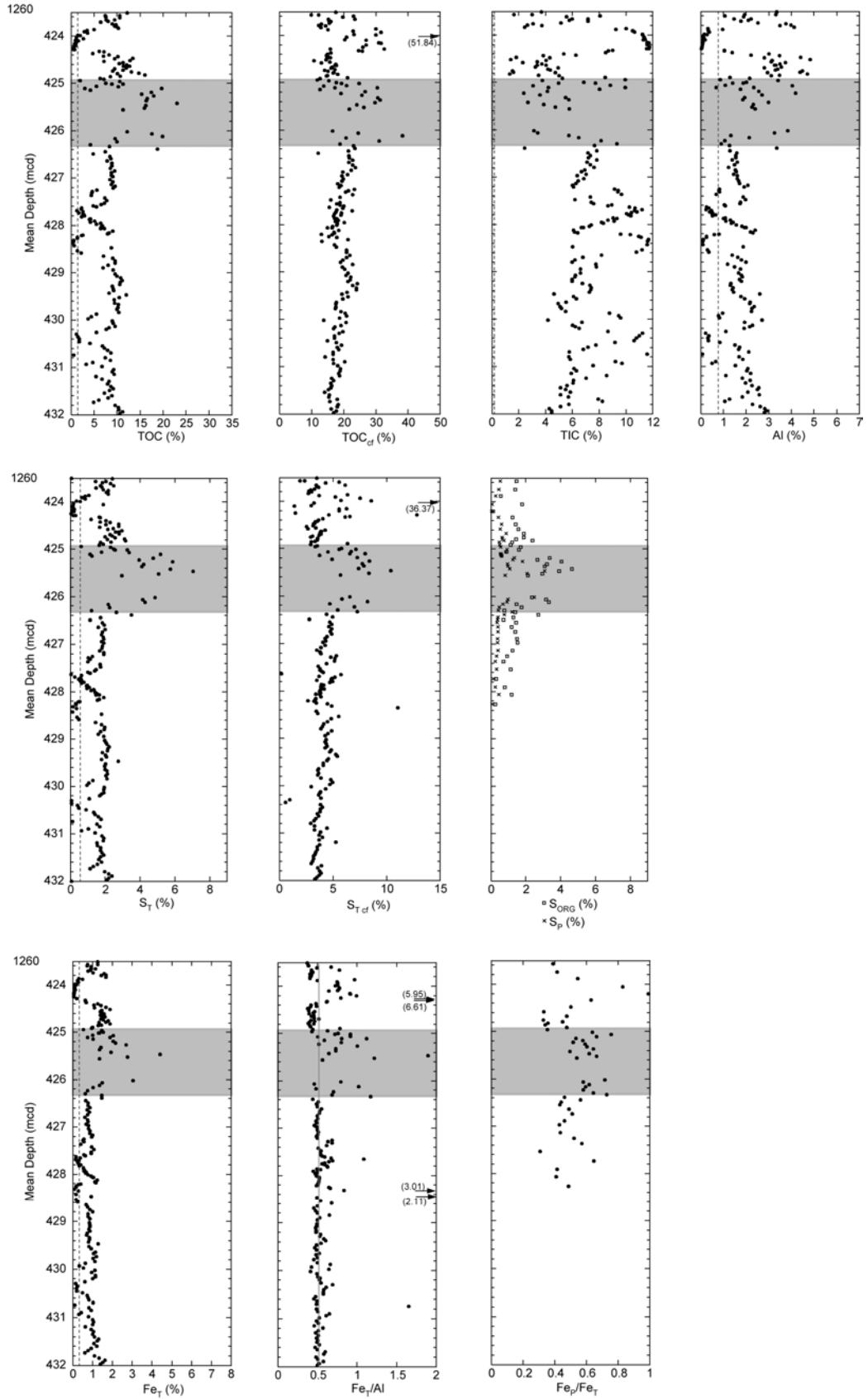


Figure 4.4 Depth-profiles for TOC, TIC, Al, S_T , S_{ORG} , S_P and Fe_T for Cenomanian/Turonian black shales at Site 1260. TOC_{cf} and $S_{T\ cf}$ are calculated for carbonate-free sediment. Fe_T/Al ratios as well as Fe_P/Fe_T ratios are also shown. Grey: OAE 2; grey solid line: element/Al ratio of 'average shale' (AS) (Wedepohl, 1971, 1991); dashed line: quantification limit (see Appendix A4.1).

Table 4.3 Comparison of average element contents and element/Al ratios Cenomanian/Turonian black shales of Demerara Rise and 'average shale'.

		1258 below OAE 2 (n=347)	1258 within OAE 2 (n=197)	1258 above OAE 2 (n=274)	1260 below OAE 2 (n=129)	1260 within OAE 2 (n=26)	1260 above OAE 2 (n=57)	Average shale (Wedepohl, 1971, 1991)
S _T	%	1.71	4.97	2.35	1.45	3.43	1.69	0.24
TIC	%	6.20	2.46	5.00	7.59	5.76	6.34	0.35
TOC	%	7.83	17.82	10.13	6.89	12.12	7.54	
Si	%	11.61	14.66	11.43	6.64	8.06	9.14	27.53
Ti	%	0.08	0.14	0.12	0.08	0.10	0.10	0.46
Al	%	1.68	2.90	2.57	1.47	2.17	2.18	8.84
Fe _T	%	0.88	2.17	1.19	0.76	1.65	0.97	4.80
Mg	%	0.47	0.46	0.57	0.47	0.47	0.60	1.60
Ca	%	21.37	9.44	18.27	26.04	20.20	22.32	1.57
Na	%	0.68	1.16	0.99	0.74	0.86	0.82	1.19
K	%	0.45	0.89	0.74	0.43	0.65	0.69	2.99
P	%	0.25	0.15	0.54	0.29	0.22	0.52	0.07
As	ppm	13	25	21	18	25	16	10
Ba	ppm	260	542	612	343	746	642	580
Co	ppm	3	13	5	3	9	4	19
Cr	ppm	121	70	149	109	82	145	90
Cu	ppm	58	68	70	53	68	63	45
Mn	ppm	7	50	27	0	14	7	850
Mo	ppm	80	40	95	62	33	38	1
Ni	ppm	126	169	149	108	144	92	68
Rb	ppm	21	30	30	19	22	26	140
Sr	ppm	593	653	716	923	952	792	300
U	ppm	12	17	18	16	18	12	4
V	ppm	1058	370	1173	1386	554	899	130
Y	ppm	12	29	23	13	23	19	41
Zn	ppm	578	138	968	879	382	701	95
Zr	ppm	28	38	36	27	33	34	160
S _{Tcf}	%	3.83	6.26	4.36	4.04	6.47	4.70	0.25
TOC _{cf}	%	17.64	22.40	18.30	18.74	22.80	19.30	
S _T /Al		1.05	1.75	1.05	1.06	1.67	1.54	0.03
TOC/Al		4.85	6.32	4.40	4.94	5.93	5.98	
Si/Al		7.79	5.81	4.76	4.49	3.72	4.24	3.11
Ti/Al		0.05	0.05	0.05	0.05	0.05	0.05	0.05
Fe _T /Al		0.55	0.76	0.50	0.58	0.80	0.74	0.54
Mg/Al		0.57	0.17	0.25	0.55	0.25	1.39	0.18
Ca/Al		42.97	4.36	11.69	43.01	13.87	121.32	0.18
Na/Al		0.43	0.41	0.42	0.57	0.42	0.58	0.13
K/Al		0.28	0.31	0.29	0.32	0.31	0.40	0.34
P/Al		0.13	0.05	0.20	0.17	0.12	0.23	0.01
As/Al	× 10 ⁻⁴	9.3	8.8	8.4	14.3	12.5	13.6	1.1
Ba/Al	× 10 ⁻⁴	190.8	188.1	239.0	271.8	345.2	531.6	65.6
Co/Al	× 10 ⁻⁴	2.1	4.4	2.3	2.2	4.4	3.2	2.1
Cr/Al	× 10 ⁻⁴	68.8	24.0	50.7	75.1	37.5	57.7	10.2
Cu/Al	× 10 ⁻⁴	36.0	24.0	27.4	38.9	30.5	45.9	5.1
Mn/Al	× 10 ⁻⁴	9.2	18.4	23.2	0.1	5.9	36.2	96.2
Mo/Al	× 10 ⁻⁴	50.0	14.3	40.4	49.4	16.7	20.3	0.1
Ni/Al	× 10 ⁻⁴	77.8	59.5	62.0	85.0	73.0	47.6	7.7
Rb/Al	× 10 ⁻⁴	11.5	10.2	11.3	12.1	10.7	10.6	15.8
Sr/Al	× 10 ⁻⁴	584.4	241.5	349.0	1019.4	541.5	1425.7	33.9
U/Al	× 10 ⁻⁴	9.7	6.2	8.5	14.5	10.8	17.9	0.4
V/Al	× 10 ⁻⁴	654.8	127.0	461.7	1010.1	294.5	439.8	14.7
Y/Al	× 10 ⁻⁴	8.9	10.1	10.2	10.6	13.1	17.0	4.6
Zn/Al	× 10 ⁻⁴	316.0	48.1	355.9	581.4	154.0	251.1	10.7
Zr/Al	× 10 ⁻⁴	20.7	13.5	14.9	22.4	17.1	31.8	18.1

Italics: average values below quantification limit (see Appendix A4.1).

Iron

Figures 4.3 and 4.4 show profiles of total iron and Al-normalized iron contents. Only for some carbonate-rich layers Fe contents are below the quantification limit of 0.33 % (e.g. ~424 mcd at Site 1260) and Fe_T/Al peaks may be exaggerated (see *Preliminary remarks*) due to inaccuracies of measurements of Fe and Al close to or below the quantification limit. Besides these peaks, the Fe_T/Al profiles show an almost constant value close to AS. Assuming severe oxygen-deficiency, as evidenced by sediment lamination for the black shale sequence of Demerara Rise, the almost constant average shale-like values of Fe_T/Al imply anoxic but not euxinic (no free H_2S in the water column) conditions during deposition. Fe_T/Al ratio of the sediment is neither decreased via mobilization of iron(hydr)oxides under suboxic conditions nor increased via precipitation of dissolved Fe species as sulfide in the overlying water column under euxinic conditions. During OAE 2 Fe_T/Al mean values increase to 0.76 (Site 1258, maximum 1.72) and 0.80 (Site 1260, maximum 1.89), owing to an increase in total Fe_T contents. This indicates an additional Fe-source during deposition of this interval. In analogy to the modern Black Sea reductive Fe mobilization in nearshore areas or enhanced fluvial input are likely causes for the observed Fe-enrichment (e.g., Lyons and Severmann, 2006). In the case of the modern Black Sea Fe_T/Al -ratios are increasing with water depth (e.g., Wijsman et al., 2001) because syngenetic iron sulfides form an increasing part of bulk sedimentary iron. This model requires truly euxinic conditions, besides the existence of a zone where reducing but non-sulfidic conditions prevail, allowing Fe transport from shallow to deep sites (e.g., Lyons and Severmann, 2006). The increase of the ratio of pyrite iron to total iron, Fe_P/Fe_T , from a mean value of 0.44 below and above to about 0.64 (Table 4.4) within OAE 2 indicates the addition of syngenetic water column-derived pyrite (Raiswell and Canfield, 1998; Poulton and Raiswell, 2002; Böttcher et al., 2006, and references therein). Together with previous measurements on the detailed reactive iron speciation of Leg 207 sediments (Böttcher et al., 2006), these findings are confirmed by the Al-normalized iron contents, as discussed above.

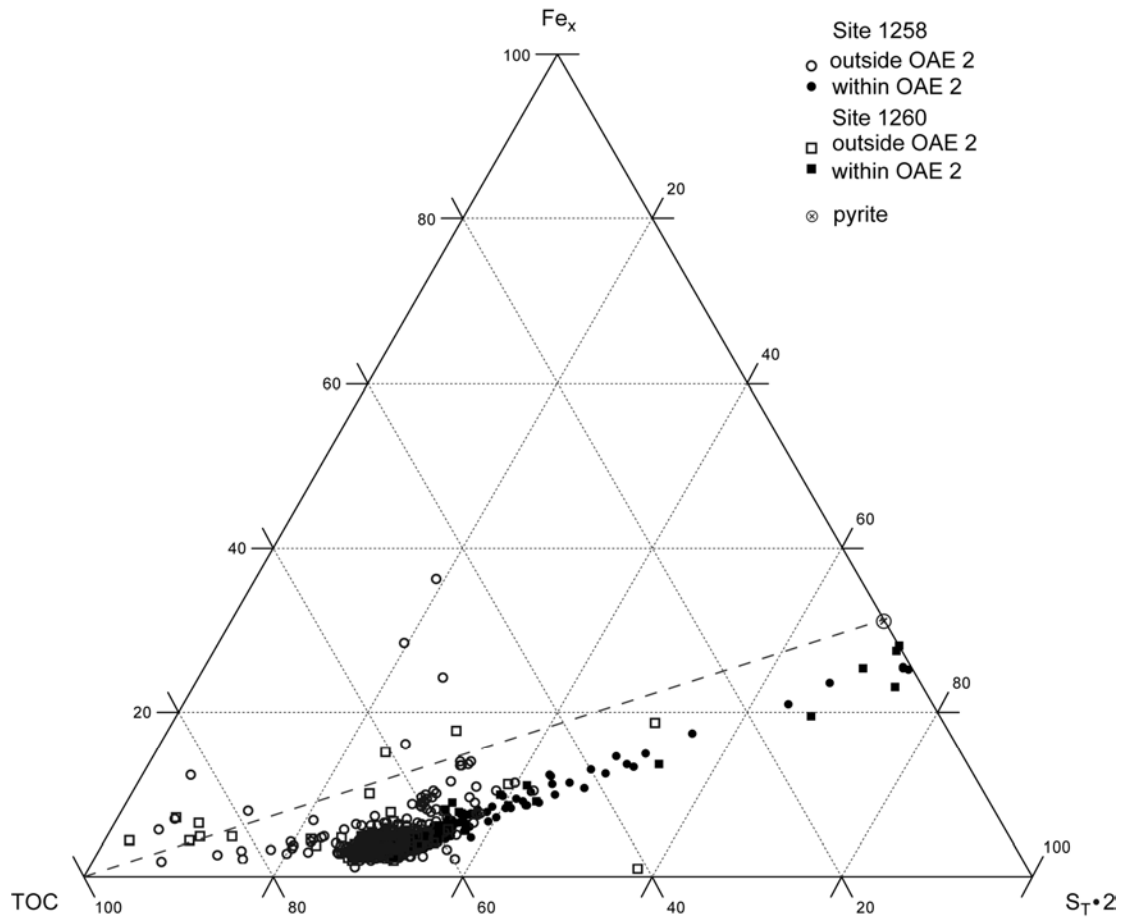


Figure 4.5 Ternary Plot: Degree of pyritization of Cenomanian/Turonian black shales at Demerara Rise in the Fe_x – TOC – $\text{S}_T \cdot 2$ system (relative weight ratios). Reactive Fe_x is calculated with $\text{Fe}_x = \text{Fe}_T - 0.25 \cdot \text{Al}$. Data point for pyrite is also shown.

Figure 4.5 presents the analytical data of Sites 1258 and 1260 in a ternary Fe_x - S_T -TOC plot (Brumsack, 1988; Dean and Arthur, 1989; Brumsack et al., 1995). The represented data within the OAE all plot below the pyrite-saturation line indicating, that under iron-limited conditions, some (excess) sulfide and/or sulfur intermediates were able to react with organic matter to form organic sulfur compounds.

Table 4.4 Average pyrite sulfur (S_P), pyrite iron (Fe_P), acid volatile sulphur (S_{AVS}), calculated organic sulfur (S_{org}) and ratio of pyrite (reactive) iron to total iron (see Table 4.3).

		1258 below OAE 2 (n=19)	1258 within OAE 2 (n=18)	1258 above OAE 2 (n=12)	1260 below OAE 2 (n=16)	1260 within OAE 2 (n=22)	1260 above OAE 2 (n=13)
S_P	%	0.42	1.68	0.60	0.38	1.14	0.52
Fe_P	%	0.36	1.46	0.52	0.33	0.99	0.45
S_{AVS}	ppm	22.4 (n=17)	0.5 (n=13)	12.2 (n=11)			
S_{org}	%	1.25	4.39	1.69	1.14	2.31	1.41
Fe_P/Fe_T		0.41	0.67	0.44	0.43	0.60	0.46

Sulfur and sulfur isotopes

Dissimilatory sulfate reduction leads to the formation of hydrogen sulfide that may transform reactive iron to iron sulfides (essentially pyrite, FeS_2 ; including framboidal pyrite Fig. 4.6) and, under iron limited conditions with organic matter to form organic sulfur compounds (e.g., Werne et al., 2004). The profiles of S_P and S_{ORG} show elevated values during OAE 2 at both sites (Fig. 4.3 and Fig. 4.4; see also Table 4.4). Below OAE 2 S_P values are $\sim 0.4\%$ (ca. 25 rel% of S_T) and $S_{ORG} \sim 1.2\%$ (respectively ca. 75 rel% of S_T). At Site 1258, S_P contents rise to $\sim 1.7\%$ (maximum $>2.5\%$) and S_{ORG} to $\sim 4.4\%$ (maximum $>7.7\%$) within the OAE 2 interval, thus the proportion of pyrite sulfur increases to ca. 28 rel% of total sulfur. Although absolute values are not as high as at Site 1258, the pyrite sulfur fraction at Site 1260 reaches even ca. 33 rel% with 1.1% S_P (maximum $>3.1\%$) and 2.3% S_{ORG} (maximum $>6.6\%$) during OAE 2. Above OAE 2 the proportional composition of different sulfur species nearly equals the composition below with $\sim 0.5\%$ S_P and $\sim 1.4\%$ S_{ORG} ($S_P:S_{ORG} = 26:74$ rel%) at both sites.

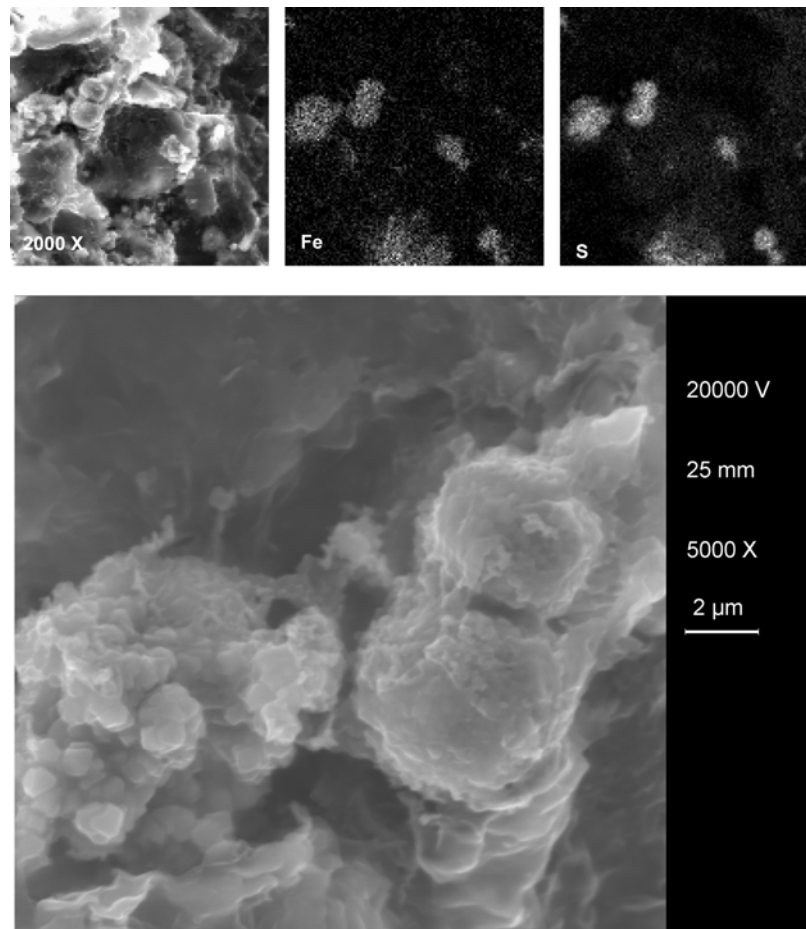


Figure 4.6 EDX-Scan and SEM of a pyrite framboid from Site 1258B-45-4 138-139cm, 422.98 mcd (within OAE 2).

The relationship of S_P with TOC data is presented in Figure 4.7a and compared to the relationship proposed for “normal marine sediments” (Berner and Raiswell, 1983). Only a few data points coincide with the relation found for clastic sediments below an oxic water column (dashed line in Fig. 4.7a). A number of data points plot above the regression line, indicating an excess of sulfur that may be due to euxinic depositional conditions. At highest TOC contents, however, most data show a relative excess of organic matter (OM). The indicated iron-limitation during black shale deposition has also been found for the modern Black Sea sapropel and Mediterranean sapropels (e.g., Lyons and Berner, 1992; Passier et al., 1999b; Böttcher et al., 2006). S_P in the investigated black shale samples makes up between 30 % and 100 % of S_T , with a decrease of the relative amount of S_P with increasing OM content. This indicates the importance of the balance between organic matter and the syngenetic metal flux to the surface sediments in controlling the sedimentary sulfur speciation. In addition to fixation of sulfide by the reaction with iron, organic matter acted as the second important sulfur trap during early diagenesis. From molecular analysis of the preservation pathways of sedimentary organic carbon in a euxinic environment Hebbing et al. (2006) proposed that sulfides produced by bacterial sulfate reduction play a major role for the reductive alteration and thus preservation of organic carbon. From the nearly linear variation of organic sulfur and organic carbon contents (Fig. 4.7b), essentially constant atomic S_{ORG}/TOC ratios are obtained. Quantitatively, the samples with TOC contents exceeding ~2 wt% have as much as 10 atom% organic sulfur. Most of the atomic S/C ratios fall in the range of 0.04 to 0.06, which is within the range reported for sapropels from the Mediterranean and Black Sea (Passier et al., 1999b; Böttcher et al., 2006). The almost linear relationship between TOC and S_{ORG} may be caused by a constant relative proportion of organic matter fractions available for diagenetic sulfurization.

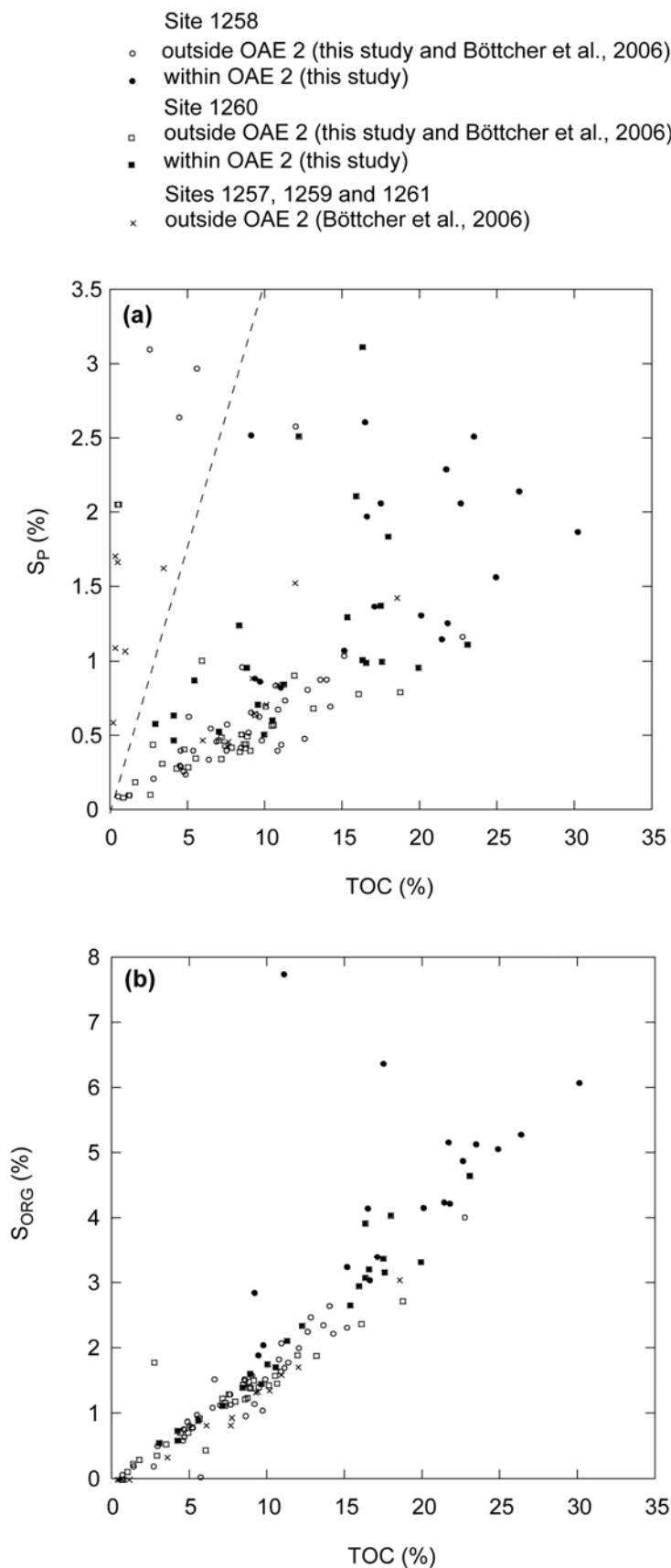


Figure 4.7 (a) Pyrite sulfur (S_P) versus TOC and (b) organic sulfur (S_{ORG}) versus TOC for Cenomanian/Turonian black shales at Site 1258 and Site 1260 (this study) and black shale samples from Sites 1257, 1259 and 1261 (Böttcher et al., 2006). Dashed line marks the relationship derived for normal marine sediments as defined by Berner and Raiswell (1983).

The downcore variation of the stable sulfur isotope composition of pyrite at Site 1258 displays a range in $\delta^{34}\text{S}$ values between -28.2 and +0.2 ‰ (average -15.4 ± 8.3 ‰; $n=41$) during OAE 2, with an inverse relationship to the $\delta^{13}\text{C}$ values (Fig.4.3, Table 4.5). The sulfur isotope variations observed in the sedimentary pyrite pool are much more pronounced than those observed in the global seawater sulfate at this time (Paytan et al., 2004). This indicates that sulfur isotope discrimination was controlled by changes in sedimentary conditions and was higher during times of enhanced burial of OM. This can be caused by a lower burial efficiency of reduced sulfur and/or higher contributions from the oxidative part of the sulfur cycle (in the water column or in surface sediments). A similar trend and magnitude of sulfur isotope discrimination was found in the C/T sediments of different sites in the Tarfaya basin (e.g., Kolonic et al., 2002; Böttcher et al., unpubl. data). For instance for the pyrite fraction Böttcher et al. (unpubl. data) obtained ranges at Site S13 (-18.9 to +2.5 ‰, average -10.2 ± 7.8 ‰; $n=9$), at S57 (-28.8 to -8.8 ‰, average -17.6 ± 5.1 ‰; $n=29$), and S75 (-20.6 to -8.7 ‰, average -15.7 ± 3.2 ‰; $n=17$). This similarity suggests a common control of the overall sedimentary sulfur isotope signal for the CTBE in the southern North Atlantic independent of paleo-water depths. The stratigraphic trend of the sulfur isotope ratios shows that pyrite isotope data go through a minimum similar to previous observations at Tarfaya (Kolonic et al., 2002; Böttcher et al., unpubl. data). We relate the most negative values to an increased contribution of syngenetic pyrite, sulfur derived from the oxidative part of the biogeochemical sulfur cycle, and mostly changes in other factors (e.g., the quality of organic matter) influencing overall sulfur isotope discrimination.

Table 4.5 Average $\delta^{34}\text{S}$ of pyrite sulfur (S_P) for Cenomanian/Turonian black shales of Site 1258.

		1258 below OAE 2 ($n=16$)	1258 within OAE 2 ($n=12$)	1258 above OAE 2 ($n=13$)
$\delta^{34}\text{S}_P$	‰	-8.4	-24.4	-15.6

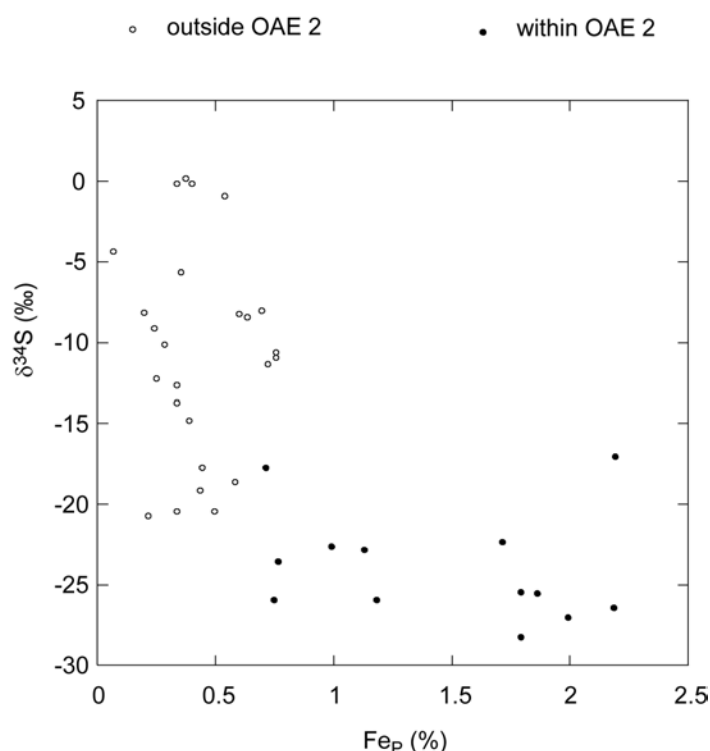


Figure 4.8 $\delta^{34}\text{S}$ of pyrite versus pyrite iron (Fe_p) for Cenomanian/Turonian black shales at Site 1258.

Most lighter sulfur isotope data are found during OAE 2 compared to sediments outside OAE 2 (Fig.4.8), and these are associated with highest contents of pyrite-iron. This is in agreement with findings of Gauthier (1987) on Cretaceous black shales from the Western Interior Seaway. Taking the sulfur isotopic composition for seawater sulfate during the Cenomanian/Turonian to be around +15 ‰ (Strauss, 1999; Paytan et al., 2004), and assuming that pyrite mainly formed under conditions that were open with respect to dissolved sulfate (Hartmann and Nielsen, 1969), e.g., in the water column or close to the sediment-water interface, an overall sulfur isotope fractionation of 15 to 42 ‰ is estimated for Site 1258. This is within the range found in studies with pure cultures of sulfate-reducing bacteria (e.g., Brunner and Bernasconi, 2005), but is smaller than values found in C/T sediments from the northern North Atlantic (Böttcher and Kuypers, unpubl. data), in the Pliocene TOC-rich sapropels of the deep Mediterranean (Passier et al., 1999a; Böttcher et al., 2003), in the modern euxinic Black Sea (Neretin et al., 2004; Böttcher et al., 2004), and in sediments from the Great Australian Bight (Wortmann et al., 2001). Higher contributions from the oxidative part of the sulfur cycle (microbial disproportionation of sulfur intermediates) and/or lower cellular sulfate reduction rates or specific bacterial communities may be responsible for the development of the different characteristic sulfur isotope signals.

*Redox-sensitive and sulfide forming trace metals*Manganese

The C/T black shales of Demerara Rise are characterized by very low Mn-concentrations (Fig. 4.9). For most of the samples the Mn contents are below the XRF quantification limit of 78 ppm. At Site 1258, for sediments below 427.7 mcd Mn values are below the detection limit, which is defined as half the quantification limit. Right below, within and above OAE 2, Mn contents are higher and reach the detection limit of 39 ppm. Within OAE 2, Mn values show a high variability between detection limit and 426 ppm, with a mean value of ~ 50 ppm and a standard deviation of the same order (49 ppm). Above OAE 2 (421.63-421.03 mcd) a clear peak in absolute Mn concentrations with a maximum value of 217 ppm can be recognized. This peak can be correlated to a peak in TIC. Since Mn concentrations often are below the quantification limit, Mn/Al ratios have to be considered with caution. A maximum Mn/Al ratio of 466×10^{-4} at 421.63-421.03 mcd represents a significant Mn enrichment in comparison to the Mn/Al ratio of 96×10^{-4} for average shale (Wedepohl, 1971, 1991). The same is true for certain intervals within OAE 2. For samples close to the onset and termination of OAE 2, the enrichments in Mn are less pronounced.

At Site 1260 Mn concentrations in all samples are below the quantification limit. Only a few samples attain the detection limit of 39 ppm: One interval above OAE 2 (423.99-424.04 mcd) reaching Mn values up to 77 ppm can again be correlated to a carbonate peak. Within OAE 2 Mn concentrations vary between 0 and 46 ppm.

Extremely low Mn/Al ratios in C/T black shales of Demerara Rise indicate that Mn was either reduced within the water column before sedimentation or upon early diagenesis in an environment open to dissolved Mn(II) loss as provided by an expanded oxygen-minimum-zone (OMZ), like the modern upwelling zones off Peru (Böning et al., 2004) or in the Gulf of California (Brumsack, 1989). Thurow et al. (1992) found a similar mobilization of Mn at the Northwest Australian margin during OAE 2. The authors described Mn-poor sediments within the OMZ and Mn-rich sediments below the OMZ, indicating oxic deep waters during the C/T interval at this location.

A possibility for the observed Mn-enrichment might be the fixation of dissolved Mn(II) as mixed Mn-Ca-carbonates under conditions where Mn was enriched. Brumsack (2006) suggests that overgrowths of early diagenetic Mn-carbonate on pre-existing carbonate tests might be responsible for Mn enrichment in Black Sea sediments. Pre-existing carbonates may act as an efficient trap for diagenetically mobilized Mn(II) (Boyle, 1983; Gingele and Kasten, 1994; Böttcher, 1997).

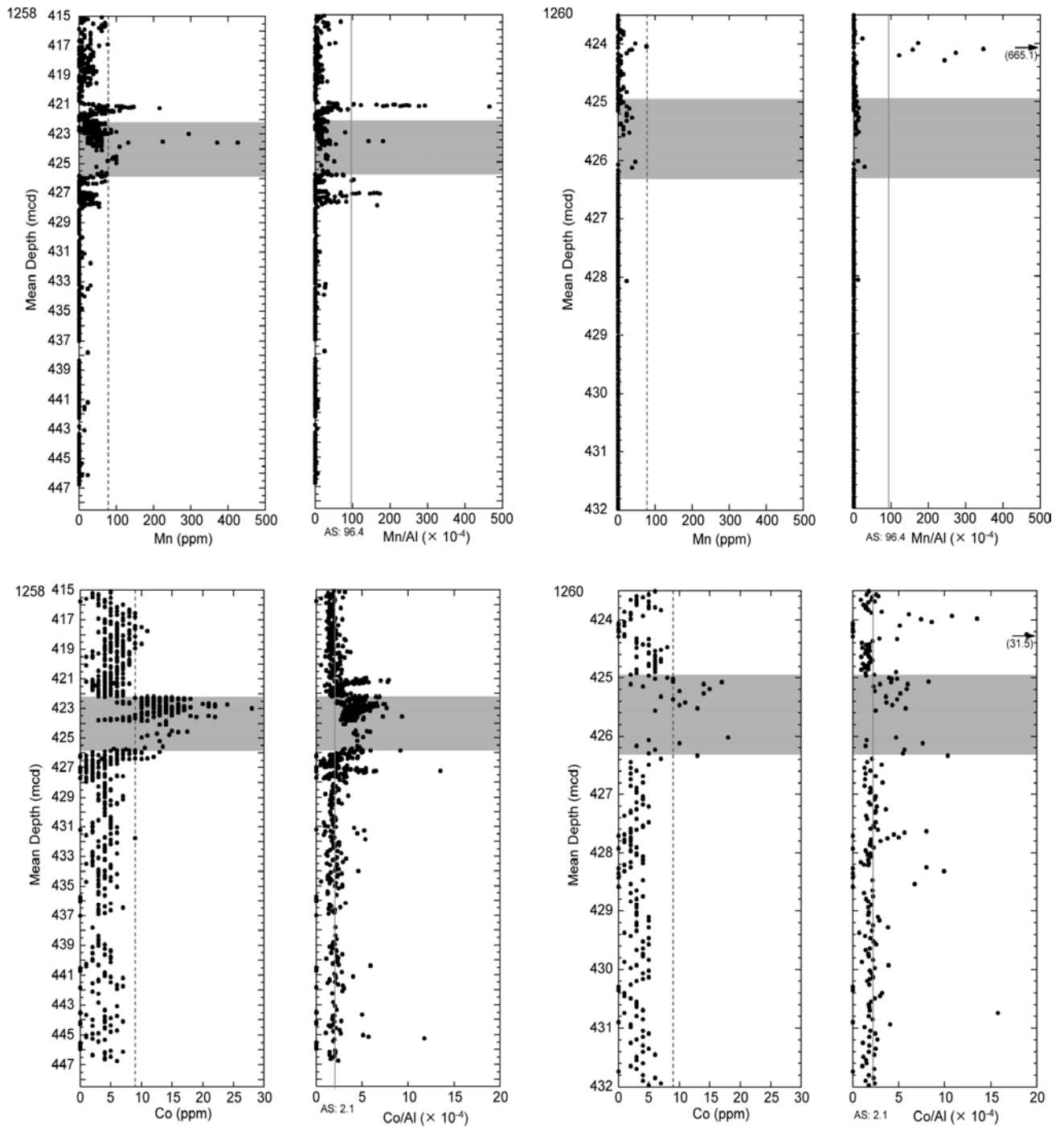


Figure 4.9 Depth-profiles for Mn, Mn/Al, Co and Co/Al for Cenomanian/Turonian black shales at Site 1258 and Site 1260. Grey: OAE 2; grey solid line: element/Al ratio of 'average shale' (AS) (Wedepohl, 1971, 1991); dashed line: quantification limit (see Appendix A4.1).

At Demerara Rise elevated Mn/Al ratios are only seen in distinct horizons with high carbonate contents below (Site 1258) and above OAE 2 (Site 1258 and Site 1260). We therefore relate these Mn/Al peaks in C/T black shales to carbonate diagenesis. There is no correlation to Fe_T/Al ratios that would point to simultaneous mobilization from suboxic sediments and precipitation under sulfidic conditions as described by Lyons and Severmann (2006).

The higher Mn contents at Site 1258 might originate from the position in greater paleo water depths. Assuming the existence of an OMZ, Site 1258 might be located below the OMZ where during times of weaker anoxia, Mn(IV)-bearing phases reached the sediment and later were transformed into mixed Ca-Mn-carbonates.

Within OAE 2, Mn values show a high variability as described above. As all OAE 2 samples with higher Mn/Al ratios are located near the presumed “ash-layers”, the import of Mn(IV)-bearing phases could also be attributed to the different detritus composition (average Mn contents: 332 ppm compared to 17 ppm mean value for all C/T black shales of this study, see Appendix A4.2c). If Mn was released to the pore space after burial, Mn concentrations in the pore water within these “ash-layers” and adjacent intervals might have been higher. Because TIC contents are not elevated (1.7-8.1 %, mean value 5.6 %), precipitation of Mn-carbonate is questionable in these intervals.

Besides increased availability of dissolved Mn, pore volume may influence the potential for precipitation of Mn-bearing minerals during diagenesis. The carbonate-rich layers with elevated Mn contents are visually affected by carbonate diagenesis, e.g., precipitation of calcite (Erbacher et al., 2004). Increased pore volume, either through the occurrence of foraminiferal packstones or of “ash-like” layers, may have favored authigenic formation of Mn-bearing minerals.

Cobalt

Under oxygen depleted conditions like in an OMZ, Mn-and Fe-oxi/hydroxide-associated Co would be mobilized and transported away. In Gulf of California upwelling sediments (Brumsack, 1989) or the Peruvian margin (Böning et al., 2004), Co is depleted similar to Mn. In contrast to Mn, which forms stable sulfides only under very special conditions, Co precipitates as CoS when free hydrogen sulfide is present (Heggie and Lewis, 1984; Gendron et al., 1986).

The profiles of Co concentration (Fig. 4.9) at Site 1258 and Site 1260 show that nearly all sediments below and above OAE 2 are characterized by very low Co concentrations (often below the quantification limit of 9 ppm). Co/Al ratios for Demerara Rise C/T black shales

below and above OAE 2 are similar to the Co/Al ratio of average shale (2.1×10^{-4} ; Wedepohl, 1971, 1991). Within OAE 2, Co/Al ratios increase to a mean value of 4.4×10^{-4} at both sites with maximum values of 9.4×10^{-4} at Site 1258 and 10.3×10^{-4} at Site 1260.

Thus, the Co distribution is quite similar to the Fe distribution: Under reducing conditions the constant average shale-like value of Co/Al rather indicates fixation of dissolved Co as sulfide than preservation of particulate Co-bearing (hydr)oxide phases. As the Co increase during OAE 2 requires an additional Co-source during deposition, we assume a transport mechanism analogous to Fe from nearshore areas, where reducing but non-sulfidic conditions mobilize additional Co, which is then fixed under truly euxinic conditions further offshore.

Zinc

Cretaceous black shales are known to be highly enriched in Zn. Brumsack (2006) gives a Zn/Al ratio 459×10^{-4} as a C/T mean value (AS = 10.7×10^{-4} ; Wedepohl 1971, 1991). Hetzel et al. (2006), found 370×10^{-4} as a mean value of the Cretaceous black shales of Demerara Rise (all sites). The high-resolution study of the C/T interval presented here reveals considerable variability in Zn/Al ratios (Fig. 4.10). The depth profile of Site 1258 shows Zn/Al ratios in the same order of magnitude as described by Hetzel et al. (2006) below and above OAE 2 (mean values of 316.0×10^{-4} and 355.9×10^{-4} , respectively; see Table 4.3). The maxima below and above OAE 2 correspond to maxima in the S_{AVS} profile, indicating the presence of metal sulfides other than pyrite. At Site 1260, the Zn/Al ratios are slightly higher below OAE 2 (mean value 581.4×10^{-4}), while above OAE 2 ratios are lower (mean value 251.1×10^{-4}). At both sites a distinct decrease in Zn/Al ratios during OAE 2 can be observed (mean values 48.1×10^{-4} at Site 1258 and 154.0×10^{-4} at Site 1260).

Addressing the distribution patterns of Co and Zn discussed above we found two different enrichments patterns for these trace metals, both known to be enriched in C/T black shales (Brumsack, 2006) by forming stable sulfides. Whereas C/T black shales from Demerara Rise are enriched in Co during OAE 2, but not before and thereafter, the enrichment in Zn is present throughout the studied interval and displays a rapid decrease in the degree of enrichment within OAE 2.

Molybdenum and Vanadium

Overall, element/Al ratios of both Mo and V show clear enrichments in C/T black shales of Demerara Rise (mean Mo/Al = 28.2×10^{-4} , AS = 0.15×10^{-4} , mean V/Al = 443.8×10^{-4} , AS = 14.7×10^{-4} ; Wedepohl 1971, 1991; Fig. 4.10). Mo and V are relatively unreactive in oxic

seawater, but are known to be concentrated in sediments overlain by anoxic waters (Brumsack and Gieskes, 1983; Brumsack, 1986).

Vanadium in oxic seawater should be present as V(V). Under moderately reducing conditions, V(IV) forms vanadyl ions (VO^{2+}) that may be removed to the sediment by surface adsorption processes or by formation of organometallic ligands (Emerson and Huested, 1991; Morford and Emerson, 1999). Under more reducing conditions, the presence of free H_2S released by bacterial sulfate reduction causes V to be further reduced to V(III), which can be taken up by geoporphyrins or be precipitated as the solid oxide V_2O_3 or hydroxide $\text{V}(\text{OH})_3$ phase (Breit and Wanty, 1991; Wanty and Goldhaber, 1992).

The stable oxidation state of Mo in oxic seawater is Mo(VI). Reduction of Mo(VI) to Mo(IV) and authigenic enrichment in sediments occur under euxinic conditions (Crusius et al., 1996) possibly via diffusion across the sediment-water interface (Emerson and Huested, 1991). Helz et al. (1996) suggested a threshold concentration for H_2S , above which Mo is transformed to particle-reactive thiomolybdates that are scavenged by forming bonds with metal-rich particles, sulfur-rich OM and pyrite.

Tribovillard et al. (2006) addressed the reconstruction of the redox environment of sediments overlain by oxygen-depleted waters via the combined use of different trace metals. While V is reduced and can accumulate under denitrifying conditions, Zn and Mo are enriched mainly under sulfate-reducing conditions. Thus, in the case of V enrichment without Mo enrichment, the authors postulate suboxic/anoxic depositional conditions without free H_2S , whereas sediments exhibiting concurrent enrichments in V and Mo reflect euxinic conditions at the sediment-water interface or in the water column (Algeo and Maynard, 2004; Tribovillard et al., 2004). As the C/T black shales of Demerara Rise are clearly enriched in both, Mo and V, this simplified distinctive feature would hint to euxinic conditions for the depositional environment.

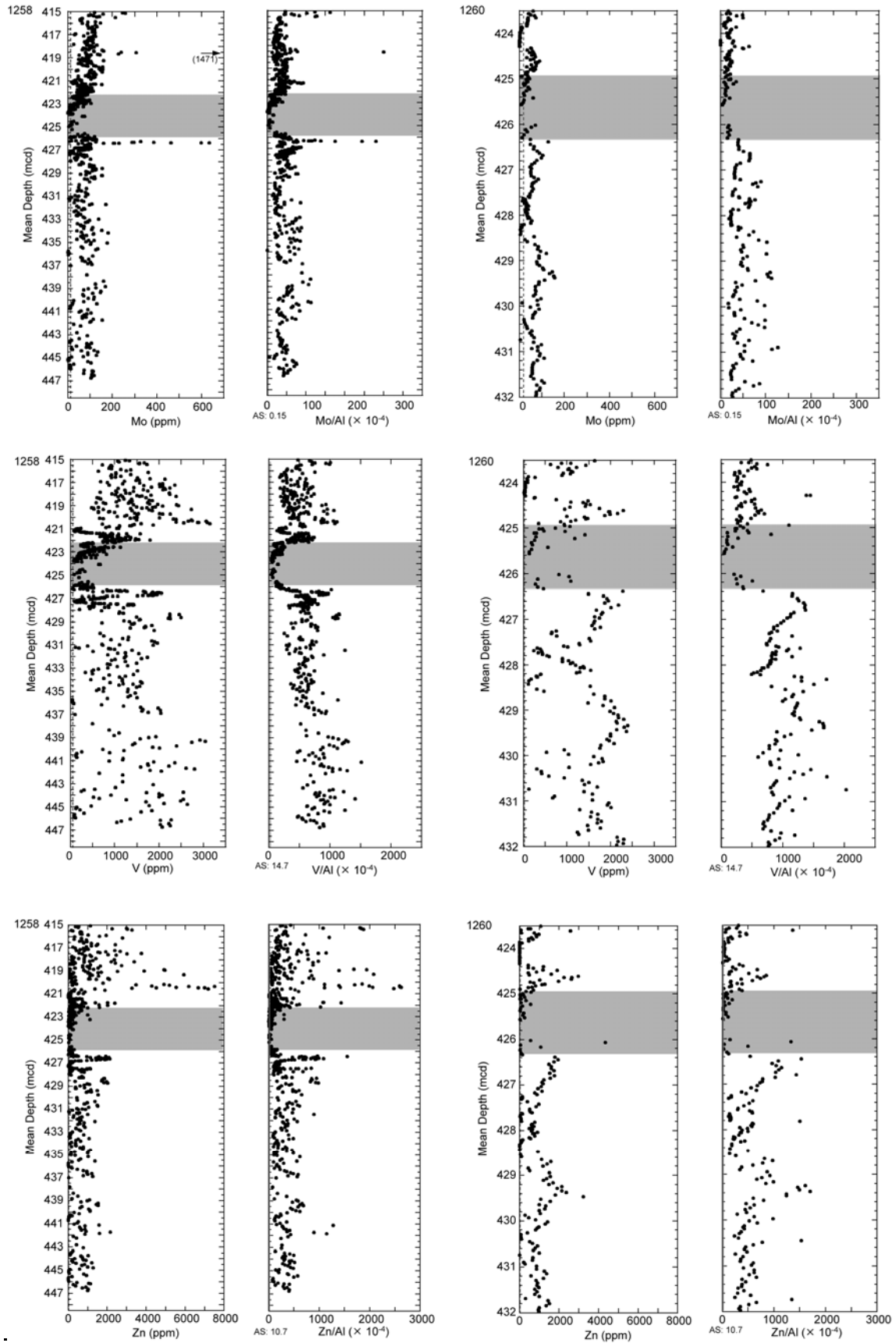


Figure 4.10 Depth-profiles for Mo, Mo/Al, V, V/Al, Zn and Zn/Al for Cenomanian/Turonian black shales of Site 1258 and Site 1260. Grey: OAE 2; grey solid line: element/Al ratio of 'average shale' (AS) (Wedepohl, 1971, 1991); dashed line: quantification limit (see Appendix A4.1).

From positive correlations of Mo with sulfurized OM in ancient marine black shales, Tribovillard et al. (2004) emphasized Mo trapping by sulfur-rich OM. No correlation of Mo with pyrite accumulation could be found. Instead, the reduced availability of reactive Fe may favor Mo accumulation, as significant OM sulfurization is only possible when reactive iron is limited. As shown above, we find iron-limitation in most of the studied intervals and an enhanced OM sulfurization during OAE 2. Following the arguments of Tribovillard et al. (2004), we would expect an increase in Mo enrichment during OAE 2. Instead, a clear decrease is visible, implying that other factors influenced Mo accumulation as well. Probably, the concentration of dissolved sulfide in the water column that affected aqueous Mo speciation may have influenced the efficiency of Mo fixation (Neubert et al., 2008).

For anoxic basins, Emerson and Huested (1991) showed that the concentrations of Mo and V in the water column are usually lower than in oxic seawater due to their uptake into highly anoxic sediments. As no systematic relationship between the deep-water Mo or V concentrations and H_2S content was found, the authors concluded that concentrations of Mo and V are rather controlled by their flux to sediments and water renewal from outside the basins than by changes in water column anoxia. Algeo and Lyons (2006) analyzed Mo-TOC relationships in sediments from anoxic environments characterized by different degrees of hydrographic restriction. In silled anoxic basins, decreasing Mo/TOC ratios with increasing degree of restriction imply that sedimentary Mo concentrations were controlled by Mo availability from the overlying water column, and thus by resupply of Mo via deepwater renewal. Algeo and Lyons (2006) termed this drawdown of Mo concentrations in deep water during stagnant intervals the “basin reservoir effect”.

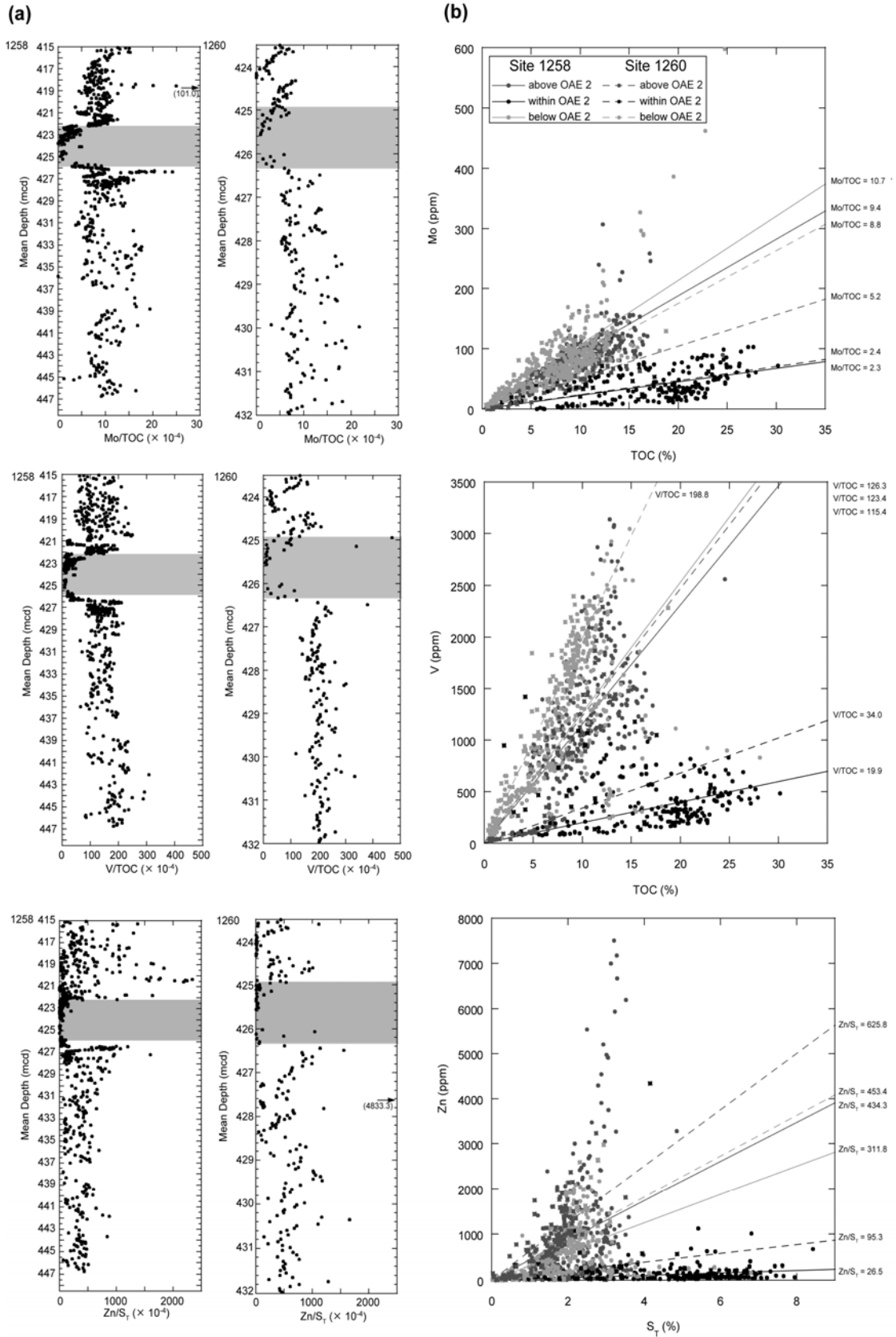


Figure 4.11 (a) Depth-profiles for Mo/TOC, V/TOC and Zn/S_T for Cenomanian/Turonian black shales at Site 1258 and Site 1260. Grey: OAE 2. (b) X-Y-Plots for Mo versus TOC, V versus TOC and Zn versus S_T. Slopes of regression lines (solid for Site 1258, dashed line for Site 1260) are given in units of 10^{-4} .

Figure 4.11 shows Mo/TOC profiles as well as X-Y-plots of Mo versus TOC. Mo/TOC values vary between $\sim 5 \times 10^{-4}$ and $\sim 20 \times 10^{-4}$ for sediments deposited before OAE 2. Similar to Mo/Al, Mo/TOC ratios decrease rapidly at the onset of OAE 2, staying low during OAE 2, before a slight increase is visible after OAE 2. The slopes of regression lines for X-Y-plots of Mo versus TOC give similar low Mo/TOC ratios for samples within the OAE 2 interval at both sites (2.3×10^{-4} at Site 1258 and 2.4×10^{-4} at Site 1260). These values are even lower than the value of $\text{Mo/TOC} = 4.5 \pm 1 \times 10^{-4}$ reported by Algeo and Lyons (2006) for the Black Sea. Regression lines for samples deposited before OAE 2 give Mo/TOC values of 10.7×10^{-4} at Site 1258 and 8.8×10^{-4} at Site 1260. The increase in Mo/TOC ratios after OAE 2 is less pronounced at Site 1260 ($\text{Mo/TOC} = 5.2 \times 10^{-4}$) than at Site 1258 ($\text{Mo/TOC} = 9.4 \times 10^{-4}$).

As V burial under anoxic conditions is also known to be linked to OM (Breit and Wanty, 1991; Emerson and Huested, 1991; Morford and Emerson, 1999), we analyzed V/TOC ratios analogues to Mo and Zn/S_T ratios as Zn is known to form stable sulfides if H₂S is present (Jacobs et al., 1985) (Fig. 4.11). Both, V and Zn, show the distinct decrease relative to TOC and S_T during OAE 2 pointing to decoupling of OM burial, sulfidization and TM availability during OAE 2.

Figure 4.12 shows the enrichment factors relative to average shales for Fe_T, Co, Mo, V and Zn for Sites 1258 and 1260, and for C/T mean values (Brumsack 2006). The enrichment factor for Fe_T is ~ 1 at Site 1258 below and above the CTBE and at Site 1260 below the CTBE, indicating Fe/Al ratios similar to average shale. The observed enrichment in sediments of Site 1260 above the CTBE may be an artefact owing to normalization of values close to the Fe and Al detection limit in carbonate-rich sediments (see Fig. 4.4, ~ 424 mcd). As described above, the distribution patterns of Co are similar to those of Fe_T. Zn, Mo and V show similar enrichment patterns, with highest values below, intermediate values above, and lowest values within OAE 2. At Site 1258, Mo, V and Zn are enriched to similar degrees below and above OAE 2. The decline of enrichment during OAE 2 is more pronounced than for Site 1260. Overall, the degrees of enrichment of Mo, V and Zn are similar to other C/T sediments listed by Brumsack (2006). Only the sediments deposited during OAE 2 at Site 1258 are characterized by less pronounced Mo, V and Zn enrichments relative to other C/T black shales.

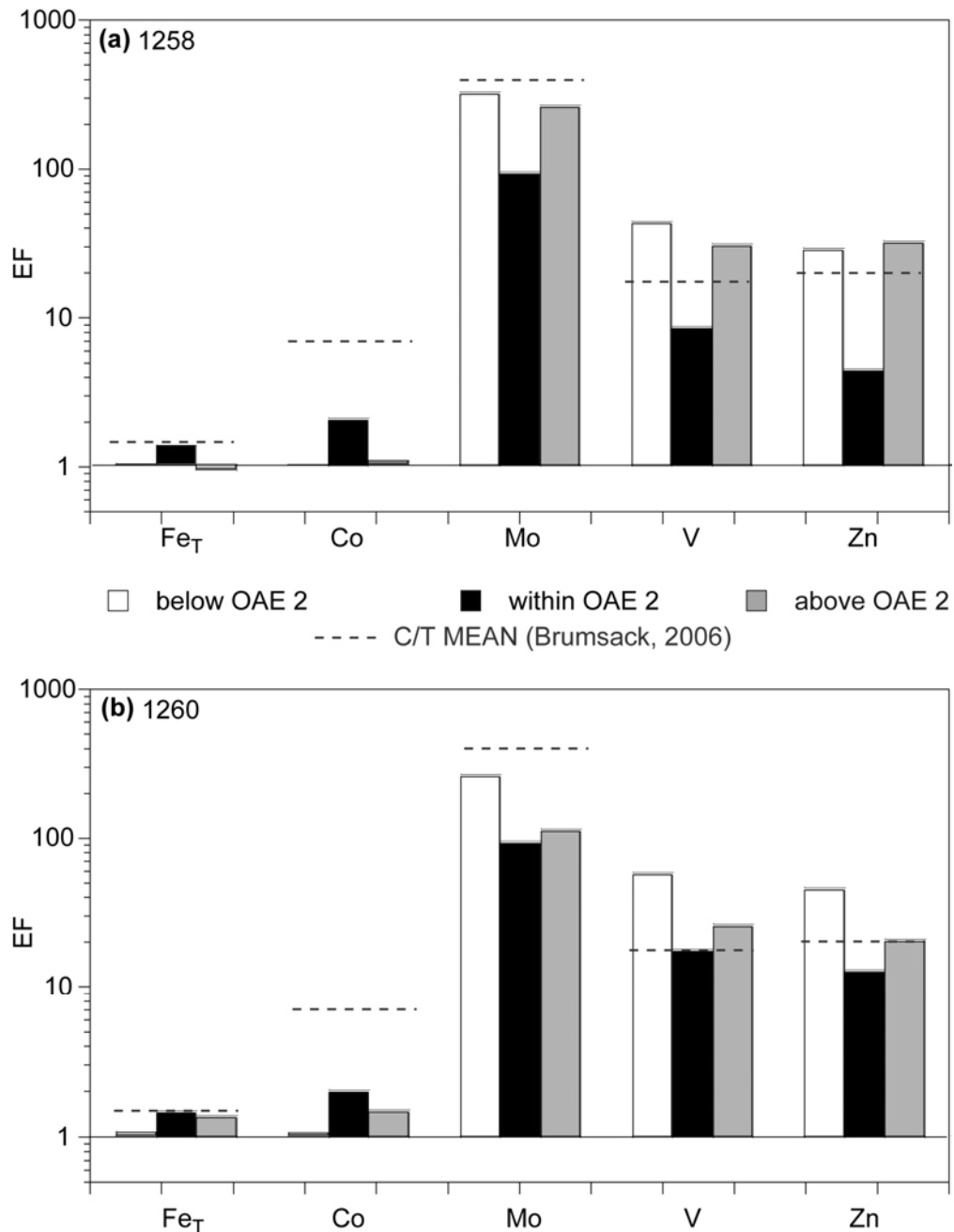


Figure 4.12 Mean enrichment factors (EF) of Fe_T, Co, Mo, V and Zn relative to 'average shale' (AS) (Wedepohl, 1971, 1991) for Cenomanian/Turonian black shales at Demerara Rise. EF = element/Al(sample)/element/Al(AS). (a) Site 1258, (b) Site 1260. Dashed lines: EF for C/T mean values (Brumsack, 2006).

In summary, we suggest two important mechanisms affecting Fe_T and trace metal distribution patterns in C/T black shales at Demerara Rise:

Locally, Mn depletion hints to reducing conditions in an open-marine environment, e.g. an OMZ. Fe_T and Co enrichments during OAE 2 indicate an expansion of this OMZ. As their seawater concentrations are generally low, at least part of the sedimentary Fe_T and Co enrichments during OAE 2 must be due to mobilization from oxygen-depleted nearshore

sediments. Whereas Fe and Co are conveyed along with Mn in suboxic waters, they will be precipitated as sulfides when hydrogen sulfide is present in the water column.

Regarding the source for TMs enriched in TOC-rich sediments, Mo and V are highly concentrated in seawater, and they may have become enriched in the sediment via diffusion from the water column. As extreme Zn enrichments in Cretaceous black shales (compared to recent TOC-rich sediments) require an additional Zn source, a higher seawater concentration of Zn due to hydrothermal input during the Cretaceous seems likely (Arthur et al., 1988; Brumsack, 2006). Under such conditions seawater might again be the dominating source for Zn enrichments. Thus, on a larger if not global scale, we emphasize a decline in seawater TM availability during OAE 2, revealed by the decrease in Mo, V and Zn enrichment.

Taking seawater as the dominant source for Mo, V and Zn, the depletion in TM/Al may reflect the global onset of black shale deposition during OAE 2 and the rapid drawdown of the seawater TM reservoir by the spreading of euxinic depositional areas. In the modern oceans, only 0.2% of the seafloor are hypoxic (Helly and Levin, 2004), while during the Cretaceous, particularly during OAE 2, such conditions were much more wide-spread. Kuypers et al. (2002) pointed out that the proto-North Atlantic Ocean was one of the main sites of carbon burial during OAE 2. Paleogeographic reconstructions show that the proto-North Atlantic Ocean was a restricted area with major seawater supply coming from the Tethys only. The black shales deposited in the Tethys and in the proto-North Atlantic Ocean during OAE 2 (e.g., Kuhnt et al., 1990) definitely formed a significant TM sink. We therefore assume that the decline in TM enrichment seen at Demerara Rise indicates a drawdown of TMs from seawater, similar to the “basin reservoir effect” described by Algeo and Lyons (2006).

Productivity proxies

Figure 4.13 show the enrichments factors for some elements used for approximation of paleoproductivity.

Phosphorus belongs to the essential nutrient elements controlling marine primary productivity (e.g., Broecker and Peng, 1982). High concentrations are found in recent upwelling sediments pointing towards enhanced nutrient supply and resulting high bioproductivity (e.g., Böning et al., 2004). Incorporated into organic material (e.g., in marine phytoplankton; Redfield, 1958) P is deposited in the sediment, where it is preferentially remineralized relative to TOC and liberated to the pore water and maybe forming authigenic phosphatic precipitates. Under oxygen-depleted conditions, when potential phosphate

scavengers such as Fe(hydr)oxides are reduced and not available, organic P release in sediments is even higher. Therefore, in TOC-rich sediments deposited under anoxic conditions the TOC/P ratio should be increased (Ingall et al., 1993 and references therein). Nederbragt et al. (2004) concluded from measurements of total phosphorus and organic carbon in C/T sediments from the Tarfaya Basin, Morocco, that the main underlying mechanism that allowed and sustained enhanced carbon burial during the mid-Cretaceous was a perturbation of the oceanic phosphorus cycle. More effective regeneration of organic phosphorus under anoxic conditions can lead to an increase in dissolved oceanic phosphate, which in turn stimulates surface-water productivity (Ingall et al., 1993; Bjerrum and Canfield, 2002; Mort et al., 2007). The Shipboard Scientific Party (2004) describes the presence of P-rich concretions in black shales of Demerara Rise. Figure 4.13 shows a clear enrichment of P relative to average shale in the sections studied. This points towards a high primary productivity comparable to coastal upwelling areas. The minor enrichment during OAE 2 hints to a decreasing nutrient supply or to partial loss of P during at least periodically truly anoxic conditions in comparison to the situation before and thereafter.

The non-lithogenic excess barium has been interpreted as a paleoproxy for bio-productivity (Schmitz, 1987; Dymond et al., 1992; Paytan et al., 1996). These biogenic barites (BaSO_4) (Bishop, 1988; Bertram and Cowen, 1997; Paytan et al., 2002; Bernstein and Byrne, 2004) are only stable under seawater sulfate concentrations (Church and Wohlgemuth, 1972). Due to the microbial sulfate reduction in TOC-rich sediments, barite may be dissolving, leading to the mobilization of Ba (Brumsack and Gieskes, 1983; McManus et al., 1998; Eagle et al., 2003). Authigenic barite may precipitate at the top of the sulfate-depletion zone forming diagenetic barite fronts within or above TOC-rich strata (Torres et al., 1996; Bréhéret and Brumsack, 2000).

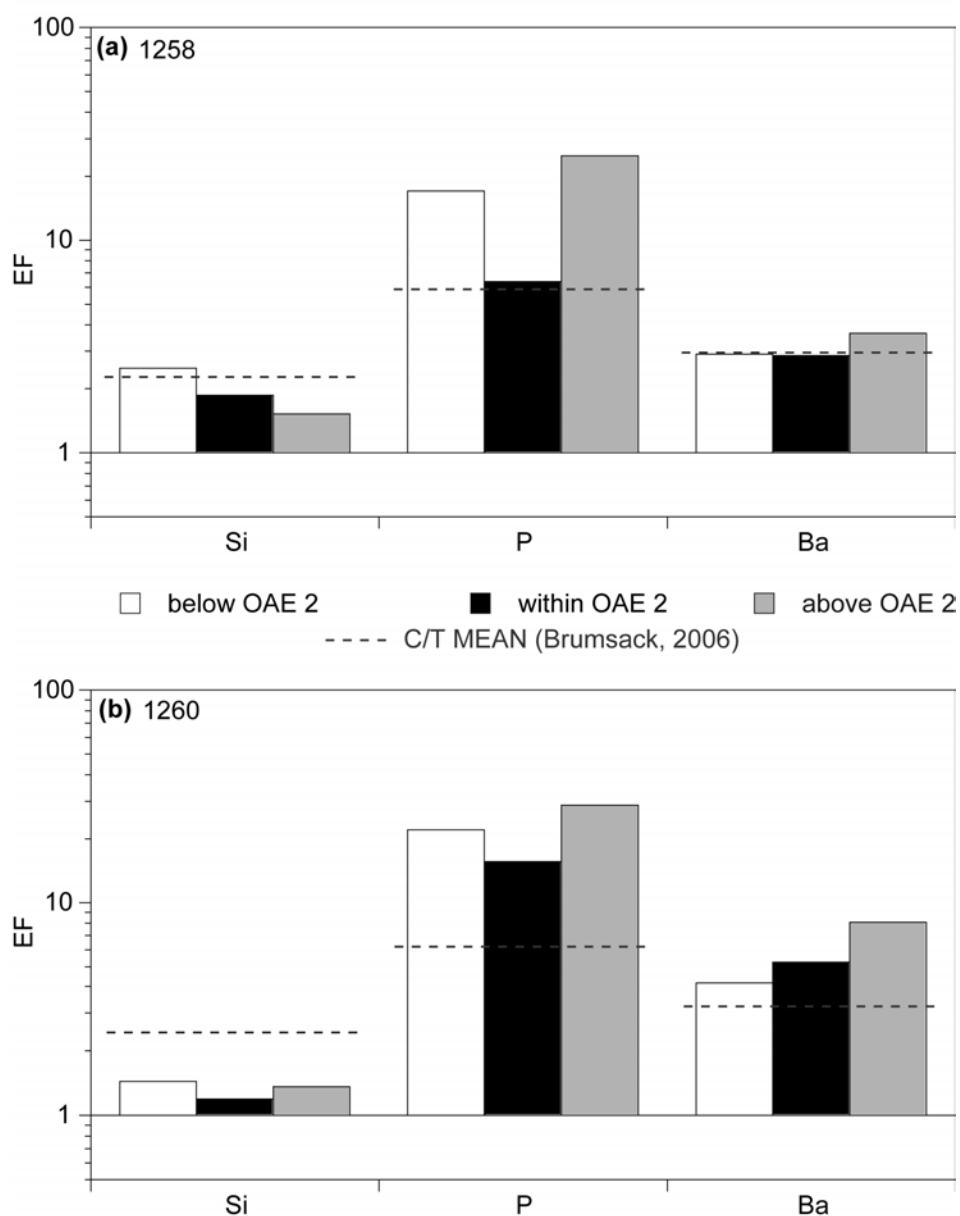


Figure 4.13 Mean enrichment factors (EF) of Si, P and Ba relative to 'average shale' (AS) (Wedepohl, 1971, 1991) for Cenomanian/Turonian black shales at Demerara Rise. EF = element/Al(sample)/element/Al(AS). (a) Site 1258, (b) Site 1260. Dashed lines: EF for C/T mean values (Brumsack, 2006).

Hetzel et al. (2006) found the highest Ba/Al above the Cretaceous black shales, while within the black shales Ba/Al ratios are still high despite of the present absence of sulfate in the pore waters (Erbacher et al., 2004). Arndt et al. (2006) showed in a transport-reaction model that not only OM degradation but also anaerobic oxidation of methane (AOM) above the black shales of Demerara Rise influences sulfate availability and therefore the remobilization of biogenic barium. These authors further showed that temporal dynamics of degradation processes caused various shifts of the barite precipitation zone during burial,

thus inhibiting the formation of an authigenic barite front or causing the dissolution of earlier formed fronts.

Figure 4.13 shows an enrichment of Ba similar to the C/T mean values from Brumsack (2006). This enrichment indicates elevated primary productivity during deposition. But a large fraction of former barite may have been remobilized and formed diagenetic barites above the black shales. For this reason the use of Ba as a paleoproxy on a quantitative level (Dymond et al., 1992) for Cretaceous settings in such an environment is highly questionable.

Paleoenvironmental implications and comparison with other paleoproxies

The paleoconditions for the depositional environment based on geochemical arguments are summarized in Figure 4.14. From analysis of TOC-Fe-S systematics and TM distribution patterns we can conclude that a depositional environment with an expanded oxygen-minimum-zone (OMZ) similar to coastal upwelling areas existed before the onset of OAE 2 (Fig 4.14a). Enrichments of TOC, P and Ba hint to enhanced bioproductivity. The depletion in Mn and enrichment in redox-sensitive TM indicate at least suboxic conditions. During OAE 2, an increase in the Fe_P/Fe_T ratio points to the rapid development of truly euxinic conditions with free hydrogen-sulfide in the water column (Fig. 4.14b). This is confirmed by a rise in Fe_T/Al and Co/Al ratios. An expansion of the OMZ, possible due to intensified paleoproductivity and/or sea level rise, leads to mobilization of Fe and Co from nearshore sediments. Thus, enrichment in Fe_T and Co in the sediments is possible, when hydrogen sulfide is present in the water column for sulfide precipitation.

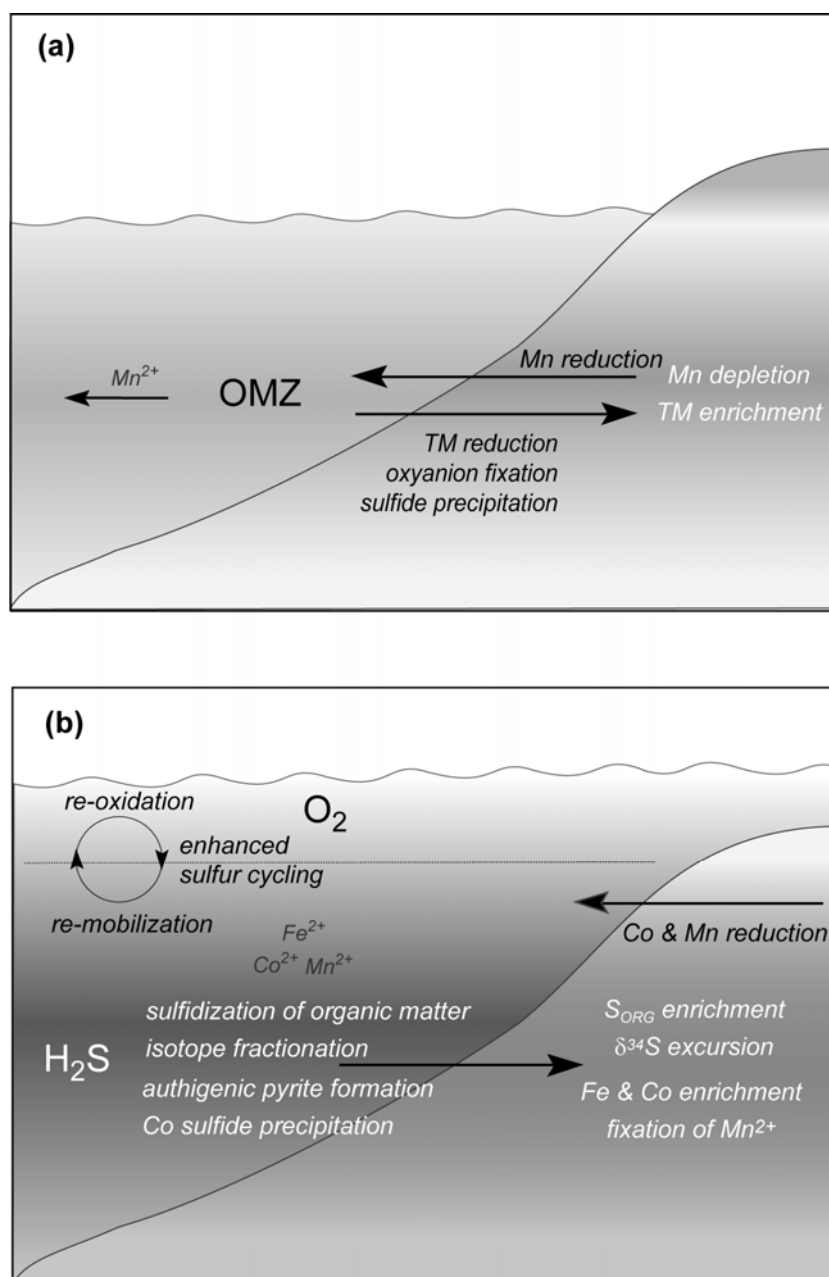


Figure 4.14 Simplified scheme of paleoenvironmental conditions as deduced from geochemical data before / after (a) and during (b) OAE 2.

Musavu-Moussavou and Danelian (2006) analyzed the radiolarian abundances across OAE 2 at Site 1258 and Site 1261. The presence of radiolarians at Site 1258 and to a lesser degree at the shallower Site 1261 below OAE 2 indicates, at least periodically, oxygenated surface waters. During OAE 2, the absence of radiolarians at Site 1261 and only rare occurrence at Site 1258 hint at the intensification of euxinic conditions, while above OAE 2 radiolarians are present again, this time with higher abundances at Site 1261 than at Site 1258. In marine sediments Si derives either from the terrigenous detritus as aluminosilicates, quartz or from a biogenous opal from siliceous plankton (diatoms or

radiolarians; Brumsack, 1989). Assuming an 'average shale'-like terrigenous background for C/T-black shales of Demerara Rise the enrichment in Si indicates the presence of additional Si other than present in the clay component. Owing to the absence of heavy mineral related elements Hetzel et al. (2006) could exclude the presence of excess quartz in Cretaceous black shales of Demerara Rise and instead assumed a biogenous origin for the excess silica. We suppose that the enrichment in Si shown in Figure 4.13 represents Si derived from radiolarian tests. The general pattern with slight enrichment of Si below and above OAE 2 fits well with the findings of Musavu-Moussavou and Danelian (2006).

Hardas and Mutterlose (2007) analyzed the calcareous nannofossil assemblages of Site 1258 and 1260. They found highest absolute abundances below OAE 2 at both sites. During OAE 2 the absolute abundance decreases and also the species assemblages change. From the now dominating species the authors conclude a higher bio-productivity. Instead of cooler temperatures, as suggested by Forster et al. (2007) at Site 1260 within OAE 2, Hardas und Mutterlose (2007) postulate a slight increase in SSTs. They suggest a possible breakdown of water column stratification and thus a shallowing of the nutricline. This fits into a picture of a euxinic water column and the decline in total abundance of nannofossils.

Regarding the redox conditions at the sediment-water interface Friedrich et al. (2006) suggest a strengthening of the OMZ during OAE 2, based on the benthic foraminifera assemblage at Sites 1258 - 1261.

Below OAE 2 the authors suggest anoxic to sometimes slightly dysoxic bottom-water conditions at the shallower sites, whereas for the deepest Site 1258 more oxygenated but still dysoxic bottom waters were proposed, possibly due its position below the OMZ. During OAE 2, the total absence of benthic foraminifera hints to anoxic conditions, but short-term re-populations may indicate bottom-water oxygenation. The authors find these events in the lower third of OAE 2 at all sites studied. Forster et al. (2007) correlate these occurrences with a cooling event at Site 1260. Benthic foraminiferal assemblages indicate continued oxygen-deficient bottom-water conditions following OAE 2 with the exception of one short-term increase in oxygenation immediately above the OAE 2. After ~0.5 Ma more oxygenated bottom-water masses are postulated.

From geochemical data we suppose euxinic conditions during OAE 2. The presence of benthic foraminifera indicates that the euxinic conditions may not have been permanent. Evidence for the short-term complete re-oxidation of the bottom water is not given by the geochemical data, although peaks in Mn/Al several decimeters above the repopulation

events of benthic foraminifera at Site 1258 may indicate a shallowing of the OMZ thus introducing Mn to the sediment.

Addressing the same questions by different paleo-proxies may lead to different results under certain circumstances. If sedimentation rates are low, and the amount of sample material required for certain analyses comprises a time-span in which several changes in depositional environment may have occurred, the chemical result would be an integrated signal due to homogenization of the sample. In contrast, analyzing fossils might give only a snapshot of paleoconditions. Contrasting results for the same intervals may therefore hint to unstable conditions. Forster et al. (2007) suggest such unstable conditions during OAE 2 at Site 1260. From our point of view a closer look is necessary, if and to what extent the presence of the “ash-like” layers, which were omitted here, may influence directly or by diagenetic effects results obtained in close vicinity to these layers.

Summary and Conclusions

From geochemical analysis the following conclusions regarding the depositional environment of C/T black shales at Demerara Rise during OAE 2 can be drawn:

Elevated Fe_P/Fe_T , Fe_T/Al , and Co/Al values within the OAE 2 confirm euxinic conditions but, at the same time, require a zone where reducing but non-sulfidic conditions enable Fe and Co mobilization in oxygen depleted nearshore sediments.

The existence of an expanded oxygen-minimum-zone (OMZ) is demonstrated by extremely low Mn/Al ratios. Elevated Mn/Al ratios are only seen in distinct horizons. Overgrowth of Mn-carbonates on pre-existing carbonate tests seems to be possible under euxinic conditions and elevated pore water alkalinities.

Mo/Al, V/Al and Zn/Al ratios are generally high throughout the investigated sequence, but a significant depletion is notable exactly during OAE 2. The decrease in enrichment for these seawater derived trace metals may reflect the global onset of black shale deposition during OAE 2 and the rapid drawdown of the seawater TM reservoir by the enlargement of euxinic depositional areas.

The enrichment in phosphorus and barium points towards high bio-productivity like in recent upwelling areas. Due to diagenesis driven by the reducing conditions a quantitative interpretation is not possible.

Besides fixation of sulfide as iron sulfide, organic matter acts as an important sulfur trap during early diagenesis. During OAE 2 the amounts of both, pyrite and organically bound sulfur increase. A negative shift in the stable sulfur isotope curve during OAE 2 indicates

changes in the overall sulfur cycle, similar to results observed previously in the Tarfaya Basin.

According to the assumed high bioproductivity and the depletion in Mn, the C/T black shales of Demerara Rise are compatible with a situation encountered in modern coastal upwelling areas within an expanded OMZ. During OAE 2 a more euxinic situation was established with the presence of free hydrogen sulfide in the water column.

Acknowledgements

We would like to thank the crew and scientific party of ODP Leg 207 for their kind support. This research used samples and / or data provided by the Ocean Drilling Program (ODP). ODP is sponsored by the U.S. National Science Foundation (NSF) and participating countries under management of Joint Oceanographic Institutions (JOI), Inc.. This contribution has benefited from the thorough reviews by Tim Lyons and an anonymous reviewer. AH is grateful to Astrid Forster and Christian März for valuable discussions, Knut Bernhardt for performing time series analysis and Imke Notholt for EDX assistance. MEB wishes to thank Andrea Schipper for technical assistance and E. Clapton, N. Futado, C. Hynde, and J. Stone for acoustical inspiration during work on the manuscript. This study was funded by Deutsche Forschungsgemeinschaft (IODP-SPP grants BR 775/16+17; BO 1584/2) and by Max Planck Society, Germany.

References

- Algeo, T.J., Lyons, T.W., 2006. Mo-total organic carbon covariation in modern anoxic marine environments: implications for analysis of paleoredox and paleohydrographic conditions. *Paleoceanography* 21, PA1016.
- Algeo, T.J., Maynard, J.B., 2004. Trace element behavior and redox facies in core shales of the Upper Pennsylvanian Kansastype cyclothems. *Chemical Geology* 206(3-4), 289-318.
- Arndt, S., Brumsack, H.-J., Wirtz, K.W., 2006. Cretaceous black shales as active bioreactors: A biogeochemical model for the deep biosphere encountered during ODP Leg 207 (Demerara Rise). *Geochimica et Cosmochimica Acta* 70(2), 408-425.
- Arthur, M.A., Dean, W.E., Pratt, L.M., 1988. Geochemical and climatic effects of increased marine organic carbon burial at the Cenomanian/Turonian boundary. *Nature* 335(6192), 714-717.
- Arthur, M.A., Schlanger, S.O., Jenkyns, H.C., 1987. The Cenomanian/Turonian Oceanic Anoxic Event, II. Palaeoceanographic controls on organic-matter production and preservation. In: Brooks, J., Fleet, A.J. (Eds.), *Marine Petroleum Source Rocks*. Geological Society, London. Special Publication 26, 401-420.
- Berner, R.A., Raiswell, R., 1983. Burial of organic carbon and pyrite sulfur in sediments over Phanerozoic time: a new theory. *Geochimica et Cosmochimica Acta* 47(5), 855-862.

- Bernstein R.E., Byrne R.H., 2004. Acantharions and marine barite. *Marine Chemistry* 86(1-2), 45-50.
- Bertram, M.A., Cowen, J.P., 1997. Morphological and compositional evidence for biotic precipitation of marine barite. *Journal of Marine Research* 55(3), 577-593.
- Bishop, J.K.B., 1988. The barite-opal-organic carbon association in oceanic particulate matter. *Nature* 332(6162), 341-343.
- Bjerrum, C.J., Canfield, D.E., 2002. Ocean productivity before about 1.9 Gyr ago limited by phosphorus adsorption onto iron oxides. *Nature* 417(6885), 159-162.
- Böning, P., Brumsack, H.-J., Böttcher, M.E., Schnetger, B., Kriete, C., Kallmeyer, J., Borchers, S.L., 2004. Geochemistry of Peruvian near-surface sediments. *Geochimica et Cosmochimica Acta* 68(21), 4429-4451.
- Böttcher, M.E., 1997. The transformation of aragonite to $\text{Mn}_x\text{Ca}_{(1-x)}\text{CO}_3$ solid-solutions at 20°C: An experimental study. *Marine Chemistry* 57(1-2), 97-106.
- Böttcher, M.E., Rinna, J., Warning, B., Wehausen, R., Howell, M.W., Schnetger, B., Stein, R., Brumsack, H.-J., Rullkötter, J., 2003. Geochemistry of sediments from the connection between the western and eastern Mediterranean Sea (Strait of Sicily, ODP Site 963). *Palaeogeography, Palaeoclimatology, Palaeoecology* 190, 165-194.
- Böttcher, M.E., Jørgensen, B.B., Kallmeyer, J., Wehausen, R., 2004. S and O isotope fractionation in the western Black Sea. *Geochimica et Cosmochimica Acta* 68(11), A345.
- Böttcher, M.E., Hetzel, A., Brumsack, H.-J., Schipper, A., 2006. Sulfur-iron-carbon geochemistry in sediments of the Demerara Rise. In: Mosher, D.C., Erbacher, J., Malone, M.J. (Eds.), *Proceedings of the Ocean Drilling Program, Scientific Results*, 207. College Station, TX (Ocean Drilling Program), 1-23.
- Bréhéret, J.G., Brumsack, H.-J., 2000. Barite concretions as evidence of pauses in sedimentation in the Marnes Bleues Formation of the Vocontian Basin (SE France). *Sedimentary Geology* 130(3-4), 205-228.
- Breit, G.N., Wanty, R.B., 1991. Vanadium accumulation in carbonaceous rocks. A review of geochemical controls during deposition and diagenesis. *Chemical Geology* 91(1-2), 83-97.
- Broecker, W.S., Peng, T.-H., 1982. *Tracers in the Sea*. Eldigio Press, Palisades, New York.
- Brumsack, H.-J., 1980. Geochemistry of Cretaceous black shales from the Atlantic Ocean (DSDP Legs 11, 14, 36, and 41). *Chemical Geology* 31, 1-25.
- Brumsack, H.-J., 1986. The inorganic geochemistry of Cretaceous black shales (DSDP Leg 41) in comparison to modern upwelling sediments from the Gulf of California. In: Summerhayes, C.P., Shackleton, N.J. (Eds.), *North Atlantic Paleocenography*. Geological Society, London. Special Publication 21, 447-462.
- Brumsack, H.-J., 1988. *Rezente, Corg-reiche Sedimente als Schlüssel zum Verständnis fossiler Schwarzschiefer*. Habilitationsschrift, Georg-August Universität Göttingen, Germany.
- Brumsack, H.-J., 1989. Geochemistry of recent TOC-rich sediments from the Gulf of California and the Black Sea. *Geologische Rundschau* 78(3), 851-882.
- Brumsack, H.-J., 2006. The trace metal content of recent organic carbon-rich sediments: implications for Cretaceous black shale formation. *Palaeogeography, Palaeoceanography, Palaeoecology* 232(2-4), 344-361.
- Brumsack, H.-J., Gieskes, J.M., 1983. Interstitial water trace-metal chemistry of laminated sediments from the Gulf of California, Mexico. *Marine Chemistry* 14(1), 89-106.
- Brumsack, H.-J., Heydemann, A., Kühn, V., Rachold, V., Usdowski, E., 1995. Geochemistry and mineralogy of Middle Aptian sediments from the Lower Saxony Basin, NW Germany. *Neues Jahrbuch für Geologie und Paläontologie, Abhandlungen* 196(2), 235-255.

- Brunner, B., Bernasconi, S.M., 2005. A revised isotope fractionation model for dissimilatory sulfate reduction in sulfate reducing bacteria. *Geochimica et Cosmochimica Acta* 69(20), 4759-4771.
- Calvert, S.E., Pedersen, T.F., 1993. Geochemistry of recent oxic and anoxic marine sediments: implications for the geological record. *Marine Geology* 113(1-2), 67-88.
- Canfield, D.E., Raiswell, R., Westrich, J.T., Reaves, C.M., Berner, R.A., 1986. The use of chromium reduction in the analysis of reduced inorganic sulfur in sediments and shale. *Chemical Geology* 54(1-2), 149-155.
- Church, T.M., Wohlgemuth, K., 1972. Marine Barite Saturation. *Earth and Planetary Science Letters* 15(1), 35-44.
- Cline, J.D., 1969. Spectrophotometric determination of hydrogen sulfide in natural waters. *Limnology and Oceanography* 14(3), 454-458.
- Crusius, J., Calvert, S., Pedersen, T., Sage, D., 1996. Rhenium and molybdenum enrichments in sediments as indicators of oxic, suboxic, and sulfidic conditions of deposition. *Earth and Planetary Science Letters* 145(1-4), 66-78.
- Dean, W.E., Arthur, M.A., 1989. Iron-sulfur-carbon-relationship in organic sequences, I. Cretaceous Western Interior Seaway. *American Journal of Science* 289, 708-743.
- Dymond, J., Suess, E., Lyle, M., 1992. Barium in deep-sea sediments: A geochemical proxy for paleoproductivity. *Paleoceanography* 7(2), 163-181.
- Eagle, M., Paytan, A., Arrigo, K.R., van Dijken, G., Murray, R.W., 2003. A comparison between excess barium and barite as indicators of carbon export. *Paleoceanography* 18(1), 1021.
- Emerson, S.R., Huested, S.S., 1991. Ocean anoxia and the concentrations of molybdenum and vanadium in seawater. *Marine Chemistry* 34(3-4), 177-196.
- Erbacher, J., Mosher, D.C., Malone, M.J., Shipboard Scientific Party, 2004. Proceedings of the Ocean Drilling Program, Initial Reports, 207. College Station, TX (Ocean Drilling Program), pp. 89.
- Erbacher, J., Friedrich, O., Wilson, P.A., Birch, H., Mutterlose, J., 2005. Stable organic carbon isotope stratigraphy across Oceanic Anoxic Event 2 of Demerara Rise, Western Tropical Atlantic. *Geochemistry, Geophysics, Geosystems* 6, Q06010.
- Forster, A., Schouten, S., Moriya, K., Wilson, P.A., Sinninghe Damsté, J.S., 2007. Tropical warming and intermittent cooling during the Cenomanian/Turonian oceanic anoxic event 2: sea surface temperature records from the equatorial Atlantic. *Paleoceanography* 22, PA1219.
- Fossing, H., Jørgensen, B.B., 1989. Measurement of bacterial sulfate reduction in sediments. Evaluation of a single-step chromium reduction method. *Biogeochemistry* 8(3), 205-222.
- Friedrich, O., Erbacher, J., 2006. Benthic foraminiferal assemblages from Demerara Rise (ODP Leg 207, western tropical Atlantic): possible evidence for a progressive opening of the equatorial Atlantic gateway. *Cretaceous Research* 27(3), 377-397.
- Friedrich, O., Erbacher, J., Mutterlose, J., 2006. Paleoenvironmental changes across the Cenomanian/Turonian Boundary Event (Oceanic Anoxic Event 2) as indicated by benthic foraminifera from the Demerara Rise (ODP Leg 207). *Revue de Micropaléontologie* 49(3), 121-139.
- Gale, A.S., Jenkyns, H.C., Kennedy, W.J., Corfield, R.M., 1993. Chemostratigraphy versus biostratigraphy: data from around the Cenomanian-Turonian boundary. *Journal of the Geological Society* 150(1), 29-32.
- Galimov, E., 2006. Isotope organic geochemistry. In: Bouillon, S., Böttcher, M.E. (Eds.), *Stable Isotopes in Biogeosciences*. *Organic Geochemistry* 37(10), 1200-1262.

- Gauthier, D.L., 1987. Isotopic composition of pyrite: relationship to organic matter type and iron availability in some North American Cretaceous shales. *Chemical Geology* 65, 293-303.
- Gendron, A., Silverberg, N., Sundby, B., Lebel, J., 1986. Early diagenesis of cadmium and cobalt in sediments of the Laurentian Trough. *Geochimica et Cosmochimica Acta* 50(1), 741-747.
- Gingele, F.X., Kasten, S., 1994. Solid-phase manganese in Southeast Atlantic sediments: Implications for the paleoenvironment. *Marine Geology* 121(3-4), 317-332.
- Hardas, P., Mutterlose, J., 2007. Calcareous nannofossil assemblages of Oceanic Anoxic Event 2 in the equatorial Atlantic: Evidence of an eutrophication event. *Marine Micropaleontology* 66(1), 52-69.
- Hartmann, M., Nielsen, H., 1969. $\delta^{34}\text{S}$ -Werte in rezenten Meeressedimenten und ihre Deutung am Beispiel einiger Sedimentprofile aus der westlichen Ostsee. *Geologische Rundschau* 58(2), 621-655.
- Hatch, J.R., Leventhal, J.S., 1992. Relationship between inferred redox potential of the depositional environment and geochemistry of the Upper Pennsylvanian (Missourian) Stark Shale Member of the Dennis Limestone, Wabaunsee County, Kansas, USA. In: Meyers, P.A., Pratt, L.M., Nagy, B. (Eds.), *Geochemistry of Metalliferous Black Shales*. *Chemical Geology* 99(1-3), 65-82.
- Hebting, Y., Schaeffer, P., Behrens, A., Adam, P., Schmitt, G., Schneckenburger, P., Bernasconi, S.M., Albrecht, P., 2006. Biomarker evidence for a major preservation pathway of sedimentary organic carbon. *Science* 312(5780), 1627-1631.
- Heggie D., Lewis T., 1984. Cobalt in pore waters of marine sediments. *Nature* 311(5985), 453-455.
- Helly, J.J., Levin, L.A., 2004. Global distribution of naturally occurring marine hypoxia on continental margins. *Deep-Sea Research Part I* 51(9), 1159-1168.
- Helz, G.R., Miller, C.V., Charnock, J.M., Mosselmans, J.F.W., Pattrick, R.A.D., Garner, C.D., Vaughan, D.J., 1996. Mechanism of molybdenum removal from the sea and its concentration in black shales: EXAFS evidence. *Geochimica et Cosmochimica Acta* 60(19), 3631-3642.
- Hetzel, A., Brumsack, H.-J., Böttcher, M. E., Schnetger, B., 2006. Inorganic geochemical characterization of lithologic units recovered during ODP Leg 207 (Demerara Rise). In: Mosher, D.C., Erbacher, J., Malone, M.J. (Eds.), *Proceedings of the Ocean Drilling Program, Scientific Results, 207*. College Station, TX (Ocean Drilling Program), 1-37.
- Ingall, E.D., Bustin, R.M., van Cappellen, P., 1993. Influence of water column anoxia on the burial and preservation of carbon and phosphorus in marine shales. *Geochimica et Cosmochimica Acta* 57(2), 303-316.
- Jacobs, L., Emerson, S., Huested, S.S., 1987. Trace metal geochemistry in the Cariaco Trench. *Deep-Sea Research Part A* 34(5-6), 965-981.
- Jacobs, L., Emerson, S., Skei, J., 1985. Partitioning and transport of metals across the $\text{O}_2/\text{H}_2\text{S}$ interface in a permanently anoxic basin: Framvaren Fjord, Norway. *Geochimica et Cosmochimica Acta* 49(6), 1433-1444.
- Kolonic, S., Wagner, T., Forster, A., Sinninghe Damsté, J.S., Walsworth-Bell, B., Erba, E., Turgeon, S., Brumsack, H.-J., Chellai, E.H., Tsikos, H., Kuhnt, W., Kuypers, M.M.M., 2005. Black shale deposition on the northwest African Shelf during the Cenomanian/Turonian oceanic anoxic event: Climate coupling and global organic carbon burial. *Paleoceanography* 20(1), PA1006.
- Kuhnt, W., Herbin, J.P., Thurow, J., Wiedmann, J., 1990. Distribution of Cenomanian-Turonian organic facies in the Western Mediterranean and along the Adjacent Atlantic Margin. In: Huc, A.Y. (Ed.), *Deposition of Organic Facies*. *AAPG Studies in Geology* 30, 133-160.

- Kuypers, M.M.M., Pancost, R.D., Nijenhuis, I.A., Sinninghe Damsté, J.S., 2002. Enhanced productivity led to increased organic carbon burial in the euxinic North Atlantic basin during the late Cenomanian oceanic anoxic event. *Paleoceanography* 17(4), 1051.
- Lyons, T.W., Berner, R.A., 1992. Carbon-sulfur-iron systematics of the uppermost deep water sediments of the Black Sea. *Chemical Geology* 99(1-3), 1-27.
- Lyons, T.W., Severmann, S., 2006. A critical look at iron paleoredox proxies: New insights from modern euxinic marine basins. *Geochimica et Cosmochimica Acta* 70(23), 5698-5722.
- McManus, J., Berelson, W.M., Klinkhammer, G.P., Johnson, K.S., Coale, K.H., Anderson, R.F., Kumar, N., Burdige, D.J., Hammond, D.E., Brumsack, H.-J., McCorkle, D.C., Rushdi, A., 1998. Geochemistry of barium in marine sediments: implications for its use as a paleoproxy. *Geochimica et Cosmochimica Acta* 62(21-22), 3453-3473.
- Morford, J.L., Emerson, S.E., 1999. The geochemistry of redox sensitive trace metals in sediments. *Geochimica et Cosmochimica Acta* 63(11-12), 1735-1750.
- Mort, H.P., Adatte, T., Föllmi, K.B., Keller, G., Steinmann, P., Matera, V., Berner, Z., Stüben, D., 2007. Phosphorus and the roles of productivity and nutrient recycling during oceanic anoxic event 2. *Geology* 35(6), 483-486.
- Musavu-Moussavou, B., Danelian, T., 2006. The Radiolarian biotic response to Oceanic Anoxic Event 2 in the southern part of the Northern proto-Atlantic (Demerara Rise, ODP Leg 207). *Revue de Micropaléontologie* 49(3), 141-163.
- Nederbragt, A.J., Thurow, J., Pearce, R., 2007. Sediment composition and cyclicity in the mid-Cretaceous at Demerara Rise, ODP Leg 207. In: Mosher, D.C., Erbacher, J., Malone, M.J. (Eds.), *Proceedings of the Ocean Drilling Program, Scientific Results, 207*. College Station, TX (Ocean Drilling Program), 1-31.
- Nederbragt, A.J., Thurow, J., Vonhof, H., Brumsack, H.-J., 2004. Modelling oceanic carbon and phosphorus fluxes: implications for the cause of the late Cenomanian Oceanic Anoxic Event (OAE2). *Journal of the Geological Society* 161(4), 721-728.
- Neretin, L.N., Böttcher, M.E., Jørgensen, B.B., Volkov, I.I., Lüschen, H., Hilgenfeldt, K., 2004. Pyritization processes and greigite formation in the advancing sulfidization front in the Upper Pleistocene sediments of the Black Sea. *Geochimica et Cosmochimica Acta* 68(9), 2081-2093.
- Neubert, N., Nägler, T., Böttcher, M.E., 2008. Sulfidity controls molybdenum isotope discrimination into euxinic sediments: Evidence from the modern Black Sea. *Geology* 36(10), 775-778.
- Nijenhuis, I.A., Brumsack, H.-J., de Lange, G.J., 1998. The trace element budget of the eastern Mediterranean during Pliocene sapropel formation. In: Robertson, A.H.F., Emeis, K.-C., Richter, C., Camerlenghi, A. (Eds.), *Proceedings of the Ocean Drilling Program, Scientific Results, 160*. College Station, TX (Ocean Drilling Program), 199-206.
- Passier, H.F., Bosch, H.-J., Nijenhuis, I.A., Lourens, L.J., Böttcher, M.E., Leenders, A., Sinninghe Damsté, J.S., de Lange, G.J., de Leeuw, J.W., 1999a. Sulfidic Mediterranean surface waters during Pliocene sapropel formation. *Nature* 397(6715), 146-149.
- Passier, H.F., Böttcher, M.E., de Lange, G.J., 1999b. Sulfur enrichment in organic matter of eastern Mediterranean sapropels: a study of sulfur isotope partitioning. *Aquatic Geochemistry* 5(1), 99-118.
- Paytan, A., Kastner, M., Chavez, F.P., 1996. Glacial to interglacial fluctuations in productivity in the equatorial Pacific as indicated by marine barite. *Science* 274(5291), 1355-1357.
- Paytan, A., Kastner, M., Campbell, D., Thieme, M.H., 2004. Seawater sulfur isotope fluctuations in the Cretaceous. *Science* 304(5677), 1663-1665.

- Paytan, A., Mearon, S., Cobb, K., Kastner, M., 2002. Origin of marine barite deposits: Sr and S isotope characterization. *Geology* 30(8), 747-750.
- Piper, D.Z., 1994. Seawater as the source of minor elements in black shales, phosphorites and other sedimentary rocks. *Chemical Geology* 114(1-2), 95-114.
- Poulton, S.W., Raiswell, R., 2002. The low-temperature geochemical cycle of iron: From continental fluxes to marine sediment deposition. *American Journal of Science* 302, 774-805.
- Prakash Babu, C., Brumsack, H.-J., Schnetger, B., 1999. Distribution of organic carbon in surface sediments along the eastern Arabian Sea: a revisit. *Marine Geology* 162(1), 91-103.
- Raiswell, R., Canfield, D.E., 1998. Sources of iron for pyrite formation in marine sediments. *American Journal of Science* 298, 219-245.
- Redfield, A.C., 1958. The biological control of chemical factors in the environment. *American Scientist* 46, 205-221.
- Rudnicki, M.D., Elderfield, H., Spiro, B., 2001. Fractionation of sulfur isotopes during bacterial sulfate reduction in deep ocean sediments at elevated temperatures. *Geochimica et Cosmochimica Acta* 65(5), 777-789.
- Schlanger, S.O., Arthur, M.A., Jenkyns, H.C., Scholle, P.A., 1987. The Cenomanian-Turonian Oceanic Anoxic Event, I. Stratigraphy and distribution of organic carbon-rich beds and the marine $\delta^{13}\text{C}$ excursion. In: Brooks, J., Fleet, A.J. (Eds.), *Marine Petroleum Source Rocks*. Geological Society, London. Special Publication 26, 371-399.
- Schlanger, S.O., Jenkyns, H.C., 1976. Cretaceous oceanic anoxic events: causes and consequences. *Geologie en Mijnbouw* 55, 179-184.
- Schmitz, B., 1987. Barium, equatorial high productivity, and the northward wandering of the Indian continent. *Paleoceanography* 2(1), 63-77.
- Shipboard Scientific Party, 2004. Leg 207 summary. In: Erbacher, J., Mosher, D.C., Malone, M.J., et al. (Eds.), *Proceedings of the Ocean Drilling Program, Initial Reports*, 207. College Station, TX (Ocean Drilling Program), 1-89.
- Strauss, H., 1999. Geological evolution from isotope proxy signals: sulfur. *Chemical Geology* 161(1-3), 89-101.
- Thurrow, J., Brumsack, H.-J., Rullkötter, J., Littke, R., Meyers, P., 1992. The Cenomanian/Turonian boundary event in the Indian Ocean - a key to understand the global picture. In: Duncan, R.A., Rea, D.K., Kidd, R.B., von Rad, U., Weissel, J.K. (Eds.), *The Indian Ocean: A Synthesis of Results from the Ocean Drilling Program*. American Geophysical Union, Geophysical Monograph 70, 253-273.
- Torres, M.E., Brumsack, H.-J., Bohrmann, G., Emeis, K.C., 1996. Barite fronts in continental margin sediments: A new look at barium remobilization in the zone of sulfate reduction and formation of heavy barites in diagenetic fronts. *Chemical Geology* 127(1-3), 125-139.
- Tribouillard, N., Algeo, T.J., Lyons, T., Riboulleau, A., 2006. Trace metals as paleoredox and paleoproductivity proxies: An update. *Chemical Geology* 232(1-2), 12-32.
- Tribouillard, N., Riboulleau, A., Lyons, T., Baudin, F., 2004. Enhanced trapping of molybdenum by sulfurized marine organic matter of marine origin in Mesozoic limestones and shales. *Chemical Geology* 213(4), 385-401.
- van der Weijden, C.V., 2002. Pitfalls of normalization of marine geochemical data using a common divisor. *Marine Geology* 184(3-4), 167-187.
- Wanty, R.B., Goldhaber, M.B., 1992. Thermodynamics and Kinetics of Reactions Involving Vanadium in Natural Systems - Accumulation of Vanadium in Sedimentary-Rocks. *Geochimica et Cosmochimica Acta* 56(4), 1471-1483.

- Wedepohl, K.H., 1971. Environmental influences on the chemical composition of shales and clays. In: Ahrens, L.H., Press, F., Runcorn, S.K., Urey, H.C. (Eds.), *Physics and Chemistry of the Earth* 8. Pergamon, Oxford, 305-333.
- Wedepohl, K.H., 1991. The composition of the upper earth's crust and the natural cycles of selected metals. Metals in natural raw materials. Natural Resources. In: Merian, E. (Ed.), *Metals and Their Compounds in the Environment*. VCH, Weinheim, 3-17.
- Werne, J.P., Hollander, D.J., Lyons, T.W., Sinninghe Damsté, J.S., 2004. Organic sulfur biogeochemistry: recent advances and future research directions. In: Amend, J., Edwards, K., Lyons, T. (Eds.), *Sulfur Biogeochemistry: Past and Present*. Geological Society of America. Special Paper 379, 135-150.
- Wijsman, J.W.M., Middelburg, J.J., Herrmann, P.M., Böttcher, M.E., Heip, C.H.R., 2001. Sulfur and iron speciation in surface sediments along the northwestern margin of the Black Sea. *Marine Chemistry* 74(4), 261-278.
- Wortmann, U.G., Bernasconi, S.M., Böttcher, M.E., 2001. Hypersulfidic deep biosphere indicates extreme sulfur isotope fractionation during single step microbial sulfate reduction. *Geology* 29(7), 647-650.
- Wortmann, U.G., Chernyavsky, B., 2007. Effect of evaporite deposition on Early Cretaceous carbon and sulphur cycling. *Nature* 446(7136), 654-656.
- Zhabina, N.N., Volkov, I.I., 1978. A method of determination of various sulfur compounds in sea sediments and rocks. In: Krumbein, W.E. (Ed.), *Environmental Biogeochemistry and Geomicrobiology (Vol. 3): Methods, Metals and Assessment*. Ann Arbor Science Publications, 735-745.

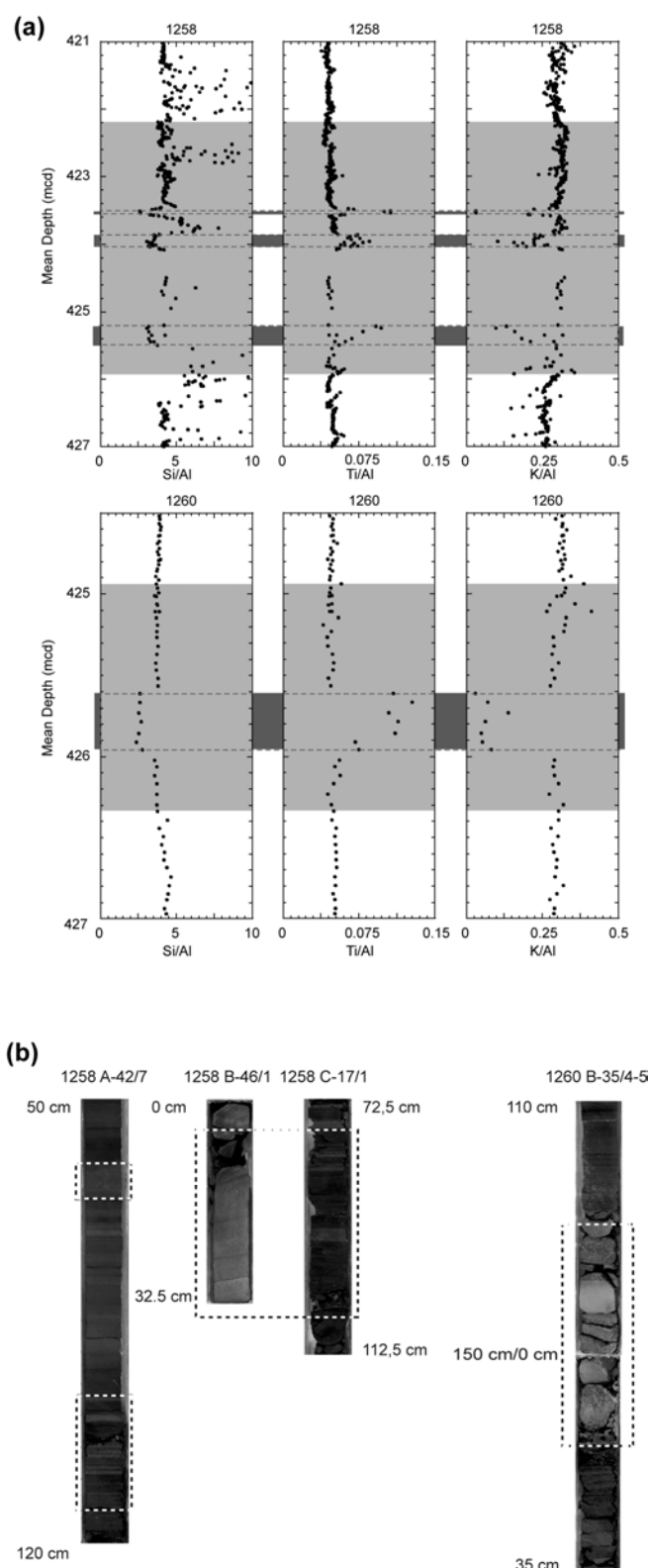
Appendix

Appendix A4.1 Quantification limit, precision and accuracy of analyzed elements. For stable isotope measurements, see section on Materials and Methods.

Element	Method	Quantification limit		Precision SD (1 σ) (rel%)	Accuracy (rel%)
S _T	IR-analyzer	0.56	%	3.0	99.9
TC	IR-analyzer	1.22	%	1.6	101.2
TIC	Coulometry	0.19	%	2.3	99.8
Si	XRF	1.94	%	1.3	99.1 - 101.0
Ti	XRF	0.03	%	1.2	98.1 - 101.0
Al	XRF	0.77	%	1.6	98.7 - 100.6
Fe _T	XRF	0.33	%	1.2	98.7 - 100.6
Mg	XRF	0.26	%	1.9	99.3 - 101.0
Ca	XRF	0.80	%	1.6	99.4 - 99.7
Na	XRF	0.21	%	5.7	90.1 - 100.6
K	XRF	0.20	%	2.6	95.5 - 100.4
P	XRF	0.04	%	6.5	98.6 - 108.8
As	XRF	4	ppm	7.0	96.0 - 100.0
Ba	XRF	77	ppm	2.5	98.8 - 102.6
Co	XRF	9	ppm	8.1	93.7 - 95.4
Cr	XRF	17	ppm	2.9	98.4 - 104.4
Cu	XRF	21	ppm	6.6	94.0 - 102.2
Mn	XRF	78	ppm	2.2	97.5 - 103.1
Mo	XRF	14	ppm	6.0	94.1 - 104.3
Ni	XRF	14	ppm	3.3	99.1 - 103.8
Rb	XRF	26	ppm	3.9	92.7 - 101.8
Sr	XRF	120	ppm	9.7	101.0 - 102.2
U	XRF	5	ppm	10.9	109.0 - 110.2
V	XRF	56	ppm	4.2	99.8 - 100.9
Y	XRF	8	ppm	5.4	98.5 - 109.5
Zn	XRF	33	ppm	3.9	95.1 - 102.4
Zr	XRF	30	ppm	3.6	96.1 - 103.7

Notes: Procedures and accuracy of all methods were checked with in-house reference materials (IR-Analyzer: PS-S (n=286); coulometry: Loess (n=387); XRF: DR-BS (n=33), TW-TUC (n=14) and PS-S (n=11)). Quantification limit is defined as 6 times the maximum standard deviation (1 σ). Precision is defined as 100% times the best estimate standard deviation (1 σ) divided by the mean of the repeats. The maximum value is given. SD = standard deviation. Accuracy is defined as 100% times the mean of the repeat analyses divided by the expected value. For XRF the range of different reference material is given.

Appendix A4.2 Identification of so-called “ash layers” (see text for details).



(a) Profiles for Si/Al, Ti/Al and K/Al for Cenomanian/Turonian black shales at Sites 1258 and 1260. Grey: OAE 2; dashed line: “ash layers”.

(b) Images of sediment intervals (available online from Erbacher et al., 2004, doi:10.2973/odp.proc.ir.207.2004). Dashed line: “ash layers”.

(c) Comparison of average element contents and element/Al ratios of omitted samples (unknown source, secondary overprinted). Cenomanian/Turonian black shales of Demerara Rise (mean values of Table 4.3, 4.4 and 4.5) and 'average shale'.

		Omitted samples (n= 34)	Average C/T black shales Demerara Rise	Average shale (Wedepohl. 1971. 1991)
S _T	%	6.03	2.60	0.24
S _P	%	(n=11) 1.67	0.79	
δ ³⁴ S _P	‰	(n=4) -15.4	-15.8	
TIC	%	2.73	5.56	0.35
TOC	%	8.55	10.39	
Si	%	14.69	10.26	27.53
Ti	%	0.36	0.10	0.46
Al	%	4.60	2.16	8.84
Fe _T	%	4.36	1.27	4.80
Mg	%	1.01	0.51	1.60
Ca	%	10.26	19.61	1.57
Na	%	1.25	0.88	1.19
K	%	0.74	0.64	2.99
P	%	0.08	0.33	0.07
As	ppm	54	20	10
Ba	ppm	511	524	580
Co	ppm	23	6	19
Cr	ppm	136	113	90
Cu	ppm	152	63	45
Mn	ppm	332	17	850
Mo	ppm	32	58	1
Ni	ppm	132	131	68
Rb	ppm	22	25	140
Sr	ppm	564	771	300
U	ppm	7	15	4
V	ppm	530	907	130
Y	ppm	17	20	41
Zn	ppm	209	608	95
Zr	ppm	35	33	160
S _{T cf}	%	12.10	4.94	0.25
TOC _{cf}	%	2.27	19.86	
S _T /Al		32.18	1.35	0.03
TOC/Al		89.00	5.40	0.02
Si/Al		3.18	5.13	
Ti/Al		0.08	0.05	0.05
Fe _T /Al		0.96	0.65	0.54
Mg/Al		0.31	0.53	0.18
Ca/Al		12.03	39.54	0.18
Na/Al		0.27	0.47	0.13
K/Al		0.17	0.32	0.34
P/Al		0.02	0.15	0.01
As/Al	× 10 ⁻⁴	12.9	11.2	1.1
Ba/Al	× 10 ⁻⁴	122.6	294.4	65.6
Co/Al	× 10 ⁻⁴	5.1	3.1	2.1
Cr/Al	× 10 ⁻⁴	30.6	52.3	10.2
Cu/Al	× 10 ⁻⁴	32.6	33.8	5.1
Mn/Al	× 10 ⁻⁴	80.4	15.5	96.2
Mo/Al	× 10 ⁻⁴	6.2	31.9	0.1
Ni/Al	× 10 ⁻⁴	28.3	67.5	7.7
Rb/Al	× 10 ⁻⁴	4.8	11.1	15.8
Sr/Al	× 10 ⁻⁴	197.9	693.6	33.9
U/Al	× 10 ⁻⁴	2.4	11.3	0.4
V/Al	× 10 ⁻⁴	119.0	498.0	14.7
Y/Al	× 10 ⁻⁴	5.2	11.7	4.6
Zn/Al	× 10 ⁻⁴	49.4	284.4	10.7
Zr/Al	× 10 ⁻⁴	10.4	20.1	18.1

5. Reconstruction of water column anoxia in the equatorial Atlantic during the Cenomanian-Turonian oceanic anoxic event using biomarker and trace metal proxies

Elisabeth van Bentum, Almut Hetzel, Hans-Jürgen Brumsack, Astrid Forster, Gert-Jan Reichart, Jaap S. Sinninghe Damsté

This chapter has been re-submitted to *Palaeogeography, Palaeoceanography, Palaeoecology*.

Abstract

The occurrence of the biomarker lycopane and the enrichment patterns of redox sensitive trace metals in black shales from Demerara Rise (western tropical Atlantic) reveal that bottom waters were anoxic during the upper Cenomanian and lower Turonian at this location. Bottom waters were clearly oxygen depleted already before oceanic anoxic event 2 (OAE-2), and continued to be so afterwards. Furthermore, the presence of fossil derivatives of isorenieratene and chlorobactene, pigments derived from green sulfur bacteria, demonstrates that the waters at the base of the photic zone occasionally contained sulfide (i.e., were euxinic). Before and after OAE-2, low concentrations of derivatives of these pigments are present, while much higher concentrations occur within the OAE-2 section. Stratification of the water column must have been strong to sustain euxinic conditions in the photic zone for prolonged periods. A substantial drop in the concentrations of isorenieratene and chlorobactene derivatives demonstrates that this stratification temporarily broke down during OAE-2. A simultaneous decrease in sea surface temperatures suggests that local ventilation was instrumental in this reoxygenation event. A rapid decrease in seawater derived trace metal burial rates at Demerara Rise, occurring in phase with the onset of the anoxia related to OAE-2, suggests an approximately synchronous onset of OAE-2 in the proto-North Atlantic.

Keywords: Demerara Rise, Ocean Drilling Program, trace metals, Oceanic Anoxic Event 2, CTBE, euxinia

Introduction

Recurring episodes of extensive deposition of marine, organic-rich, fine-grained, laminated, silicilastic sediments (so-called black shales) are characteristic for the mid-Cretaceous. The black shales deposited during this time are often enriched in certain trace metals (TMs) (Goldschmidt, 1954, see Brumsack, 2006, for a recent overview). These episodes of increased organic matter deposition are referred to as oceanic anoxic events (OAEs) and are primarily known from the Cretaceous (Schlanger and Jenkyns, 1976), the Jurassic (Jenkyns, 1985) and the Permian/Triassic boundary (Grice et al., 2005, Hays et al., 2007). One of the most extreme Cretaceous OAEs is OAE-2 at the Cenomanian-Turonian boundary (93.5 My, Gradstein et al., 2004, Sageman et al., 2006), also known as the Bonarelli event. OAE-2 is characterized by a large positive carbon isotope excursion (Arthur et al., 1988) both in marine carbonates (up to 2.5‰) and organic matter (OM) (up to 6‰) (Kuypers et al., 2002b, Tsikos et al., 2004, Erbacher et al., 2005). This positive excursion is most likely the result of the preferential removal of ^{12}C associated with the burial of OM, leaving the remaining carbon reservoir enriched in ^{13}C .

The high concentrations of organic carbon in OAE-2 black shales have been attributed to both enhanced preservation of OM by anoxic water column conditions, possibly related to a slowdown in oceanic circulation (e.g., Bralower and Thierstein, 1987, Sinninghe Damsté and Köster, 1998) and to increased productivity leading to higher OM accumulation rates (Schlanger and Jenkyns, 1976). Increased productivity will also lead to an enhanced oxygen demand for mineralization, which may overwhelm the oxidation potential of the ocean and cause water column anoxia (e.g., Schlanger and Jenkyns, 1976, Kuypers et al., 2002b). At present, the high OM content in OAE-2 black shales is therefore generally considered to be the result of a combination of increased productivity and enhanced preservation by anoxia (e.g., Kuypers et al., 2002b, Kolonic et al., 2005).

Several factors might have played a role in creating the specific environmental conditions that promoted the occurrence of OAEs during the mid-Cretaceous. Most noticeably, the climate was extraordinarily warm at the time, probably due to high atmospheric CO_2 concentrations caused by increased volcanism (Arthur et al., 1985, Bice et al., 2006, Sinninghe Damsté et al., 2008, Turgeon and Creaser, 2008). The resulting warmer ocean waters possibly gave rise to halothermal rather than thermohaline ocean circulation (Horne, 1999), consequently producing lower deep water ventilation rates, as warm water contains less oxygen. Moreover, large scale deposition of evaporates in the South Atlantic during the Early Cretaceous (Wortmann and Chernyavsky, 2007) would have changed the salt

balance of the ocean, creating less saline water and therefore slower circulation (Hay et al., 2006). In addition, the increased seafloor spreading, submarine volcanism and hydrothermal activity at this time would have had a strong effect on ocean circulation and TM cycling (Hays and Pitman, 1973, Paytan et al., 2004).

Specific biomarkers can be powerful tools for the reconstruction of bottom water anoxia and photic zone euxinia. The lycopane to *n*-alkane ratio ((lycopane+*n*-C₃₅)/*n*-C₃₁), for instance, can be used as an indicator for the palaeoxicity of the sediment/water interface (Sinninghe Damsté et al., 2003). Although the primary biological sources of lycopane are still unclear, this molecular compound is predominantly preserved in anoxic settings. The lycopane to *n*-alkane ratio, (lycopane+*n*-C₃₅)/*n*-C₃₁, can therefore be used as an indicator for the palaeoxicity of the sediment/water interface (Sinninghe Damsté et al., 2003). (Lycopane+*n*-C₃₅)/*n*-C₃₁ ratios observed in sediments deposited in anoxic waters in the present day oxygen minimum zone (OMZ) of the Arabian Sea are around 1 (Sinninghe Damsté et al., 2003). In contrast, sediments deposited in oxic bottom waters, above and below the OMZ, have ratios ≤ 0.5 . Elevated lycopane ratios in the sediments, therefore, demonstrate bottom waters were anoxic. Furthermore, the presence of isorenieratene or its diagenetic derivatives, indicates that at least the base of the photic zone (typically 50-150 m below sea surface; Hedgpeth, 1957) was euxinic, i.e., the water column contained free sulfide and no oxygen (Summons and Powell, 1986, Koopmans et al., 1996, Sinninghe Damsté and Köster, 1998, Kuypers et al., 2002b, Pancost et al., 2004). Isorenieratene is a carotenoid specific for Chlorobiaceae, the brown strain of the green sulfur bacteria. These photosynthetic bacteria are strict anaerobes and require both light and free sulfide, and can therefore only survive when part of the photic zone is euxinic. The presence of chlorobactene or its diagenetic derivatives points to an even shallower depth of photic zone euxinia, as chlorobactene occurs predominantly in the green colored strain of green sulfur bacteria, which requires a higher light intensity than the brown strain (Van Gernerden and Mas, 1995). These compounds are most likely autochthonous when found in sediments, since both these aromatic carotenoids are relatively labile and rarely survive transport over longer distances (Sinninghe Damsté et al., 2001, Sinninghe Damsté and Hopmans, 2008). At several North Atlantic sites the presence of these carotenoids established that euxinia reached all the way into the photic zone during OAE-2 (Sinninghe Damsté and Köster, 1998, Kuypers et al., 2002b, Kuypers et al., 2004. See Figure 5.2 for occurrences of isorenieratene and derivatives). An upward excursion of euxinic conditions in the oceans, and subsequent S out-gassing into the atmosphere, is thought to have contributed to the

Cenomanian-Turonian, Permian/Triassic and Late Devonian extinction events (Grice et al., 2005, Kump et al., 2005, Hays et al., 2007). During the Cenomanian-Turonian, an estimated amount of $8 \cdot 10^{16}$ kg SO₂ along with a significant amount of H₂S was introduced by plume-related volcanism (e.g., the formation of the Caribbean plateau, Kerr, 1998), which could have advanced the expansion of euxinic conditions (Sinninghe Damsté and Köster, 1998).

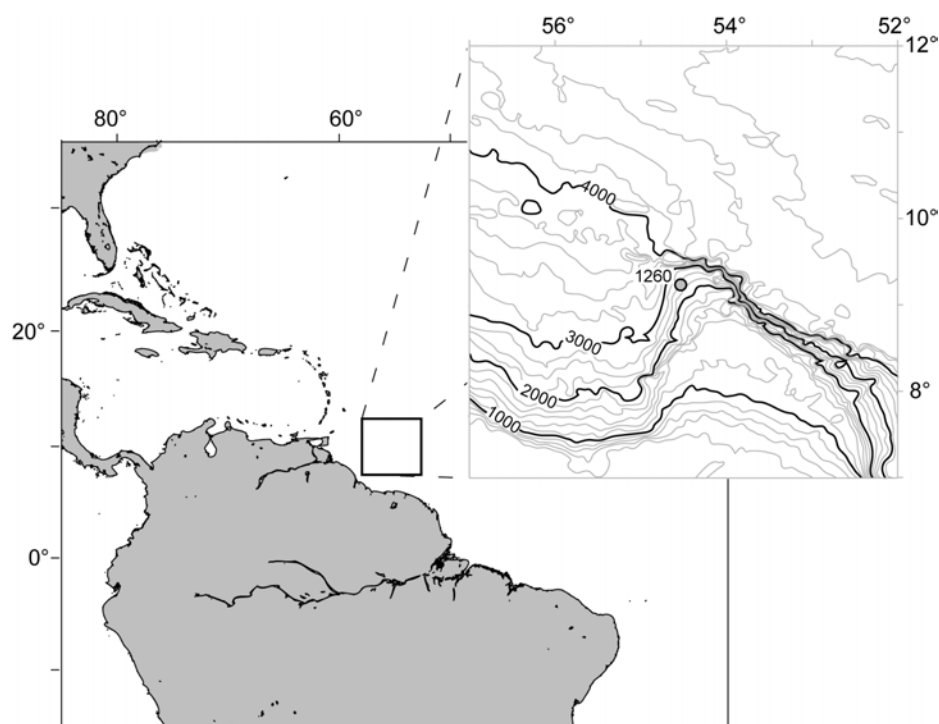


Figure 5.1 Map showing the present-day location of Demerara Rise Site 1260. Depth in meters, modified from ODP website.

Records of redox sensitive TMs are useful in elucidating redox conditions of oceanic bottom waters. Generally, some redox sensitive elements (e.g., V and U) are immobilized under anoxic, non-sulfidic conditions and therefore enriched in the sediment during anoxia (Calvert and Pedersen, 1993, Brumsack, 2006). Other elements, in contrast, are mobile under anoxic, non-sulfidic conditions (e.g., Mn) and as a result become depleted in sediments deposited during anoxia. In addition, under euxinic conditions, the abundantly present sulfide immobilizes chalcophile TMs (mainly Cu, Zn, and Cd, but also Co, Fe, and Ni) as metal sulfides, most likely by co-precipitation in pyrite (Huerta-Diaz and Morse, 1992, Tribouillard et al., 2006). Consequently, sediments deposited under euxinic conditions are usually enriched in these elements. Both Mo and As become enriched under anoxic and sulfidic conditions.

Despite intensive studies, causes and effects of OAEs are still poorly understood. To reconstruct the development of bottom water, water column and potentially photic zone anoxia during OAE-2 at Demerara Rise, we used both biomarker and TM proxies. Demerara Rise is a submarine plateau located off the coast of Suriname (Figure 5.1 and Figure 5.2) with excellently preserved biomarker records (e.g., Forster et al., 2004). These sediments are thus uniquely suited to compare biomarker and TM records.

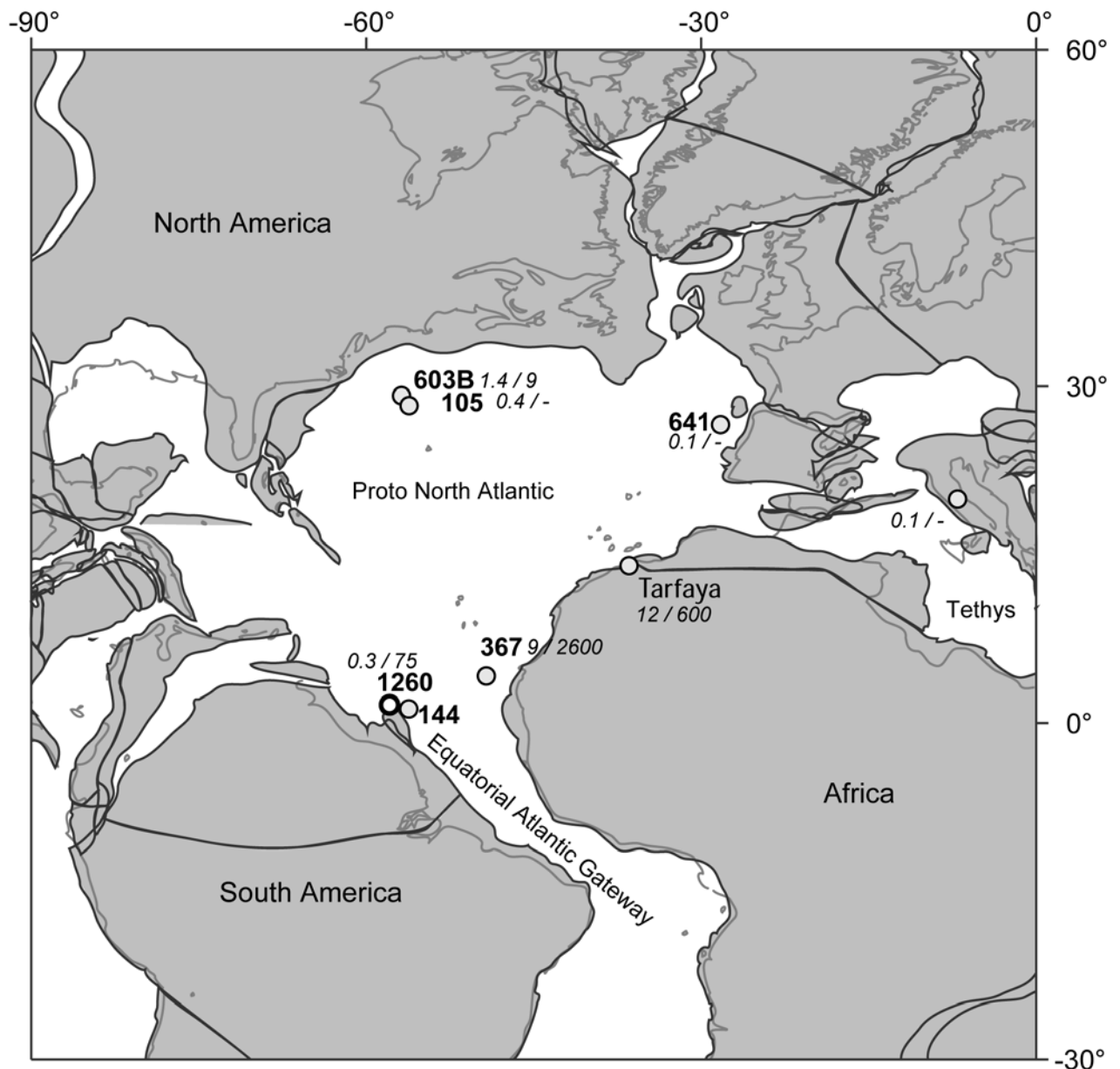


Figure 5.2 Sites where isorenieratane or its derivatives were found within the OAE-2 interval (DSDP Sites 144, 367, 368 and Tarfaya, Sinninghe Damsté and Köster, 1998, DSDP Sites 105 and 603B, Kuypers, 2001, Kuypers et al., 2004, S13 at Tarfaya, Kolonic et al., 2005).

Bold: Site numbers. Italics OAE-2 OC accumulation rates ($\text{g/m}^2/\text{yr}$) / maximum OAE-2 isorenieratane accumulation rates ($\mu\text{g/m}^2/\text{yr}$).

The sites are plotted on a palaeogeographical map showing the proto North Atlantic during the mid-Cretaceous (~94 Ma), created with GEOMAR map generator; www.odsn.de/odsn/services/paleomap/paleomap.html.

Geological setting and Stratigraphy

Demerara Rise is a NW-SE oriented, gently dipping submarine plateau located off the coast of Suriname (Figure 5.1). During the Cenomanian-Turonian, Demerara Rise was situated in the tropics (14-15°N) in the proto-North Atlantic (Figure 5.2). Sediments used for this study were collected during Ocean Drilling Program (ODP) Leg 207 at Site 1260, holes A and B (Erbacher et al., 2004a). The recovered Albian to Pleistocene sequence contains a total of 509 meters of sediments and includes the Cenomanian-Turonian boundary. The Cretaceous sediments at Site 1260 were most likely deposited at intermediate water depth, probably between 500-1500 m (Erbacher et al., 2004b, Suganuma and Ogg, 2006) but certainly below the storm wave base (200 m). The Cenomanian-Coniacian sediments of this sequence are typically laminated, dark, carbonaceous, calcareous mud- to marlstones (black shales) occasionally interbedded with sandy limestones and thin calcareous layers (Erbacher et al., 2004a). Most noticeable are a 25 cm thick carbonate layer (here referred to as the lower carbonate layer) at 425.91-425.66 meters composite depth (mcd) and another thick carbonate bed above the OAE-2 interval (the upper carbonate layer, at 424.3-423.9 mcd). Both beds consist of almost pure calcium carbonate most likely of diagenetic origin (Hetzl et al., 2009), with TOC (total organic carbon) values below 1 % (Figure 5.3B). Apparently, the carbonate compensation depth was never shallow enough to cause appreciable carbonate dissolution at Demerara Rise.

OM from Demerara Rise is thermally immature and well preserved, mostly of marine origin with organic carbon contents of up to 20 % (Erbacher et al., 2004a, Erbacher et al., 2004b, Forster et al., 2004, Meyers et al., 2006). Both TOC and sulfur concentrations are higher than levels generally encountered in OAE-2 black shales (Brumsack, 2006, Hetzel et al., 2009). Although TOC content is already high throughout the entire sequence (with the exception of some carbonate beds), there is a clear increase from, on average, 8 to 16 % TOC at the onset of OAE-2 (Forster et al., 2007) (Figure 5.3B).

Stratigraphy is based on shipboard results, chemostratigraphy and nannofossil biostratigraphy (Erbacher et al., 2004a, Hardas and Mutterlose, 2006, Forster et al., 2007). The exact stratigraphic position of OAE-2 was determined by the positive isotope excursion in bulk organic carbon ($\delta^{13}\text{C}_{\text{org}}$) accompanying OAE-2 (Figure 5.3A) (cf. Erbacher et al., 2005, Forster et al., 2007). The OAE-2 carbon isotope excursion can be divided into three phases (cf. Kuypers et al., 2002a, Forster et al., 2007). The onset of the excursion up to the first isotopic maximum, a positive shift in $\delta^{13}\text{C}_{\text{org}}$ values of approximately 6 ‰, is termed phase A (426.41-426.11 mcd). Phase A is equivalent to the “first build-up” phase used for

the proposed European reference section at Eastbourne (Paul et al., 1999). Phase B (426.11-425.27 mcd) contains a decline of 2.5 ‰ in $\delta^{13}\text{C}_{\text{org}}$ values, followed by a second increase of almost 3 ‰ and ends with an interval of steadily high $\delta^{13}\text{C}_{\text{org}}$ values (at ca. -22 ‰). Phases A and B together make up OAE-2. By comparing Site 1260 to the well-dated Pueblo record of Sageman et al. (2006) an approximate duration of 550 kyr is established for OAE-2 at this site. During phase C (425.27-424.81), the so-called “recovery phase”, carbon isotopic ratios gradually return almost to the initial, pre-excursion values.

Methods

Biomarkers and trace metals were analyzed on aliquots of samples previously used to determine TOC content, carbonate (CaCO_3) content, stable carbon isotopes of bulk organic carbon ($\delta^{13}\text{C}_{\text{org}}$) and sea surface temperatures (SSTs) using the TEX_{86} paleothermometry proxy (data set of Forster et al., 2007, method details given therein). Briefly, the TEX_{86} index is based on molecular compounds derived from the cell membranes of unicellular marine microorganisms, the Crenarchaeota. The number of cyclopentane rings occurring in these specific membrane lipids has been shown to co-vary with the ambient sea water temperature (Schouten et al., 2002), therefore the TEX_{86} index can be used as a temperature proxy. Numerous studies have recently applied the TEX_{86} proxy for SST reconstructions in the geological past (e.g., Dumitrescu et al., 2006).

Sediment samples (3 to 5 g dry mass) were taken approximately every 10 cm above and below the OAE-2 black shales, while within the OAE-2 section, samples were taken every 2-5 cm. This sampling campaign resulted in 61 samples from a section of approximately 10 m covering the Cenomanian-Turonian transition.

Sediments were freeze-dried, powdered and for biomarker analysis subsequently extracted with an Accelerated Solvent Extractor (Dionex) using a dichloromethane (DCM) - methanol mixture (9:1, v/v). Elemental sulfur was removed from the extracts using activated copper. The extracts were then separated into apolar and polar fractions using a column of activated alumina by elution with hexane/DCM (9:1, v/v) and DCM/methanol (1:1, v/v), respectively.

Raney Nickel desulfurisation and subsequent hydrogenation (Sinninghe Damsté et al., 1993) were used to release sulfur-bound biomarkers from polar fractions. This was only performed on samples that produced polar fractions weighing >5 mg to ensure a sufficient yield. The desulfurised fraction was separated further into apolar and polar fractions as stated above. Both the original apolar fraction and the apolar fraction obtained from the

desulfurised polar fraction were separated into their saturated aliphatic, unsaturated aliphatic and aromatic fractions by column chromatography using AgNO₃-impregnated silica as the stationary phase and hexane, hexane/DCM (9:1, v/v) and hexane/DCM (1:1, v/v) as eluents.

All fractions were analyzed on a HP gas chromatograph (GC) fitted with a flame ionization detector (FID) and a sulfur-selective flame photometric detector (FPD). Samples were injected on-column, on a CP-sil 5CB fused silica column (50 m x 0.32 mm i.d.) with helium as carrier gas set at constant pressure (100 KPa). The oven program started at 70 °C, was heated by 20 °C/min to 120 °C and subsequently by 4 °C/min to 320 °C and held isothermally at 320 °C for 15 min. To identify compounds the samples were measured on a GC-MS (Thermo Trace GC Ultra) with a mass range m/z 50-800 using a similar column and heating program as for the GC, set at constant flow. Biomarkers were identified by comparing mass spectra and retention times to those of compounds described in literature (e.g., Schaeffer et al., 1997). Phytane and isorenieratane were quantified by integration of the peak areas of these compounds on the GC mass chromatogram and comparing them with the peak area of the internal standard (D₂-C₂₂-anteisoalkane). Chlorobactane concentrations were calculated by comparing the peak area of the m/z 133 GC-MS mass chromatogram of chlorobactane to the area of the m/z 133 peak of isorenieratane, which was quantified relative to the internal standard.

Major, minor and trace elements were determined by X-ray fluorescence (XRF) at the Institute for Chemistry and Biology of the Marine Environment (ICBM), University Oldenburg. 600 mg of the powdered sample was mixed with 3600 mg of a 1:1 mixture of dilithiumtetraborate (Li₂B₄O₇) and lithiummetaborate (LiBO₂), or with 100% dilithiumtetraborate for carbonate rich samples and pre-oxidized at 500°C in porcelain crucibles for 5 h with approximately 1 g of ammonium nitrate (NH₄NO₃, p.a.). After cooling, the samples were melted at 1200°C in Pt-Au crucibles and cooled in Pt-Au disk moulds. The disks were analysed with a Philips® PW2400 XRF spectrometer. Analytical precision was verified by the preparation and analysis of several in-house standards. Relative precision and accuracy was found to be better than 5 rel% for all major elements, except for P (better than 10 rel%), and better than 11 rel% for minor elements. A few elements were present in concentrations lower than the quantification limit of the XRF. This is the case for Mn and Co for most of the sequence studied and for Fe within the upper carbonate layer mentioned above. As SO₃ is partly lost during the melting process, the XRF S values are not very accurate and reflect only a minimum content.

To compensate for the highly variable Ca concentration, which dilutes the trace metal content, element concentrations were calculated on a carbonate free basis. Trace metal, major element and bulk sulfur concentrations are plotted on a carbonate free basis (CF) against depth in Figure 5.4.

$$\text{Element}_{\text{CF}} = \text{element} \cdot 100 / (100 - \text{CaCO}_3)$$

Enrichment factors were calculated to compare the Demerara Rise records to trace element records from different settings (Figure 5.5). Enrichment factors (EF's) were calculated as in Brumsack (2006);

$$\text{EF}_{\text{element}} = (\text{element}/\text{Al})_{\text{sample}} / (\text{element}/\text{Al})_{\text{average shale}}$$

Average shale here refers to the average chemical composition measured in hundreds of shale samples (Wedepohl, 1971). This “average shale” is typically used as the standard of comparison between these types of sediments. If $\text{EF}_{\text{element}}$ is greater than 1 the element is enriched relative to average shale, when $\text{EF}_{\text{element}}$ is less than 1 it is depleted.

The average organic carbon accumulation rate (AR_{OC}) for OAE-2 at Site 1260 was estimated from the thickness of the OAE section (1.15 m), the duration of OAE-2 (550 ky) and the TOC content.

Results

Biomarkers

Biomarkers that were bound in macromolecular aggregates through incorporation of sulfur during early diagenesis (cf., Brassell et al., 1986, Sinninghe Damsté et al., 1989) were released by Raney Nickel desulfurisation and subsequently hydrogenated. This way, chlorobactane and isorenieratane, derived from the aromatic carotenoids chlorobactene and isorenieratene of photosynthetic green sulfur bacteria (Sinninghe Damsté et al., 1993, Schaeffer et al., 1997), were recovered. Isorenieratane concentrations fluctuate strongly between ~ 0 and $270 \mu\text{g g}^{-1}$ TOC (Figure 5.3F). Below the interval representing OAE-2, isorenieratane concentrations are $<5 \mu\text{g g}^{-1}$ TOC, concentrations then increase rapidly at the start of the OAE-2 interval (426.31 mcd), where highest concentrations ($270 \mu\text{g g}^{-1}$ TOC) are found. Subsequently, still within the early stages of the OAE-2 interval (426.06-425.96 mcd), isorenieratane concentrations decrease again to $<5 \mu\text{g g}^{-1}$ TOC. Within the carbonate layer (425.91-425.66 mcd) extraction yields were insufficient to apply desulfurisation and isorenieratane concentrations could not be determined. Above the carbonate layer, values increase again to a maximum of $130 \mu\text{g g}^{-1}$ TOC in phase C (425.01 mcd). Subsequently, isorenieratane concentrations quickly decrease to $<5 \mu\text{g g}^{-1}$

TOC (424.43 mcd). These low concentrations continue in the sediments deposited above phase C.

Chlorobactane concentrations at Site 1260 range from 0.2 to 32 $\mu\text{g g}^{-1}$ TOC with the chlorobactane record generally following that of isorenieratane. Showing increasing concentrations at the start of the OAE-2 section, and decreasing concentrations just below the carbonate layer. Highest chlorobactane concentrations occur within the OAE-2 interval just above the carbonate layer (425.6 mcd) (Figure 5.3G).

Lycopane is present in all apolar fractions of the analysed sediments. Calculated $(\text{lycopane} + n\text{-C}_{35})/n\text{-C}_{31}$ ratios (Sinninghe Damsté et al., 2003) ranged from 1.3 to 34, but are predominantly between 4 and 8 (Figure 5.3E).

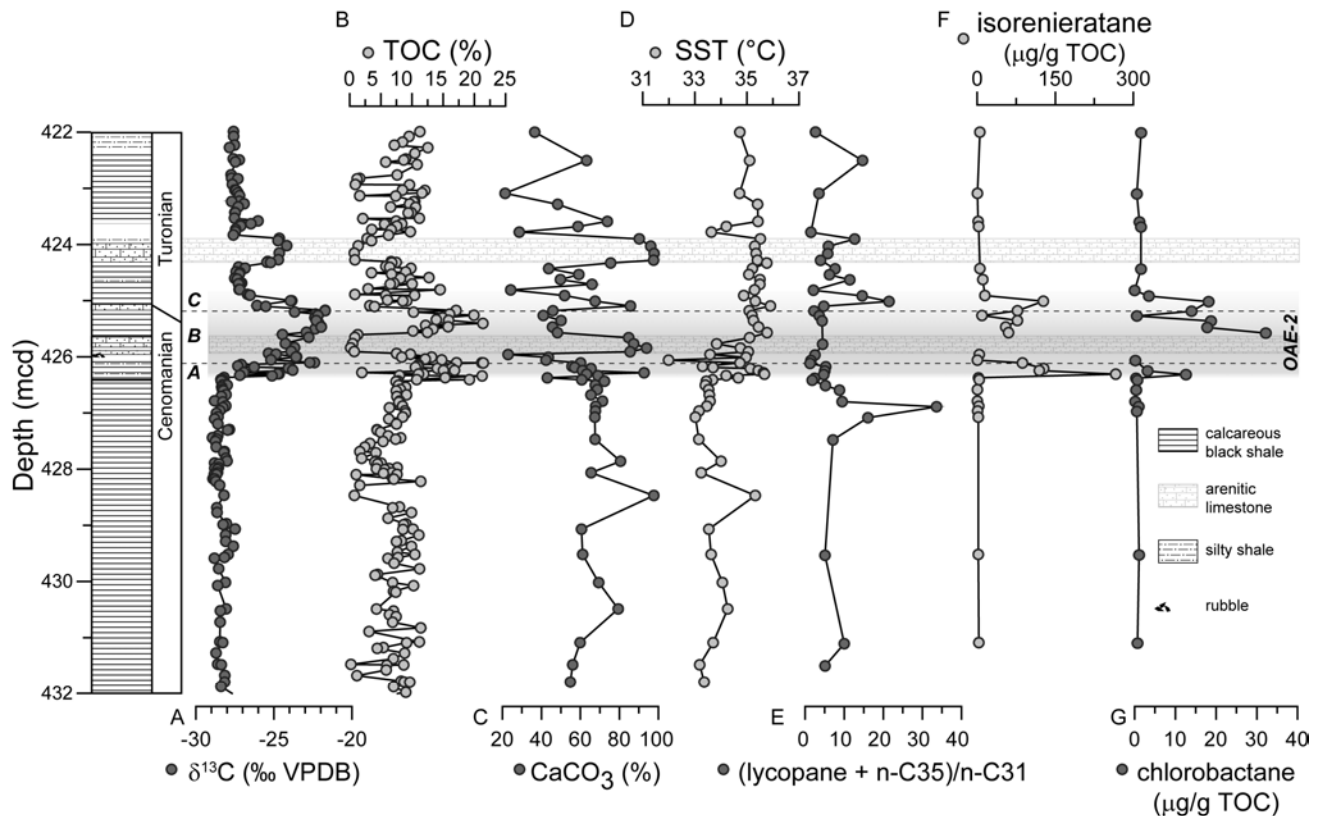


Figure 5.3 Lithology, stratigraphy, stable isotope and biomarker data for OAE-2 at Demerara Rise, ODP Site 1260. (A) Isotope values of bulk organic carbon ($\delta^{13}\text{C}_{\text{org}}$) in ‰ VPDB, (B) total organic carbon content (TOC) in weight %, (C) calcium carbonate (CaCO_3) content in weight %, (D) sea surface temperatures (SST) in °C as reconstructed by TEX_{86} (all from Forster et al. 2007), (E) the $(\text{lycopane} + n\text{-C}_{35})/n\text{-C}_{31}$ ratio, (F) isorenieratane and (G) chlorobactane concentrations in $\mu\text{g/g TOC}$. Grey shaded areas mark phases A, B and C of OAE-2 (see text for explanation). Scale in meters composite depth (mcd).

Trace metals and major elements

Trace metal, major element and bulk sulfur concentrations are plotted on a carbonate free basis (CF) against depth in Figure 5.4. Due to dilution effects, samples from the carbonate layers contain extremely low concentrations of certain TMs. The trace elements Co, Fe and Mn were occasionally present in concentrations lower than the quantification limit of the XRF. Co concentrations are under the quantification limit (10 ppm) in all samples below and above OAE-2 interval and Mn concentrations are below the quantification limit (155 ppm) in all but three samples. Fe is below the quantification limit (0.2 %) in one of the samples. The TMs that are below the quantification limit are represented with empty circles in Figure 5.4. Overall, Al_{CF} , Si_{CF} and Ti_{CF} concentrations are relatively uniform except for an increase in the lower carbonate layer, and a decrease in the upper carbonate layer. Mg_{CF} mostly follows the same pattern, except for an increase of Mg_{CF} in the upper carbonate layer. For most samples at Site 1260, Mn_{CF} concentrations are below the XRF quantification limit although Mn_{CF} concentrations are slightly higher within the carbonate layer.

Downcore S_{CF} , Co_{CF} , As_{CF} and Fe_{CF} concentrations are low before the OAE-2 interval, increase slightly at the onset of OAE-2 and remain at this level until deposition of the lower carbonate layer, where concentrations strongly increase. Above the carbonate layer, As_{CF} , Co_{CF} and Fe_{CF} concentrations decrease again, but remain higher than before OAE-2. In the remaining part of the OAE-2 interval and phase C concentrations stay at this level apart from an increase in the upper carbonate layer. Cu_{CF} follows this pattern although concentrations are slightly higher before the OAE-2 interval.

Concentrations of Mo_{CF} , U_{CF} , V_{CF} , Zn_{CF} and Ni_{CF} increase prior to the OAE (starting at 426.9 mcd) and subsequently reveal a considerable depletion at the onset of OAE-2. Concentrations remain low during the entire OAE-2 interval (Figure 5.4) and only increase again after phase C.

Downcore P_{CF} concentrations show an increase prior to, and immediately after the OAE-2 interval, while within the OAE-2 interval concentrations are very low. Y_{CF} concentrations show a pattern similar to P_{CF} but also increase in both carbonate layers. Sr_{CF} concentrations are mostly very low, except for in the upper carbonate layer. K_{CF} increases after the OAE-2 interval and shows a strong drop within the two carbonate layers.

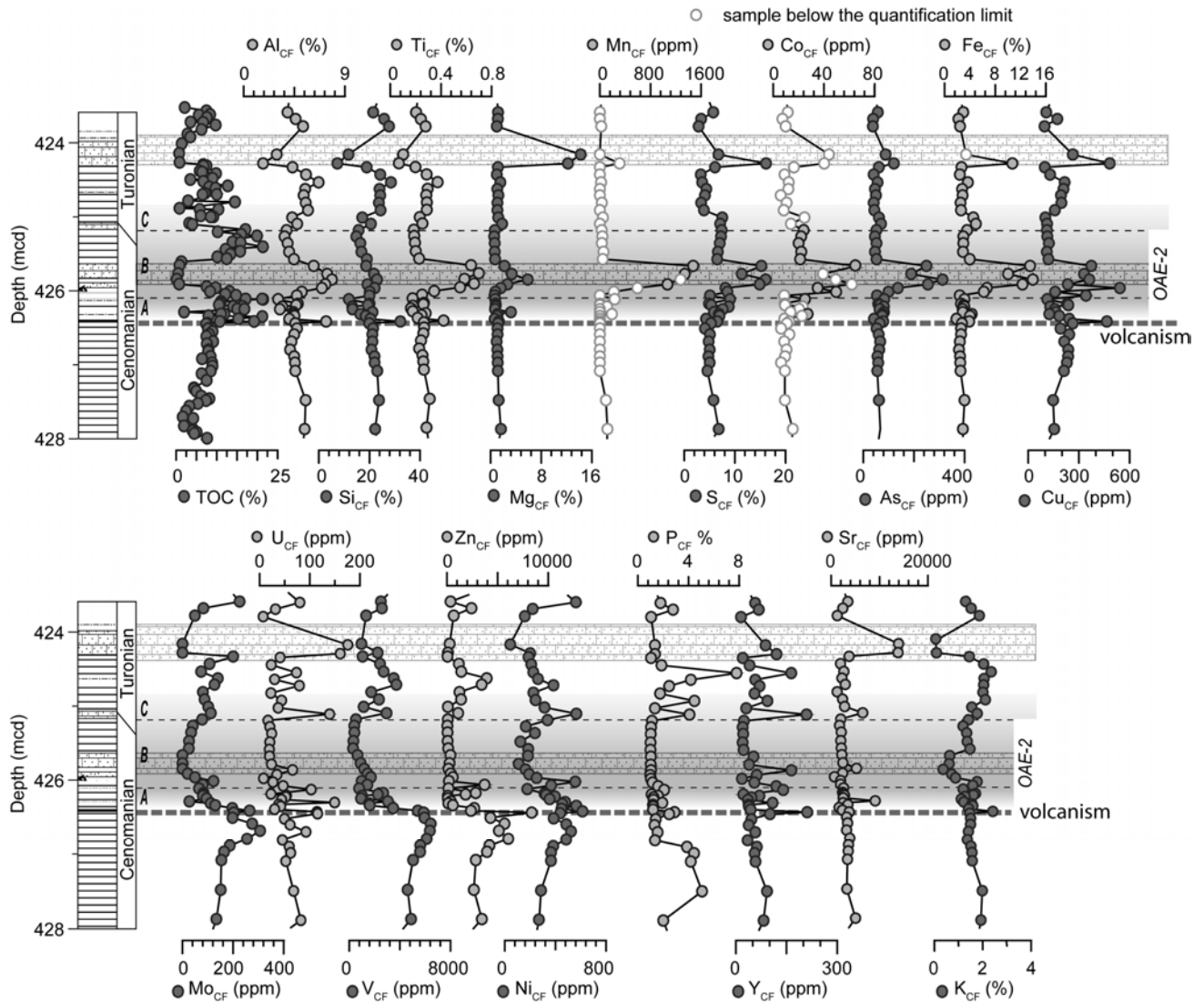


Figure 5.4 Major elements and trace metals (all, except TOC, on a carbonate free basis) plotted against depth. The lower carbonate layer indicated at 425.91-425.66 mcd, upper carbonate layer at 424.3-423.9 mcd. The grey shaded areas indicate the division of OAE-2. Phase A, corresponds to the build-up phase, B, to the stable plateau and C, the gradual decline to pre-exursion values, for further details see text. The unfilled circles represent samples below the XRF quantification limit.

Calculated trace metal enrichment factors (EFs) from Site 1260 are plotted for elements of which the deposition is influenced by changes in bottom water redox conditions (Figure 5.5). Most TMs are enriched compared to average shale (Wedepohl, 1971; $EF > 1$) both within and outside the OAE-2 black shale section. Only for Mn, depletion is indicated by $EF < 1$, both within and outside the OAE-2 section. The EFs of As, Ba, Cu, Fe and S and are similar for sediments deposited during the entire investigated interval. However, when Fe, Cu and As are plotted on a carbonate free basis (Figure 5.4), these elements show increased concentrations during OAE-2. The EFs of Cr, Mo, P, U, V, and Zn decrease during the OAE, while the EFs of Co and Ni increase slightly (Figure 5.5).

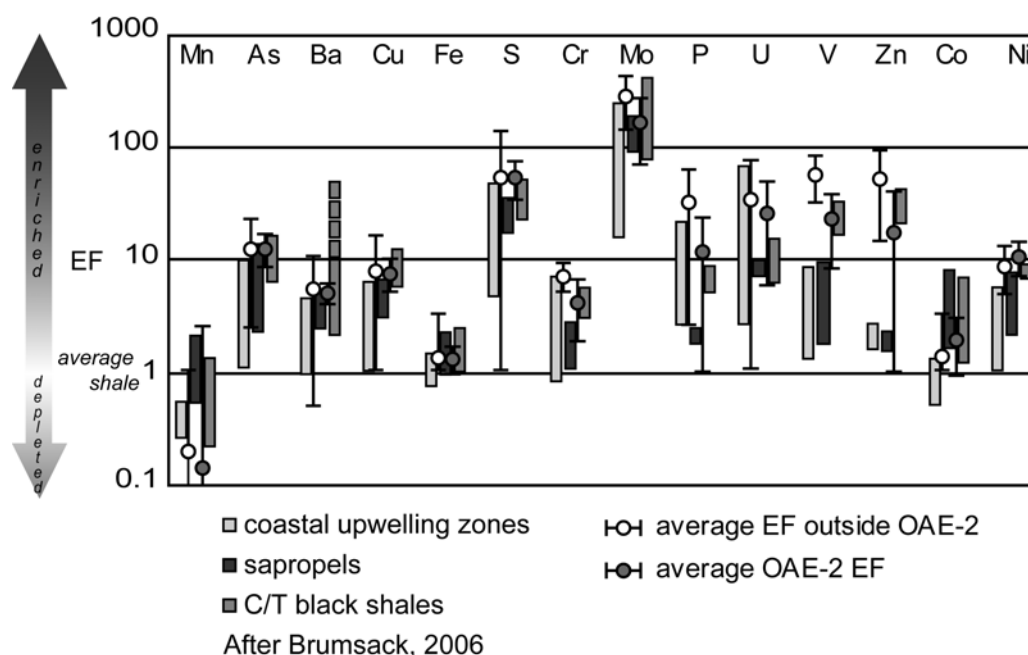


Figure 5.5 Enrichment factors of several trace metals and selected major elements at Demerara Rise relative to 'average shale' (Wedepohl, 1971). $EF_{\text{element}} = (\text{element}/\text{Al})_{\text{sample}} / (\text{element}/\text{Al})_{\text{average shale}}$. Open dots: average enrichment factors outside OAE-2. Filled dots: average enrichment factors during OAE-2, disregarding the samples from the carbonate layer. Also plotted are EFs for 3 different depositional settings (data from: Brumsack, 2006). EFs at Site 1260 are generally higher than normally encountered in sapropels and upwelling sites, however, at Demerara Rise Site 1260 most EFs do not increase during OAE-2, even though there is evidence for stronger photic zone euxinia at that time.

Discussion

Anoxia and water column stratification at Site 1260

The lycopane to *n*-alkane ratio, $(\text{lycopane} + n\text{-C}_{35})/n\text{-C}_{31}$, can be used as an indicator for the palaeoanoxicity of the sediment/water interface (Sinninghe Damsté et al., 2003). The generally elevated and sometimes extremely high lycopane ratios in the sediments from Site 1260 (Figure 5.3E), therefore, demonstrate bottom waters were anoxic. However, the use of the lycopane ratio implicitly assumes a relatively constant input of resistant long-chain *n*-alkanes (including the *n*-C₃₁ alkane that is used in the ratio). The relatively low input of these components at Site 1260 may have skewed the ratio towards comparatively high values. Still, as lycopane is a labile compound unable to survive prolonged exposure to oxygen, the high lycopane concentrations alone already indicate excellent preservation of the OM and imply permanently anoxic bottom water conditions during deposition of the complete interval studied. The absence of bioturbation and the extremely low concentrations of Mn_{CF}, which is remobilized during anoxic conditions, are further evidence for permanent bottom water anoxia at Site 1260.

Prior to the OAE-2 interval, Cu_{CF} , Mo_{CF} , Ni_{CF} , V_{CF} and, although more scattered, U_{CF} concentrations increase (Figure 5.4), this could be interpreted as an indication of water column conditions becoming more oxygen depleted. However, the simultaneous rise in Zn_{CF} concentrations together with increasing Os concentrations (Turgeon and Creaser, 2008) suggests that the increase in these TMs is more likely related to enhanced hydrothermal input (Arthur et al., 1990). Increased hydrothermal input during the Cenomanian-Turonian is certainly likely, as volcanic activity was enhanced shortly before and during the Cenomanian-Turonian interval (Sinton and Duncan, 1997, Snow et al., 2005, Kuroda et al., 2007).

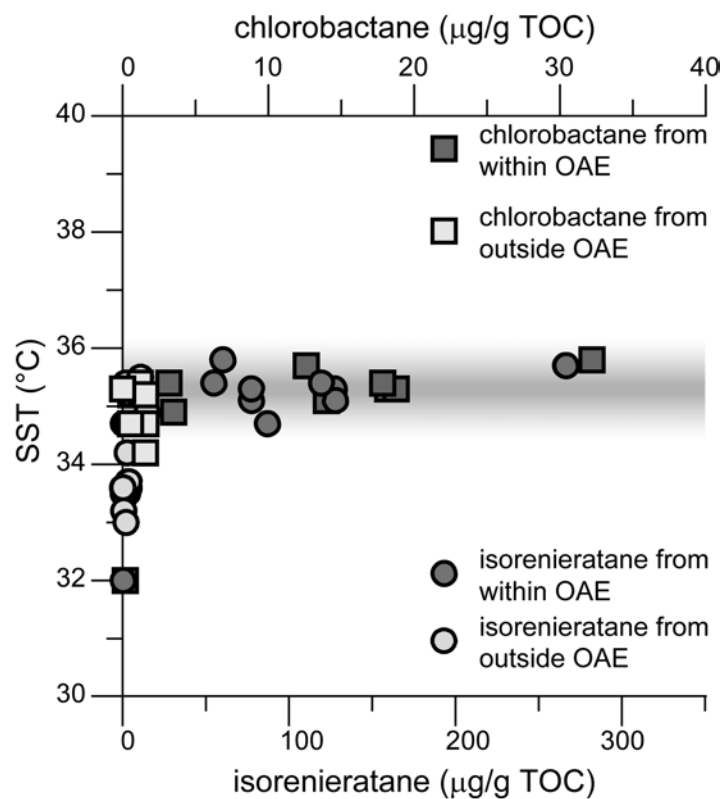


Figure 5.6 During the Cenomanian-Turonian-transition at ODP Site 1260, elevated isorenieratane and chlorobactane concentrations are found mainly during times of high sea surface temperatures (SSTs). Dark grey circles represent isorenieratane concentrations from OAE-2 samples, while light grey circles represent isorenieratane concentrations from samples from above or below the OAE at this site. Dark grey squares represent chlorobactane concentrations from OAE-2 samples; light grey squares represent chlorobactane concentrations from samples from above or below the OAE.

Although the high lycopane to *n*-alkane ratios (Figure 5.3E) demonstrate that bottom water conditions remained continuously anoxic during the interval studied, conditions in the photic zone were more variable. Isorenieratane and chlorobactane are present in low concentrations before OAE-2, revealing that the base of the photic zone occasionally

became euxinic before the OAE-2 (Figure 5.3F and 5.3G). At the start of the OAE-2 interval, extremely high concentrations of isorenieratane are encountered for the first time. The major increase in isorenieratane and chlorobactane concentrations at the start of OAE-2 demonstrates that euxinic conditions expanded into the base of the photic zone. These high concentrations suggest that photic zone euxinia was strongest at the beginning of OAE-2. The small increase in As_{CF} , Co_{CF} and Fe_{CF} concentrations at the start of the OAE-2 interval is in line with an expansion of anoxic conditions in the water column.

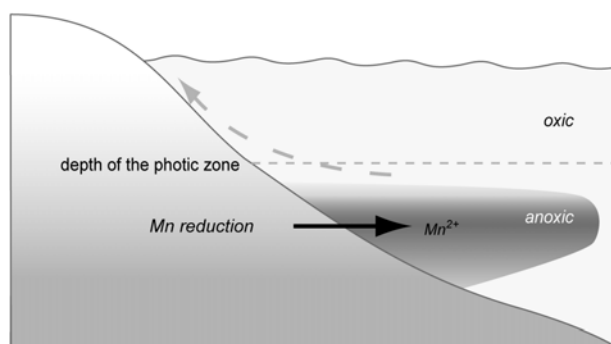
The maximum isorenieratane concentrations at the start of OAE-2 coincide with a rapid increase by two degrees in SSTs (Forster et al., 2007) (Figure 5.3D and 5.3F). Isorenieratane and chlorobactane concentrations plotted against SSTs show that the highest concentrations of these compounds occur at higher SSTs (Figure 5.6). As stratification develops by density differences of water masses in the ocean, these differences can be due to changes either in salinity or in temperature. Apparently, high SSTs resulted in stronger ocean stratification, enabling the chemocline to shoal into the base of the photic zone at Demerara Rise.

Following the strong euxinic photic zone conditions at the start of OAE-2, there is a substantial decrease in isorenieratane concentrations (426.0-425.6 mcd, just below the lower carbonate layer, Figure 5.3F). Interestingly, this drop coincides with relatively lower SSTs. Apparently, during the later part of phase A of OAE-2, there was a period of surface-water cooling, which might have led to enhanced convective overturn and subsequent re-oxygenation of the base of the photic zone. This mid-OAE-2 cooling could well be equivalent to the “Plenus Cold Event” in Europe (as defined by Gale and Christensen, 1996, Forster et al., 2007). This temporary cooling within OAE-2 was originally based on the southward migration of boreal fauna in NW-Europe (Jefferies, 1962, Gale and Christensen, 1996, Voigt et al., 2004). The “benthonic zone”, a period of oxygenated bottom waters during OAE-2 in the Western Interior Seaway of the U.S (Leckie et al., 1998) was probably synchronous with the Plenus cold event. Therefore, it seems likely that there was a, perhaps worldwide, period of cooling and associated oceanic mixing during OAE-2 (Jenkyns et al., 1994, Keller and Pardo, 2004, Forster et al., 2007). A short benthic foraminiferal repopulation event, observed in all Demerara Rise cores (Friedrich et al., 2006), reveals that even bottom waters were ventilated during this interval of cooling. Based on the faunal characteristics the bottom water changed from anoxic to dysoxic. Additional evidence for dysoxic conditions rather than fully oxic bottom water comes from the absence of strongly elevated Mn concentrations (“a Mn spike”) during this repopulation

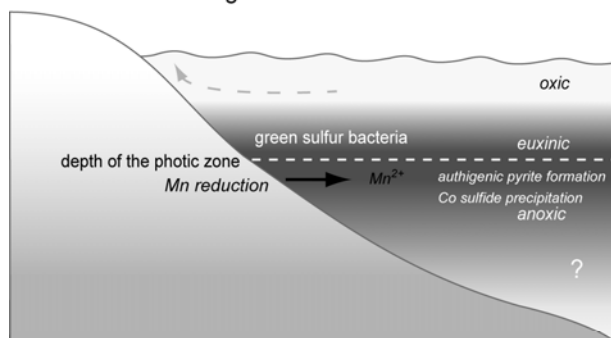
event (Figure 5.4). Dissolved Mn^{2+} in the anoxic water column would precipitate during complete reoxygenation, resulting in a major flux to the sea floor. Alternatively, the possibility exists that bottom waters did become completely oxic but remobilisation of Mn during a later stage of anoxia might have erased most of this spike. The small increase in Mn and Co concentrations in the samples above the foraminiferal repopulation level could then suggest that bottom waters did remain oxygenated/suboxic for a longer period. However, even though Mn_{CF} concentrations increase slightly, concentrations generally remain lower than would be expected for fully oxygenated bottom water conditions. Enrichment factors of Mn in these samples are around 1, which corresponds to typically low oxygen environments such as sapropels and Cenomanian-Turonian sediments from other sites (Brumsack, 2006). The modestly increased Mn and Co concentrations are more likely associated with the formation of pyrite (Huerta-Diaz and Morse, 1992). Moreover the lack of bioturbation and the continuously high values for the lycopane proxy (Figure 5.3E) are clearly in line with persistent anoxic to dysoxic bottom waters (Figure 5.7). Presumably, the foraminiferal repopulation event represents a short term, snapshot view of the situation at the time, while biomarkers and TM show a longer, averaged out representation of events. Biomarkers could not be studied in the lower carbonate layer (425.91-425.66 mcd) due to low TOC levels. Both carbonate layers demonstrate a major change in mineralogical composition. The concentration of Ti_{CF} and Al_{CF} increase, while K_{CF} decreases (Figure 5.4). This could be the result of an ash layer intercalated within the overall pelagic sediments. Authigenic carbonates could then have precipitated in these relatively porous ash layers (Hein et al., 1979, Hetzel et al., 2009). In general, biogenic carbonates are rich in Sr (Brumsack, 1980). Consequently, the relatively low Sr/Ca ratios in the carbonate layers indicate this carbonate is probably authigenic, rather than biogenic. At the deeper Demerara Rise site 1258, several, centimeter-thick ash layers are observed during this interval (Hetzel et al., 2009), suggesting that the lower single carbonate layer at Site 1260 actually represents a succession of thinner ash layers. Above the lower carbonate layer (425.57 mcd), an increase in isorenieratane and chlorobactane concentrations demonstrates that the base of the photic zone became euxinic again (Figure 5.3F and 5.3G). Chlorobactane concentrations are highest at the end of phase B and during phase C, suggesting that at this time, photic zone anoxia reached the shallowest water levels. At the same time, SSTs increase again and then remain stable at around 35 °C.

No clear changes occur in the TM or biomarker records at the boundary between phase A and phase B. However, in phase C, simultaneously increasing isorenieratane and TM concentrations (Fe, As) indicate conditions became again more euxinic. After phase C, isorenieratane concentrations drop to pre-OAE values, indicating that conditions at the base of the photic zone were generally oxic (Figure 5.7). However, TM patterns and the occurrence of lycopane demonstrate bottom waters remained anoxic.

A Before and after OAE-2



B Stratification during OAE-2



C Mixing during OAE-2

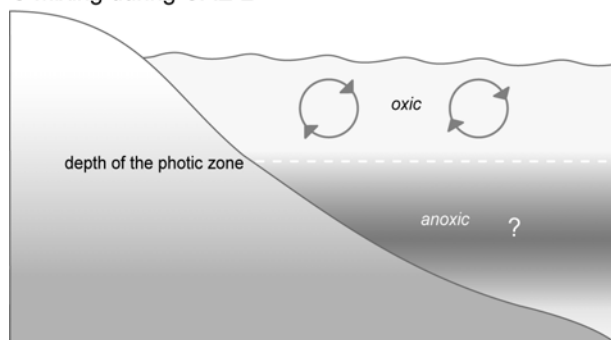


Figure 5.7 Simplified schemes of paleoenvironmental changes on Demerara Rise: (A) Before OAE-2. (B) During OAE-2, when high sea surface temperatures and strong stratification occurred. The occurrence of isorenieratane and chlorobactane demonstrates the presence of green sulfur bacteria and therefore photic zone euxinia. (C) During OAE-2, when surface water mixing and cooler temperatures prevailed. Lower isorenieratane and chlorobactane concentrations indicate water column mixing, the presence of lycopane suggests bottom water remained anoxic.

Trace metal drawdown during OAE-2

During OAE-2 the area in the proto-North Atlantic characterized by anoxic bottom waters expanded significantly. Burial of redox sensitive elements immobilized under oxygen-depleted conditions consequently increased, resulting in an overall decrease of concentrations of these elements in seawater. The considerable depletion in Mo, Ni, U, V and Zn at the start of OAE-2 (Figure 5.4), thus, may reflect such a decreased oceanic TM inventory (Algeo, 2004, Hetzel et al., 2009), related to an expansion of anoxic bottom water conditions. Before the OAE-2 interval, when sea water TM concentration were at their “regular” Cretaceous values, the anoxic conditions at Demerara Rise resulted in enhanced local immobilization of redox sensitive TMs. Directly following the onset of the OAE, a basin wide drawdown of redox sensitive elements decreased the accumulation of these elements at Demerara Rise. This decrease in TM concentrations occurred, even though, water column anoxia expanded locally, as shown by the strong increase in S-bound isorenieratane and chlorobactane concentrations. After OAE-2 concentrations of Mo_{CF}, Ni_{CF}, U_{CF}, V_{CF} and Zn_{CF} increase again in phase C (Figure 5.4), while, at the same time, high lycopane, isorenieratane and chlorobactane concentrations indicate that local water column conditions remained euxinic (Figure 5.3F and 5.3G). This increase may be due to a restoration of the seawater TM inventory to “regular” Cretaceous values.

A sudden and drastic drop in the seawater TM inventory requires large parts of the ocean floor becoming anoxic at the same time. The abrupt depletion of Mo_{CF}, Ni_{CF}, U_{CF}, V_{CF}, Zn_{CF} and possibly Cu_{CF} at the start of the OAE at Demerara Rise thus seem to reflect a proto-North Atlantic wide synchronous onset of OAE-2. This change in the TM inventory is further illustrated when plotting records of V, Mo, U and Zn against TOC (for a more detailed explanation see Hetzel et al. 2009).

Water column anoxia in the North Atlantic during OAE-2

Most of the hitherto investigated North Atlantic sites also show signs of bottom water anoxia and photic zone euxinia during OAE-2. Anoxia and euxinia, however, did not occur everywhere to the same extent (Bralower and Thierstein, 1987, Sinninghe Damsté and Köster, 1998). In the northern and eastern part of the proto-North Atlantic for instance, there is clear evidence of occasional bioturbation and therefore bottom water re-oxygenation during OAE-2 (Figure 5.2; DSDP Sites 105 and 603B, Herbin et al., 1987, Kuypers et al., 2004, Tarfaya Basin, Kolonic et al., 2005). Bottom water anoxia seems to have been more intense in the south, where bottom waters stayed anoxic during the entire OAE-2 interval (Figure 5.2; DSDP sites 367 and 144, Kuypers et al., 2002b, ODP Site 1260, this study).

From the widespread occurrence of isorenieratane derivatives during OAE-2 it becomes clear that euxinia reached the base of the photic zone at several locations (DSDP Sites 144, 367, 368 and Tarfaya Basin, Sinninghe Damsté and Köster, 1998, Kuypers et al., 2002b, DSDP Sites 105 and 603B, Kuypers et al., 2004, ODP Site 1260, this study). While in the north and southeast of the proto-North Atlantic, isorenieratane already occurs regularly before and after the OAE-2 interval (sites S13, 367 and 603B Kuypers et al., 2002b, Kolonic et al., 2005), isorenieratane was only observed in one sample predating the OAE-2 interval at Demerara Rise Site 144 (Kuypers et al., 2002b). This was explained by a shallower position of the chemocline in the southeast of the basin (Kuypers et al., 2002b). At Demerara Rise Site 1260, isorenieratane occurs also before and after OAE-2, albeit in low concentrations, indicating that the chemocline was not necessarily shallower in the southeast North Atlantic. On the contrary, at the northern proto North Atlantic sites (DSDP Sites 105 and 603B) isorenieratane abundances are much lower (Kuypers et al., 2004) during OAE-2 than in the south. Previously measured values range from 7 ng g⁻¹ TOC (Kuypers et al., 2004) to 150 µg g⁻¹ TOC (Kuypers et al., 2002b). To the best of our knowledge, the concentration of 270 µg g⁻¹ TOC observed at site 1260 at the onset of the OAE is the highest isorenieratane concentration measured in any OAE-2 site up to now, indicating that, at least during OAE-2, photic zone euxinia occurred probably much more frequent in the south.

The occurrence of S-bound chlorobactane demonstrates that extremely shallow photic zone anoxia occurred in the south and southeast of the proto-North Atlantic. At Tarfaya, S-bound chlorobactane was found in sediments deposited prior to, during and after the OAE-2 interval (Kolonic et al., 2005), while at DSDP Sites 367 and 144 S-bound chlorobactane was only found within the OAE-2 section, although here, the upper part of OAE-2 was not recovered during drilling (Kuypers et al., 2002b). Since chlorobactane concentrations are highest during the OAE-2 interval at most locations in the proto-North Atlantic, it seems photic zone anoxia became more pronounced during OAE-2. Although large parts of the North Atlantic clearly experienced photic zone anoxia during the OAE-2 interval, the slight increase in Fe_{CF} concentrations during OAE-2 at Site 1260 (Figure 5.4) requires an additional source of iron during deposition of this interval. Fe-enrichment can occur during euxinic conditions at the depositional site as long as there is a zone with anoxic but non-sulfidic conditions, in the same basin, allowing reductive Fe mobilization and subsequent Fe transport (Lyons and Severmann, 2006). Similarly, the extremely low Mn concentrations at Site 1260 demonstrate that there must have been oxygenated areas elsewhere in the North

Atlantic, where Mn presumably was deposited (Hetzl et al., 2009). Possibly the lack of a significant Mn enrichment in the proto-North Atlantic was due to the export of Mn in oxygen-depleted waters to the proto-Pacific. At the Northwest Australian margin, Mn-poor sediments were deposited within the OMZ during OAE-2, while sediments extremely rich in Mn were deposited below the OMZ, indicating oxic deep waters during the Cenomanian-Turonian interval at this location (Thurrow et al., 1992).

OM accumulation rates in the North Atlantic

The AR_{OC} at Site 1260 of ca. $0.3 \text{ gC m}^{-2} \text{ yr}^{-1}$, is substantially lower than the 9 and $12 \text{ gC m}^{-2} \text{ yr}^{-1}$ calculated previously for Site 367 (Kuypers et al., 2002b) and Tarfaya Basin (Kolonic et al., 2005), respectively (Figure 5.2). The AR_{OC} s from Tarfaya and Site 367 were calculated using shorter durations for OAE-2 (400 kyr for Site 367 and 490 kyr for Tarfaya), however when these AR_{OC} s are adjusted for a duration of 550 kyr for OAE-2, they are still an order of magnitude higher than the AR_{OC} s calculated for Site 1260. The AR_{OC} is influenced by both the rate of primary production and the degree of preservation of OM exported from the ocean surface to the sediment. Our TM and biomarker data indicate that organic matter preservation at Site 1260 was excellent. Furthermore, the excellently preserved laminations make post-depositional loss of sediments through winnowing unlikely. Preservation being excellent and post depositional loss of organic matter ruled out, primary production rates must have been relatively low compared to other locations in the southern proto-North Atlantic Ocean. Since biogenic barium was almost completely removed during diagenesis at Site 1260 (Brumsack, 1986, Arndt et al., 2006) it can no longer be used to test this hypothesis. Although both P and Y are commonly associated with phosphates, and high concentrations of these elements are thus indicative for enhanced productivity, P is also lost from the sediment during truly anoxic/euxinic conditions (Ingall et al., 1993).

Relatively low productivity during the OAE at Demerara Rise could be caused by the Cenomanian-Turonian transgression (Hancock and Kauffman, 1979, Haq et al., 1987) which resulted in an extended shelf area, trapping sediment and nutrients from the South American continent. Simultaneously, low productivity and a reduced sediment input resulted in suspension free waters, facilitating light penetration into the deeper euxinic part of the water column, creating an ideal environment for the growth of green sulfur bacteria (Figure 5.7).

Conclusions

Demerara Rise experienced anoxic bottom water conditions, not only during OAE-2, but also during most of the Cenomanian-Turonian transition. During OAE-2, the water column became euxinic from the bottom waters up to, at least, the lower part of the photic zone. The anoxic setting during OAE-2 was interrupted by a period of re-oxygenation, during which, the photic zone became temporarily oxygenated and bottom waters probably became suboxic. The decrease in TM enrichment factors during OAE-2 suggests a decline in the supply of trace metals to the Demerara Rise area. The increase of isorenieratane concentrations, while at the same time trace metal concentrations decrease, suggests that the onset of OAE-2 occurred approximately synchronous in the proto-North Atlantic.

Acknowledgements

We thank Marianne Baas for technical advice and Christian März for helpful comments on the manuscript. The comments of two anonymous reviewers are gratefully acknowledged. This research used samples and data provided by the Integrated Ocean Drilling Program (IODP). Funding by the Deutsche Forschungsgemeinschaft (SPP IODP-ICDP) to HJB is gratefully acknowledged.

References

- Algeo, T.J., 2004. Can marine anoxic events draw down the trace element inventory of seawater? *Geology* 32(12), 1057-1060.
- Arndt, S., Brumsack, H.-J., Wirtz, K.W., 2006. Cretaceous black shales as active bioreactors: A biogeochemical model for the deep biosphere encountered during ODP Leg 207 (Demerara Rise). *Geochimica et Cosmochimica Acta* 70(2), 408-425.
- Arthur, M.A., Dean, W.E., Pratt, L.M., 1988. Geochemical and climatic effects of increased marine organic carbon burial at the Cenomanian/Turonian boundary. *Nature* 335(6192), 714-717.
- Arthur, M.A., Dean, W.E., Schlanger, S.O., 1985. Variations in the global carbon cycle during the Cretaceous related to climate, volcanism and changes in atmospheric CO₂. In: Sundquist, E.T., Broecker, W.S. (Eds.), *The carbon cycle and atmospheric CO₂: Natural variations archean to present*. AGU Geophysical Monograph 32, 504-529.
- Arthur, M.A., Jenkyns, H.C., Brumsack, H.-J., Schlanger, S.O., 1990. Stratigraphy, geochemistry, and paleo-oceanography of organic carbon-rich Cretaceous sequences. In: Ginsburg, R.N., Beadoin, B. (Eds.), *Cretaceous resources, events and rhythms; background and plans for research*. NATO ASI Series C Vol. 304, Kluwer Academic Publishers, Dordrecht, 75-119.
- Bice, K.L., Birgel, D., Meyers, P.A., Dahl, K.A., Hinrichs, K.-U., Norris, R.D., 2006. A multiple proxy and model study of Cretaceous upper ocean temperatures and atmospheric CO₂ concentrations. *Paleoceanography* 21, PA2002.

- Brassel, S.C., Lewis, C.A., de Leeuw, J.W., de Lange, F., Sinninghe Damsté, J.S., 1986. Isoprenoid thiophenes: novel products of sediment diagenesis? *Nature* 320(6058), 160-162.
- Bralower, T.J., Thierstein, H.R., 1987. Organic carbon and metal accumulation rates in Holocene and mid-Cretaceous sediments: palaeoceanographic significance. In: Brooks, J., Fleet, A.J. (Eds.), *Marine Petroleum Source Rocks*. Geological Society, London. Special Publication 26, 345-369.
- Brumsack, H.-J., 1980. Geochemistry of Cretaceous black shales from the Atlantic Ocean (DSDP Legs 11, 14, 36, and 41). *Chemical Geology* 31, 1-25.
- Brumsack, H.-J., 1986. The inorganic geochemistry of Cretaceous black shales (DSDP Leg 41) in comparison to modern upwelling sediments from the Gulf of California. In: Summerhayes, C.P., Shackleton, N.J. (Eds.), *North Atlantic Paleocenography*. Geological Society, London. Special Publication 21, 447-462.
- Brumsack, H.-J., 2006. The trace metal content of recent organic carbon-rich sediments: implications for Cretaceous black shale formation. *Palaeogeography, Palaeoceanography, Palaeoecology* 232(2-4), 344-361.
- Calvert, S.E., Pedersen, T.F., 1993. Geochemistry of recent oxic and anoxic marine sediments: implications for the geological record. *Marine Geology* 113(1-2), 67-88.
- Dumitrescu, M., Brassel, S.C., Schouten, S., Hopmans, E.C., Sinninghe Damsté, J.S., 2006. Instability in tropical Pacific sea-surface temperatures during the early Aptian. *Geology* 34(10), 833-836.
- Erbacher, J., Friedrich, O., Wilson, P.A., Birch, H., Mutterlose, J., 2005. Stable organic carbon isotope stratigraphy across Oceanic Anoxic Event 2 of Demerara Rise, Western Tropical Atlantic. *Geochemistry, Geophysics, Geosystems* 6, Q06010.
- Erbacher, J., Mosher, D.C., Malone, M.J., ODP Leg 207 Shipboard Scientific Party, 2004b. Drilling probes past carbon cycle perturbations on the Demerara Rise. *EOS* 85(6), 57-63.
- Erbacher, J., Mosher, D.C., Malone, M.J., Shipboard Scientific Party, 2004a. Proceedings of the Ocean Drilling Program, Initial Reports, 207. College Station, TX (Ocean Drilling Program), pp. 89.
- Forster, A., Schouten, S., Moriya, K., Wilson, P.A., Sinninghe Damsté, J.S., 2007. Tropical warming and intermittent cooling during the Cenomanian/Turonian oceanic anoxic event 2: sea surface temperature records from the equatorial Atlantic. *Paleoceanography* 22, PA1219.
- Friedrich, O., Erbacher, J., Mutterlose, J., 2006. Paleoenvironmental changes across the Cenomanian/Turonian Boundary Event (Oceanic Anoxic Event 2) as indicated by benthic foraminifera from the Demerara Rise (ODP Leg 207). *Revue de Micropaléontologie* 49(3), 121-139.
- Gale, A.S., Christensen, W.K., 1996. Occurrence of the belemnite *Actinocamax plenus* in the Cenomanian of SE France and its significance. *Bulletin of the Geological Society of Denmark* 43, 68-77.
- Goldschmidt, V.M., 1954. *Geochemistry*. In: Muir, A.E. (Ed.), *The International Series of Monographs on Physics*. Clarendon Press, Oxford.
- Gradstein, F.M., Ogg, J.G., Smith, A.G., Bleeker, W., Lourens, L.J., 2004. A new Geologic Time Scale, with special reference to Precambrian and Neogene. *Episodes* 27(2), 83-100.
- Grice, K., Cao, C., Love, G.D., Böttcher, M.E., Twitchett, R.J., Grosjean, E., Summons, R.E., Turgeon, S.C., Dunning, W., Jin, Y., 2005. Photic zone euxinia during the Permian-Triassic superanoxic event. *Science* 307(5710), 706-709.
- Hancock, J.M., Kauffman, E.G., 1979. The great transgressions of the Late Cretaceous. *Journal of the Geological Society* 136(2), 175-186.

- Haq, B.U., Hardenbol, J., Vail, P.R., 1987. Chronology of fluctuating sea levels since the Triassic (250 million years ago to present). *Science* 235(4793), 1156-1167.
- Hardas, P., Mutterlose, J., 2006. Calcareous nannofossil biostratigraphy of the Cenomanian/Turonian boundary interval of ODP Leg 207 at the Demerara Rise. *Revue de Micropaléontologie* 49(3), 165-179.
- Hay, W.W., Migdisov, A., Balukhovsky, A.N., Wold, C.N., Flögel, S., Söding, E., 2006. Evaporites and the salinity of the ocean during the Phanerozoic: implications for climate, ocean circulation and life. *Palaeogeography, Palaeoclimatology, Palaeoecology* 240(1-2), 3-46.
- Hays, J.D., Pittman, W.C., 1973. Lithospheric plate motion, sea level changes and climatic and ecological consequences. *Nature* 246(5427), 18-22.
- Hays, L.E., Beatty, T., Henderson, C.M., Love, G.D., Summons, R.E., 2007. Evidence for photic zone euxinia through the end-Permian mass extinction in the Panthalassic Ocean (Peace River Basin, Western Canada). *Palaeoworld* 16(1-3), 39-50.
- Hedgepeth, J.W., 1957. Classification of marine environments. In: Ladd, H.S. (Ed.), *Treatise on marine ecology and paleoecology*. I. Ecology. Geological Society of America, Memoir 67, 17-28.
- Hein, J.R., O'Neil, J.R., Jones, M.G., 1979. Origin of authigenic carbonates in sediment from the deep Bering Sea. *Sedimentology* 26(5), 681-705.
- Herbin, J.P., Masure, E., Roucaché, J., 1987. Cretaceous formations from the lower continental rise off Cape Hatteras: organic geochemistry, dinoflagellate cysts, and the Cenomanian/Turonian boundary event at Sites 603 (Leg 93) and 105 (Leg 11). *Deep Sea Drilling Program, Initial Reports* 93, 1139-1162.
- Hetzel, A., Böttcher, M.E., Wortmann, U.G., Brumsack, H.-J., 2009. Paleo-redox conditions during OAE 2 reflected in Demerara Rise sediment geochemistry (ODP Leg 207). *Palaeogeography, Palaeoceanography, Palaeoecology* 273(3-4), 302-328.
- Horne, E.D., 1999. Ocean circulation modes of the Phanerozoic: Implications for the antiquity of deep-sea benthonic invertebrates. *Crustaceana* 72(8), 999-1018.
- Huerta-Diaz, M.A., Morse, J.W., 1992. Pyritization of trace metals in anoxic marine sediments. *Geochimica et Cosmochimica Acta* 56(7), 2681-2702.
- Jefferies, R.P.S., 1962. The palaeoecology of the Actinocamax Plenus subzone (lowest Turonian) in the Anglo-Paris Basin. *Palaeontology* 4(4), 609-647.
- Jenkyns, H.C., 1985. The Early Toarcian and Cenomanian-Turonian anoxic event in Europe: comparisons and contrasts. *Geologische Rundschau* 74(3), 505-518.
- Jenkyns, H.C., Gale, A.S., Corfield, R.M., 1994. Carbon-isotope and oxygen-isotope stratigraphy of the English chalk and Italian Scaglia and its paleoclimatic significance. *Geological Magazine* 131(1), 1-34.
- Keller, G., Pardo, A., 2004. Age and paleoenvironment of the Cenomanian-Turonian global stratotype section and point at Pueblo, Colorado. *Marine Micropaleontology* 51(1-2), 95-128.
- Kerr, A.C., 1998. Oceanic plateau formation: a cause of mass extinction and black shale deposition around the Cenomanian-Turonian boundary? *Journal of the Geological Society* 155(4), 619-626.
- Kolonic, S., Wagner, T., Forster, A., Sinninghe Damsté, J.S., Walsworth-Bell, B., Erba, E., Turgeon, S., Brumsack, H.-J., Chellai, E.H., Tsikos, H., Kuhnt, W., Kuypers, M.M.M., 2005. Black shale deposition on the northwest African Shelf during the Cenomanian/Turonian oceanic anoxic event: Climate coupling and global organic carbon burial. *Paleoceanography* 20(1), PA1006.
- Koopmans, M.P., Köster, J., van Kaam-Peters, H.M.E., Kenig, F., Schouten, S., Hartgers, W.A., de Leeuw, J.W., Sinninghe Damsté, J. S., 1996. Diagenetic and catagenetic

- products of isorenieratene: Molecular indicators for photic zone anoxia. *Geochimica et Cosmochimica Acta* 60(22), 4467-4496.
- Kump, L.R., Pavlov, A., Arthur, M.A., 2005. Massive release of hydrogen sulfide to the surface ocean and atmosphere during intervals of oceanic anoxia. *Geology* 33(5), 397-400.
- Kuroda, J., Ogawa, N.O., Tanimizu, M., Coffin, M.F., Tokuyama, H., Kitazato, H., Ohkouchi, N., 2007. Contemporaneous massive subaerial volcanism and late cretaceous Oceanic Anoxic Event 2. *Earth and Planetary Science Letters* 256(1-2), 211-223.
- Kuypers, M.M.M., 2001. Mechanisms and biogeochemical implications of the mid-Cretaceous global organic carbon burial events. University of Utrecht.
- Kuypers, M.M.M., Blokker, P., Hopmans, E.C., Kinkel, H., Pancost, R.D., Schouten, S., Sinninghe Damsté, J.S., 2002a. Archaeal remains dominate marine organic matter from the early Albian oceanic anoxic event 1b. *Palaeogeography, Palaeoclimatology, Palaeoecology* 185(2), 211-234.
- Kuypers, M.M.M., Lourens, L.J., Rijpstra, W.R.C., Pancost, R.D., Nijenhuis, I.A., Sinninghe Damsté, J.S., 2004. Orbital forcing of organic carbon burial in the proto-North Atlantic during oceanic anoxic event 2. *Earth and Planetary Science Letters* 228(3-4), 465-482.
- Kuypers, M.M.M., Pancost, R.D., Nijenhuis, I.A., Sinninghe Damsté, J.S., 2002b. Enhanced productivity led to increased organic carbon burial in the euxinic North Atlantic basin during the late Cenomanian oceanic anoxic event. *Paleoceanography* 17(4), 1051.
- Leckie, R.M., Yureteich, R.F., West, O.L.O., Finkelstein, D., Schmidt, M., 1998. Paleooceanography of the southwestern Western Interior Sea during the time of the Cenomanian-Turonian boundary (Late Cretaceous). In: Dean, W.E., Arthur, M.A. (Eds.), *Stratigraphy and Paleoenvironments of the Cretaceous Western Interior Seaway, USA. SEPM Concepts in Sedimentology and Paleontology*, No. 6, Society for Sedimentary Geology (SEPM), Tulsa, Oklahoma, 101-126.
- Lyons, T.W., Severmann, S., 2006. A critical look at iron paleoredox proxies: New insights from modern euxinic marine basins. *Geochimica et Cosmochimica Acta* 70(23), 5698-5722.
- Meyers, P.A., Bernasconi, S.M., Forster, A., 2006. Origins and accumulation of organic matter in expanded Albian to Santonian black shale sequences on the Demerara Rise, South American margin. *Organic Geochemistry* 37(12), 1816-1830.
- Pancost, R.D., Crawford, N., Magness, S., Turner, A., Jenkyns, H.C., Maxwell, J.R., 2004. Further evidence for the development of photic-zone euxinic conditions during Mesozoic oceanic anoxic events. *Journal of the Geological Society* 161(3), 353-364.
- Paul, C.R.C., Lamolda, M.A., Mitchell, S.F., Vaziri, M.R., Gorostidi, A., Marshall, J.D., 1999. The Cenomanian-Turonian boundary at Eastbourne (Sussex, UK): a proposed European reference section. *Palaeogeography Palaeoclimatology Palaeoecology* 150(1-2), 83-121.
- Paytan, A., Kastner, M., Campbell, D., Thieme, M.H., 2004. Seawater sulfur isotope fluctuations in the Cretaceous. *Science* 304(5677), 1663-1665.
- Sageman, B.B., Meyers, S.R., Arthur, M.A., 2006. Orbital time scale and new C-isotope record for Cenomanian-Turonian boundary stratotype. *Geology* 34(2), 125-128.
- Schaeffer, P., Adam, P., Wehrung, P., Albrecht, P., 1997. Novel aromatic carotenoid derivatives from sulfur photosynthetic bacteria in sediments. *Tetrahedron Letters* 38(48), 8413-8416.
- Schouten, S., Hopmans, E.C., Schefuß, E., Sinninghe Damsté, J.S., 2002. Distributional variations in marine crenarchaeotal membrane lipids: A new tool for reconstructing ancient sea water temperatures? *Earth and Planetary Science Letters* 204(1-2), 265-274.

- Sinninghe Damsté, J.S., Hopmans, E.C., 2008. Does fossil pigment and DNA data from Mediterranean sediments invalidate the use of green sulfur bacterial pigments and their diagenetic derivatives as proxies for the assessment of past photic zone euxinia? *Environmental Microbiology* 10(6), 1392-1399.
- Sinninghe Damsté, J.S., Köster, J., 1998. A euxinic southern North Atlantic Ocean during the Cenomanian/Turonian oceanic anoxic event. *Earth and Planetary Science Letters* 158(3-4), 165-173.
- Sinninghe Damsté, J.S., Kuypers, M.M.M., Pancost, R.D., Schouten, S., 2008. The carbon isotopic response of algae, (cyano)bacteria, archaea and higher plants on the late Cenomanian perturbation of the global carbon cycle: Insights from biomarkers in black shales from the Cape Verde Basin (DSDP Site 367). *Organic Geochemistry* 39(12), 1703-1718.
- Sinninghe Damsté, J.S., Kuypers, M.M.M., Schouten, S., Schulte, S., Rullkötter, R., 2003. The lycopane/C-31 n-alkane ratio as a proxy to assess palaeoxicity during sediment deposition. *Earth and Planetary Science Letters* 209(1-2), 215-226.
- Sinninghe Damsté, J.S., Rijpstra, W.I.C., Kock-van Dalen, A.C., de Leeuw, J.W., Schenck, P., 1989. Quenching of labile functionalised lipids by inorganic sulfur species: evidence for the formation of sedimentary organic sulfur compounds at the early stages of diagenesis. *Geochimica et Cosmochimica Acta* 53(6), 1343-1355.
- Sinninghe Damsté, J.S., Schouten, S., van Duin, A.C.T., 2001. Isorenieratene derivatives in sediments: Possible controls on their distribution. *Geochimica et Cosmochimica Acta* 65(10), 1557-1571.
- Sinninghe Damsté, J.S., Wakeham, S.G., Kohnen, M.E.L., Hayes, J.M., de Leeuw, J.W., 1993. A 6,000-year sedimentary molecular record of chemocline excursions in the Black-Sea. *Nature* 362(6423), 827-829.
- Sinton, C.W., Duncan, R.A., 1997. Potential links between ocean plateau volcanism and global ocean anoxia at the Cenomanian-Turonian boundary. *Economic Geology* 92(7-8), 836-842.
- Snow, L.J., Duncan, R.A., Bralower, T.J., 2005. Trace element abundances in the Rock Canyon Anticline, Pueblo, Colorado, marine sedimentary section and their relationship to Caribbean plateau construction and oxygen anoxic event 2. *Paleoceanography* 20, PA4099.
- Suganuma, Y., Ogg, J.G., 2006. Campanian through Eocene magnetostratigraphy of Sites 1257-1261, ODP Leg 207, Demerara Rise (western equatorial Atlantic) In: Mosher, D.C., Erbacher, J., Malone, M.J. (Eds.), *Proceedings of the Ocean Drilling Program, Scientific Results*, 207. College Station, TX (Ocean Drilling Program), 1-48.
- Thurrow, J., Brumsack, H.-J., Rullkötter, J., Littke, R., Meyers, P., 1992. The Cenomanian/Turonian boundary event in the Indian Ocean - a key to understand the global picture. In: Duncan, R.A., Rea, D.K., Kidd, R.B., von Rad, U., Weissel, J.K. (Eds.), *The Indian Ocean: A Synthesis of Results from the Ocean Drilling Program*. American Geophysical Union, *Geophysical Monograph* 70, 253-273.
- Tsikos, H., Jenkyns, H.C., Walsworth-Bell, B., Petrizzo, M.R., Forster, A., Kolonic, S., Erba, E., Premoli Silva, I., Baas, M., Wagner, T., Sinninghe Damsté, J.S., 2004. Carbon-isotope stratigraphy recorded by the Cenomanian-Turonian oceanic anoxic event; Correlation and implications based on three key localities: *Journal of the Geological Society* 161(4), 711-719.
- Turgeon, S.C., Creaser, R.A., 2008. Cretaceous oceanic anoxic event 2 triggered by a massive magmatic episode. *Nature* 454(7202), 323-326.
- van Gemerden, H., Mas, J., 1995. Ecology of phototrophic sulfur bacteria. In: Blankenship, R.E., Madigan, M.T., Bauer, C.E. (Eds.), *Anoxygenic photosynthetic bacteria*. Kluwer Academic Publishers, Dordrecht, 49-85.

- Voigt, S., Gale, A.S, Flögel, S., 2004. Midlatitude shelf seas in the Cenomanian-Turonian greenhouse world: Temperature evolution and North Atlantic circulation. *Paleoceanography* 19, PA4020.
- Wedepohl, K.H., 1971. Environmental influences on the chemical composition of shales and clays. In: Ahrens, L.H., Press, F., Runcorn, S.K., Urey, H.C. (Eds.), *Physics and Chemistry of the Earth* 8. Pergamon, Oxford, 305-333.
- Wortmann, U.G., Bernasconi, S.M., Böttcher, M.E., 2001. Hypersulfidic deep biosphere indicates extreme sulfur isotope fractionation during single step microbial sulfate reduction. *Geology* 29(7), 647-650.

6. Evolution of organic matter degradation in Cretaceous black shales inferred from authigenic barite: A reaction-transport model

Sandra Arndt, Almut Hetzel, Hans-Jürgen Brumsack

This chapter was published 2009 in *Geochimica et Cosmochimica Acta* 73(7), 2000-2022.

Abstract

A reaction-transport model was used to infer the long-term evolution of anaerobic organic matter degradation in Cretaceous black shales from the distribution of authigenic barite in sediments drilled at Demerara Rise (ODP Leg 207, Site 1258). In these sediments, sulfate-reduction and methanogenesis are the major pathways of organic matter decomposition and the depth-distribution of authigenic barite serves as an indicator for the temporal evolution of the sulfate-methane transition zone (SMTZ), the strength of the biogenic methane flux and, ultimately, the organic matter reactivity in the black shales over geological timescales. Organic matter degradation is described according to the reactive continuum model approach and parameters values are determined by inverse modeling, based on present-day porewater and authigenic barite profiles. Fully transient simulations were performed over a period of 100 Myrs and indicate that important features of the biogeochemical dynamics are associated to changes in the boundary forcing. Hiatuses in sediment accumulation rate result in quasisteady-state conditions and lead to distinct accumulations of authigenic barites in the SMTZ. The inversely determined parameters reveal that the reactivity of the organic matter was already low (apparent first order rate constant $k \approx 10^{-4} \text{ yr}^{-1} - 10^{-6} \text{ yr}^{-1}$) at the time of its deposition in the Cretaceous. The geochemical characteristics of sediments drilled at Demerara Rise, as well as the presence of specific biomarkers, suggest that this low reactivity is most likely due to the euxinic palaeo-conditions which favored the sulfurization of the organic matter. Simulation results predict average initial organic carbon contents between 8.1 and 9.5 wt%, implying a high preservation efficiency of the organic matter (between 79% and 89%). Calculated mass accumulation rates (between 0.43 and $0.5 \text{ g C m}^{-2} \text{ year}^{-1}$) compare well with estimations for the western basin of the Cretaceous southern North Atlantic. Simulation results thus indicate that the enhanced preservation of organic matter under euxinic conditions may

have been the main cause for the formation of organic-rich Cretaceous black shales at Demerara Rise.

Keywords: Reaction-transport model, Cretaceous black shales, organic matter degradation, organic matter burial, sulfate methane transition zone, authigenic barite, Demerara Rise, ODP Leg 207

Introduction

On a global scale, mid-Cretaceous (120 to 80 Myrs) sediments are characterized by relatively thick layers of organic-rich black shales (Stein et al., 1986). These black shale sequences are linked to a series of significant perturbations in the ocean-atmosphere system, the so-called oceanic anoxic events, OAE, (e.g. Schlanger and Jenkyns, 1976; Jenkyns, 1980; Arthur et al., 1990). The enhanced sequestration of organic carbon during these extreme events not only had a significant impact on Cretaceous ocean chemistry and climate, but also played an important role in the formation of petroleum source rocks. However, the exact nature and functioning of the palaeo-environment that fostered the massive and almost ubiquitous deposition of organic carbon-rich sediments is still a matter of debate.

In the past, Cretaceous black shale formation has often been related to an increased organic matter preservation in an anoxic ocean (e.g. Demaison and Moore, 1980), increased oceanic productivity (e.g. Pederson and Calvert, 1990) or a combination of both (e.g. Erbacher et al., 2001; Wilson and Norris, 2001; Brumsack, 2006). However, results from the analysis of shale organic carbon (e.g. Arthur et al., 1987, 1988; Meyers et al., 2001; Lyons et al., 2003), diagenetic modeling (e.g. Berner, 1980; Westrich and Berner, 1984; Middelburg, 1989; Boudreau and Ruddick, 1991; Tromp et al., 1995; Wallmann et al., 2006) as well as observations from modern day analogs (e.g. Emerson, 1985; Tyson and Pearson, 1991; Canfield, 2001) substantially advanced the general understanding of organic carbon burial over the past decades and primary production, sedimentation/dilution and microbial degradation have been identified as the main controls for organic carbon burial in marine sediments (e.g. Emerson and Hedges, 1988; Arthur and Sageman, 1994; Canfield, 1994; Tyson, 2001). Nonetheless, the relative importance of each of these processes is difficult to assess (Demaison and Moore, 1980; Ibach, 1982; Pederson and Calvert, 1990; Sageman et al., 2003; Burdige, 2007). This is particularly true for ancient sediments, such as Cretaceous black shales. In these sediments, long-term trends in sedimentation rates can be comparably well constrained by dating of the ocean drill core. However, the estimation of palaeo-productivity is generally complicated by the strong diagenetic overprint of palaeoproxies (e.g. barite). More important, our quantitative understanding of microbial degradation processes over geological time scales is very limited. A better quantification of organic matter degradation during burial could therefore provide important insights into the mechanisms of black shale formation and could thus ultimately shed light on the functioning of the mid-Cretaceous carbon cycle. Generally, a

pronounced decrease in organic matter degradation rates during burial has been documented for different environments and over time scales ranging from hours to millions of years (Middelburg, 1989; Boudreau and Ruddick, 1991). Nevertheless, observations and diagenetic modeling results show that the organic matter in ancient, deeply buried organic carbon-rich strata still provides a suitable substrate for ongoing microbial degradation (Krumholz et al., 1997; Coolen et al., 2002; Krumholz et al., 2002; Moodley et al., 2005; Arndt et al., 2006).

The reconstruction of the diagenetic history in these sediments is complicated by the superposition of various diagenetic signals and the limited availability of observations. Nevertheless, the distribution of authigenic mineral phases may be key to a deeper understanding of long-term biogeochemical dynamics, since it provides a detailed record of the spatio-temporal redox dynamics and related microbial activities. Authigenic pyrites, for instance, indicate the migration of redox-fronts and a later sulfidization of underlying sediments as described for sediments below sapropels of the Kau Basin (Middelburg, 1991), the Eastern Mediterranean (Passier et al., 1996), the Baltic Sea (Böttcher and Lepland, 2000), or the Black Sea (Jørgensen et al., 2004). Authigenic barite fronts may serve as indicators for the past and present location of redox fronts, methane fluxes or hiatuses in sedimentation rate (Brumsack, 1986; van Os et al., 1991; Bréhéret and Brumsack, 2000; Dickens, 2001; Arndt et al., 2006). Yet, authigenic minerals are also sensitive to diagenetic alteration. Earlier formed authigenic fronts, for instance, may redissolve at later stages or may be superimposed by more recent accumulations. The interpretation of this record can therefore be seriously compromised. In this respect, mathematical modeling is a powerful tool to “rewind the tape”. Transient reaction-transport models (RTMs) can help to resolve the diagenetic history that created the observed distribution. A model that reproduces the observed present-day depth-distribution of authigenic minerals and the depth-profiles of interstitial waters can provide a quantitative understanding of diagenetic processes, deposition and burial fluxes over geological time scales. And yet, the application of RTMs over geological time scales is severely limited by data constraints. Black shale sequences and interstitial water gradients obtained by deep sea drilling are usually not analyzed at a sufficiently high resolution for a detailed interpretation of past environmental change and possible diagenetic overprints.

Sediment sequences drilled at Site 1258 during ODP Leg 207 (Ocean Drilling Program) at Demerara Rise provide an excellent and comprehensive data set (Erbacher et al., 2004). These sections contain deep-seated extended Cretaceous black shale sequences, which

still provide a suitable substrate for ongoing metabolic activity in a modern day deep biosphere setting (Erbacher et al., 2004; Arndt et al., 2006). Steady-state simulations of the present-day situation revealed that authigenic barite dynamics are controlled by the depth of the sulfate-methane transition zone (SMTZ) and thus by the diffusive flux of biogenic methane out of the black shale sequences (Arndt et al., 2006). Arndt et al. (2006) therefore hypothesized that the distribution of authigenic barites above the black shales serves as an indicator for the temporal evolution of the SMTZ, the strength of the biogenic methane flux and ultimately for the evolution of organic matter reactivity in the black shales over the past 100 Myrs. In this study, the black shale overlying sediments are sampled with a high enough spatial resolution to obtain a detailed barite depth-profile within the model-determined, critical depth range. The new high-resolution barite depthprofile offers, in combination with the comprehensive standard ODP data set and a total number of 152 interstitial water samples, sufficient information to constrain a transient RTM which can be used to hindcast the evolution of biogeochemical fluxes and transformations over the past 100 Myrs and to test the earlier formulated hypothesis. Simulation results allow estimates of the initial organic matter content and its reactivity, as well as their long-term evolution from the shallow subsurface to the deep biosphere. These quantifications shed light on the functioning of the sedimentary carbon sink during the Cretaceous, the nature of the depositional environment and the controls of organic carbon preservation in Cretaceous black shales.

Materials and Methods

Site description

Demerara Rise is a prominent submarine plateau located at approximately 5°N off the coasts of Suriname and French Guyana (Fig. 6.1). It is built on rifted continental crust of Precambrian and early Mesozoic age and was one of the last areas in contact with West Africa prior to the opening of the equatorial Atlantic. The rise stretches approximately 380 km along the coast and reaches a width of around 220 km from the shelf break to the northeastern escarpment, where water depths increase sharply from 1000 to over 4500 m. While most of the plateau lies in shallow water (700 m), the northwest margin is a gentle ramp that reaches depths of 3000-4000 m. Here the plateau is covered by 2-3 km of pelagic sediment down to water depths >4000 m. Sediment sequences drilled at the northern flank of Demerara Rise during ODP Leg 207 are of lower Albian to Neogene origin, thus reflecting a significant part of the palaeoceanographic history of the tropical

Atlantic Ocean. Upper Albian sediments are mostly green clayey carbonate siltstones. The Cenomanian to Santonian sequence consists almost exclusively of laminated carbonate-rich, calcareous black shales with occasional stringers of limestone and chert. In total, about 650 m of black shales were recovered during ODP Leg 207 (Erbacher et al., 2004). Critical intervals recovered include multiple copies of OAE 2 and 3. Campanian to Paleogene sediments are calcareous to siliceous oozes and chalks. A prominent submarine channel system and erosional surface developed in the late Oligocene to early Miocene. The channels carried sediment east-to-west over the flank of the plateau and into feeder channels for a submarine fan that formed northwest of the Demerara Rise. The channel system was short-lived and most of the Neogene sediments are thin (a few meters) or absent from the distal portions of the plateau.

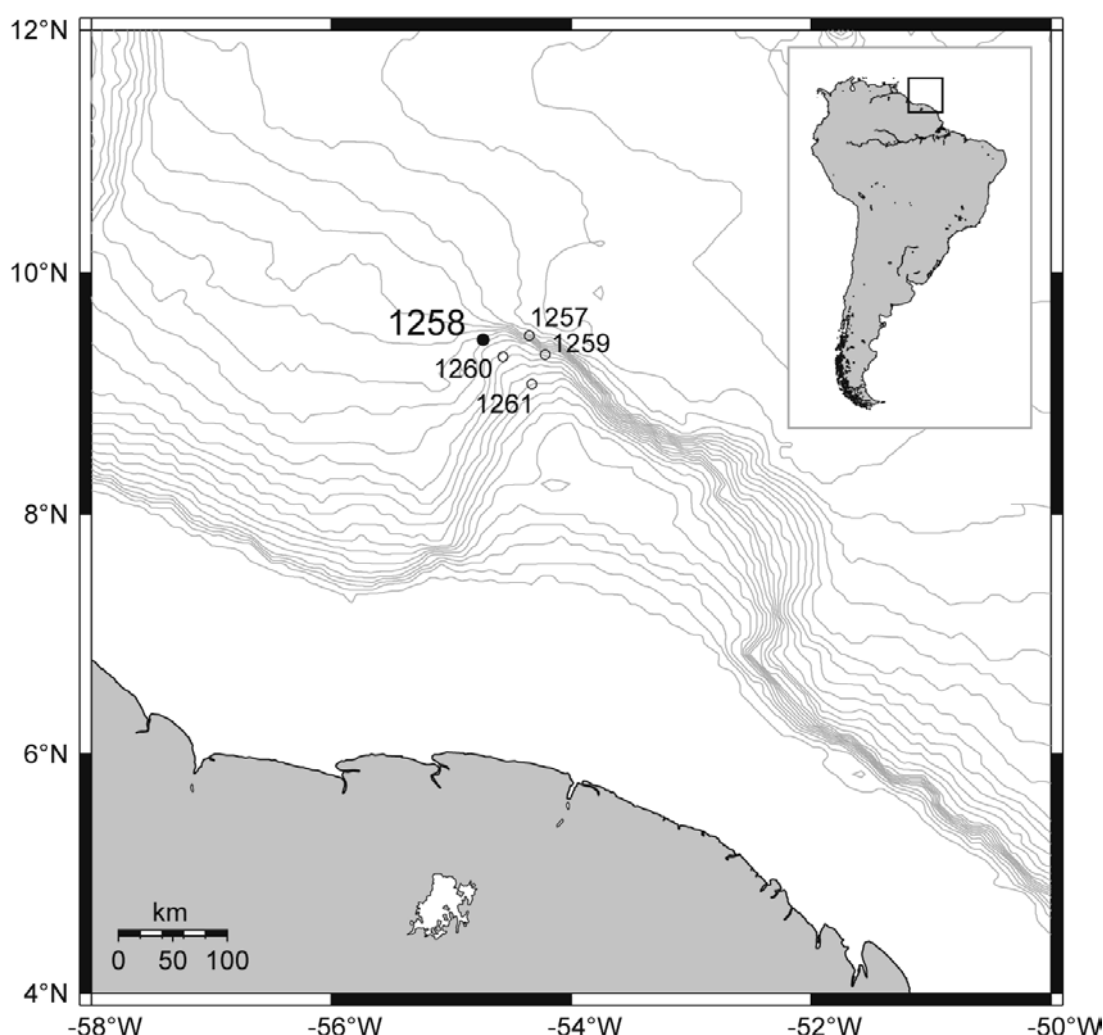


Figure 6.1 Location of ODP drill Sites (1257-1261) on Demerara Rise (ODP Leg 207, Equatorial Atlantic). The presented study focuses on observations from drill Site 1258.

Previous work and modeling strategy

At Demerara Rise, sediment sequences were drilled at five drill Sites (Site 1257-1261, Erbacher et al., 2004). All drilled sections are characterized by the presence of a distinct, deep-seated (150-500 mbsf) Cretaceous black shale sequence, which still exhibits very high total organic carbon contents (TOC) of up to 30 wt% (Fig. 6.2). In contrast, overlying Campanian to Pleistocene chalks and oozes reveal relatively low TOC contents. Interstitial sulfate (SO_4) concentrations decrease linearly from the sediment-water interface to the top of the black shale sequence. The depletion in interstitial SO_4 is accompanied by an increase in ammonium and methane (CH_4) concentrations within the black shale layer (Fig. 6.2). Observed interstitial water depth-profiles thus indicate that almost 100 Myrs after their deposition, deeply buried Cretaceous black shales still act as active bioreactors at great sediment depths and control the biogeochemical reaction network in these sediments (Erbacher et al., 2004).

On the basis of the collected data set, Arndt et al. (2006) designed a steady-state RTM to identify and quantify the importance of the biogeochemical transformation processes in the present-day, deep biosphere setting at Demerara Rise. Reaction rate constants were determined through inverse modeling techniques and provide a first estimate of the most pertinent biogeochemical rate constants. Simulation results show that the Cretaceous black shales still provide a suitable substrate for an ongoing metabolic activity in these sediments. Methanogenesis is a key process, dominating not only the organic matter degradation in the black shales but also the SO_4 availability through the anaerobic oxidation of methane (AOM) above the black shales (Arndt et al., 2006). The complete depletion of SO_4 within the black shale sequences results in an undersaturation of pore waters with respect to barite (BaSO_4) and, therefore, promotes the remobilization of biogenic barium (Ba). Remobilized Ba diffuses out of the black shale layer and reprecipitates as authigenic BaSO_4 in the SMTZ, where the presence of SO_4 increases the saturation state of the interstitial waters. Therefore, Arndt et al. (2006) argued that elevated authigenic BaSO_4 contents should coincide with the SMTZ and may serve as an indicator for the AOM, the intensity of the biogenic CH_4 production in the black shales and ultimately for the reactivity of the bulk organic matter (Arndt et al., 2006).

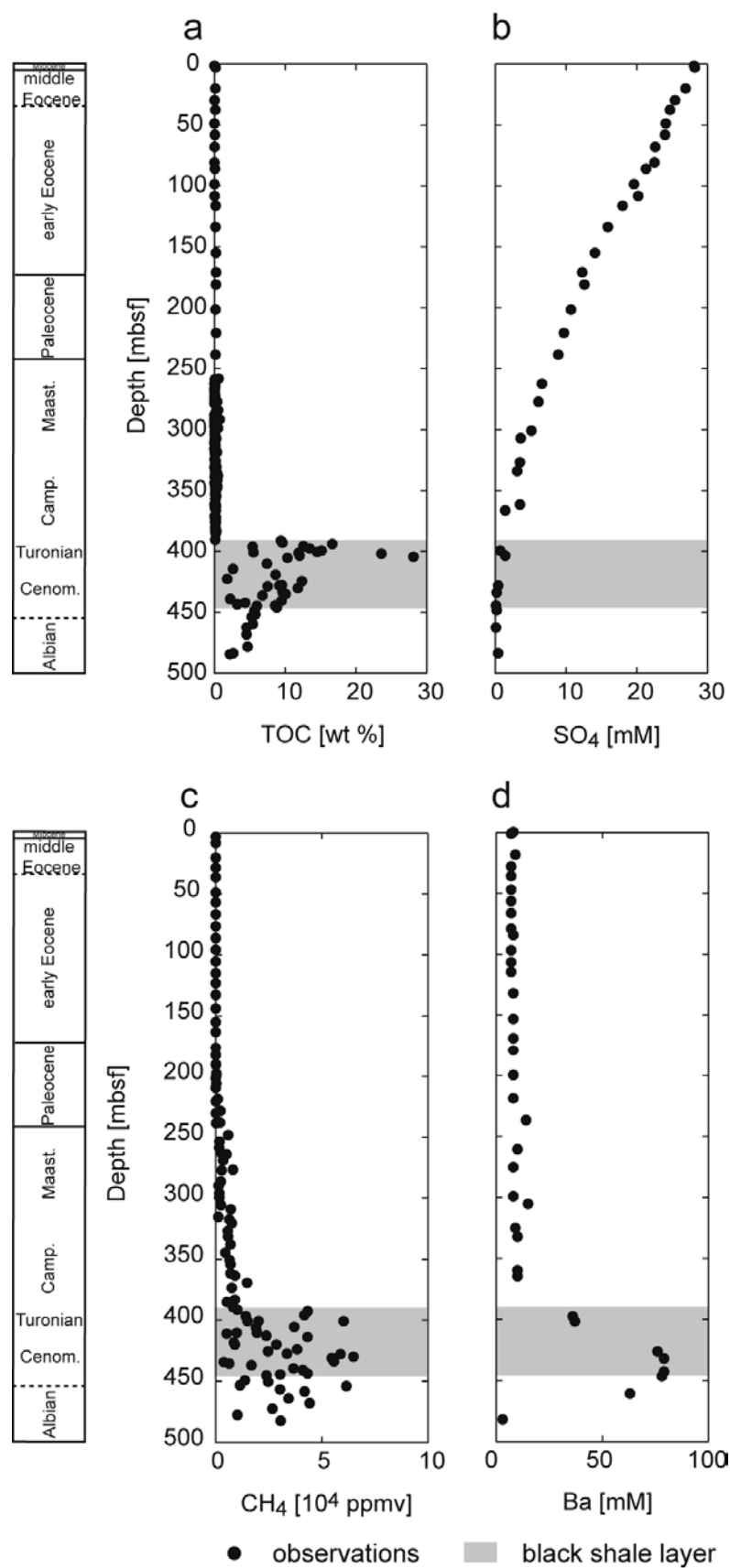


Figure 6.2 Observed (a) TOC, (b) SO_4 , (c) CH_4 and (d) Ba concentration depth-profiles in sediments drilled at Site 1258 (ODP Leg 207, Demerara Rise). The location of the Cretaceous black shale sequence is indicated by a gray box. A corresponding geological time scale is illustrated on the left of the depth scales.

However, core observations as well as a very limited data set of solid-phase barium excess values did not reveal the presence of a single, pronounced authigenic BaSO_4 front in the vicinity of the SMTZ. In fact, authigenic BaSO_4 crystals of mm to cm scale were frequently observed over the whole length of Campanian to Paleogene sediment sequences (Erbacher et al., 2004; Arndt et al., 2006). Arndt et al. (2006) hypothesized, that the absence of a distinct authigenic front may indicate varying intensities of CH_4 production during burial. The resulting variations in CH_4 flux would have induced important shifts of the SMTZ and, therefore, would have inhibited the formation of a single front or would have led to the dissolution of already formed fronts. This hypothesis was supported by the results of a sensitivity study, which revealed that the SMTZ is, indeed, extremely sensitive to the rate of methanogenesis in the black shales. Under steady-state conditions, a doubling of the rate constant of methanogenesis shifts the SMTZ about 100 m up in the sediment (Arndt et al., 2006). The authigenic BaSO_4 distribution above the black shales thus provides a detailed record of the past and present location of the SMTZ and the temporal evolution of organic matter degradation. Unfortunately, the spatial resolution of the available BaSO_4 depth-profiles was too coarse (ca. 10 - 30 m) to allow inferring these information. Instead, Arndt et al. (2006) provided first, rough estimates of the initial organic matter reactivity by applying the power model within a reasonable range of initial organic matter contents. They concluded that the initial reactivity of black shale organic matter was probably orders of magnitude lower than in modern marine sediments. Based on observations from similar black shale bearing sites, they speculated that this apparent refractory nature of the black shale organic matter might be related to an anoxic/euxinic character of the depositional environment. However, the proposed hypotheses and estimates had to remain purely speculative, since the available BaSO_4 did not allow verifying the estimated initial reactivity and its evolution. In addition, little was known about the nature of the depositional environment during the black shale formation at Demerara Rise.

Based on these simulation results, a new analytic and modeling strategy is designed to test and refine the earlier formulated hypothesis and to provide a quantitative understanding of the long-term evolution of biogeochemical transformations and fluxes accompanying organic matter breakdown on geological time scales. The black shales overlying chalks and calcareous claystones of Site 1258A (Units III to IIc, Erbacher et al., 2004) are sampled with high resolution (ca. 50 cm) to obtain a detailed BaSO_4 depth-profile within a critical depth range identified by the steady-state simulation results. The resulting highly resolved depth-distribution of BaSO_4 provides a detailed record of the past and present location of the

SMTZ and, therefore offers, in combination with the growing ODP Leg 207 data set, a unique opportunity to study the long-term biogeochemical dynamics at Demerara Rise. A direct interpretation of this record is however complicated by the strong diagenetic overprint and the superposition of various signals. Therefore, a transient RTM is designed on the basis of the mechanistic understanding developed in the steady-state modeling study. The modeling procedure has to be carried out backwards, since the model attempts to reconstruct past conditions based on indirect evidence. In other words, the problem mainly consists in finding a set of parameters that reproduces the observed BaSO_4 distribution and the present-day depth-profiles. Such an extraction of model parameter values from available data is called an inverse problem. In general, inverse modeling is hampered by two problems. First, models often contain a number of free parameters that may not be fully determinable on the basis of available data. Second, a number of different models may explain a given data set equally well, at least in the sense of measures of misfit. However, previous modeling efforts revealed that the long-term redox dynamics below the shallow subsurface at Demerara Rise are mainly controlled by the degradation of organic matter in the distinct black shale layer (Arndt et al., 2006). Therefore, the presented inverse modeling approach focuses on the parameters describing organic matter degradation. The parameter values of the additional biogeochemical and transport processes, such as AOM or BaSO_4 precipitation/dissolution are adopted from the previous steady-state model (Arndt et al., 2006). This approach reduces the number of free parameters and, therefore, the number of models that may potentially fit the data equally well. In addition, it uses the available data efficiently to constrain the most sensitive parameters. Furthermore, the growing, comprehensive ODP data set also limits the number of possible model scenarios. Therefore, the parameter set that reproduces the high-resolution BaSO_4 distribution and the observed interstitial water depth-profiles may help constrain the timedependent evolution of organic matter reactivity on time scales that fall far beyond the reach of laboratory experimentation. The RTM can then be used to resolve the diagenetic history, recorded in the observed present-day depth distribution of authigenic BaSO_4 . The presented model approach may shed light on the functioning of the sedimentary carbon sink during the Cretaceous. It may further offer insight into the conditions that may have prevailed at the seafloor during episodes of enhanced organic carbon sequestration in marine sediments, such as during OAEs.

Sampling methods

During ODP Leg 207 interstitial waters, covering a depth range from the sediment/seawater interface to 548 mcd (meters composite depth), were collected and processed using standard ODP methods (Gieskes et al., 1991). CH₄ measurements were performed in the framework of the routine monitoring of interstitial gas contents and a special microbial gas study (Meyers et al., 2004). A faint odor of hydrogen sulfide was noticeable in sediment samples from the black shale sequence, but the gas could not be detected with the natural gas analyzer in headspace samples. The amount of total organic carbon (TOC) was calculated as the difference between total carbon and inorganic carbon, which were determined using an infrared analyzer and a CO₂ coulometer coupled to an acidification module, respectively. A detailed description of the standard shipboard operations and analysis can be found in Erbacher et al. (2004) and Hetzel et al. (2006). On board, splits of all squeeze cakes (pore water squeezing residues) were taken, freeze-dried, and stored in polyethylene bags. In addition, the black shales overlying chalks and calcareous claystones of Site 1258A (Units III to IIc, Erbacher et al., 2004) were sampled post-cruise in the Bremen Core Repository. Sediment splits were taken every approximately 0.5 m spanning a depth range of 258.1–385.3 mbsf. At the ICBM, freeze-dried sediment splits were ground and homogenized in an agate ball mill. Sedimentary barium concentrations, Ba_t , were determined by X-ray fluorescence (XRF) analysis. For this purpose, 600 mg of sample powder were mixed with 3600 mg of a 1:1 mixture of dilithiumtetraborate (Li₂B₂O₇) and lithiummetaborate (LiBO₂), pre-oxidized at 500 °C with NH₄NO₃ (p.a.) and fused into glass beads. The glass beads were analyzed by XRF (Philips PW 2400) calibrated with 29 carefully selected geostandards. Procedures and accuracy of the methods were checked with two in-house reference materials. Analytical precision (defined as 100% times the best estimated standard deviation (1σ) divided by the mean of the repeats) was better than 3.1%. Analytical accuracy (defined as 100% times the mean of the repeat analyses divided by the expected value) was 105.0%. Since the sedimentary barite composition consists mainly of barite and detrital aluminosilicates (Schenau et al., 2001; Robin et al., 2003), barium excess concentrations, Ba_{xs} , were corrected for the barium incorporated in aluminosilicates by applying the minimum barium-aluminum ratio found in sediments at Site 1258 (Ba_t/Al) = 0.003433:

$$Ba_{xs}(z) = Ba_t(z) - Al(z) \cdot Ba_t/Al \quad (1)$$

The corrected barium excess concentrations were used to calculate barite concentrations.

Model Description

Transport

The one-dimensional conservation of dissolved and solid species C_i (e.g. Berner, 1980; Boudreau, 1997) is given by:

$$\frac{\partial C_i}{\partial t} = -\frac{\partial F_i}{\partial z} + \sum R_i \quad (2)$$

The change in concentration of chemical species i is balanced by the divergence of mass flux, F_i , and the sum of biogeochemical reactions, $\sum R_i$, affecting species i . For a dissolved species undergoing transport by molecular diffusion and compaction-influenced advection, the conservation equation reads:

$$\frac{\partial \phi C_i}{\partial t} = D'_i \frac{\partial C_i^2}{\partial z^2} + \left(\frac{D'_i}{\phi} \frac{\partial \phi}{\partial z} + \frac{\partial D'_i}{\partial z} - \frac{\phi_\infty \cdot \omega}{\phi} \right) \frac{\partial C_i}{\partial z} + \phi \sum R_i \quad (3)$$

where ϕ is the porosity, ϕ_∞ is the constant porosity at depth and ω is the sedimentation rate. The effective diffusion coefficients, D'_i , are determined by correcting the diffusion coefficients in free solution $D_{0,i}$ for tortuosity, Θ^2 , where the tortuosity is calculated by means of porosity according to a modified Weissberg relation (Boudreau, 1997). Solid species are only affected by advection and sediment compaction. Biological transport processes, such as biodiffusion or bioirrigation have a negligible effect at the considered depth (>1 m) and time scales (>1 Myr). The conservation equation therefore reads:

$$\frac{\partial (1-\phi)C_i}{\partial t} = -\frac{(1-\phi_\infty) \cdot \omega}{(1-\phi)} \cdot \frac{\partial C_i}{\partial z} + (1-\phi) \sum R_i \quad (4)$$

Porosity is assumed to decrease exponentially with depth (Erbacher et al., 2004) according to:

$$\phi(z) = 0.4 + 0.3 \cdot e^{(-z/150)} \quad (5)$$

Reaction network

The diagenetic reaction network accounts for the degradation of organic matter by sulfate reduction and methanogenesis, anaerobic oxidation of methane and barite dissolution/precipitation. The RTM does not account for CH_4 gas formation. CH_4 enters a gaseous state if the dissolved CH_4 concentration exceeds the local solubility concentration, CH_4^* . CH_4^* varies with salinity, temperature and pressure. Duan et al. (1992) proposed a numerical solution for the solubility of CH_4 as a function of salinity, temperature and pressure. A range of realistic values for CH_4^* can be calculated assuming a maximum sediment depth of 550 m, palaeo-waterdepth which increases from 500 m in the Cretaceous to a modern depth of 3200 m (Arthur and Natland, 1979), a constant salinity and a downcore increase in temperature according to the geothermal gradient. Under these

conditions, calculated solubility concentrations, CH_4^* , are very high (90-200 mM) and, therefore, CH_4 gas formation can be neglected.

Following Arndt et al. (2006), AOM is described by a linear dependence on CH_4 concentration and a Monod dependence on SO_4 concentration (e.g. Treude et al., 2003).

$$R_{AMO} = k_{AMO} \cdot [CH_4] \frac{[SO_4^{2-}]}{K_{S,AMO} + [SO_4^{2-}]} \quad (6)$$

The total depletion of SO_4 in the sulfate reduction zone can promote the dissolution of biogenic $BaSO_4$ in sediments due to a shift in equilibrium. The relatively fast rate of mineral dissolution and precipitation allows a solely thermodynamic formulation. Reaction rates of dissolution and precipitation are expressed in form of empirical rate laws following experimental results (Christy and Putnis, 1993; Bosbach, 2002):

$$R_{BaSO_4,diss} = k_{BaSO_4,diss} [BaSO_4] (\Omega - 1) \quad (7)$$

for $\Omega < 1$ and

$$R_{BaSO_4,prec} = k_{BaSO_4,prec} (1 - \Omega)^2 \quad (8)$$

for $\Omega > 1$

where $k_{BaSO_4,diss}$ and $k_{BaSO_4,prec}$ are the rate constants for dissolution and precipitation, respectively. The state of saturation of the pore water solution Ω is defined by the ratio of the ion activity product over the corresponding solubility product K_{sp} :

$$\Omega = \frac{[SO_4^{2-}][Ba^{2+}]}{K_{sp}} \quad (9)$$

Values of K_{sp} are calculated as a function of salinity and temperature using an empirical relation provided by Rushdi et al. (2000). The rate constants for AOM and barite dissolution/precipitation are chosen according to Arndt et al. (2006) and are detailed in Table 6.1.

Table 6.1 Rate constants for anaerobic oxidation of methane k_{AMO} , barite dissolution $k_{diss,BaSO_4}$ and barite precipitation $k_{prec,BaSO_4}$ are based on previous steady-state simulations (Arndt et al., 2006).

Rate constant	Units	Value
k_{AMO}	$[yr^{-1}]$	$2 \cdot 10^{-4}$
$k_{diss,BaSO_4}$	$[yr^{-1}]$	$3 \cdot 10^{-8}$
$k_{prec,BaSO_4}$	$[\mu Myr^{-1}]$	$5 \cdot 10^{-4}$

In the steady-state version of the model (Arndt et al., 2006), organic matter degradation is described by the so-called multi-G model (e.g. Berner, 1980; Boudreau, 1997). However, this approach requires an empirical determination of reactive types and associated

reactivities by curve fitting. Middelburg (1989) and Boudreau and Ruddick (1991) point out that the identification of reactive types is rather a function of the selectivity of the method of analysis and, therefore, does not provide any information about the distribution of organic matter types. In addition, the multi G-model requires the choice of a relatively large number of parameters. Yet, the available information is not sufficient to constrain the number of reactive types, as well as the distribution of organic matter and its reactivity among these types. A more realistic alternative to the discrete multi-G approach is a continuous distribution of reactive types. Two decades ago, Jansen (1984) and Middelburg (1989) described the distribution of empirically derived organic matter reactivity over time by a power law, thus relating the apparent reactivity, k , of the bulk organic matter to time rather than to a change of composition. Middelburg (1989) proposed the following relationship to describe the decrease of the rate of organic matter degradation, R_G , with time:

$$R_G(t) = 0.16 \cdot (ia + t)^{-0.95} \cdot G(t) \quad (10)$$

where ia denotes the apparent initial age of the deposited organic matter. A number of other authors proposed alternative approaches that describe bulk organic matter as the integral of a distribution function, $g(k, t)$, over all possible values of k (Aris, 1968; Carpenter, 1981; Bosatta and Agren, 1985; Boudreau and Ruddick, 1991). However, Bosatta and Agren (1995) illustrated that their model of organic matter degradation, the q-theory, reduces to the reactive continuum model or the power model under specific assumptions. In addition, Tarutis (1993) showed that the reactive continuum model and the power model are mathematically equivalent for a simple closed-system decay (i.e. no bioturbation) if the reactive continuum model is based on a Gamma distribution and the exponent of power model equals one. However, the power and the reactive continuum model are conceptually very different. While the power model uses a single time-dependent reaction rate coefficient, the reactive continuum model explicitly integrates the effect of compound-specific reactivities on organic matter degradation. Isotopic evidence indicates that the reactive continuum model is as a more realistic conceptual basis for organic matter degradation rates in marine sediments (Aller and Blair, 2004). In addition, Boudreau and Ruddick (1991) found important similarities of apparent reaction orders for organic matter from different environments and of different ages. A comparison of the apparent order of reaction with the one determined for Cretaceous black shales could potentially provide further insights into the functioning of the organic carbon sink during the Cretaceous OAEs. Therefore, we use the reactive continuum approach to describe organic matter degradation over geological time scales.

The reactive continuum model represents the total amount of organic matter, $G(t)$, as the integral of the distribution function of reactive types, $g(k, t)$, over the entire range of possible degradation rate constants, k . Each member is degraded according to a first order rate law. Following Aris (1968) and Ho and Aris (1987), Boudreau and Ruddick (1991) propose the Gamma distribution as an initial distribution, $g(k, 0)$:

$$g(k, 0) = \frac{g_0 \cdot k^{\nu-1} \cdot e^{-a \cdot k}}{\Gamma(\nu)} \quad (11)$$

The concentration of organic matter is then given by:

$$G(t) = \int_0^\infty g(k, t) dk = \int_0^\infty g(k, 0) \cdot e^{-k \cdot t} dk \quad (12)$$

where the rate constant k is treated as a continuous variable and $\Gamma(\nu)$ is the Gamma function (e.g. Abramowitz and Stegun, 1972). The free parameters a and ν completely determine the shape of the initial distribution of organic matter reactivities. The parameter a describes the average life-time of the more reactive components of the spectrum, while ν defines the shape of the distribution near $k = 0$. Therefore, ν serves as an indicator for the reactivity of the bulk organic matter. Low ν values reflect a predominance of unreactive types, while high ν values characterize a more uniform distribution of the bulk organic matter among the different reactive types. The rate of organic matter degradation, R_G , is then given by:

$$R_G(t) = -\frac{\nu}{a \cdot G(0)^{1/\nu}} \cdot G(t)^{1+1/\nu} = -\nu \cdot (a + t)^{-1} \cdot G(t) \quad (13)$$

where $G(0)$ is the initial content of organic matter. Small ν values thus result in apparent higher orders of reaction, even though each reactive-type decays linearly. Eq. (13) shows that, for certain assumptions, the reactive continuum model is mathematically equivalent to a power law with the pre-factor $\nu = 0.16$ and an exponent of -1 (Ref. Eq. (10)).

At Demerara Rise, organic matter is assumed to be only consumed by sulfate reduction R_{G,SO_4} and methanogenesis R_{G,CH_4} . Therefore, the total organic matter degradation rate R_G is divided into the contributions of the two metabolic pathways, applying a pseudo-kinetic approach, which determines the sequence of the pathways a priori and reflects the decreasing standard Gibbs free energy yield of the reaction (e.g. Berner, 1980; Van Cappellen and Wang, 1996; Boudreau, 1997). The contribution of the degradation pathways is mathematically described by the sum of a limitation and inhibition term. The limitation of sulfate reduction by low SO_4 concentrations is described by a Monodtype hyperbolic expression using a half-saturation constant K_{SO_4} . Methanogenesis is not limited since no external oxidant is involved. The suppression of methanogenesis by the

energetically more favorable sulfate reduction is formulated by an inhibition function. The inhibition constant equals the half-saturation constant K_{SO_4} , so that the R_G is simply given by the sum of the two pathways, R_{G,SO_4} and R_{G,CH_4} :

$$R_G = R_{G,SO_4} + R_{G,CH_4} \quad (14)$$

$$R_{G,SO_4} = R_G \cdot \frac{SO_4}{SO_4 + K_{SO_4}} \quad (15)$$

$$R_{G,CH_4} = R_G \cdot \frac{K_{SO_4}}{K_{SO_4} + SO_4} \quad (16)$$

Other electron acceptors may also have played a role during the early stages of black shale deposition. The benthic foraminifera assemblage at Site 1258, for instance, reveals short-term re-populations in the lower third of OAE 2, which may indicate short-term bottom-water oxygenation (Friedrich and Erbacher, 2006). Model-determined Cretaceous organic matter contents and fluxes therefore represent maximum estimates.

Numerical Solution

Transient model simulations are performed for a period of 100 Myr (Cretaceous - present day). Based on the operator splitting approach, transport and reaction equations are treated separately. The transport equation for dissolved species is numerically integrated applying the semi-implicit Crank-Nicholson scheme with an iteration through successive over-relaxation, a Chebyshev acceleration and odd-even ordering. The numerical scheme for solid transport must conserve the sharp concentration front that characterizes the black shale layer over the simulated 100 Myrs. High-resolution numerical schemes generally display very good results in the case of advection-dominated problems. Therefore the advective term is integrated using a third-order accurate total variation diminishing algorithm with flux limiters, ensuring monotonicity. The reaction network is integrated by a simple Euler-Forward method with an automatically adjusting time-step, which guarantees numerical accuracy and stability. The algorithm was run with a maximum time step of $\Delta t = 10\text{yr}$ on an unevenly spaced grid, with a grid size increasing downcore from the sediment/water interface to the maximum simulated depth ($z = 500\text{ mbsf}$) from $\Delta z = 1\text{ cm}$ to $\Delta z = 1\text{ m}$.

External forcing and initial conditions

Boundary conditions and forcings connect the system to its environment. They exert an important influence on model performance, since their temporal resolution controls the error associated with a potential aliasing and ultimately determines the scales on which system dynamics can be resolved. The presented model, which is designed to integrate

biogeochemical dynamics over geological time scales, can only provide a long-term trend of these dynamics. The temporal resolution of the available external forcing is coarse (>1 Myr) and, therefore, does not resolve short-term variations over the considered geological time scale.

Sedimentation rates are constrained on the basis of an age-depth model, which was established for Site 1258 by combining biostratigraphic and magnetostratigraphic data (Erbacher et al., 2004, Table 6.2). Linear sedimentation rates have been estimated by dividing the resulting age-depth distribution into different linear segments for specific time intervals. Calculated sedimentation rates reveal five different intervals of approximately constant sedimentation rates separated by distinctive hiatuses (Erbacher et al., 2004). The coarse resolution of available biostratigraphic and magnetostratigraphic data cannot resolve potential orbital-scale variations.

Table 6.2 Sedimentation rate used in the model. Estimates are based on an age-depth model established for Site 1258 (Erbacher et al., 2004).

Epoch	Time (Myrs BP)	Simulation Time (Myrs)	Sedimentation rate (m•Myrs)
Cenomanian-Turonian	100-83	0-17	3
Turonian-Campanian	83-79	17-28	0
Campanian-Maastrichian	79-65.2	29-34.8	10
Maastrichian-early Paleocene	65.2-64.5	34.8-35.5	10
early Paleocene-late Paleocene	64.5-60.9	35.5-39.1	0
late Paleocene-middle Eocene	60.9-45.2	39.1-54.8	15
Neogene	45.2-0	54.8-100	0.04

A Dirichelet boundary condition is applied for dissolved species at the sediment-water interface while an open flux boundary condition specifies the concentration 50 mbsf below the bottom of the black shale sequence, i.e. at the bottom of the sediment column. At the sediment/water interface, dissolved Ba and CH₄ concentrations are assumed to be constant in time and chosen according to modern day seawater values (Table 6.3). However, oceanic SO₄ concentrations varied significantly during the Phanerozoic (Horita et al., 2002; Lowenstein et al., 2001). The analysis of fluid inclusions in marine halites suggests that the seawater SO₄ concentration was low during the early Palaeozoic and subsequently increased to its modern value (Fig. 6.3). Yet, the temporal resolution of these analysis is extremely coarse and, therefore, they can merely provide a very general trend. In addition, measurement error bars can reach as much as 79% of the estimated concentration (Horita

et al., 2002). Therefore, the estimated evolution of seawater sulfate concentration proposed by Horita et al. (2002) is used as a baseline sulfate concentration scenario (best scenario) (Fig. 6.3). Maximum (high scenario) and minimum (low scenario) estimates help to constrain the sensitivity of simulation results to different SO_4 boundary concentration scenarios.

Table 6.3 Boundary conditions used in the model.

Symbol	Description	Unit	Value
C_{SO_4}	SO_4 concentration at the sediment/water interface	μm	Var.
C_{CH_4}	CH_4 concentration at the sediment/water interface	μm	0
C_{Ba}	Ba concentration at the sediment/water interface	μm	20
F_{BaSO_4}	BaSO_4 flux at the sediment/water interface	$\text{mmol}/(\text{m}^2 \text{ Myr})$	$11.5 \cdot 10^4 \cdot (1 - \phi) \cdot \omega$ for $t = (0-17 \text{ Myrs})$ 0 for $t > 17 \text{ Myrs}$
F_{OM}	OM flux at the sediment/water interface	$\text{mmol}/(\text{m}^2 \text{ Myr})$	$G(0) \cdot (1 - \phi) \cdot \omega$ for $t = (0-17 \text{ Myrs})$ 0 for $t > 17 \text{ Myrs}$

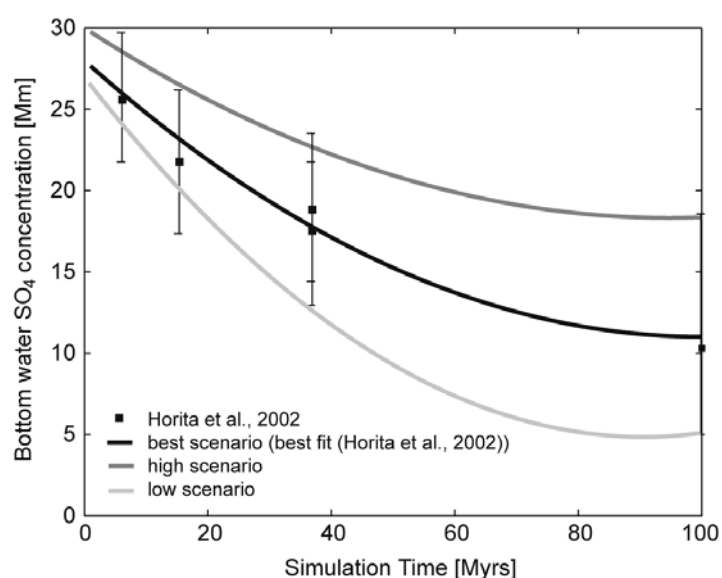


Figure 6.3 Evolution of seawater sulfate concentration over the past 100 Myrs, as measured in fluid inclusions from marine halites (Horita et al., 2002). Three different sulfate boundary condition scenarios (solid lines) are chosen according to the best fit to the measured data (best, black line), to the lower limits of the error bars (low, light gray) and to the higher limits of the error bars (high, dark gray).

The black shale layer is characterized by generally high, but very variable TOC contents between 0.1 and 28.3 wt% (Fig. 6.2). Part of this variability is associated with the finely laminated alternations of dark claystones and thin calcite layers (Erbacher et al., 2004; Meyers et al., 2004). In addition, variable TOC contents may reflect short-term fluctuations in organic matter accumulation rates similar to the orbital cycles observed elsewhere (e.g. Wagner et al., 2004; Kolonic et al., 2005). However, the sample spacing and the rough estimate of sedimentation rate do not permit an unambiguous identification of such short-term fluctuations. Therefore, we use the mean TOC content of the Cretaceous black shale sequence to estimate a long-term organic matter flux, which reflects the enhanced deposition of organic carbon during the mid-Cretaceous. The organic matter flux to the sediment, F_{OM} can be estimated via the initial mean TOC content $G(0)$, applying the reactive continuum model and using the mean present-day content of TOC in the black shales sequence (400–450 mbsf) $G(10^8 \text{ yr}) = 7.8 \text{ wt\%}$:

$$G(0) = \frac{G(10^8 \text{ yr})}{\left(\frac{a}{a+10^8}\right)^v} \quad (17)$$

$$F = G(0) \cdot (1 - \phi) \cdot \omega \quad (18)$$

The Cretaceous anoxic events are assumed to be the only period of organic matter deposition, influencing the longterm biogeochemical dynamics below the shallow subsurface at Demerara Rise, over the past 100 Myrs. After the Cretaceous, background organic matter fluxes are likely to be comparable to depositional fluxes observed in open ocean settings. The amount of organic matter that reached the sediments was probably consumed by aerobic degradation or denitrification in the shallow subsurface (<1.5 m). Therefore, it is realistic to assume that this organic matter had very little influence on SO_4 consumption. The simulated organic matter flux thus ceases after the deposition of the black shales sequence. At site 1258, dark-colored Albian clayey siltstones, with comparably high average TOC contents of 4.6 wt% (Fig. 6.2), indicate that a period of increased organic matter deposition precedes the deposition of the Cenomanian-Santonian black shales. However, TOC contents of age-equivalent units at the other drilling sites are significantly lower (0.6 wt%). These deposits are currently not believed to contain any of the known Albian OAE 1 events (Erbacher et al., 2004; Meyers et al., 2006). Due to its singular occurrence and the largely unknown character of the depositional environment, we exclude the underlying sediments from our analysis and only focus on the distinct Cretaceous black shale layer. This approach could potentially lead to a slight overprediction of estimated organic matter reactivities and contents.

The average deposition flux of biogenic barite is estimated by assuming that biogenic barite was only redistributed by diagenesis. The Cretaceous biogenic barite content of the black shale layer thus equals the present, depth-integrated (0-484 mbsf) barite content of sediments at Site 1258.

The choice of initial conditions for dissolved species is not straightforward. The RTM cannot account for shortterm dynamics (<1 Myr), which may exert an important influence on the balance between the biogeochemical consumption/production and transport processes during the initial stage of the black shale deposition event. Therefore, only TOC dynamics are explicitly simulated for the black shale deposition period (0-17 Myrs simulation time). Observation results show that the burial of organic matter in the black shale sequence is associated with an enrichment of all analyzed sulfur fractions: total, pyrite, and organicbound sulfur (Böttcher et al., 2006; Hetzel et al., 2009). These findings indicate a dominance of microbial sulfate reduction and the associated formation of sedimentary sulfur compounds. Therefore, biogenic barite is assumed to be conserved in the black shale sequence for the initial 17 Myrs. The resulting TOC and BaSO₄ profiles at $t = 17$ Myrs are used to calculate steady-state profiles for dissolved species. These steady-state profiles are applied as initial conditions for the numerical integration of the full RTM, which starts at the beginning of the hiatus following the black shale deposition period at Demerara Rise (17 Myrs).

Inverse modeling

The parameters, a and ν , are free parameters, which require calibration. They are extracted from the observed, present-day depth-profiles of SO₄, CH₄, Ba and the information recorded in the BaSO₄ distribution. The transient RTM is run forward over a period of 100 Myrs with randomly chosen parameter couples (a , ν) and the resulting simulated, present-day depth profiles are compared with the observations. Assuming that the rank of the optimal parameter combination depends on the similarity between simulated and measured depth profiles, a and ν are determined by minimizing a cost function $M(a, \nu)$, which represents the measure of the misfit between simulation results and observations:

$$M(a, \nu) = \frac{1}{i} \sum_i M_i(a, \nu) \quad (19)$$

$$M_i(a, \nu) = \frac{1}{n_z} \sum_{n_z} \left(\frac{C_i^{obs}(\Delta z) - C_i^{sim}(\Delta z, a, \nu)}{\sigma_i} \right)^2 \quad (20)$$

The total cost function, $M(a, \nu)$, to be minimized is the sum of the species-specific cost functions, $M_i(a, \nu)$. $M_i(a, \nu)$ is given by the sum of least-square differences between simulated average concentration/content C_i^{sim} and measured average

concentration/content C_i^{obs} for each depth interval Δz , weighted by the factor σ_i^2 and normalized by the number of depth intervals n_z . The weighting factors are defined as the sum of the respective measurement errors and a factor, f which reflects the importance given to the minimization of the respective misfit. Barite measurements are available with a high spatial resolution and sulfate depth-profiles are a sensitive indicator of the present-day location of the SMTZ. Therefore, their species-specific cost function is additionally weighted by a factor, $f = 1/2$. The sampling of the two-dimensional parameter space is realized in two steps. First, an extended parameter space ($a \in [10^1-10^6]$, $v \in [10^{-3}-5 \cdot 10^{-1}]$) was sampled systematically with a coarse step size ($\log \Delta a = 1$, $\log v = 0.5$). Hereafter, sampling was concentrated around the global minimum. The inverse modeling approach thus tests the feasibility of a large number of different reactivity scenarios. In addition, the procedure was repeated for each of the three estimated (1-low, 2-best, 3-high) sulfate scenarios to quantify the uncertainty associated with the weakly constrained boundary condition.

Results and Discussion

Distribution of barite

Figure.6.4 illustrates the highly resolved barite depth profile, which is observed in sediments from Site 1258. BaSO_4 contents are highest at sediment depths between 300 and 400 mbsf, while the Cretaceous black shale layer is characterized by comparably low contents. These findings are in agreement with previous observation and model results, which indicate that biogenic BaSO_4 is mobilized in the black shales and reprecipitates as authigenic BaSO_4 in the vicinity of the SMTZ (Arndt et al., 2006). In addition, the highly resolved sampling within the 300 to 400 mbsf depth range provides new insights into the detailed depth-distribution of authigenic BaSO_4 above the black shales. Two distinct peaks can be identified at approximately 320 and 375 mbsf. These distinct peaks suggest that the temporal dynamics of organic matter degradation caused various shifts in the BaSO_4 precipitation zone, followed by longer periods of quasi steady-state conditions, during which prominent accumulations of authigenic BaSO_4 formed. A direct interpretation of the record is however complicated by the strong diagenetic overprint and the potential superposition of various signals. Earlier formed authigenic fronts, for instance, may redissolve at later stages or may be superimposed by more recent accumulations. Transient RTM simulations will help to resolve the temporal evolution recorded in the BaSO_4 profile.

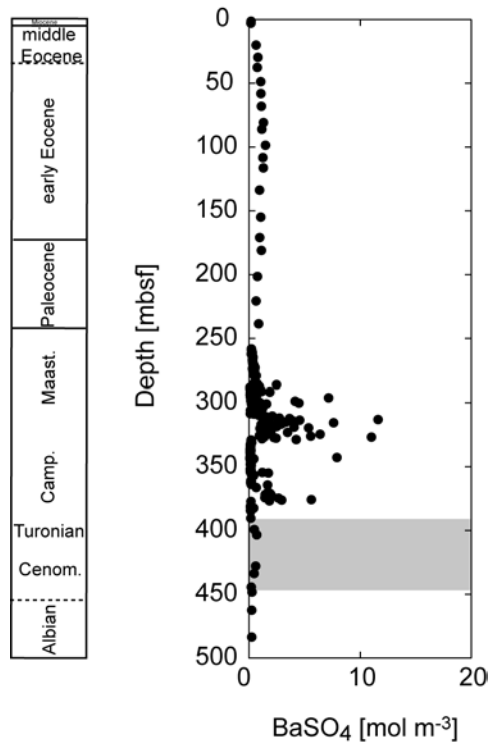


Figure 6.4 High-resolution BaSO_4 depth-profile in sediments drilled at Site 1258 (ODP Leg 207, Demerara Rise). The location of the Cretaceous black shale sequence is indicated by a gray box.

Inverse modeling

The parameters of the reactive continuum model can be extracted from the newly obtained, highly resolved distribution of BaSO_4 and the interstitial water depth-profiles. Figure 6.5 illustrates the distributions of the cost function $M(a, v)$ over the two-dimensional parameter space in the vicinity of the respective global minimum for each of the three sulfate scenarios. The cost function reveals little variability along the a -axis, since the evolution of k is mainly determined by the term v/t , beyond a transient time a (Eq. (13)). Realistic values for a (10^1 - 10^4 yr, (Boudreau and Ruddick, 1991)) are orders of magnitude lower than the simulated period (10^8 years) and a thus exerts a very limited influence on the long-term dynamics. In addition, the observed BaSO_4 depth profile represents a record of the long-term (>1 Myr) biogeochemical dynamics and, does not allow a to be determined by inverse modelling. Therefore, the exponential relationship between the average life-span a (yr) and the sedimentation rate ω (cm kyr^{-1}) proposed by Boudreau and Ruddick (1991) is used as a rationale to constrain a . Boudreau and Ruddick (1991) argued that the average life-span of the fast decaying types should increase with decreasing sedimentation rate due to its rapid removal in the upper sediment column:

$$a = 4970 \cdot e^{-0.0296 \cdot \omega} \quad (21)$$

Organic matter in black shales deposited at Demerara Rise would thus be characterized by an average life-span a of 4926 years. However, the extrapolation to low sedimentation rates in the original fit of this equation is uncertain and, therefore, a is not well constrained. Nevertheless, the exact choice of a within the realistic range has little influence on the simulated long-term biogeochemical dynamics. This estimate is thus used in the presented simulations of long-term biogeochemical dynamics (see Section *Evolution of Biogeochemical Dynamics at Demerara Rise*). Yet, the estimates of initial TOC content, $G(0)$, and reactivity, $k(0)$, are always calculated for a realistic range of average life spans ($a = 10^1$ - 10^6 yr), since these estimates are sensitive to the choice of a .

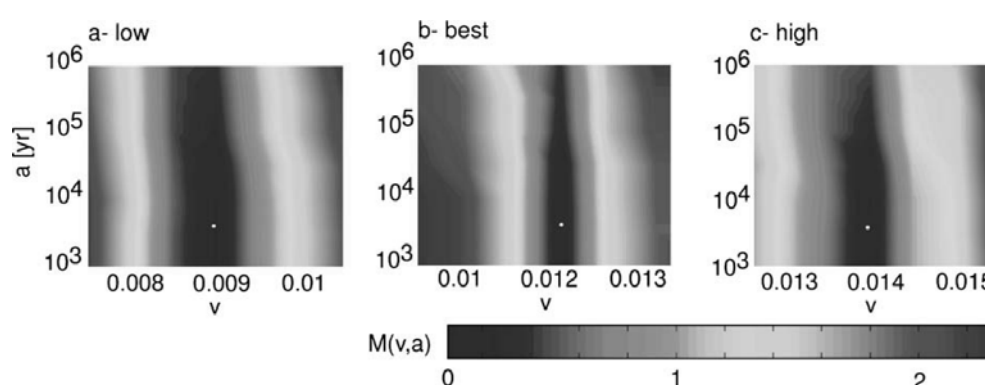


Figure 6.5 Distribution of the cost function $M(v, a)$ over the two-dimensional parameter space for the a-low, b-best and c-high sulfate boundary concentration scenario. White dots correspond to the chosen parameter combination.

In contrast to the a -axis, the cost function reveals a pronounced variability along the v -axis (Fig. 6.5). This parameter serves as an indicator for the reactivity of the bulk organic matter since it controls the shape of the gamma function near $k = 0$. Low v values reflect a predominance of unreactive types, while high v values characterize a more uniform distribution of the bulk organic matter among the different reactive types. Therefore, high v values results in higher CH_4 fluxes out of the black shales, a shallower sulfate zone, the formation of BaSO_4 accumulations at shallower sediment depth and thus an increased misfit to observations. Low v values have the opposite effect and lead to a downcore shift of the SMTZ. Therefore, the cost function first decreases with a decrease in v . It reaches a minimum before it increases again in the region of very low v values. Here, the low organic matter reactivity results in low degradation rates and an enhanced availability of SO_4 that inhibits the dissolution of biogenic BaSO_4 in the black shales. The best estimate for v increases with an increasing SO_4 availability and global minima for the low, best and high

sulfate scenarios are therefore reached for $\nu = 0.009$, $\nu = 0.0123$ and $\nu = 0.014$, respectively (Fig. 6.5a-c). The cost function reveals a sharp minimum, indicating that neither high-reactivity nor very low-reactivity scenarios provide a satisfactory fit to the observed profiles. Because the slope of the cost function reflects the sensitivity of the simulated profiles to changes in m , such a pronounced minimum also indicates that the shape of the simulated present-day depth-profiles strongly depends on the long-term evolution of organic matter degradation determined by ν/t .

Evolution of biogeochemical dynamics at Demerara Rise

Transient model simulations are performed over a period of 100 Myrs for each of the three SO_4 scenarios (low, best and high), the ν values determined by inverse modeling and the average life-span, a , of 4926 years. Transient simulation results reveal that long-term fluctuations in sedimentation rate trigger prominent shifts in the redox-zonation of the sediment and control the long-term evolution of biogeochemical dynamics. Based on these long-term trends in sedimentation rate, the diagenetic history can be divided in five different periods (see subsections). Figure 6.6 shows selected snapshots of simulated TOC, SO_4 , CH_4 , Ba and BaSO_4 depth-profiles that are representative for the main stages of the diagenetic evolution. The corresponding evolution of depth-integrated biogeochemical reaction rates is illustrated in Figure 6.7.

Cenomanian-Campanian (0-21 Myr)

At Site 1258, the deposition of expanded late Cretaceous black shale sequences begins in the Cenomanian (0 Myr) and lasts until the Campanian (17 Myr), followed by a four million year hiatus (17-21 Myr). A ca. 50-m-thick black shale layer, the local representation of widespread organic-rich sedimentation in the southern part of the mid-Cretaceous North Atlantic, accumulates during this period (Fig. 6.6a). The enhanced availability of organic matter in the sediment leads to an increase in the depth-integrated organic matter degradation rate over the time of black shale deposition (Fig. 6.7a). The exceptionally low reactivity of the organic matter within the black shale sequence (apparent $k(0-51 \text{ m}) = 10^{-6}$ - 10^{-8} yr^{-1}) results in comparably low degradation rates that do not completely consume the diffusive SO_4 flux. Organoclastic sulfate reduction outcompetes methanogenesis (Fig. 6.7) and is the only SO_4 consumption process. Therefore, SO_4 is not rapidly consumed in the upper sediment, a phenomena which is often observed in subsurface, organic matter-rich sediments, where the high organic matter degradation and AOM generally results in a shallow SMTZ. The availability of SO_4 at depth maintains the oversaturation of interstitial

waters with respect to BaSO_4 and biogenic BaSO_4 is therefore preserved in the black shale layer (Fig. 6.6a).

Campanian-early Paleocene (21-35.5 Myr)

In the late Cretaceous and early Paleocene, organic matter degradation rates decrease due to the decrease in organic matter reactivity during burial (Fig. 6.7a-c). The elevated sedimentation rates lead to a progressive burial of the Cretaceous black shales and 145 m of sediment accumulate on top of the black shale layer during this period (Fig. 6.6b). The burial of the black shales to increasing sediment depths has important consequences for the biogeochemical dynamics. It leads to a progressive increase in diffusion length and, therefore, reduces the SO_4 flux at depth. The reduced diffusive SO_4 flux cannot supply sufficient SO_4 to satisfy the metabolic needs in the black shale layer. SO_4 becomes depleted in the deepest part of the black shale sequence (Fig. 6.6b) and promotes the onset of methanogenesis (Fig. 6.7c). The associated production of biogenic methane leads to an upcore shift of the SMTZ and, therefore, triggers a fast switch in the dominant degradation pathway. Biogenic CH_4 , which is produced at the bottom of the black shale sequences drives an additional consumption of SO_4 by AOM (Fig. 6.7d). The reduced availability of SO_4 at depth further increases the importance of methanogenesis in the black shales and enhances the CH_4 flux, which in turn drives higher AOM rates (Fig. 6.7c and d). The increased SO_4 consumption ultimately pushes the SO_4 penetration depth out of the black shales (Fig. 6.6b). This upcore movement of the SMTZ and the associated switch to methanogenesis occurs earlier for the low and the best sulfate scenario, while a higher SO_4 flux can maintain the dominance of sulfate reduction for a longer time (Fig. 6.7b). Authigenic BaSO_4 bear the testimony of this biogeochemical evolution in the late Cretaceous. The progressive depletion of interstitial SO_4 promotes the remobilization of biogenic BaSO_4 in the black shale sequence (Figs. 6.6b and 6.7e). Ba diffuses out of the black shales and reprecipitates as authigenic BaSO_4 in the SMTZ (Figs. 6.6b and 6.7f).

Figure 6.6 (next page) Snapshots of simulated depth-profiles for the different sulfate scenario (best = black, high = dark gray and low = light gray). The six snapshots correspond the five distinct stages of the diagenetic history and the present-day situation (see respective subsections of Section *Evolution of biogeochemical dynamics at Demerara Rise*). The duration of the distinct stages (1-5), as well as the corresponding sedimentation rates are illustrated in the time bar on the top of the figure. The simulated time is indicated in the time bar above each group of depth-profiles (a-f). Simulated present-day profiles (f) are compared to measured depth-profiles.

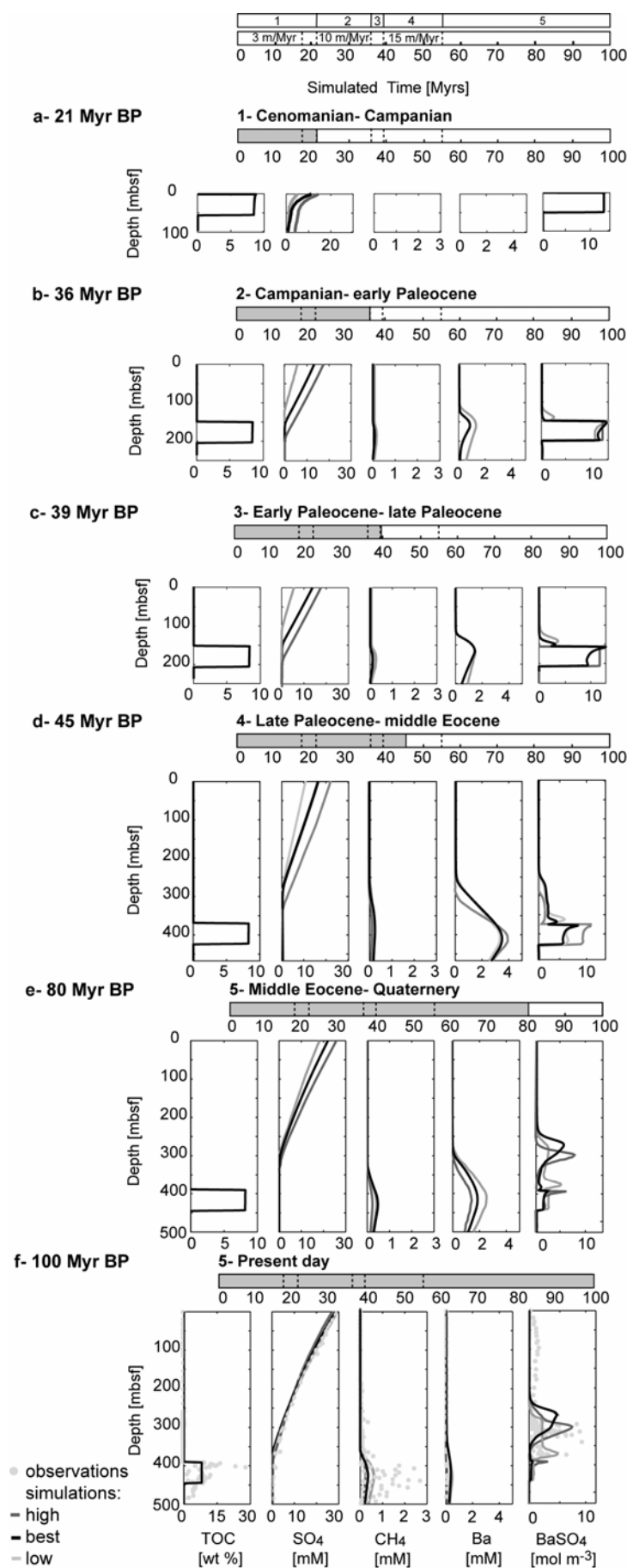


Figure 6.6

Early Paleocene-late Paleocene (35.5-39.1 Myr)

In the early Paleocene, a hiatus in sedimentation rate creates a short period of quasi-steady-state conditions. Authigenic BaSO_4 therefore accumulates in the SMTZ just above the top of the black shale sequence (Fig. 6.6c). Yet, higher SO_4 boundary concentrations support an increased SO_4 availability in the high SO_4 scenario. The switch from sulfate reduction to methanogenesis therefore occurs later and BaSO_4 dissolution is inhibited (Fig. 6.7e).

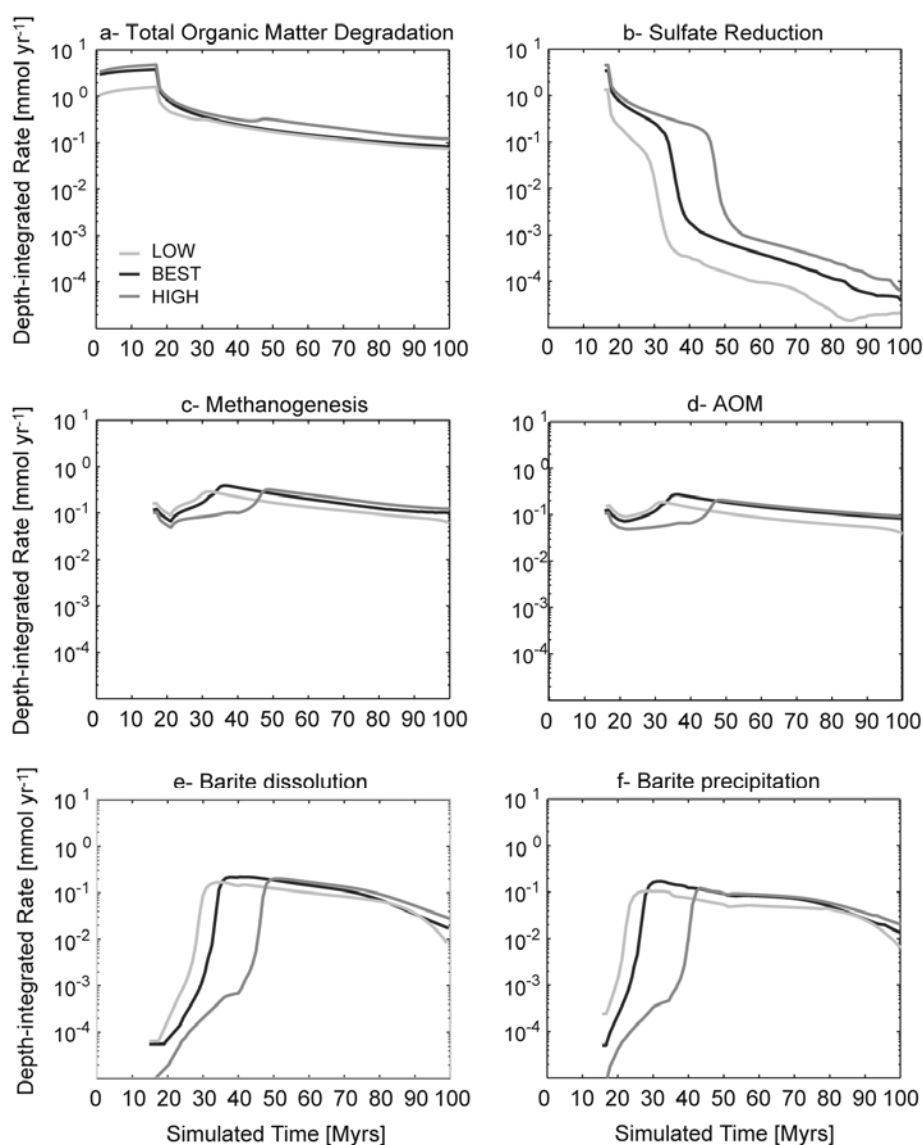


Figure 6.7 Simulated evolution of the depth-integrated (a) total organic matter degradation rate, (b) sulfate reduction rate, (c) methanogenesis rate, (d) AOM rate, (e) barite dissolution rate and (f) barite precipitation rate for the low (light gray), best (black) and high (dark gray) sulfate scenario. Only organic matter degradation is explicitly simulated for the first 17 Myrs of simulation. See Section *External forcing and initial conditions* for further explanation.

Late Paleocene-middle Eocene (39.1-54.8 Myr)

The subsequent increase in sedimentation rate during the late Paleocene/Eocene interval leads to a rapid burial of the black shale layer. Increasing diffusion lengths and ongoing SO_4 consumption at depth (Fig. 6.7) drive an upcore shift of the SMTZ (Fig. 6.6d). This transient behavior, imposed by the increase in sedimentation rates, cannot be compensated by the increase in bottom water SO_4 concentration (Fig. 6.3). Biogenic, as well as earlier formed authigenic BaSO_4 dissolve below the SMTZ, while authigenic BaSO_4 reprecipitates along the migration path of the SMTZ (Fig. 6.6d). At the end of the late Paleocene/Eocene sedimentation period, the SMTZ is situated 100-150 m above the top of the black shale sequence.

Middle Eocene-Quaternary (54.8-100 Myr)

During the late Paleogene, a strong reduction in sedimentation rate results in a second period of quasi-steadystate conditions. Authigenic BaSO_4 accumulate in the SMTZ and form a second peak in the BaSO_4 depth-profile (Fig. 6.6e). However, a rapid increase in bottom water SO_4 concentrations leads to a downcore shift of the SMTZ. This downcore shift is further promoted by the decrease in organic matter degradation rate and thus AOM (Fig. 6.7a and d). The transient behavior, which is induced by these processes, proceeds relatively slowly and authigenic BaSO_4 accumulate over an extended depth section (Fig. 6.6e).

At present day, the SMTZ is again located close to the top of the black shale layer in the vicinity of the early Palaeocene BaSO_4 accumulation (Fig. 6.6f). Organic matter degradation proceeds at very slow rates, which are characteristic for the deep biosphere ($R_G = 10^{-1}$ - 10^{-2} mmol yr^{-1} , Fig. 6.7). However, the long diffusion length of almost 400 m and the ongoing SO_4 consumption by AOM, and to a lesser extent by BaSO_4 precipitation, maintain the dominance of methanogenesis (Fig. 6.7). The main trends in the observed depth-profiles are well captured by the simulated profiles. However, the model underestimates observed CH_4 concentrations in the black shale layer. This deviation arises due to the uncertainties in paleo-boundary conditions and the inverse modeling strategy. Transient simulation results reveal that the dynamics of the SMTZ is essentially determined by the long-term trends in sedimentation rate. The rapid burial during the late Paleocene-middle Eocene period, for instance, induced a prominent upcore shift of the SMTZ. The pace of the subsequent downcore movement is mainly controlled by the increase in bottom water SO_4 concentrations and the magnitude of the CH_4 flux from the black shales. Arndt et al. (2006) showed that the location of the SMTZ in the present-day deep biosphere setting is

extremely sensitive to the production of biogenic CH_4 in the black shale layer. A simple doubling of the degradation rate constant results in significantly higher CH_4 concentrations and an upward shift of the SMTZ by ca. 100 m. Hence, a less pronounced upcore movement of the SMTZ, resulting from lower Paleocene/Eocene sedimentation rates or higher bottom water SO_4 concentrations, would allow for higher biogenic CH_4 production in the Quarternary and a better fit to the observed CH_4 profile. A similar effect can be observed for the BaSO_4 depth profile. BaSO_4 depth-profiles simulated by applying the three sulfate concentration scenarios, display differences in the height, width and exact location of the two authigenic barite peaks. The deviations between the simulation results obtained with the three different SO_4 scenarios thus illustrate the uncertainty induced by the paleo-boundary concentrations.

Reactivity and preservation of black shale organic matter at Demerara Rise

The inversely determined parameter ν provides important insights into the nature of the black shale organic matter and the long-term evolution of its reactivity over the past 100 Myrs. Boudreau and Ruddick (1991) determined ν values between 0.1 and 0.2 for five organic matter profiles from various shallow and deep-water sediments. The inversely determined ν values (0.009-0.014) for the black shale organic matter are thus one order of magnitude lower than those determined for a wide range of modern sedimentary environments. These results indicate that the organic matter in the Cretaceous black shales is dominated by relatively unreactive components. Its microbial decomposition has thus proceeded with continuously low rates since the Cretaceous.

Figure 6.8a and b compare the Cretaceous, apparent first-order rate constants ($k(0) = \nu/a$) determined for the three different SO_4 scenarios and the average life-span, a , of 4926 yr, with those predicted by empirical relationships proposed in the literature. Error bars indicate the range of rate constants calculated for different a values ($a = 10^{-1}$ - 10^{-6} yr). Estimates thus reflect the range of uncertainty associated with both the weakly constrained a value and SO_4 concentration at the sediment/water interface. Initial apparent first-order rate constants at Demerara Rise are orders of magnitude lower than oxic decay constants estimated by using the Cretaceous sedimentation rate. However, the relationships between compacted burial velocities and anoxic decay constants proposed by Tromp et al. (1995), Toth and Lerman (1977) and Berner (1978) yield lower rate constants. Yet, these estimates are based on rates measured in the anoxic part of the sediment and are thus characteristic for the residual organic matter pool, which is buried below the oxic zone. In addition, Cretaceous black shales are generally characterized by relatively low sedimentation rates

but very high organic matter contents (e.g. Stein et al., 1986) and empirically-found $k - \omega$ relationships may not be applicable to such untypical situation. Emerson (1985) and Murray and Kuivilla (1990) argued that first-order rate constants correlate much better with organic matter rain rate. The comparison between model determined $k(0)$, observations and a power law correlation fitted to the observations (Boudreau, 1997) reveals that degradation rate constants at Demerara Rise fall well below these estimates.

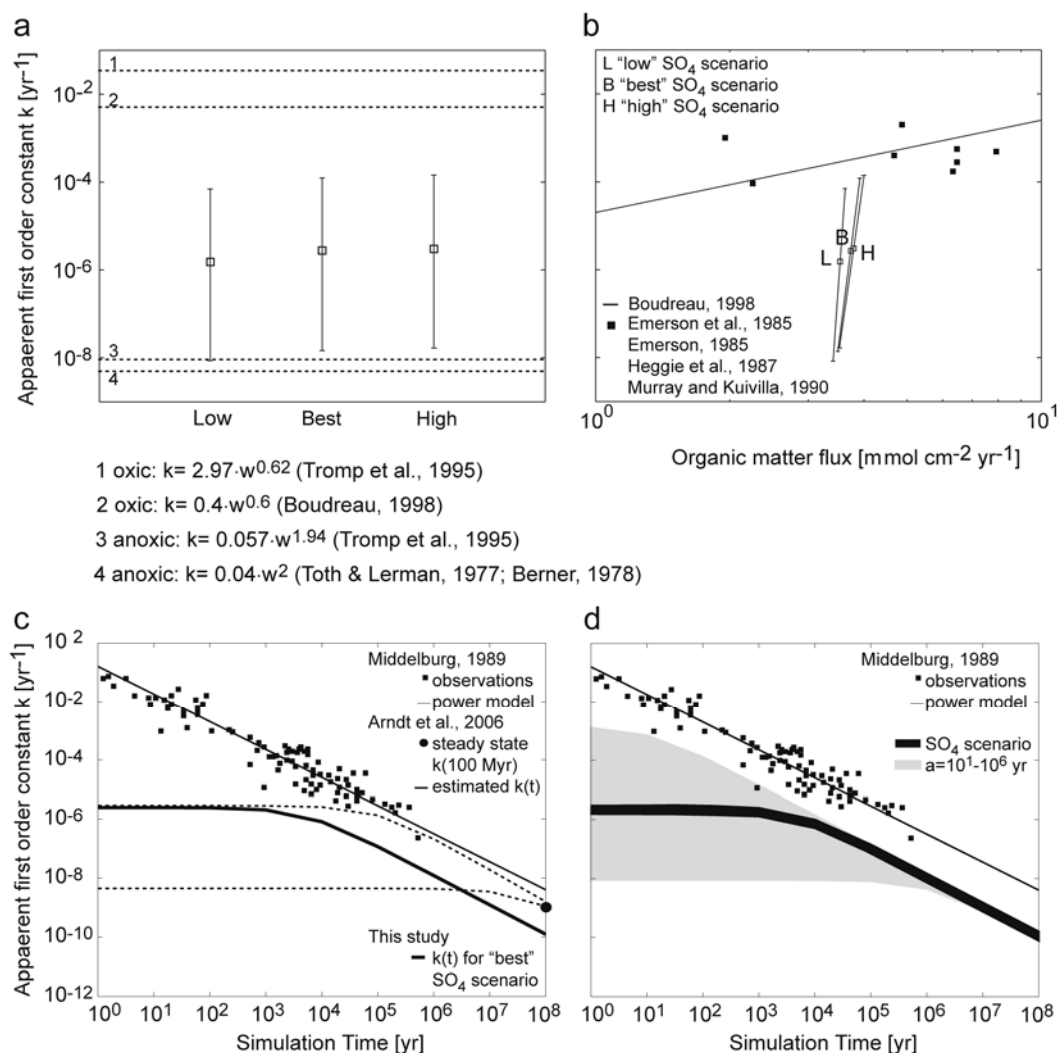


Figure 6.8 Estimated initial reactivity of black shale organic matter compared to reactivity estimates based on empirical (a) $k - \omega$ and (b) $k - F_{org}$ relationships. The squares represent the estimates calculated with a value of $a = 4926$ yr, while error bars reflect the range of rate constants calculated with different a values ($a = 10^{-1}$ – 10^6 yr). The estimated evolution of organic matter reactivity at Demerara Rise (c) is compared to the power-model and observations compiled by Middelburg (1989), as well as steady-state estimates for the present day Arndt et al. (2006). The uncertainty in $k(t)$, which is associated with the SO_4 boundary scenario and the exact value of a is shown in (d).

In contrast, $k(0)$ agrees well with the earlier, speculative estimates, which were calculated based on Middelburg's power model, model-determined, present-day degradation rate constants, and a reasonable range of initial organic matter contents (Arndt et al., 2006). These calculations revealed that a very low apparent initial age is required to calculate realistic initial organic carbon contents (<50 wt%). The determined apparent initial age results in a rate constant of organic matter degradation ($k(0) < 10^{-4} \text{ yr}^{-1}$) that is orders of magnitude lower than the rate constants provided by the original fit of the power model to field and laboratory data (i.e. $k(0) = 0.16$, Fig. 6.8c). Although the reactive continuum model (this study) and the power model (Arndt et al., 2006) result in similar initial rate constants, the reactive continuum model predicts a faster decrease of k with time (Fig. 6.8c) due to the difference between the pre-factor of the power model (0.16) and the ν value of the reactive continuum model ($\nu = 0.009\text{-}0.014$). The constant pre-factor of the power model implies that organic matter degradation follows the same reactivity decrease with time, independent of the composition of the organic matter or the depositional environment. While this assumption is, to a certain extent, supported by the similarity of ν values determined for different environments (Boudreau and Ruddick, 1991), it seems not to be applicable to the long-term evolution of organic matter degradation in the Cretaceous black shales. Inverse model results suggest that the Cretaceous black shales at Demerara Rise are controlled by comparably low, long-term degradation rates, which cannot be represented with the original form of the power model, i.e. a pre-factor of 0.16. Furthermore, the present-day rate constant, k (10^8yr) is almost one order of magnitude lower than the methanogenic degradation rate constants determined by steady-state modeling (Arndt et al., 2006). This difference indicates that the system is not at steady state and that the past evolution of biogeochemical transformations and fluxes has important implications for the present location of the SMTZ. The comparably large depth scale and the low pace of biogeochemical reactions in the deep biosphere result in a slow response of redox-fronts to changing conditions. Therefore, the significant upcore movement of the SMTZ during the late Palaeocene/Eocene sedimentation period, requires lower simulated CH_4 fluxes and thus lower methanogenic rate constants to allow for the subsequent downcore movement of the SMTZ. Figure 6.8d illustrates the uncertainty in $k(t)$, which is associated with the exact choice of a and the SO_4 boundary condition. In general, the temporal evolution of k reveals little variability for the different SO_4 boundary scenarios (black band, Fig. 6.8d), but strongly depends on the choice of a (gray band, Fig. 6.8d). On short time scales (<1 Myr), the weakly constrained parameter a induces large uncertainties in k . However, the uncertainty

rapidly decreases for longer timescales (> 1 Myr), where the evolution of k is mainly determined by the comparably well constrained value of ν . Despite these uncertainties, Figure 6.8d shows that, even within the range of uncertainty, $k(t)$ is on all timescales lower than the observed organic matter reactivities.

The identification of the mechanisms that caused the apparent, refractory character of the black shale organic matter at Demerara Rise could potentially shed new light on the functioning of the sedimentary carbon sink during the mid-Cretaceous OAEs. In general, the apparent reactivity of bulk organic carbon is the result of a large number of interacting factors, such as organic carbon sources, physical protection, geopolymerization, metabolite inhibition or the redox zonation of the depositional environment (e.g. Canfield, 1994; Burdige, 2007). Especially the euxinic nature of the Cretaceous, southern North Atlantic, as indicated by the presence of isorenieratene derivatives in black shales (Sinninghe Damsté et al., 1998), may have played an important role for the enhanced sequestration of organic carbon in this region. At Demerara Rise, the presence of certain biomarkers, as well as the geochemical characteristics of the drilled sediments also provide strong evidence for an euxinic paleo-environment. Isorenieratene derivatives are found in sediments drilled at Demerara Rise (Kuypers et al., 2002). In addition, high lycopane concentrations, a labile compound that is unable to survive prolonged exposure to oxygen, imply stable water column anoxia during deposition (Forster et al., 2004). High ratios of reactive to total iron (> 0.38), a high degree of pyritization ($DOP = 0.5-0.8$), large pyrite contents (0.5-3 wt%) and the presence of framboidal pyrite indicate euxinic depositional conditions (Böttcher et al., 2006; Hetzel et al., 2009). Furthermore, a decline in seawater derived trace metal enrichment indicates an expansion of euxinic conditions at the global onset of black shale deposition during OAE 2 (Hetzel et al., 2009). The enhanced preservation of organic matter is often related to such an anoxic or euxinic depositional environment (e.g. Toth and Lerman, 1977; Demaison and Moore, 1980; Reimers and Suess, 1983; Emerson, 1985; Moodley et al., 2005; Burdige, 2007). However, a number of studies showed that a direct relationship between water column anoxia and enhanced organic matter preservation only holds below a threshold sedimentation rate (Stein et al., 1986; Tyson, 2001). Black shales are generally characterized by relatively low sedimentation rates (< 5 cm/kyr, e.g. Stein et al., 1986) and, therefore, anoxic or euxinic conditions may play a key role for enhanced organic matter preservation in these sediments.

The reasons given to explain the relationship between organic matter preservation and anoxic/euxinic conditions include lower free energy from suboxic respiration, the need for

complex microbial consortia, reduced bioturbation and grazing, microbial inhibition by the accumulation of metabolites and the presence of non-hydrolyzable substrates which resist fermentative breakdown (e.g. Canfield, 1994; Hedges and Keil, 1995). In addition, water column suboxia generally promote preferential degradation of labile, N-rich compounds during sinking. The remaining non-amino acid fraction of the bulk organic matter is largely resistant to degradation under suboxic conditions (Van Mooy et al., 2002). Dauwe et al. (1999) also found a correlation between an amino-acid based degradation index and the first-order degradation rate constant. At Demerara Rise, high average C/N ratios of 31.2 may reflect a suppressed organic matter degradation associated with low-oxygen conditions in the water column that favored preservation of nitrogen-poor over nitrogen-rich components (Meyers et al., 2006; Junium and Arthur, 2007). In addition, euxinic conditions promote an intense sulfurization of the deposited organic matter. This natural vulcanization significantly increases the bioresistance of organic matter (Sinninghe Damsté et al., 1990; Aizenshtat et al., 1995; Sinninghe Damsté et al., 1998; Burdige, 2007) and is known to play a key role in the formation of ancient, organic matter-rich, marine sediments (Sinninghe Damsté et al., 1998; Kolonic et al., 2002; Moodley et al., 2005). At Demerara Rise, a significant enrichment of organic sulfur ($S/C = 0.04-0.06$) in the black shale sequences, as well as the presence of hopanoid thiophenes (Forster et al., 2004; Böttcher et al., 2006; Hetzel et al., 2009) indicate an intense sulfurization of organic matter. The distribution of pyrite sulfur over TOC contents reveals a relative excess of organic carbon at high TOC values, indicating a certain degree of iron limitation during black shale deposition (Böttcher et al., 2006). The limitation of reactive iron probably promoted the incorporation of diagenetically formed sulfides into the black shale organic matter, especially during the early, sulfate-dominated stages.

Implications for black shale deposition at Demerara Rise

Little is known about the quantitative significance of microbial degradation in marine sediments for the preservation and burial of black shale organic carbon. Generally, it is assumed that only a small fraction (approximately 10%) of the depositing organic matter escapes degradation in the sediment (e.g. Emerson and Hedges, 1988). However, the model-determined, low organic matter reactivity suggests an enhanced preservation of black shale organic matter at Demerara Rise. Figure 6.9 compares model-determined preservation efficiencies with observed preservation efficiencies from different non-deltaic depositional environments (Canfield, 1994). The preservation efficiency of black shale organic carbon is calculated as the percentage of the average initial organic carbon

content, which is still preserved in the sediments, $G(10^8 \text{ yr})$. The average initial organic carbon content of the black shale layer, $G(0)$, is simply given by the integrated organic carbon oxidation rate. This approach is similar to the approach adopted by Canfield (1994), who defines the depositional flux as the sum of the organic carbon burial flux and the integrated organic carbon oxidation rate. In addition, preservation efficiencies are calculated for the three SO_4 concentration scenarios and the whole range of realistic α values. The resulting range of preservation efficiencies thus accounts for the uncertainty associated with SO_4 boundary condition and the choice of the parameter α .

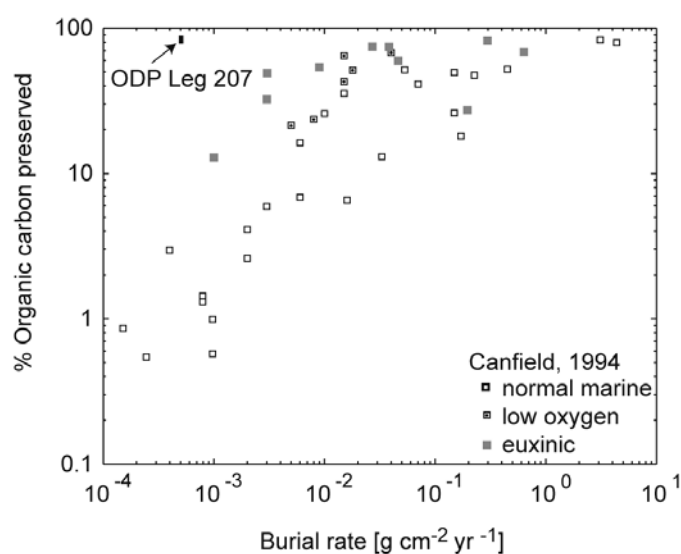


Figure 6.9 Preservation efficiency of organic matter in oxic, suboxic and anoxic depositional environments as a function of the burial rate (Canfield, 1994), compared to the range of preservation efficiencies determined for the black shale sequences drilled at Demerara Rise for a realistic range of α values ($\alpha = 10^1$ - 10^6 yr) and the three SO_4 boundary scenarios.

Observed preservation efficiencies range from an almost complete organic matter preservation to an almost complete consumption (e.g. Arthur and Sageman, 1994; Canfield, 1994; Burdige, 2007). This variability is often related to sedimentation rates and water column oxygenation (e.g. Stein et al., 1986; Henrichs and Reeburgh, 1987; Betts and Holland, 1991; Canfield, 1994). In general, enhanced preservation efficiencies are favored by high sedimentation rates and low-oxygen or euxinic water column conditions (Canfield, 1994; Moodley et al., 2005). Yet, sediments underlying an anoxic water column do not show uniformly enhanced preservation efficiencies. Calculated preservation efficiencies for Cretaceous black shale organic matter drilled at Demerara Rise range from 79% to 89% and, therefore, plot well above observations from other euxinic environments (Fig. 6.9). Nonetheless, it should be noted that these estimates represent an average preservation

efficiency for the bulk organic matter in the black shale layer. They do not reflect short-term variations and preservation efficiencies are likely to be variable across the black shale layer. In addition, these estimates are associated with a certain degree of uncertainty. The rough estimation of sedimentation rates affects the calculation of sediment burial rates. Furthermore, potential, short-term bottom water oxygenation events may have resulted in enhanced organic matter degradation rates and model-determined preservation efficiencies may thus be slightly overestimated. Despite these uncertainties, the model-determined bulk preservation efficiency is significantly higher than preservation efficiencies expected for such a low burial rate (Fig. 6.9).

The high degree of organic matter preservation in the Cretaceous black shales implies that their initial organic carbon content was comparable to the observed presentday content. Based on general assumptions and simulated initial carbon contents, rough estimates of Cretaceous bulk organic carbon mass accumulation and primary production rates can be calculated and compared with previous estimates. Average organic carbon contents between 8.1 and 9.5 wt% predict organic carbon mass accumulation rates between 0.43 and 0.5 g C m² yr⁻¹ at the Cretaceous Demerara Rise. These values agree well with organic matter contents and organic carbon accumulation rates estimated for other North Atlantic sites. Stein et al. (1986) report accumulation rates between 0.2 and 0.5 g C m² yr⁻¹ for black shales drilled in the eastern North Atlantic, while accumulation rates range generally between 0.2 and 1 g C m² yr⁻¹ in the western North Atlantic. Assuming that 1-4% (Suess, 1980; Arthur and Sageman, 1994; Sinninghe Damsté et al., 1998) of the oceanic primary production is preserved in an euxinic water column, estimated primary production rates would reach average values between 11 and 50 g C m² yr⁻¹. The estimated values are orders of magnitude lower than primary production rates reported for present-day upwelling areas (200-3600 g C m² yr⁻¹). Therefore, the enhanced preservation of organic matter in the sediment may explain the comparably high organic matter contents of black shales drilled in the southern North Atlantic, without having to assume exceptionally high primary production rates.

Model results, observations from Demerara Rise, as well as previous studies thus indicate that the enhanced preservation of organic carbon in marine sediments may have operated as an important control for organic carbon burial in ancient black shales. Environmental factors associated with euxinic conditions in the sediment and the water column apparently reduced the susceptibility of the black shale organic matter to degradation and significantly increased the efficiency of the sedimentary carbon sink. This notion is supported by other

modeling studies and observations from similar sites. Sinninghe Damsté et al. (1998), for instance, argued that the enhanced preservation of organic matter under euxinic conditions may have been the main driver for black shale formation around the C/T boundary in the southern North Atlantic. In addition, Kolonic et al. (2005) conclude that preservation of organic carbon was considerably enhanced during Cretaceous black shale deposition in the euxinic paleo-environment at the Tarfaya shelf. Recently, Meyers et al. (2005) and Meyers (2007) showed that a reduced supply of reactive iron to the sediment results in high porewater sulfide concentrations and a shoaling of the sulfate reduction zone, which leads to an enhanced preservation of organic matter in these sediments. They demonstrated that this biogeochemical mechanism was particularly important for the formation of black shales.

Uncertainties and Model Limitations

The complexity of the Earth system, as well as the inability of observations to fully resolve all of the characteristic spatial and temporal scales of change challenge simple, straightforward answers. In this respect, RTM studies represent an important tool in the study of the paleo-environments as they offer a means to bridge spatial and temporal scales. They are therefore fully complementary to experimental observations, which provide snapshots of instantaneous dynamics, within the context of the system that evolved over millions of years. Nevertheless, the explanatory power of paleo-modeling studies is limited by the scarcity of data and the knowledge of the paleo boundary conditions required to run the model.

In this study, the rough estimates of sedimentation rates merely capture the long-term evolution of sediment deposition at Demerara Rise. Furthermore, the evolution of oceanic SO_4 concentration over the last 100 Myrs is not well constrained. The available data from fluid inclusions in marine halites only provide a general trend of increasing oceanic SO_4 concentration. Constant TOC and biogenic BaSO_4 depositional fluxes are applied throughout the period of black shale deposition to match the temporal scale of change that can be resolved by the available boundary conditions and forcings. Therefore, simulation results capture the long-term evolution of biogeochemical dynamics at Demerara Rise. They provide insights into the general nature of bulk black shale formation, but do not resolve the observed heterogeneity within the black shale layer, associated with short-term fluctuations at the sediment-water interface. Apart from their temporal resolution, uncertainties in boundary conditions also affect the model performance. The accuracy of estimated sedimentation rates is compromised by the combination of hiatuses, limited

biostratigraphic zonal markers, and the absence of magnetic reversals. This uncertainty influences the estimation of accumulation rates. In addition, measurements of SO_4 concentrations in fluid inclusions are associated with large uncertainties. Yet, simulation results display a large sensitivity to bottom water SO_4 concentrations, since they control the magnitude of the simulated degradation rates and thus the estimated organic matter content. Therefore, three different boundary concentration scenarios, which span the range of observed variability help quantifying the influence of these uncertainties on simulation results. Furthermore, we assume that organic matter degradation within the black shale sequence is completely dominated by sulfate reduction and methanogenesis. However, the benthic foraminifera assemblage at Site 1258 reveals short-term repopulations in the lower third of OAE 2, which may indicate short-term bottom-water oxygenation. A temporary oxygenation of bottom waters could have enhanced organic matter degradation and, therefore, estimated Cretaceous organic matter contents and depositional fluxes might be underestimated. In addition, the depth-integrated BaSO_4 contents may not be completely representative for the initial biogenic BaSO_4 content in the Cretaceous black shales and, therefore induce uncertainties in model estimates.

Potential uncertainties also stem from the open flux conditions which is applied at the lower boundary. This treatment assumes that the influence of underlying sediments on the simulated biogeochemical dynamics is negligible. Nevertheless, a diffusion of CH_4 from lower sources, e.g. underlying Albian sediments, cannot be completely ruled out. In this case, the choice of an open flux boundary condition for CH_4 could result in an overestimation of the calculated organic matter reactivity, since the simulated biogenic CH_4 flux would have to compensate for the neglected influx of CH_4 through the lower boundary.

Uncertainties also arise from the RTM and the inverse model approach itself. The building process is not unique and subjective by nature. A number of models, differing in process formulations, parameter choice or boundary conditions might potentially explain the observed data equally well. Nonetheless, the presented RTM was built on the mechanistic understanding gained from the previous steady-state modeling study and the comprehensive ODP data set. The presented scenario is thus comparably well constrained and represents the most plausible scenario that reproduces the data and can be constrained by available observations.

Despite these uncertainties and limitations, the presented study reveals how RTMs can hindcast the diagenetic history that created the observed distributions of authigenic minerals. Therefore, RTMs provide a rational support for a detailed, quantitative

understanding of the biogeochemical dynamics over geological timescales. Model estimates are orders of magnitude lower than in modern day environments. Previous modeling studies, the results of the inverse modeling, the quantification of uncertainties associated with weakly constrained parameters, a comprehensive set of biomarker, isotope and geochemical data, as well as the results of modeling and observational studies from similar drill sites, help verify the model formulation and support the formulated conclusions. However, any attempt to infer the nature of paleo-environments from present-day observations should be viewed as a work in progress and should be constantly reevaluated and tested in the context of our evolving mechanistic understanding of these environments.

Conclusions

Marine sediments act as the ultimate sink for organic carbon, sequestering otherwise rapidly cycling carbon for geologic timescales. During the mid-Cretaceous OAEs, the globally enhanced organic carbon burial rates may have effectively reduced the CO₂ concentrations of the mid-Cretaceous greenhouse atmosphere. However, the mechanisms which led to the increased organic carbon burial during these events are still controversial. In the past, conceptual and mathematical models of black shale formation often focused on the contribution of primary depositional processes, such as increased primary production and/or water column anoxia, to the intense organic carbon sequestration. So far, little attention has been given to the role of organic matter breakdown in marine sediments. However, a quantitative assessment of the long-term evolution of organic matter degradation in Cretaceous black shales and the associated biogeochemical transformations and fluxes could provide important insights into the functioning of the sedimentary carbon sink during these events.

In this study, a highly-resolved barite depth-profile is used in combination with a transient RTM to unravel the evolution of biogeochemical transformations and fluxes in black-shale bearing sediments drilled at Demerara Rise (ODP Leg 207). Simulation results indicate that long-term variations in sedimentation rate induce prominent shifts in the redox-zonation of the sediment and promote the formation of distinct authigenic fronts. These results confirm the earlier formulated hypothesis that the distribution of authigenic barites provides a detailed record of the longterm evolution of the SMTZ and, therefore, offers important insights into the evolution of the organic matter reactivity within the Cretaceous black shale sequence.

Simulation results show that the reactivity of the organic matter was already low at the time of its deposition in the Cretaceous. The inversely determined range of initial apparent first-order rate constant of organic matter degradation (10^{-4} - 10^{-8} yr⁻¹) is orders of magnitude lower than those calculated based on empirical relationships for oxic and anoxic environments. However, it agrees well with rough estimates of initial rate constants, which have been calculated with the power model (Arndt et al., 2006). Nonetheless, the inverse model results show that the temporal evolution of the redox-dynamics at Demerara Rise, as recorded in the authigenic BaSO₄ distribution, indicates low organic matter degradation rates, which are not well-captured by the power model. The refractory nature of the organic matter results in a high preservation efficiency of 79-89%.

The geochemical characteristics of sediments drilled at Demerara Rise, as well as the presence of certain biomarkers indicate that euxinic conditions in both the water column and the sediment may have caused an enhanced preservation of organic matter in the Cretaceous black shales. In particular, the intense sulfurization of organic matter in the sulfidic and iron-limited sediments could have significantly reduced the susceptibility of the organic matter to degradation. The enhanced preservation of organic matter may have played a prominent role in the formation of Cretaceous black shales in the euxinic southern North Atlantic. It may have increased the efficiency of the global sedimentary carbon sink and may have effectively reduced the CO₂ content of the Cretaceous atmosphere.

These findings suggest that the extreme environmental conditions, which prevailed in the Cretaceous greenhouse, increased the importance of factors that favor organic matter preservation. Consequently, the functioning of the Cretaceous sedimentary carbon sink and its effect on the Cretaceous climate system may not be well-described by simplified parametric laws, based on empirical relationships from modern day observations. Therefore, the results emphasize the need for a mechanistic understanding of long-term organic matter degradation dynamics that integrates the environmental controls on organic matter preservation.

Acknowledgements

This manuscript has greatly benefited from discussions with P. Regnier, P. Van Cappellen and extremely constructive and helpful reviews from Robert Aller, Christian Hensen and two anonymous reviewers. This study was financially supported by the Deutsche Forschungsgemeinschaft (Br 775/16) within the IODP/ICDP Special Research Program.

References

- Abramowitz, M., Stegun, I.A., 1972. Handbook of Mathematical Functions with Formulas, Graphs and Mathematical Tables. National Bureau of Standards, Washington DC.
- Aizenshtat, Z., Krein, E., Vairavamurthy, M., Goldstein, T., 1995. Role of sulfur in the transformation of sedimentary organic matter: A mechanistic overview. ACS Symposium Series 612, 378-396.
- Aller, R. C., Blair, N. E., 2004. Early diagenetic remineralization of sedimentary organic C in the Gulf of Papua deltaic complex (Papua New Guinea): Net loss of terrestrial C and diagenetic fractionation of C isotopes. *Geochimica et Cosmochimica Acta* 68(8), 1815-1825.
- Aris, R., 1968. Prolegomena to the rational analysis of systems of chemical reactions, II. *Archiv Rational Mechanics Analysis* 27, 539-548.
- Arndt, S., Brumsack, H.-J., Wirtz, K.W., 2006. Cretaceous black shales as active bioreactors: A biogeochemical model for the deep biosphere encountered during ODP Leg 207 (Demerara Rise). *Geochimica et Cosmochimica Acta* 70(2), 408-425.
- Arthur, M.A., Jenkyns, H.C., Brumsack, H.-J., Schlanger, S.O., 1990. Stratigraphy, geochemistry, and paleo-oceanography of organic carbon-rich Cretaceous sequences. In: Ginsburg, R.N., Beadoin, B. (Eds.), *Cretaceous resources, events and rhythms; background and plans for research*. NATO ASI Series C Vol. 304, Kluwer Academic Publishers, Dordrecht, 75-119.
- Arthur, M.A., Dean, W.E., Pratt, L.M., 1988. Geochemical and climatic effects of increased marine organic carbon burial at the Cenomanian/Turonian boundary. *Nature* 335(6192), 714-717.
- Arthur, M.A., Natland, J.H., 1979. Carbonaceous sediments in the North and South Atlantic: The role of salinity in stable stratification of Early Cretaceous basins. In: Talwani, M., Hay, W., Ryan, W.B.F. (Eds.), *Deep Drilling Results in the Atlantic Ocean: Continental Margins and Paleoenvironment*. American Geophysical Union, Maurice Ewing Series 3, 375-401.
- Arthur, M.A., Sageman, B.B., 1994. Marine black shales: Depositional mechanisms and environments of ancient deposits. *Annual Reviews of Earth and Planetary Sciences* 22, 499-551.
- Arthur, M.A., Schlanger, S.O., Jenkyns, H.C., 1987. The Cenomanian/Turonian Oceanic Anoxic Event, II. Palaeoceanographic controls on organic-matter production and preservation. In: Brooks, J., Fleet, A.J. (Eds.), *Marine Petroleum Source Rocks*. Geological Society, London. Special Publication 26, 401-420.
- Berner, R.A., 1978. Sulfate reduction and the role of deposition of marine sediments. *Earth and Planetary Science Letters* 37, 492-498.
- Berner, R.A., 1980. *Early Diagenesis: A theoretical approach*. Princeton University Press, Princeton, New Jersey.
- Betts, J.N., Holland, H.D., 1991. The oxygen content of ocean bottom waters, the burial efficiency of organic carbon, and the regulation of atmospheric oxygen. *Palaeogeography, Palaeoclimatology, Palaeoecology* 97(1-2), 5-18.
- Bosatta, E., Agren, G., 1985. Theoretical analysis of decomposition of heterogeneous substrates. *Soil Biology and Biochemistry* 17(5), 601-610.
- Bosatta, E., Agren, G., 1995. The power and reactive continuum models as particular case of the q-theory of organic matter dynamics. *Geochimica et Cosmochimica Acta* 59(18), 3833-3835.
- Bosbach, D., 2002. Linking molecular-scale barite precipitation mechanisms with macroscopic crystal growth rates. *Geochemical Society, Houston. Special Publications* 7, 97-110.

- Böttcher, M.E., Hetzel, A., Brumsack, H.-J., Schipper, A., 2006. Sulfur-iron-carbon geochemistry in sediments of the Demerara Rise. In: Mosher, D.C., Erbacher, J., Malone, M.J. (Eds.), *Proceedings of the Ocean Drilling Program, Scientific Results*, 207. College Station, TX (Ocean Drilling Program), 1-23.
- Böttcher, M.E., Lepland, A., 2000. Biogeochemistry of sulfur in a sediment core from the West-Central Baltic Sea: Evidence from stable isotopes and pyrite textures. *Journal of Marine Systems* 25(3-4), 299-312.
- Boudreau, B.P., 1997. *Diagenetic Models and their Implementation*. Springer Verlag, Hamburg.
- Boudreau, B., Ruddick, B., 1991. On a reactive continuum representation of organic matter diagenesis. *American Journal of Science* 291, 507-538.
- Bréhéret, J.G., Brumsack, H.-J., 2000. Barite concretions as evidence of pauses in sedimentation in the Marnes Bleues Formation of the Vocontian Basin (SE France). *Sedimentary Geology* 130(3-4), 205-228.
- Brumsack, H.-J., 1986. The inorganic geochemistry of Cretaceous black shales (DSDP Leg 41) in comparison to modern upwelling sediments from the Gulf of California. In: Summerhayes, C.P., Shackleton, N.J. (Eds.), *North Atlantic Paleocenography*. Geological Society, London. Special Publication 21, 447-462.
- Brumsack, H.-J., 2006. The trace metal content of recent organic carbon-rich sediments: implications for Cretaceous black shale formation. *Palaeogeography, Palaeoceanography, Palaeoecology* 232(2-4), 344-361.
- Burdige, D.J., 2007. Preservation of organic matter in marine sediments: Controls, mechanisms and an imbalance in sediment organic carbon budgets? *Chemical Reviews* 107(2), 467-485.
- Canfield, D.E., 1994. Factors influencing organic carbon preservation in marine sediments. *Chemical Geology* 114(3-4), 315-329.
- Canfield, D.E., 2001. Isotope fractionation by natural populations of sulfate-reducing bacteria. *Geochimica et Cosmochimica Acta* 65(7), 1117-1124.
- Carpenter, S.R., 1981. Decay of heterogeneous detritus: A general model. *Journal of Theoretical Biology* 89(4), 539-547.
- Christy, A.G., Putnis, A., 1993. The kinetics of barite dissolution and precipitation in water and sodium chloride brines at 44-85 °C. *Geochimica et Cosmochimica Acta* 57(10), 2161-2168.
- Coolen, M., Cypionka, H., Sass, A., Sass, H., Overmann, J., 2002. Ongoing modification of Mediterranean Pleistocene sapropels mediated by prokaryotes. *Science* 296(5577), 2407-2410.
- Dauwe, B., Middelburg, J.J., Herman, P.M.J., Heip, C.H.R., 1999. Linking diagenetic alteration of amino acids and bulk organic matter reactivity. *Limnology and Oceanography* 44(7), 1809-1814.
- Demaison, G.J., Moore, G.T., 1980. Anoxic environments and oil source bed genesis. *AAPG Bulletin* 64(8), 1179-1209.
- Dickens, G. R., 2001. Sulfate profiles and barium fronts in sediment on the Blake Ridge: Present and past methane fluxes through a large gas hydrate reservoir. *Geochimica et Cosmochimica Acta* 65(4), 529-543.
- Duan, Z., Moeller, N., Greenberg, J., Weare, J.H., 1992. The prediction of methane solubility in natural waters to high ionic strength from 0 to 250°C and from 0 to 1600 bar. *Geochimica et Cosmochimica Acta* 56(4), 1451-1460.
- Emerson, S. R., 1985. Organic carbon preservation in marine sediments. In: *The Carbon Cycle and Atmospheric CO₂: Natural Variations Archean to Present*. Proceedings of the Chapman Conference on Natural Variations in Carbon Dioxide and the Carbon Cycle. American Geophysical Union, Tarpon Springs, FL, 77-78.

- Emerson, S., Hedges, J. I., 1988. Processes controlling the organic carbon content of open ocean sediments. *Palaeoceanography* 3(5), 621-634.
- Erbacher, J., Huber, B.T., Norris, R.D., Markey, M. 2001. Increased thermohaline stratification as a possible cause for an oceanic anoxic event in the Cretaceous period. *Nature* 409(6818), 325-327.
- Erbacher, J., Mosher, D.C., Malone, M.J., Shipboard Scientific Party, 2004. Proceedings of the Ocean Drilling Program, Initial Reports, 207. College Station, TX (Ocean Drilling Program), pp. 89.
- Forster, A., Sturt, H., Meyers, P.A., ODP Leg 207 Shipboard Scientific Party 2004. Molecular Biogeochemistry of Cretaceous Black Shales from the Demerara Rise: Preliminary Shipboard Results from Sites 1257 and 1258, Proceedings of the Ocean Drilling Program, Initial Reports, 207. College Station, TX (Ocean Drilling Program), 1-23.
- Friedrich, O., Erbacher, J., 2006. Benthic foraminiferal assemblages from Demerara Rise (ODP Leg 207, western tropical Atlantic): possible evidence for a progressive opening of the equatorial Atlantic gateway. *Cretaceous Research* 27(3), 377-397.
- Gieskes, J., Gamo, T., Brumsack, H.-J., 1991. Chemical methods for interstitial water analysis aboard Joides Resolution. Ocean Drilling Program, Technical Note 15, College Station, TX (Ocean Drilling Program).
- Hedges, J.I., Keil, R.G., 1995. Sedimentary organic matter preservation: an assessment and speculative synthesis. *Marine Chemistry* 49(2-3), 81-115.
- Henrichs, S.M., Reeburgh, W.S., 1987. Anaerobic mineralization of marine organic matter: Rates and the role of anaerobic processes in the oceanic carbon economy. *Geomicrobiology* 5(3), 191-237.
- Hetzel, A., Böttcher, M.E., Wortmann, U.G., Brumsack, H.-J., 2009. Paleo-redox conditions during OAE 2 reflected in Demerara Rise sediment geochemistry (ODP Leg 207). *Palaeogeography, Palaeoceanography, Palaeoecology* 273(3-4), 302-328.
- Hetzel, A., Brumsack, H.-J., Böttcher, M. E., Schnetger, B., 2006. Inorganic geochemical characterization of lithologic units recovered during ODP Leg 207 (Demerara Rise). In: Mosher, D.C., Erbacher, J., Malone, M.J. (Eds.), Proceedings of the Ocean Drilling Program, Scientific Results, 207. College Station, TX (Ocean Drilling Program), 1-37.
- Hills, R.G., Fisher, K.A., Kirkland, M.R., Wierenga, P.J., 1994. Application of flux corrected transport to the Las Cruces trench Site. *Water Resource Research* 30(8), 2377-2385.
- Ho, T.C., Aris, R., 1987. On apparent second-order kinetics. *American Institute of Chemical Engineering Journal* 33, 1050-1051.
- Horita, J., Zimmermann, H., Holland, H.D., 2002. Chemical evolution of seawater during the Phanerozoic. *Geochimica et Cosmochimica Acta* 66(21), 3733-3756.
- Ibach, L.E.J., 1982. Relationship between sedimentation rate and total organic carbon content in ancient marine sediments. *AAPG Bulletin* 66(2), 170-188.
- Jansen, B.H., 1984. A simple method for calculating decomposition and accumulation of 'young' soil organic matter. *Plant and Soil* 76(1-3), 287-304.
- Jenkyns, H. C., 1980. Cretaceous anoxic events: From continents to oceans. *Journal of the Geological Society* 137(3), 171-188.
- Jørgensen, B.B., Böttcher, M.E., Lüschen, H., Neretin, L.N., Volkov, I.I., 2004. Anaerobic methane oxidation and a deep H₂S sink generate isotopically heavy sulfides in Black Sea sediments. *Geochimica et Cosmochimica Acta* 68(9), 2095-2118.
- Junium, C.K., Arthur, M.A., 2007. Nitrogen cycling during the Cretaceous, Cenomanian-Turonian Oceanic Anoxic Event II. *Geochemistry, Geophysics, Geosystems* 8, Q03002.
- Kolonic, S., Wagner, T., Forster, A., Sinninghe Damsté, J.S., Walsworth-Bell, B., Erba, E., Turgeon, S., Brumsack, H.-J., Chellai, E.H., Tsikos, H., Kuhnt, W., Kuypers, M.M.M.,

2005. Black shale deposition on the northwest African Shelf during the Cenomanian/Turonian oceanic anoxic event: Climate coupling and global organic carbon burial. *Paleoceanography* 20(1), PA1006.
- Kolonic, S., Sinninghe Damsté, J.S., Böttcher, M.E., Kuypers, M.M.M., Kuhnt, W., Beckmann, B., Scheeder, G., Wagner, T., 2002. Geochemical characterization of Cenomanian/Turonian black shales from the Tarfaya Basin (SW Morocco): Relationships between palaeoenvironmental conditions and early sulphurization of sedimentary organic matter. *Journal of Petroleum Geology* 25(3), 325-350.
- Krumholz, L.R., Harris, S.H., Suflita, J.M., 2002. Anaerobic microbial growth from components of Cretaceous shales. *Geomicrobiology Journal* 19(6), 593-602.
- Krumholz, L.R., McKinley, J.P., Ulrich, G.A., Suflita, J.M., 1997. Confined subsurface microbial communities in Cretaceous rocks. *Nature* 386(6620), 64-66.
- Kuypers, M.M.M., Pancost, R.D., Nijenhuis, I.A., Sinninghe Damsté, J.S., 2002. Enhanced productivity led to increased organic carbon burial in the euxinic North Atlantic basin during the late Cenomanian oceanic anoxic event. *Paleoceanography* 17(4), 1051.
- Lowenstein, T.K., Timoeff, M.N., Brennan, S.T., Hardie, L.A., Demicco, R.M., 2001. Oscillations in Phanerozoic seawater chemistry: evidence from fluid inclusion. *Science* 294(5544), 1086-1088.
- Lyons, T.W., Werne, J.P., Hollander, D.J., Murray, R.W., 2003. Contrasting sulfur geochemistry and Fe/Al and Mo/Al ratios across the last oxic-to-anoxic transition in the Cariaco Basin, Venezuela. *Chemical Geology* 195(1), 131-157.
- Manheim, F.T., Sayles, F.L., 1974. Composition and origin of interstitial waters of marine sediments, based on deep sea drill cores. In: Goldberg, E.D. (Ed.), *The Sea* (Vol. 5): Marine Chemistry: The Sedimentary Cycle. Wiley, New York, 527-568.
- Meyers, P.A., 1997. Organic geochemical proxies of paleoceanographic, paleolimnologic, and paleoclimatic processes. *Organic Geochemistry* 27(5), 213-250.
- Meyers, P.A., Bernasconi, S.M., Forster, A., 2006. Origins and accumulation of organic matter in expanded Albian to Santonian black shale sequences on the Demerara Rise, South American margin. *Organic Geochemistry* 37(12), 1816-1830.
- Meyers, P.A., Forster, A., Sturt, H., ODP Leg 207 Shipboard Scientific Party, 2004. Microbial gases in black shale sequences on the Demerara Rise. *Proceedings of the Ocean Drilling Program, Initial Reports, 207*. College Station, TX (Ocean Drilling Program), 1-23.
- Meyers, S.R., 2007. Production and preservation of organic matter: The significance of iron. *Paleoceanography* 22, PA4211.
- Meyers, S.R., Sageman, B.B., Hinnov, L.A., 2001. Integrated quantitative stratigraphy of the Cenomanian-Turonian Bridge Creek limestone member using evolutive harmonic analysis and stratigraphic modeling. *Journal of Sedimentary Research* 71(4), 627-643.
- Meyers, S.R., Sageman, B.B., Lyons, T., 2005. Organic carbon burial rate and the molybdenum proxy: Theoretical framework and application to Cenomanian-Turonian OAE II. *Paleoceanography* 20, 2002.
- Middelburg, J.J., 1989. A simple rate model for organic matter decomposition in marine sediments. *Geochimica et Cosmochimica Acta* 53(7), 1577-1581.
- Middelburg, J.J., 1991. Organic carbon, sulphur, and iron in recent semi-euxinic sediments of Kau Bay, Indonesia. *Geochimica et Cosmochimica Acta* 55(3), 815-828.
- Moodley, L., Middelburg, J.J., Herman, P.M.J., Soetaert, K., de Lange, G.J., 2005. Oxygenation and organic-matter preservation in marine sediments: Direct experimental evidence from ancient organic carbon-rich deposits. *Geology* 33(11), 889-892.

- Murray, J.W., Kuivilla, K.M., 1990. Organic matter diagenesis in the north-east Pacific, transition from aerobic clay to suboxic hemipelagic sediments. *Deep-Sea Research* 37(1), 59-80.
- Murray, R.W., Miller, D.J., Kryc, K.A., 2000. Analysis of major and trace elements in rocks, sediments, and interstitial waters by inductively coupled plasma-atomic emission spectrometry (ICP-AES). Ocean Drilling Program, Technical Note 29, College Station, TX (Ocean Drilling Program).
- Passier, H.F., Middelburg, J.J., van Os, B.J.H., de Lange, G.J., 1996. Diagenetic pyritization under eastern Mediterranean sapropels caused by downward sulphide diffusion. *Geochimica et Cosmochimica Acta* 60(1), 751-763.
- Pederson, T.F., Calvert, S.E., 1990. Anoxia vs. productivity: What controls the formation of organic-carbon-rich sediments and sedimentary rocks? *AAPG Bulletin* 74(4), 454-466.
- Reimers, C.E., Suess, E., 1983. The partitioning of organic carbon fluxes and sedimentary organic matter decomposition rates in the ocean. *Marine Chemistry* 13(2), 141-168.
- Robin, E., Rabouille, C., Martinez, G., Lefevre, I., Reyss, J.-L., van Beek, P., Jeandel, C., 2003. Direct barite determination using SEM/EDS-ACC system: implication for constraining barium carriers and barite preservation in marine sediments. *Marine Chemistry* 82(3-4), 289-306.
- Rushdi, A.I., McManus, J., Collier, R.W., 2000. Marine barite and celestite saturation in seawater. *Marine Chemistry* 69(1-2), 19-31.
- Sageman, B.B., Murphy, A.E., Werne, J.P., Ver Straeten, C.A., Hollander, D.J., Lyons, T.W., 2003. A tale of shales: the relative roles of production, decomposition, and dilution in the accumulation of organic-rich strata, Middle-Upper Devonian, Appalachian basin. *Chemical Geology* 195(1-4), 229-273.
- Schenau, S.J., Prins, M.A., de Lange, G.J., Monnin, C., 2001. Barium accumulation in the Arabian Sea: Controls on barite preservation in marine sediments. *Geochimica et Cosmochimica Acta* 65(10), 1545-1556.
- Schlanger, S.O., Jenkyns, H.C., 1976. Cretaceous oceanic anoxic events: causes and consequences. *Geologie en Mijnbouw* 55, 179-184.
- Sinninghe Damsté, J.S., de Leeuw, J.W., 1990. Analysis, structure and geochemical significance of organically-bound sulfur in the geosphere: State of the art and future research. *Organic Geochemistry* 16(4-6), 1077-1101.
- Sinninghe Damsté, J.S., Kok, M.D., Köster, J., Schouten, S., 1998. Sulfurized carbohydrates: An important sedimentary sink for organic carbon. *Earth and Planetary Science Letters* 164(1), 7-13.
- Sinninghe Damsté, J.S., Rijpstra, W.I.C., Reichart, G.-J., 2002. The influence of oxic degradation on the sedimentary biomarker record II: Evidence from the Arabian Sea sediments. *Geochimica et Cosmochimica Acta* 66(15), 2737-2754.
- Stein, R., Rullkötter, J., Welte, D., 1986. Accumulation of organic-carbon-rich sediments in the late Jurassic and Cretaceous Atlantic - a synthesis. *Chemical Geology* 56, 1-32.
- Suess, E., 1980. Particulate organic carbon flux in the oceans - Surface productivity and oxygen utilization. *Nature* 288(5788), 260-263.
- Tarutis, W.J., 1993. On the equivalence of the power and reactive continuum models of organic matter diagenesis. *Geochimica et Cosmochimica Acta* 57(6), 1349-1350.
- Toth, D.J., Lerman, A., 1977. Organic matter reactivity and sedimentation rates in the ocean. *American Journal of Science* 277, 465-485.
- Treude, T., Boetius, A., Knittel, K., Wallmann, K., Jørgensen, B.B., 2003. Anaerobic oxidation of methane above gas hydrates at Hydrate Ridge, NE Pacific Ocean. *Marine Ecology Progress Series* 264, 1-14.

- Tromp, T.K., van Cappellen, P., Key, R.M., 1995. A global model for the early diagenesis of organic carbon and organic phosphorus in marine sediments. *Geochimica et Cosmochimica Acta* 59(7), 1259-1284.
- Tyson, R.V., 2001. Sedimentation rate, dilution, preservation and total organic carbon: Some results of a modeling study. *Organic Geochemistry* 32(2), 333-339.
- Tyson, R.V., Pearson, T.H., 1991. Modern and ancient continental shelf anoxia: an overview. In: Tyson, R.V., Pearson, T.H. (Eds.), *Modern and ancient continental shelf anoxia*. Geological Society, London. Special Publication 58, 1-24.
- van Cappellen, P., Wang, Y., 1996. Cycling of iron and manganese in surface sediments: A general theory for the coupled transport and reaction of carbon, oxygen, nitrogen, sulfur, iron and manganese. *American Journal of Science* 296, 197-243.
- van Mooy, B.A.S.V., Keil, R.G., Devol, A.H., 2002. Impact of suboxia on sinking particulate organic carbon: Enhanced carbon flux and preferential degradation of amino acids via denitrification. *Geochimica et Cosmochimica Acta* 66(3), 457-465.
- van Os, B.J.H., Middelburg, J.J., de Lange, G.J., 1991. Possible diagenetic mobilization of barium in sapropelic sediment from the eastern Mediterranean. *Marine Geology* 100(1-4), 125-136.
- Wagner, T., Sinninghe Damsté, J.S., Hofmann, P., Beckmann, B., 2004. Euxinia and primary production in Late Cretaceous eastern equatorial Atlantic surface waters fostered orbitally driven formation of black shales. *Paleoceanography* 19, PA3009.
- Wallmann, K., Aloisi, G., Haeckel, M., Obzhairov, A., Pavlova, G., Tishchenko, P., 2006. Kinetics of organic matter degradation, microbial methane generation, and gas hydrate formation in anoxic marine sediments. *Geochimica et Cosmochimica Acta* 70(15), 3905-3927.
- Wehausen, R., Schnetger, B., Brumsack, H.-J., Lange, G.D., 1999. Determination of major and minor ions in brines by X-ray fluorescence spectrometry: comparison with other common analytical methods. *X-ray Spectrometry* 28, 168-172.
- Westrich, J.T., Berner, R.A., 1984. The role of sedimentary organic matter in bacterial sulfate reduction: the G model tested. *Limnology and Oceanography* 29(2), 236-249.
- Wilson, P.A., Norris, R.D., 2001. Warm tropical ocean surface and global anoxia during the mid-Cretaceous period. *Nature* 412(6845), 425-429.

7. Geochemical environment of Cenomanian – Turonian black shale deposition at Wunstorf (northern Germany) – a new reference section for Oceanic Anoxic Event 2

Almut Hetzel, Hans-Jürgen Brumsack

This chapter has been submitted to Cretaceous Research.

Abstract

High resolution investigations of major and minor elements were carried out on a sediment drill core from Wunstorf (N. Germany), including the black shale bearing Hesseltal Formation with the Oceanic Anoxic Event 2 (OAE 2), also referred to as Cenomanian-Turonian Boundary Event (CTBE). Seven black shale packages, each containing several black shale layers, were defined by TOC values, with black shale packages 1 – 4 deposited during OAE 2. As packages 5 - 7 extend above the level of the positive carbon isotope excursion defining OAE 2, the circumstances favouring organic carbon burial obviously prevailed longer in the Wunstorf basin than globally. Geochemical analysis revealed no significant differences between black shale packages deposited during OAE 2 and thereafter. Regarding palaeoenvironmental conditions during black shale deposition, enrichment patterns of sulphur, iron and redox-sensitive and sulphide-forming trace metals hint to suboxic to anoxic conditions at the sediment-water interface, whereas sulphidic conditions prevailed deeper in the sediment. Variations in element/Al ratios follow cyclic patterns which we interpret as climatically induced changes in sediment supply. Reduced vertical mixing leads to water column stratification causing black shale deposition.

Keywords: Wunstorf, Oceanic Anoxic Event 2, Cenomanian-Turonian Boundary Event, trace metals, black shales, palaeoenvironment

Introduction

In the mid-Cretaceous, marine sediments recorded several distinct periods of wide-spread organic-rich black shale deposition. The enhanced burial of organic carbon during these so-called Oceanic Anoxic Events (OAEs; Schlanger and Jenkyns, 1976) is thought to arise from enhanced bio-productivity, enhanced preservation of organic matter during anoxic conditions, or a combination of both (e.g., Arthur et al., 1987, 1988; Schlanger et al., 1987). The Cenomanian-Turonian Boundary Event (CTBE = OAE 2; ca. 93.5 Ma) is one of the best-studied global OAEs. It is characterized by a global organic carbon burial episode and a positive shift in $\delta^{13}\text{C}$ values of organic carbon and carbonate (e.g., Schlanger et al., 1987; Arthur et al., 1988; Gale et al., 1993; Erbacher et al., 2005). At Wunstorf (northern Germany), a continuous core was drilled in 2006 which recovered 76 m of middle Cenomanian to middle Turonian sediments. The CTBE is represented by a 26.5 m thick sedimentary succession consisting of rhythmically bedded laminated black shales, dark organic-rich marls and marly limestones (Erbacher et al., 2007). A high-resolution carbonate $\delta^{13}\text{C}$ curve resolves all known features of the positive $\delta^{13}\text{C}$ anomaly related to OAE 2 with high accuracy (Voigt et al., 2008).

Strong enrichments of redox-sensitive elements in organic carbon-rich sediments are usually related to anoxic bottom waters. Under reducing conditions, these elements may either be precipitated as sulphides, co-precipitated with iron sulphides, or bound to organic matter (Brumsack, 1980, 1989; Jacobs et al., 1985, 1987; Breit and Wanty, 1991; Hatch and Leventhal, 1992; Calvert and Pedersen, 1993; Piper 1994; Nijenhuis et al., 1998). Recent reviews by Brumsack (2006) and Tribovillard et al. (2006) examined environmental parameters controlling trace element enrichment in comparable modern settings (e.g. semi-restricted basins, upwelling regions). Enrichment/depletion patterns of selected trace elements are emphasized for reconstructing palaeodepositional conditions, most notably palaeoproductivity and palaeoredox. Brumsack (2006) discussed the enrichment of trace metals in Cretaceous black shales and attempted to evaluate whether enhanced bio-productivity or widespread water column stagnation triggered black shale formation.

Here we present an inorganic geochemical study from a Cretaceous black shale succession drilled at Wunstorf. Major and minor element composition provides insight into the relative proportions of major components in marine sediments: terrigenous detritus, biogenous material, and diagenetic products. Elements and element ratios related to terrigenous material may further help to identify provenance characteristics and related

changes in climate and/or sediment supply. Changes in palaeoproductivity are mirrored by elements related to biogenous processes, and the oxygenation state of the water column may be deduced from the abundance of redox-sensitive elements.

Material and Methods

Site description

The Wunstorf core was drilled in 2006 close to the city of Hannover, Germany, next to the Wunstorf quarry (TK 25 Wunstorf, no. 3522, R: 3,532,774, H: 5,807,412). The Hannover area encompasses the basinal section of an intra-shelf basin (with water depths in the order of 100-150 m; Wilmsen, 2003) that was formed during the Cenomanian transgression as part of the extended epicontinental shelf sea (Fig. 7.1). During the CTBE, the basin was subjected to episodically occurring dysoxic and anoxic conditions at the sea floor.

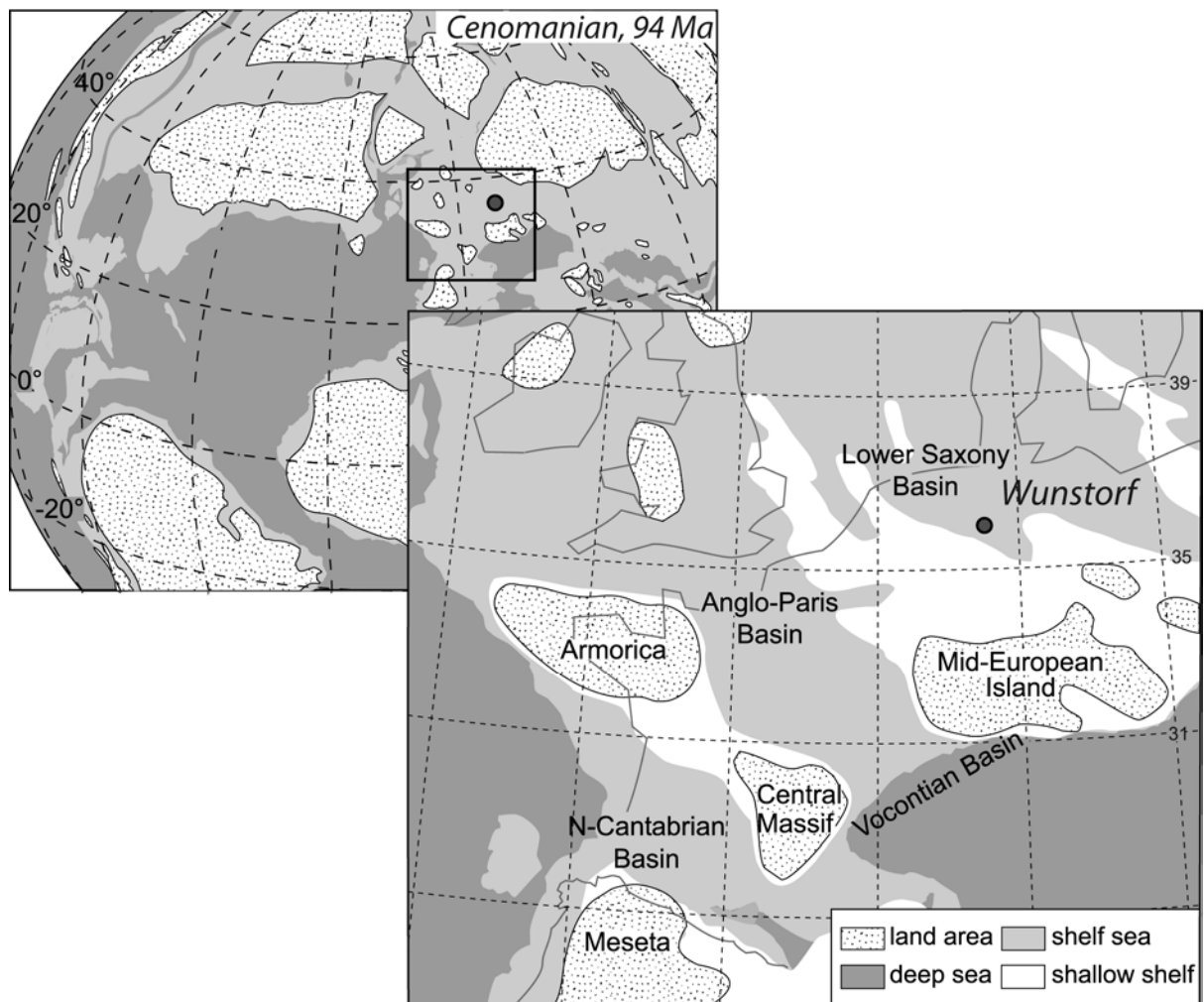


Figure 7.1 Late Cenomanian palaeogeography of the Central European shelf sea, showing the location of the Wunstorf core. Map modified after Voigt et al. (2004).

The Wunstorf core section consists of four lithostratigraphic units which represent - from base to top - parts of the Baddeckenstedt Formation, the Brochterbeck Formation, the Hesseltal Formation and parts of the Söhlde Formation (Voigt et al., 2008). This study focuses on sediments of the Hesseltal Formation (49.6-23.1 m), comprising a 26.5 m thick succession of alternating black shales, grey to green marls, marly limestones, and light-grey limestones (Fig. 7.2). The underlying Brochterbeck Formation consists of white and light-grey marly limestones. The stratigraphic boundary between both formations is marked by the Facies Change ("Fazieswechsel") as described by Ernst et al. (1983). The black shale beds of the Hesseltal Formation occur in packages of up to several meters thickness. Voigt et al. (2008) describe three major units: The lower black shale horizon (48.7-47.4 m) comprises an alternation of four black shale beds with intercalated light marly limestones and contains the basin-wide occurring *Chondrites* Event (47.55-47.35 m). A further marker bed is the *Plenus* Bed (47.30-46.85 m), a basin-wide occurring limestone layer in the lower part of the Hesseltal Formation (Ernst et al. 1983). The middle black shale package (44.1-41.6 m) often yields fish remains and is traditionally called Fish Shale ("Fischschiefer"). Thin-shelled inoceramids occur in the upper prominent black shale succession (37.3-35.0 m) which is termed the *Watinoceras* Bed because of ammonite occurrences in coeval outcrops.

Each aggregation of black shale beds of the Hesseltal Formation comprises a bundle of several (four to five, Voigt et al., 2008) black shale couplets, with cyclic patterns for each decimeter-thick single couplet: Starting with laminated black shale, the degree of bioturbation increases up-section, and the couplet grades into greenish to grey marl, grey marly limestone and finally into a light-grey limestone. In those black shale bundles, the basal couplets are characterized by thick and predominantly laminated black shales, whereas the upper couplets are thinner and carbonate-dominated. Usually the bundles are terminated by prominent limestone layers. The overlying Söhlde Formation consists of grey-greenish, bioturbated, marly limestones with scattered inoceramid debris and occasional inoceramid shell layers.

Stable isotope stratigraphy (Voigt et al., 2008) shows the prominent positive carbon isotope excursion of OAE 2 at 49.6-36.0 m (Fig. 7.2). The high-resolution carbonate $\delta^{13}\text{C}$ curve reflects all known detailed features of OAE 2 in Europe (Jarvis et al., 2006; Voigt et al., 2007), including 1) an initial small rise in $\delta^{13}\text{C}$ above the Facies Change terminated by a small negative inflection; 2) a major rise towards the first maximum (A); 3) a trough interval followed by a rise towards a second maximum (B); 4) a 'plateau' phase containing an

intermittent positive inflection (C); and 5) a final fourth maximum (D) (Fig. 7.2). This precise chemostratigraphic correlation provides an excellent age model and thus allows embedding the studied OAE 2 black shales into a global context.

Analytical methods

Focusing on the black shale-bearing Hesseltal Formation (49.6-23.1 m), sediment splits were taken every ~50 cm between 52.5 and 49.7 m and every ~10 cm between 49.7 and 19.7 m. All 319 samples were freeze-dried, ground and homogenized in an agate ball mill. Element concentrations were determined by X-ray fluorescence (XRF) analysis. 600 mg sample powder was mixed with 3,600 mg dilithiumtetraborate ($\text{Li}_2\text{B}_2\text{O}_7$), pre-oxidized at 500°C with ammonium nitrate (NH_4NO_3 , p.a.) and fused into glass beads in platinum crucibles. The glass beads were analyzed by XRF (Philips® PW 2400 X-ray spectrometer) calibrated with 29 carefully selected geostandards. Total sulphur (S) and total carbon (TC) were analyzed using an ELTRA® CS-500 IR-analyzer. Total inorganic carbon (TIC) was determined coulometrically by a UIC® CM 5012 CO_2 coulometer coupled to a CM 5130 acidification module. Total organic carbon (TOC) was calculated as the difference between TC and TIC. Procedures and accuracy of the methods were checked with in-house reference materials (see Appendix) and are comparable to those obtained by Prakash Babu et al. (1999).

Results and Discussion

The results from geochemical analysis are summarized in Table 7.1. The limestones of the Brochterbeck Formation, the Söhlde formation as well as the limestones of the Hesseltal formation are characterized by high carbonate contents and very low contents of terrigenous-detrital material. Thus, some elements are only present in trace quantities close to the XRF detection limit owing to carbonate dilution.

Table 7.1 Comparison of average element contents and element/Al ratios with standard deviation (1 σ) for Wunstorf and 'average shale'. To be continued.

		Average Shale	Brochterbeck Fm (n=10)	Söhlde Fm (n=34)	Hesseltal Fm	
					limestones (n=175)	Plenus Bed (n=2)
S	%	0.24	<0.1	<0.1	<0.1	<0.1
TIC	%	0.35	10.34 ± 0.47	9.56 ± 0.49	8.42 ± 1.34	10.96 ± 0.01
TOC	%		<0.1	<0.1	<0.1	<0.1
Si	%	27.53	3.81 ± 1.22	5.58 ± 1.08	8.84 ± 3.45	2.28 ± 0.16
Ti	%	0.46	0.07 ± 0.02	0.10 ± 0.02	0.13 ± 0.05	0.03 ± 0.00
Al	%	8.84	1.22 ± 0.35	1.84 ± 0.33	2.29 ± 0.82	0.60 ± 0.04
Fe	%	4.80	0.57 ± 0.14	0.94 ± 0.16	1.23 ± 0.48	0.45 ± 0.02
Mg	%	1.60	0.39 ± 0.05	0.53 ± 0.04	0.63 ± 0.15	0.40 ± 0.01
Ca	%	1.57	34.76 ± 1.73	31.80 ± 1.66	27.91 ± 4.38	36.45 ± 0.61
Na	%	1.19	<0.11	<0.11	<0.11	0.19 ± 0.27
K	%	2.99	0.35 ± 0.11	0.51 ± 0.09	0.67 ± 0.26	0.18 ± 0.02
P	%	0.07	0.03 ± 0.01	0.02 ± 0.00	0.05 ± 0.03	0.02 ± 0.00
As	ppm	10	1 ± 1	1 ± 1	2 ± 3	2 ± 1
Ba	ppm	580	60 ± 16	99 ± 59	106 ± 44	42 ± 7
Co	ppm	19	<5	<5	12 ± 23	6 ± 2
Cr	ppm	90	<15	<15	<15	<15
Cu	ppm	45	<5	<5	14 ± 14	<5
Mn	ppm	850	1728 ± 270	801 ± 86	3102 ± 1448	3416 ± 22
Mo	ppm	1	<5	<5	<5	<5
Ni	ppm	68	<10	<10	13 ± 34	<10
Pb	ppm	22	4 ± 1	6 ± 5	10 ± 11	3 ± 2
Rb	ppm	140	18 ± 6	29 ± 5	36 ± 13	9 ± 1
Sr	ppm	300	956 ± 31	715 ± 45	858 ± 103	897 ± 7
U	ppm	4	2 ± 1	<2	2 ± 1	2 ± 0
V	ppm	130	23 ± 6	35 ± 7	43 ± 16	14 ± 1
Y	ppm	41	13 ± 2	11 ± 2	17 ± 5	12 ± 0
Zn	ppm	95	18 ± 7	21 ± 4	32 ± 53	<10
Zr	ppm	160	33 ± 10	41 ± 7	53 ± 24	22 ± 2
Si/Al		3.11	3.09 ± 0.17	3.03 ± 0.06	3.85 ± 0.52	3.79 ± 0.00
Ti/Al		0.05	0.05 ± 0.00	0.05 ± 0.00	0.05 ± 0.00	0.05 ± 0.00
Fe/Al		0.55	0.48 ± 0.05	0.51 ± 0.02	0.54 ± 0.09	0.76 ± 0.02
Mg/Al		0.18	0.33 ± 0.06	0.29 ± 0.03	0.29 ± 0.04	0.66 ± 0.06
Ca/Al		0.18	31.17 ± 10.70	18.01 ± 4.22	14.09 ± 6.23	60.86 ± 5.19
Na/Al		0.13				0.30 ± 0.42
K/Al		0.34	0.28 ± 0.01	0.28 ± 0.01	0.29 ± 0.03	0.30 ± 0.02
P/Al		0.01	0.03 ± 0.00	0.01 ± 0.00	0.02 ± 0.01	0.04 ± 0.00
As/Al	× 10 ⁻⁴	1.1	0.6 ± 0.7	0.5 ± 0.4	1.0 ± 1.6	2.5 ± 1.0
Ba/Al	× 10 ⁻⁴	65.6	49.8 ± 9.1	56.0 ± 46.2	48.2 ± 16.5	69.7 ± 7.0
Co/Al	× 10 ⁻⁴	2.1			5.6 ± 13.1	9.1 ± 2.9
Cr/Al	× 10 ⁻⁴	10.2				
Cu/Al	× 10 ⁻⁴	5.1			5.9 ± 5.9	
Mn/Al	× 10 ⁻⁴	96	1543 ± 518	454 ± 118	1569 ± 989	5698 ± 354
Mo/Al	× 10 ⁻⁴	0.1				
Ni/Al	× 10 ⁻⁴	7.7			5.9 ± 17.3	
Pb/Al	× 10 ⁻⁴	2.5	3.8 ± 1.7	3.6 ± 3.1	4.5 ± 4.5	4.3 ± 3.8
Rb/Al	× 10 ⁻⁴	15.8	14.7 ± 0.6	16.0 ± 0.8	16.0 ± 2.0	14.1 ± 0.2
Sr/Al	× 10 ⁻⁴	34	849 ± 262	403 ± 88	425 ± 172	1497 ± 114
U/Al	× 10 ⁻⁴	0.4	1.4 ± 0.7		0.9 ± 0.5	3.3 ± 0.2
V/Al	× 10 ⁻⁴	14.7	19.3 ± 2.9	19.1 ± 1.4	18.7 ± 3.2	23.4 ± 4.0
Y/Al	× 10 ⁻⁴	4.6	11.0 ± 2.0	6.2 ± 1.0	7.7 ± 2.0	19.4 ± 1.3
Zn/Al	× 10 ⁻⁴	10.7	16.1 ± 9.9	11.7 ± 2.1	15.1 ± 28.8	
Zr/Al	× 10 ⁻⁴	18.1	27.3 ± 2.8	22.6 ± 1.9	23.0 ± 3.6	32.7 ± 6.6

Quotation "<X": average values below detection limit X (defined as half the quantification limit).
 El/Al ratio not determined. Quotation in italics: average values below quantification limit (see
 Appendix 7.1). El/Al ratio grey.

Continuation of Table 7.1 Comparison of average element contents and element/Al ratios with standard deviation (1σ) for Wunstorf and 'average shale'. To be continued.

		Hesseltal Fm – black shale packages			
		0.25≤TOC≤0.5 (n=31)	bs 1-x (n=6)	bs 2-x (n=19)	bs 3-x (n=10)
S	%	0.16 ± 0.27	0.37 ± 0.56	0.89 ± 0.80	0.58 ± 0.53
TIC	%	7.24 ± 2.190	5.14 ± 2.25	6.02 ± 1.28	5.81 ± 1.42
TOC	%	0.34 ± 0.07	0.95 ± 0.62	1.13 ± 0.49	1.38 ± 0.88
Si	%	11.66 ± 5.62	16.52 ± 6.29	14.09 ± 3.97	14.48 ± 4.23
Ti	%	0.16 ± 0.09	0.25 ± 0.10	0.20 ± 0.06	0.20 ± 0.06
Al	%	2.87 ± 1.39	4.55 ± 1.61	3.51 ± 0.92	3.57 ± 1.02
Fe	%	1.64 ± 0.79	2.27 ± 0.49	2.35 ± 0.57	2.14 ± 0.47
Mg	%	0.71 ± 0.24	0.97 ± 0.25	0.84 ± 0.20	0.86 ± 0.20
Ca	%	24.17 ± 7.11	17.50 ± 7.17	20.42 ± 4.09	19.99 ± 5.04
Na	%	<0.11	<0.11	<0.11	<0.11
K	%	0.89 ± 0.45	1.40 ± 0.50	1.12 ± 0.27	1.12 ± 0.31
P	%	0.07 ± 0.05	0.13 ± 0.05	0.10 ± 0.04	0.08 ± 0.02
As	ppm	5 ± 6	37 ± 42	13 ± 12	8 ± 6
Ba	ppm	125 ± 43	171 ± 51	150 ± 22	153 ± 34
Co	ppm	26 ± 26	131 ± 223	32 ± 21	31 ± 21
Cr	ppm	16 ± 14	37 ± 16	32 ± 10	30 ± 10
Cu	ppm	19 ± 13	35 ± 3	28 ± 6	25 ± 9
Mn	ppm	2918 ± 1434	701 ± 402	1725 ± 657	1825 ± 1430
Mo	ppm	<5	<5	<5	<5
Ni	ppm	37 ± 46	181 ± 253	35 ± 21	32 ± 17
Pb	ppm	12 ± 9	25 ± 10	17 ± 4	16 ± 5
Rb	ppm	48 ± 22	72 ± 23	58 ± 15	60 ± 17
Sr	ppm	820 ± 122	698 ± 104	798 ± 128	754 ± 93
U	ppm	2 ± 1	3 ± 1	3 ± 1	3 ± 1
V	ppm	54 ± 23	97 ± 22	90 ± 27	73 ± 17
Y	ppm	19 ± 6	26 ± 8	23 ± 5	19 ± 2
Zn	ppm	48 ± 40	60 ± 26	59 ± 24	48 ± 19
Zr	ppm	71 ± 43	118 ± 46	86 ± 30	86 ± 28
Si/Al		4.07 ± 0.44	3.60 ± 0.15	4.00 ± 0.16	4.06 ± 0.26
Ti/Al		0.06 ± 0.00	0.05 ± 0.00	0.06 ± 0.00	0.06 ± 0.00
Fe/Al		0.59 ± 0.13	0.54 ± 0.19	0.71 ± 0.27	0.62 ± 0.13
Mg/Al		0.26 ± 0.03	0.22 ± 0.03	0.24 ± 0.01	0.24 ± 0.02
Ca/Al		10.96 ± 5.90	5.01 ± 4.01	6.61 ± 3.25	6.46 ± 3.51
Na/Al			0.01 ± 0.01	0.02 ± 0.05	0.01 ± 0.00
K/Al		0.31 ± 0.02	0.31 ± 0.02	0.32 ± 0.01	0.31 ± 0.01
P/Al		0.02 ± 0.00	0.03 ± 0.00	0.03 ± 0.01	0.02 ± 0.01
As/Al	× 10 ⁻⁴	2.3 ± 3.1	8.7 ± 8.9	4.6 ± 5.1	2.6 ± 2.3
Ba/Al	× 10 ⁻⁴	46.0 ± 6.8	38.6 ± 4.3	44.8 ± 9.2	44.3 ± 9.9
Co/Al	× 10 ⁻⁴	11.4 ± 15.1	27.7 ± 42.5	10.7 ± 10.1	9.3 ± 8.0
Cr/Al	× 10 ⁻⁴	5.0 ± 2.2	8.0 ± 1.7	9.3 ± 3.0	8.4 ± 2.4
Cu/Al	× 10 ⁻⁴	7.1 ± 4.9	8.7 ± 3.7	8.4 ± 2.1	7.1 ± 2.8
Mn/Al	× 10 ⁻⁴	1328 ± 811	213 ± 210	575 ± 352	659 ± 702
Mo/Al	× 10 ⁻⁴				
Ni/Al	× 10 ⁻⁴	15.2 ± 22.6	36.9 ± 48.2	11.7 ± 10.1	9.4 ± 5.7
Pb/Al	× 10 ⁻⁴	4.3 ± 1.8	5.4 ± 1.0	4.9 ± 0.8	4.3 ± 0.8
Rb/Al	× 10 ⁻⁴	16.8 ± 1.5	16.2 ± 1.6	16.4 ± 0.6	16.9 ± 1.1
Sr/Al	× 10 ⁻⁴	355 ± 170	185 ± 112	254 ± 114	235 ± 98
U/Al	× 10 ⁻⁴	0.9 ± 0.6	0.7 ± 0.4	0.7 ± 0.3	0.8 ± 0.4
V/Al	× 10 ⁻⁴	19.8 ± 5.6	22.3 ± 3.6	26.9 ± 10.3	21.0 ± 4.3
Y/Al	× 10 ⁻⁴	7.2 ± 1.3	6.0 ± 0.7	6.8 ± 1.3	5.8 ± 1.6
Zn/Al	× 10 ⁻⁴	19.1 ± 16.4	14.2 ± 5.6	17.0 ± 5.8	13.5 ± 5.0
Zr/Al	× 10 ⁻⁴	23.8 ± 3.1	25.5 ± 1.8	23.8 ± 2.8	24.0 ± 2.3

Quotation "<X": average values below detection limit X (defined as half the quantification limit).
 El/Al ratio not determined. Quotation in italics: average values below quantification limit (see
 Appendix 1). El/Al ratio grey.

Continuation of Table 7.1 Comparison of average element contents and element/Al ratios with standard deviation (1 σ) for Wunstorf and 'average shale'.

		Hesseltal Fm – black shale packages			
		bs 4-x (n=21)	bs 5-x (n=4)	bs 6 (n=2)	bs 7-x (n=5)
S	%	0.86 ± 0.82	0.93 ± 1.01	0.51 ± 0.53	1.16 ± 1.05
TIC	%	7.58 ± 0.82	8.36 ± 1.16	8.80 ± 0.11	9.03 ± 0.32
TOC	%	1.07 ± 0.45	1.20 ± 0.72	0.89 ± 0.08	1.50 ± 0.52
Si	%	9.81 ± 2.72	7.54 ± 2.48	6.70 ± 0.56	4.77 ± 0.79
Ti	%	0.13 ± 0.04	0.10 ± 0.03	0.09 ± 0.01	0.07 ± 0.01
Al	%	2.43 ± 0.59	2.01 ± 0.69	1.89 ± 0.12	1.62 ± 0.30
Fe	%	2.24 ± 0.56	1.93 ± 0.75	1.46 ± 0.45	1.77 ± 0.88
Mg	%	0.67 ± 0.14	0.66 ± 0.06	0.55 ± 0.01	0.48 ± 0.03
Ca	%	25.16 ± 2.71	27.92 ± 2.99	29.19 ± 0.90	31.05 ± 2.34
Na	%	<0.11	<0.11	<0.11	<0.11
K	%	0.80 ± 0.21	0.65 ± 0.24	0.64 ± 0.02	0.48 ± 0.08
P	%	0.08 ± 0.04	0.06 ± 0.05	0.09 ± 0.08	0.03 ± 0.02
As	ppm	23 ± 24	14 ± 12	19 ± 19	20 ± 16
Ba	ppm	113 ± 17	101 ± 23	100 ± 2	85 ± 15
Co	ppm	30 ± 16	18 ± 9	24 ± 15	33 ± 19
Cr	ppm	29 ± 15	25 ± 21	<15	25 ± 15
Cu	ppm	25 ± 6	19 ± 11	22 ± 2	20 ± 5
Mn	ppm	3220 ± 938	2906 ± 1376	2060 ± 99	1544 ± 836
Mo	ppm	<5	<5	<5	<5
Ni	ppm	41 ± 21	33 ± 34	22 ± 20	34 ± 28
Pb	ppm	13 ± 4	11 ± 5	12 ± 1	9 ± 4
Rb	ppm	44 ± 12	36 ± 13	36 ± 3	27 ± 5
Sr	ppm	816 ± 78	837 ± 130	994 ± 64	1055 ± 68
U	ppm	3 ± 1	3 ± 1	2 ± 1	2 ± 1
V	ppm	116 ± 66	140 ± 108	67 ± 24	100 ± 52
Y	ppm	19 ± 3	13 ± 3	19 ± 6	13 ± 2
Zn	ppm	77 ± 40	62 ± 38	60 ± 16	47 ± 9
Zr	ppm	57 ± 16	42 ± 13	39 ± 2	32 ± 3
Si/Al		4.00 ± 0.22	3.77 ± 0.38	3.55 ± 0.06	2.95 ± 0.10
Ti/Al		0.05 ± 0.00	0.05 ± 0.00	0.05 ± 0.00	0.04 ± 0.00
Fe/Al		0.97 ± 0.33	1.01 ± 0.34	0.78 ± 0.29	1.08 ± 0.49
Mg/Al		0.28 ± 0.02	0.37 ± 0.15	0.29 ± 0.01	0.30 ± 0.05
Ca/Al		11.13 ± 3.54	16.33 ± 9.83	15.52 ± 1.49	20.00 ± 6.17
Na/Al					
K/Al		0.33 ± 0.02	0.32 ± 0.03	0.34 ± 0.01	0.30 ± 0.01
P/Al		0.03 ± 0.02	0.03 ± 0.02	0.05 ± 0.04	0.02 ± 0.01
As/Al	× 10 ⁻⁴	11.3 ± 13.2	7.5 ± 5.7	10.2 ± 10.8	11.7 ± 9.9
Ba/Al	× 10 ⁻⁴	47.7 ± 7.5	52.3 ± 9.4	52.8 ± 2.3	52.7 ± 2.7
Co/Al	× 10 ⁻⁴	13.0 ± 7.7	10.1 ± 6.1	12.7 ± 8.7	19.1 ± 11.0
Cr/Al	× 10 ⁻⁴	12.7 ± 7.6	11.3 ± 7.8		14.4 ± 9.0
Cu/Al	× 10 ⁻⁴	10.5 ± 3.2	9.6 ± 3.7	11.5 ± 1.9	12.8 ± 2.9
Mn/Al	× 10 ⁻⁴	1438 ± 644	1616 ± 880	1096 ± 124	1072 ± 896
Mo/Al	× 10 ⁻⁴				
Ni/Al	× 10 ⁻⁴	17.2 ± 9.7	16.8 ± 14.3	12.0 ± 11.3	19.9 ± 17.0
Pb/Al	× 10 ⁻⁴	5.3 ± 1.2	5.8 ± 2.7	6.1 ± 0.8	5.8 ± 2.8
Rb/Al	× 10 ⁻⁴	18.2 ± 1.3	17.7 ± 2.7	19.1 ± 0.3	16.9 ± 0.6
Sr/Al	× 10 ⁻⁴	360 ± 111	497 ± 325	529 ± 69	665 ± 111
U/Al	× 10 ⁻⁴	1.1 ± 0.6	1.3 ± 0.5	1.1 ± 0.8	1.3 ± 0.4
V/Al	× 10 ⁻⁴	52.0 ± 38.5	70.1 ± 42.8	36.0 ± 15.1	59.4 ± 30.0
Y/Al	× 10 ⁻⁴	8.0 ± 1.7	7.1 ± 2.1	10.1 ± 4.1	8.4 ± 1.0
Zn/Al	× 10 ⁻⁴	33.1 ± 19.0	33.1 ± 19.4	31.6 ± 6.2	30.3 ± 9.1
Zr/Al	× 10 ⁻⁴	23.3 ± 1.4	20.9 ± 1.6	20.6 ± 0.5	20.2 ± 2.9

Quotation "<X": average values below detection limit X (defined as half the quantification limit).
 El/Al ratio not determined. Quotation in italics: average values below quantification limit (see Appendix 1). El/Al ratio grey.

Bulk parameters and major components

Figure 7.2 shows the TOC depth profiles for the upper Cenomanian to lower Turonian black shale of the Wunstorf core. The analyzed limestones of the Brochterbeck Formation are basically free of organic carbon (TOC <0.1 %). The described pattern of black shale packages with alternating black shales, marls and limestones of the Hesseltal Formation can be identified in the TOC profile: Highest TOC values (up to 2.8 %) are found in the black shale beds, whereas the marls are characterized by moderate to low TOC contents (~0.5 %) and the limestones are essentially free of TOC. The same is true for the limestones of the overlying Söhlde Formation.

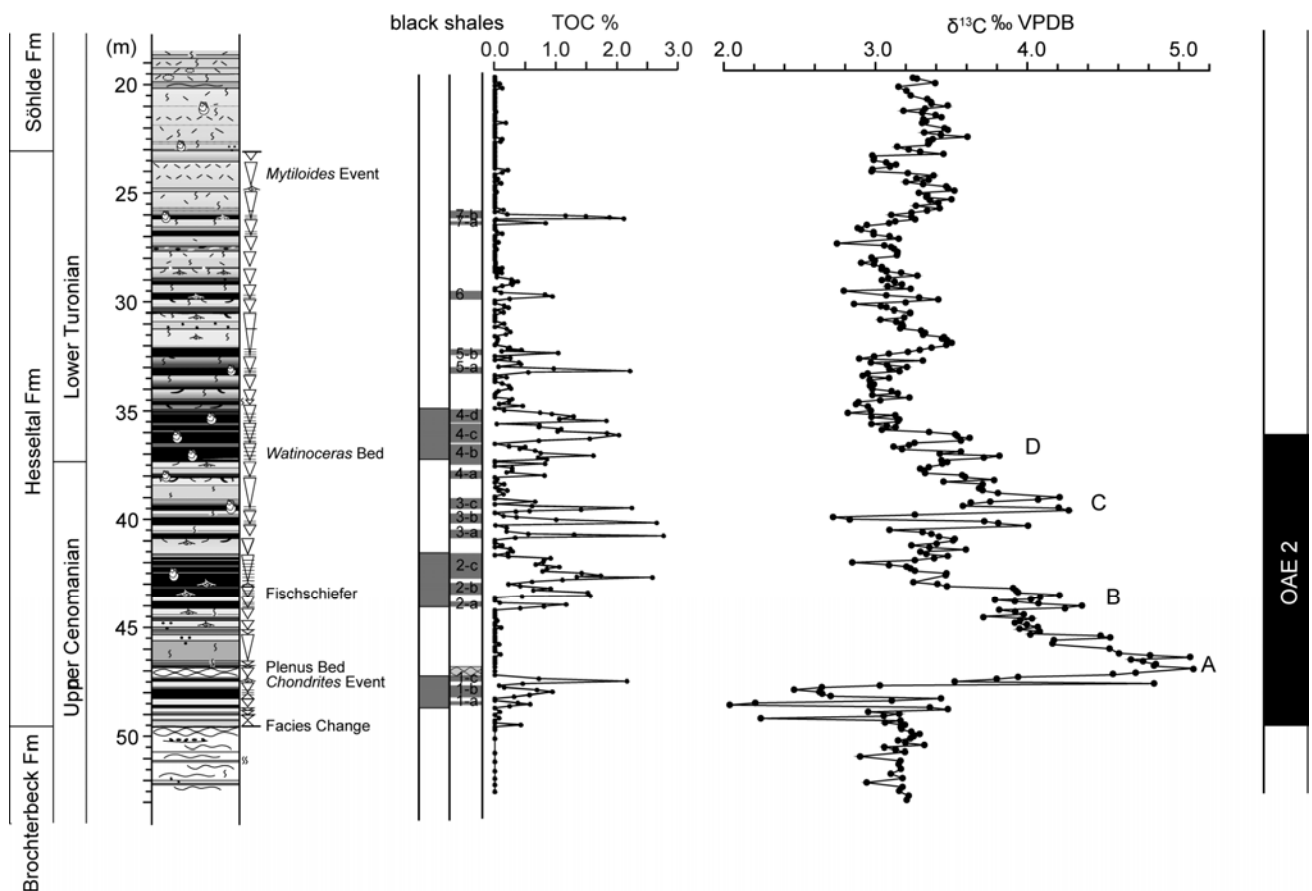


Figure 7.2 Carbon isotope stratigraphy of the studied Wunstorf core section (Voigt et al., 2008). Three major black shale packages as suggested by these authors, numbering deduced from Total Organic Carbon contents (this study).

While Voigt et al. (2008) describe three major black shale packages, we identified seven black shale packages (1 - 7, Fig. 7.2) with TOC >0.5 % with several couplets (one to four, labeled X-a, X-b, etc.). Black shale package 1 (48.6-47.4 m) consists of three black shale bundles, with 1-c corresponding to the *Chondrites* Event described by Voigt et al. (2008).

Adopting the definition of OAE 2 from carbon isotope stratigraphy (49.6-36.0 m), black shale layer 1-a is the first within OAE 2. The following black shale package 2 (44.1-41.6 m) matches the “Fischschiefer”. Below the *Watinoceras* Bed we identified a black shale package 3 (40.8-39.1 m) with three bundles. Based on TOC distribution, we expand package 4 (*Watinoceras* Bed, 37.3-35.0 m; Voigt et al., 2008) to 38.0-35.0 m. Thus, black shale layer 4-c is the last black shale layer within OAE 2. Above the *Watinoceras* Bed, we identified three more black shale packages (33.3-32.3 m, 29.8-29.7 m and 26.4-26.0 m), with packages 5 and 7 containing two black shale layers each, and package 6 containing one single layer.

Figure 7.3A shows the depth profiles of the bulk parameters TOC, S and CaCO_3 , assuming all TIC is present as pure CaCO_3 . Within the limestone sequences, S contents are <0.1 %. Within the black shale packages, S values mostly vary between 0.3 and 1.0 %. Distinct peaks with S contents reaching 2.9 % appear in black shale layers.

In a very simplistic way, marine sediments consist of variable mixtures of terrigenous detritus (represented by Al_2O_3 and SiO_2) and biogenous material (represented by CaCO_3 and SiO_2). As expected, the limestones of the Brochterbeck and the Söhlde Formations are characterized by high carbonate contents ($\text{CaCO}_3 > 70\%$). Within the Hesseltal Formation, carbonate contents vary between 15.1 and 91.3 %. Abrupt changes from lower to higher values are detected in black shale packages with alternating marls and limestones. The inverse distribution patterns for CaCO_3 and Al_2O_3 (Fig. 7.3A), the latter representing the terrigenous detritus, show the dilution effect of biogenous carbonate. The SiO_2 profile seems to match the one of Al_2O_3 .

To compare the major components contributing to sediment composition, the relative proportions of CaO (mostly carbonate), SiO_2 (quartz/opal and aluminosilicates), and Al_2O_3 (aluminosilicates) are plotted in a triangle diagram (Fig. 7.4; Brumsack, 1989). For comparison, average shale (AS, Wedepohl, 1971), K-feldspar, and kaolinite are also plotted. Sediments plot slightly below the mixing line between carbonate and AS documenting the dominance of these two components. However, samples appear to either contain a clay component lower in Al than AS or are reflecting small quantities of additional SiO_2 , possibly biogenous opal. As no shift towards Al-rich components is detectable (as would be expected from a higher kaolinite proportion), intense weathering did not play a major role in the depositional history at Wunstorf.

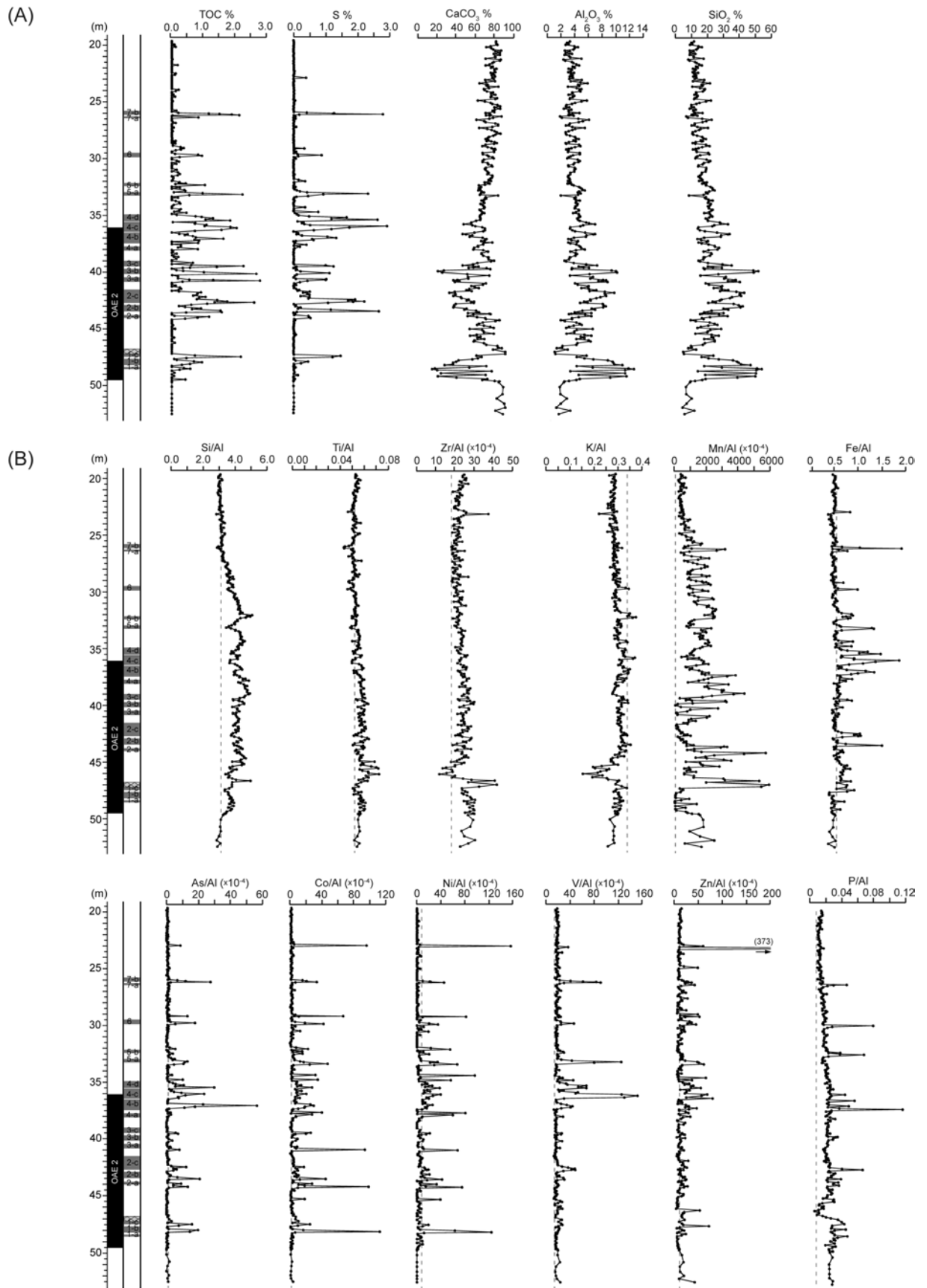


Figure 7.3 (A) Depth profiles for bulk parameters and major components. (B) Depth-profiles for selected element/Al ratios. Dashed line: Element/Al ratio of average shale (AS) (Wedepohl, 1971, 1991).

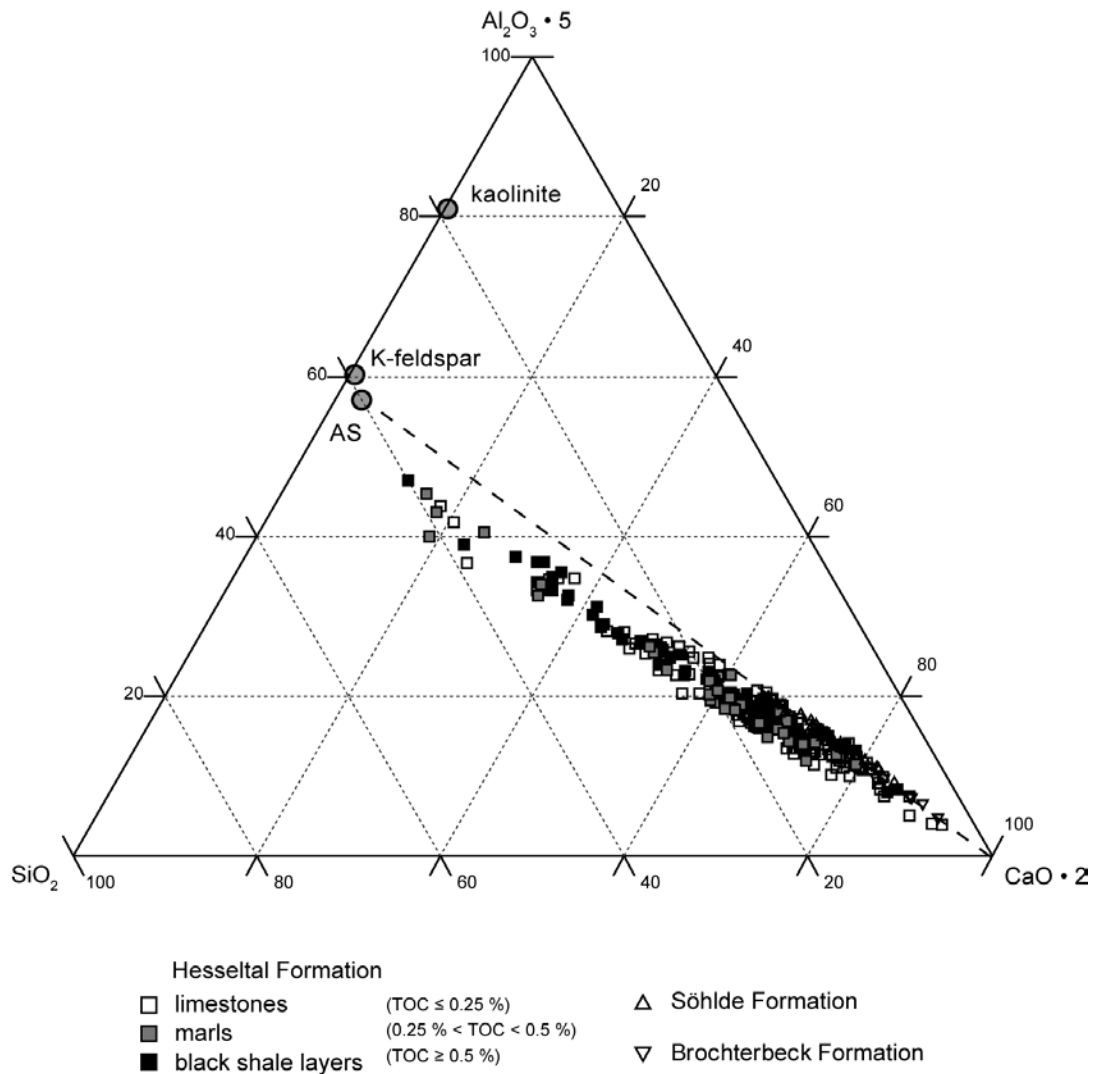


Figure 7.4 Ternary Plot: Major geochemical components of the Wunstorf core in the system $\text{Al}_2\text{O}_3 \cdot 5$ - SiO_2 - $\text{CaO} \cdot 2$ (relative weight ratios). Data points for average shale (AS; Wedepohl, 1971) and K-feldspar are shown for comparison.

Terrigenous material and cyclostratigraphy

Some elements, like Al, Ti, K and Zr, are only present in the detrital component and are not influenced by biogenic or diagenetic processes. This is especially true for proximal and shallow epicontinental seas such as the Cretaceous Wunstorf Basin. To account for dilution effects by varying input of carbonate or organic matter, element contents are normalized to Al (El/Al ratio). Significant variations in Al ratios of detrital elements therefore reveal changes in provenance and/or specific depositional processes (e.g. turbidites, winnowing bottom currents). Figure 7.3B shows the profiles of Si/Al, Ti/Al, and Zr/Al. The Si/Al ratio of sediments from the basal Brochterbeck Formation is similar to AS (3.11). With the onset of the Hesseltal Formation, Si/Al ratios slightly increase upcore, reaching a maximum value of 5.06, and decrease again to the AS level in the upper part of the Hesseltal Formation.

There are different possibilities for explaining increased Si/Al ratios. Either, there might be changes in the aluminosilicate composition (lower Al and higher Si content) owing to, e.g., changes in weathering conditions. Alternatively, the Si excess might be due to input of quartz and/or biogenic opal. As quartz and heavy minerals are closely associated in the coarser grain size fraction and are thus indicators of high-energy environments (e.g., Dellwig et al., 2000), elevated Ti/Al and Zr/Al ratios in correlation with elevated Si/Al would hint to the presence of quartz. However, the values of Ti/Al and Zr/Al (Fig. 7.3B) are similar to AS (0.05 and 18.1×10^{-4} , respectively) and show only little variation within the sequence studied, despite some interruptions between black shale package 1 and 2 (46.9–44.1 m) containing the Plenus bed, marls and limestones. Therefore, it may be assumed that the SiO_2 excess is related to enhanced input/preservation of biogenic opal. This assumption is confirmed by two observations. First, if the clay mineral fraction, represented by the Al_2O_3 content (Fig. 7.3A), is calculated on a carbonate-free basis to remove variable dilution by biogenic carbonate, it exhibits a pattern that mirrors Si/Al. Thus, there seems to be another component that dilutes the detrital input, possibly biogenic opal. Second, the increase in the Mn/Al ratio across the Hesseltal Formation (Fig. 7.3B) is unexpected as Mn is usually mobilized from sediments deposited under oxygen-depleted conditions (see below). Yet, higher biogenic opal contents in these deposits may offer higher pore space for the early diagenetic formation of authigenic Mn phases (e.g., carbonates) even under anoxic conditions (see Sangiorgi et al., 2008; März et al., in prep.). Thus, we strongly suggest that the formation of CTBE black shales in the Wunstorf Basin was accompanied by enhanced production of opal-shelled organisms, and that this biogenic SiO_2 contributes to the elevated bulk Si/Al ratio.

The K/Al ratio (Fig. 7.3B) shows a slight increase in the upper part of the Brochterbeck formation. Above the Plenus bed lower values indicate changes in the composition of the detrital material (46.65 – 45.00 m). For CTBE black shales from Demerara Rise Hetzel et al. (2009) identified several sediment layers of one centimeter to several decimeters thickness by characteristic element/Al ratios: low K/Al and Si/Al, high Ti/Al ratios. The latter can also be found in the Ti/Al profile of Wunstorf. A decrease in Si/Al ratios might be obscured by other mechanisms controlling Si distribution (see discussion above). From macroscopic observation the authors postulated that these layers at Demerara Rise are most likely diagenetically altered ash beds. At Wunstorf a change in sediment supply is not evident from macroscopic observations.

Comparison with the carbon isotopic curve shows that the decrease in K/Al coincides with the trough between maximum A and B. Lithostratigraphically it appears in the greenish-grey marls at the top of the Plenus Bed comprising a significant sandy component (Prauss, 2006). The interval is part of a Highstand systems tract (HST) following sea level lowstand at the *Chondrites* event (see Fig. 7.2). HST's coarsen slightly upward and show increasing signs of winnowing (Wilmsen, 2003). The Plenus Bed itself describes a cooling episode during OAE 2 that has been widely recognized based on the pulsed occurrence and southward migration of boreal faunal elements in midlatitude shelf seas in NW Europe (Voigt et al. 2004). Voigt et al. (2006) stated that it is likely that cooling reduced the rate of sea level rise or even stopped it entirely. Based on stratigraphic studies, we think that for the Wunstorf succession the decrease in K/Al accompanied by an increase in Ti/Al can be best explained by sediment sorting: During times of reduced sea level rise after sea level lowstand and enhanced circulation the sediment surface might be exposed to wave bases for longer times allowing winnowing of light K-bearing aluminosilicates.

Parallel to the European cooling event (Plenus Bed) a brief period of intensified sea-floor oxygenation and intermittent surface-water cooling is also documented for OAE 2 at Demerara Rise (Friedrich et al. 2006; Forster et al. 2007). Thus, besides the contemporaneous decrease in the temperature record, a change in the detrital composition is noticeable both in the Central European Shelf Sea and the tropical proto-North Atlantic. Assuming a coeval occurrence, we conclude that this is rather a result of increasing palaeocurrents than simultaneous ash ejection. However, as admitted by Hetzel et al. (2009) diagenetic overprinting and limitations of interpretation of bulk element concentrations leave the origin of the “ash layers” at Demerara Rise unexplained.

Above this interval K/Al values are ~ 0.3 and show only little variation until a gradual decrease is visible beginning above black shale package 4. Concluding, despite of slight deviations from the base level, no major changes in the terrigenous sediment supply can be deduced from El/Al ratios above 45 m.

Figure 7.5 provides details of TOC and El/Al ratios of Si, Zr and K for black shale packages 2-4. These are compared to the cyclostratigraphy for this sequence as published by Voigt et al. (2008). On this enlarged scale, changes in El/Al ratios follow the described cyclic pattern of black shale deposition. Both Si/Al and Zr/Al minima are paralleled by TOC maxima, while the cyclic pattern of K/Al is less pronounced.

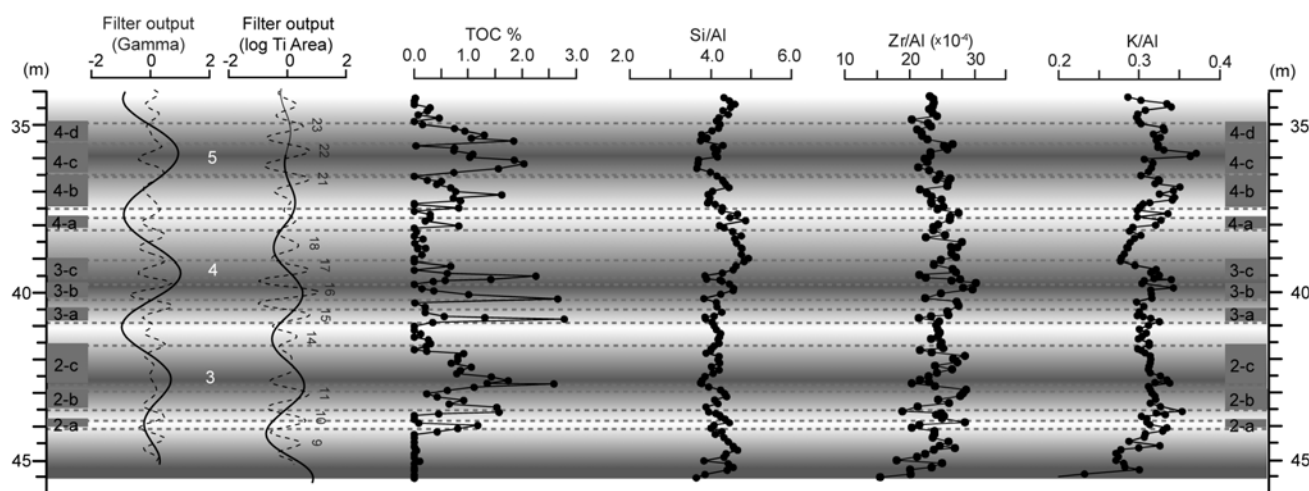


Figure 7.5 Cyclostratigraphy of the Wunstorf core black shale section (Voigt et al., 2008), applying downhole gamma ray data and XRF-scanning Ti counts. Short eccentricity-related cycles (solid line) as well as precession-related cycles (dashed line) were extracted by Gaussian filtering. Comparison with black shale deposition (TOC) and terrigenous detritus (Si/Al, Zr/Al and K/Al) for black shale packages 2, 3 and 4.

From cyclostratigraphic spectral analysis, Voigt et al. (2008) concluded that the black shale-limestone bedding cycles are climatically induced, and forced by short eccentricity-modulated precessional cyclicity. From our data, we postulate that input pathways of the detrital material follow precession cycles as well. Decreased values of Si/Al, Ti/Al and Zr/Al occur during intervals of black shale deposition. Cross-correlation analysis of excess Si with Ti and Zr indicates a co-enrichment in a more energetic environment for intercalated marls and limestones.

Manganese

The profile of the Mn/Al ratio of the Wunstorf core is shown in Figure 7.3B. Mn/Al values are higher than AS (96×10^{-4}) apart from some samples in black shale layer 1-a (minimum 42×10^{-4}). Overall, Mn/Al values show two major maxima. The first one is located above black shale package 1 (comprising the Plenus Bed), the second one forms a broad peak with gradual boundaries above black shale layer 2 (“Fischschiefer”) up to the top of the Hesseltal formation. This broad pattern is affected by local variability, e.g., local Mn/Al minima in black shale layers of black shale package 3 (see TOC profile for comparison), and local maxima following the profile of CaCO_3 (33-26 m).

Mn/Al values above AS values suggest oxic conditions and related deposition of Mn (oxyhydr)oxides. During early diagenetic reduction, these layers may act as a source for dissolved Mn(II). Mn(II)-rich pore waters enable Mn carbonate overgrowths on calcite surfaces or even lead to the precipitation of individual Mn carbonate minerals (like ankerite)

in reducing alkalinity-enriched settings. Thus Mn in anoxic sediments is assumed to be predominantly a carbonate-bound element (Pratt et al., 1991). A loss of Mn before and shortly after sediment deposition may occur under oxygen-deficient conditions at the sediment-seawater interface. Thus, apart from variable dilution by biogenic or detrital material, bottom water redox conditions during deposition, the pore water regime, sedimentary carbonate contents as well as biogenic opal-related porosity may influence Mn distribution.

Within pelagic carbonate sequences, Mn/Al contents are supposed to follow sea level changes. According to Jarvis et al. (2001) lowstand systems tracts are characterized by low Mn contents, whereas transgressive system tracts are characterized by higher Mn contents, with maxima around maximum flooding surfaces. Thus, the Mn maximum at and above the Plenus Bed in the Wunstorf section may be related to the highstand systems tract beginning at the base of the Plenus Bed up to the base of the “Fischschiefer” (Prauss, 2006). The author further concludes a lowstand system tract within the “Fischschiefer” followed by a transgressive system tract. This is in agreement with our findings of a broad Mn peak. In addition, the enhanced input of biogenic opal (see above) most probably induced the increase of the Mn/Al ratios during the black shale period due to diagenesis in porous opal-rich sediments. Thus sea level-related variations likely are obscured.

Productivity proxies

Phosphorus belongs to the essential nutrient elements controlling marine primary productivity (e.g., Broecker and Peng, 1982). High concentrations are found in recent upwelling sediments, pointing towards enhanced nutrient supply and resulting high bioproductivity (e.g., Böning et al., 2004; Schenau et al., 2005). Incorporated into organic material (e.g., in marine phytoplankton; Redfield, 1958), P is deposited in the sediment, where it is preferentially remineralized relative to TOC, liberated to bottom and pore waters, and may in the latter case form authigenic phosphate precipitates (e.g. hydroxyapatite) (Föllmi, 1996; Delaney, 1998).

The P/Al ratios (Fig. 7.3B) of the Brochterbeck Formation (mean value 0.03) are higher than AS values (0.008). Within the Hesseltal Formation, P/Al ratios stay high until a prominent dropdown right above the Plenus Bed, with superimposed local maxima within black shale package 1 between single black shale layers. Above this general broad minimum, P/Al ratios increase again, reaching values >0.02 below black shale package 2. Further upcore, they remain on this “basis level” up to black shale package 4, where P/Al ratios decrease slightly and gradually until values ~ 0.01 are reached above black shale package 7 and

within the Söhlde Formation. Within black shale packages, some isolated local P/Al maxima occur. The fact that these peaks in P/Al ratio are not always coincident with maxima in TOC might be a result of OM degradation and P diagenesis, i.e. precipitation of authigenic apatite layers. Another potential explanation for P-rich layers are fish bones, which may either accumulate in certain layers due to abrupt fish mortality, or serve as sources for dissolved P during their diagenetic dissolution. Overall, the enrichment of P within the black shale packages points towards enhanced nutrient availability and primary productivity during deposition. In addition, the “porosity effect” suggested for the Mn enrichment within the black shale interval might also lead to higher P background values via enhanced precipitation of authigenic apatite.

The non-lithogenic excess Ba has been interpreted as a palaeoproxy for bio-productivity (e.g., Schmitz, 1987; Dymond et al., 1992; Paytan et al., 1996). As biogenic barites (Dehairs et al., 1980; Bishop, 1988; Dehairs et al., 1990; Bertram and Cowen, 1997; Paytan et al., 2002, Bernstein and Byrne, 2004) are supposedly forming in the water column in association with organic particles or certain microorganisms, several authors investigated the relationship between excess Ba and water depth (Dymond et al., 1992, von Breymann et al., 1992, Schenau et al., 2001). Von Breymann et al. (1992) showed a general lack of biogenic Ba enrichments in shallow environments (<1000 m). As we assume a palaeo-water depth between 100 and 150 m for Cenomanian-Turonian sediments at Wunstorf, biogenic barite is not expected to be present in significant amounts. Therefore Ba contents or Ba/Al ratios cannot be used as proxies for palaeoproductivity at this location. The overall low Ba/Al ratios (see Tab. 7.1) support the “water depth – biogenic barite” relationship (von Breymann et al., 1992), but do not necessarily exclude enhanced bioproductivity.

Carbon-Sulphur-Iron systematics and redox-sensitive and sulphide-forming trace metals

The oxydation state of the overlying water column and the redox conditions of the surface sediment form crucial variables for the preservation of organic material and the formation of sedimentary pyrite (FeS₂). Under oxygen deficiency, dissimilatory sulphate reduction leads to the formation of hydrogen sulphide that may further interact with reactive iron to precipitate as pyrite (Berner, 1970, 1984). Therefore, the contents and interrelations of TOC, S and Fe allow to draw conclusions about the palaeoenvironment during deposition of the sediment.

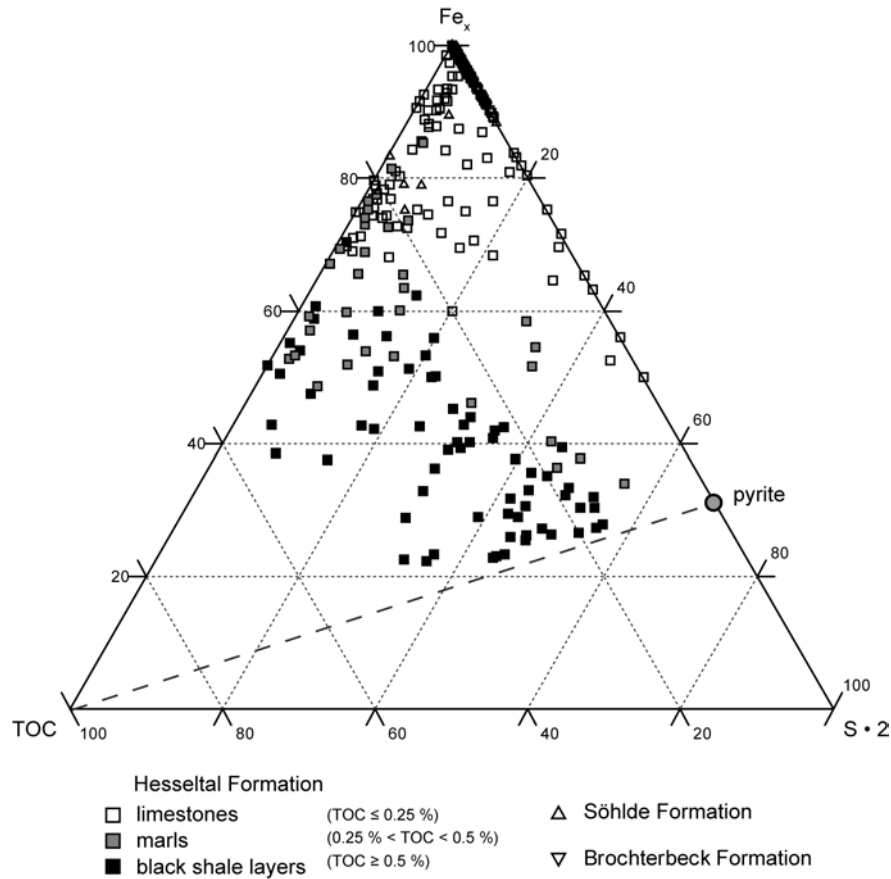


Figure 7.6 Ternary Plot: Degree of pyritization of sediments from the Wunstorf core in the system Fe_x – TOC – S · 2 (relative weight ratios). Reactive Fe_x is calculated with Fe_x = Fe – 0.25 · Al. Data point for pyrite is also shown.

The degree of pyritization based on bulk geochemical sediment analysis is visualized in a ternary Fe_x-TOC-S diagram (Fig. 7.6; Brumsack, 1988; Dean and Arthur, 1989; Brumsack et al., 1995). The content of reactive Fe (Fe_x) is estimated empirically ($\text{Fe}_x = \text{Fe} - 0.25 \cdot \text{Al}$) assuming that a certain fraction of aluminosilicate-bound Fe is not available for pyrite formation (Canfield et al., 1992). The presented data all plot above the pyrite saturation line, indicating that pyrite formation was not limited by reactive Fe availability. Nevertheless, some samples of the black shale layers plot close to the pyrite saturation line, and are assumed to be pyritized to a high degree. Comparison of different black shale packages and single layers indicates no general differences in the degrees of pyritization (data not shown).

Figure 7.3B shows the depth profile of Fe/Al. Most values are rather similar to AS (0.55). However, especially within the black shale packages, several distinct peaks occur (maximum Fe/Al 1.90) which cannot be explained by redistribution processes within the sedimentary column. Comparison with the S depth profile indicates a match of peaks in S

and Fe/Al, hinting to the formation of iron sulphides. Increased Fe/Al contents require an additional Fe source during deposition. Reductive Fe mobilization from near-shore areas or enhanced fluvial Fe input are likely causes for the observed Fe enrichments.

Several trace metals (TM) are known to be enriched in TOC-rich sediments, such as As, Co, Cu, Mo, Ni, U, V and Zn. As listed in Table 7.1, the concentrations of these TM are often below the XRF quantification limit within the limestone sequences. The black shale packages are characterized by higher values, notwithstanding absolute concentrations are relatively low due to carbonate dilution. Thus, Mo and U contents often are close or fall below the XRF detection limit. The profiles of selected element/Al ratios are given in Figure 7.3B. Figure 7.7 shows the enrichment factor (EF) - calculated from mean TM/Al ratios relative to TM/Al of AS – for different black shale packages studied and for C/T mean values (compared to a global compilation made by Brumsack, 2006).

A comparison of the TM/Al profiles with each other, as well as with the TOC and S profiles shows that not all peaks appear in parallel, and that the degree of TM enrichment is different for different TM. For example, black shale package 1 is highly enriched in As, Co and Ni. However, regarding the TM/Al profiles, layer 1-a is not distinguishable from surrounding limestones, while layer 1-b and 1-c can be readily identified. Layer 1-b shows minor peaks in S and As, but extreme peaks in Co and Ni. Layer 1-c shows higher values for S, similar values for As/Al, but lower values for Co/Al and Ni/Al relative to 1-b. Fe/Al ratios are elevated within layer 1-c, but not in 1-a or 1-b. Some single peaks in TM/Al ratios occur outside black shale layers (defined by their TOC contents). For example, within package 1, a distinct peak in Zn/Al occurs without accumulation of organic material just below layer 1-b. At 22.99 m, a peak in all TM/Al ratios as well as in S and Fe/Al profiles is present, but no TOC enrichment. Thus, the TM distribution within black shale layers of the Wunstorf section does not reveal a uniform enrichment pattern. Hence, no general TM-based model for palaeoredox and palaeoenvironmental conditions leading to black shale deposition in this setting can be established.

However, some information regarding redox conditions can still be derived from the TM records of the Wunstorf drill core. Although it bears much simplification, we may deduce from Figure 7.7 that the black shale packages of the Wunstorf section (except package 1) are enriched in Fe relative to C/T mean values.

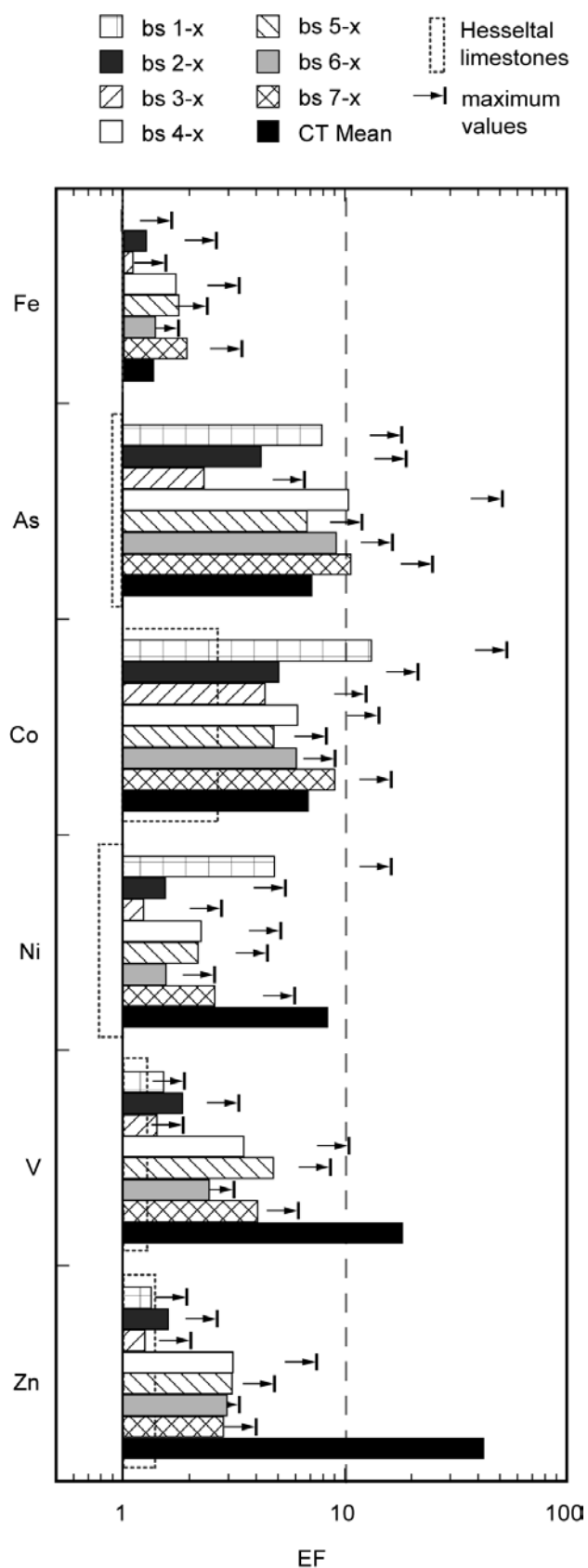


Figure 7.7 Mean enrichment factors (EFs) of redox-sensitive and sulphide-forming elements (Fe, As, Co, Ni, V and Zn) relative to average shale (AS) (Wedepohl, 1971, 1991) for Wunstorf core black shale layers, in comparison with mean values for Cenomanian-Turonian black shales (Brumsack, 2006) and Hesselstal limestones. $EF = \text{element}/Al(\text{sample})/\text{element}/Al(AS)$. Arrows indicate maximum values.

The enrichment of As and Co for most black shale packages is in the same order of magnitude as the C/T mean value, while the EFs of Ni, V and Zn are well below. Different pathways for the introduction of redox-sensitive and sulphide-forming TMs to TOC-rich sediments have been suggested. Most oxyanions (like U and Mo) are primarily derived from seawater and enter the sediments most probably via diffusion across the sediment-water interface if the surface sediments are sub- to anoxic. Other TM (Co, Cu, Ni) are deposited via bio-detritus in association with high primary productivity, or are adsorbed onto sinking particles like Fe- or Mn(oxyhydr)oxides or organic matter. For some elements (As, V, Zn), a combination of different enrichment mechanisms seems possible (Smedley and Kinniburgh, 2001, Brumsack, 2006, Tribovillard et al., 2006, Böning, 2009).

The oxyanions Mo, U and V show different behaviour under various redox conditions (Tribovillard et al., 2006). While U and V may be reduced and accumulated under denitrifying (suboxic-anoxic) conditions, Mo is enriched mainly under sulfate-reducing (anoxic-sulfidic) conditions. Thus, in the case of U and V enrichment without parallel Mo enrichment, suboxic/anoxic depositional conditions without free hydrogen sulphide are suggested. Reduced U and V may be incorporated into organic matter, but do not form stable sulphides. In contrast to these metals, As is either taken up by solid sulphide phases under anoxic-sulfidic conditions, (if high amounts of free hydrogen sulphide are present) precipitated as As sulphides, or co-precipitated with other sulphide minerals such as pyrite (Smedley and Kinniburgh, 2002). In addition, As is not supplied to the sediment via diffusion, but is adsorbed onto Fe(oxyhydr)oxides before being released during decomposition of organic matter and reductive dissolution of Fe(oxyhydr)oxides.

Co shows a similar behaviour like Mn in seawater and sediments and an association of Co with Fe and Mn(oxyhydr)oxides under oxic conditions is likely. Under oxygen-depleted conditions in an open environment like in an oxygen minimum zone (OMZ), adsorbed Co will be mobilized and transported away (Heggie and Lewis, 1984, Böning, 2009). Under sulphidic conditions, Co precipitates as CoS when free hydrogen sulphide is present (Huerta-Diaz and Morse, 1992). The elements Cu, Ni and Zn are among those being involved in biogenic cycling. Thus, they primarily enter the sediment via bio-detritus but may as well be adsorbed onto Mn or Fe(oxyhydr)oxides. Under reducing conditions in the sediment, these TM may be incorporated into Fe sulphides or form their own sulphide phases. Alternatively, Ni can be incorporated in organic matter, similar to U and V.

As the black shale layers of the Wunstorf succession are only moderately enriched in redox-sensitive and sulphide forming trace metals (e.g. As, Co, Ni, V, Zn), and at the same

time lack Mo enrichments, we assume suboxic rather than euxinic conditions during their deposition. However, because most of the TM enriched here are sulphide-forming, we further assume sulphidic conditions at or shortly below the sediment-water interface, trapping TM after reductive mobilization. As the TM involved in biogenic cycling and/or incorporated post-depositionally in organic matter (Ni, V, Zn) are more enriched within intermediate black shale packages 4 and 5, we further suggest changes in the amount and/or nature of delivered organic material. This could be due to increased primary productivity (as indicated by P/Al ratios), but also due to lower input of refractory, non-reactive terrigenous organic material into the Wunstorf basin.

Comparison to other C/T black shale sections

Although OAE 2 is thought to be a global event as concluded from positive carbon isotopic excursions, organic carbon burial differs in its geographic expression. Suboxic, anoxic or even euxinic conditions developed in oxygen minimum zones along continental margins of the tropical Tethys, in restricted epicontinental seas, and in the widening North and South Atlantic Ocean basins. These conditions led to deposition of rhythmically bedded sedimentary sequences including organic-rich black shale (Leckie et al., 2002). The Bonarelli level representing OAE 2 in the Umbria-Marche Basin of Central Italy defines a characteristic discrete black shale level within a calcareous sequence. On Demerara Rise, a submarine plateau in the tropical North Atlantic, CTBE black shales form part of a thick black shale interval (thickness up to 90 m) encompassing the Albian to Santonian (Erbacher et al., 2004). There, the sediments deposited during OAE 2 are characterized by extremely high organic carbon content with maximum values up to 30.2 % with mean values of about 15 % (Hetzl et al., 2009), whereas TOC contents of the Bonarelli level (mean value 2.60 %; Turgeon and Brumsack, 2006) are much more comparable to values for black shales of the Wunstorf succession. TOC, TIC and S contents as well as element/Al ratios for selected elements for OAE 2 sediments of Demerara Rise (ODP Sites 1258 and 1260) and the Umbria-Marche Basin (Furlo) in comparison to the Wunstorf succession are listed in Table 7.2. Additionally, values for underlying “black levels” of Furlo and values for AS are shown. Among the sites listed, Wunstorf represents the shallowest site located in the Central European shelf sea whereas Furlo and Demerara Rise were located at greater water depth (Site 1260: 500m; Site 1258: 1000 m, Furlo: 1500 m).

Table 7.2 Comparison of average element contents and element/Al ratios for different C/T black shale sections (Wunstorf, Furlo, Demerara Rise) and 'average shale'.

		Wunstorf North German Basin	Furlo Umbria-Marche Basin Livello Bonarelli Black Levels		Demerara Rise proto-North Atlantic Site 1258 Site 1260		Average Shale
		this study	Turgeon and Brumsack (2006)		Hetzel et al.(2009)		Wedepohl (1971, 1991)
water depth	(m)	100 -150 ¹	1500		1000 ³	500 ³	
sedimentation rate	cm/kyr	2.1 - 3.0 ²	0.29	0.26	1	0.25	
S	%	0.76	0.81	0.41	4.97	3.43	0.24
TIC	%	7.25		6.84	2.46	5.76	0.35
TOC	%	1.16	2.60	2.80	17.82	12.12	
Si/Al	$\times 10^{-4}$	3.70	20	5	5.81	3.72	3.11
Fe/Al	$\times 10^{-4}$	0.82	0.80	0.99	0.76	0.80	0.54
P/Al	$\times 10^{-4}$	0.03	0.12	0.05	0.05	0.12	0.01
As/Al	$\times 10^{-4}$	8.1	8.8	11.0	8.8	12.5	1.1
Ba/Al	$\times 10^{-4}$	47.6	3520	369	188.1	345.2	65.6
Co/Al	$\times 10^{-4}$	14.7	4.7	37	4.4	4.4	2.1
Cu/Al	$\times 10^{-4}$	9.8	64.0	76	24.0	30.5	5.1
Mn/Al	$\times 10^{-4}$	952.8	15.0	172	18.4	5.9	96.2
Mo/Al	$\times 10^{-4}$	0.1	5.6	2.0	14.3	16.7	0.1
Ni/Al	$\times 10^{-4}$	17.7	26	91	59.5	73.0	7.7
U/Al	$\times 10^{-4}$	1.0	2.5	1.9	6.2	10.8	0.4
V/Al	$\times 10^{-4}$	41.1	220	241	127.0	294.5	14.7
Zn/Al	$\times 10^{-4}$	24.7	229	302	48.1	154.0	10.7

¹ Wilmsen (2003)² Voigt et al. (2008)³ Friedrich et al. (2008)

At Demerara Rise, black shales deposited during OAE 2 are clearly depleted in Mn but enriched in redox-sensitive and sulphide forming TM such as As, Co, Cu, Mo, Ni, U, V, and Zn. Nevertheless the enrichment in seawater-borne elements like Mo is less pronounced during OAE 2 than before and after this event. This might be related to the global extent of oxygen-depleted conditions leading to black shale deposition and thus forming a significant TM sink. Paleogeographic reconstructions show that the proto-North Atlantic Ocean was a restricted area with major seawater supply coming from the Tethys only. Hetzel et al. (2009) assumed that the decline in TM enrichment seen at Demerara Rise indicates a drawdown of TMs from seawater, similar to the "basin reservoir effect" described by Algeo and Lyons (2006). If TM seawater concentrations were actually reduced during OAE 2, an enrichment

of seawater derived TM within the CTBE black shales at Wunstorf might have been inhibited.

High values of P/Al and Ba/Al indicate high primary productivity (Hetzl et al., 2009). From high-resolution element/Al profiles and Fe and S specification Hetzel et al. (2009) concluded that euxinic conditions prevailed during OAE 2 whereas sediments deposited before and thereafter are more compatible with a situation encountered in modern coastal upwelling areas within an expanded OMZ. For the Furlo section Turgeon and Brumsack (2006) concluded differences in depositional environments for the Bonarelli level and the “black levels” below. The Mn depletion in the Bonarelli sediments shows that bottom waters were oxygen-depleted during this time and that open marine conditions permitted the export of Mn. This contrasts with the elevated Mn/Al ratios in the black levels which indicate that Mn was trapped during these times and that the (sub-)basin or the OMZ was more restricted.

Most redox-sensitive or sulphide-residing trace elements are strongly enriched for both settings indicating periodic depletion of oxygen and potential availability of hydrogen sulphide in the water column. Black levels are characterized by higher Co and Ni enrichments and higher Re/Mo ratios demonstrate more oxygenated bottom waters during deposition of the “black levels” than during OAE 2, where elevated Ba concentrations are indicative of high paleoproductivity in this area, which is further supported by the high P concentrations.

As stated above, among the locations listed TOC contents are lowest in the black shale of the Wunstorf section, whereas S contents are comparable to the Bonarelli level but much lower than CTBE black shales at Demerara Rise, where sulphidic conditions lead to a sulphurization of organic matter (Hetzl et al., 2009). Concerning primary productivity, P and Ba contents indicate high productivity within the Umbria-Marche Basin during OAE 2, whereas at Demerara Rise productivity was slightly enhanced similar to black shales deposited before and after OAE 2 (Hetzl et al., 2009). Since Ba contents cannot be used as a paleo-proxy for the Wunstorf succession (see section *Productivity proxies*), we conclude that productivity at Wunstorf was more comparable to the preceding deposition of black levels in the Umbria-Marche basin than to the deposition of the Bonarelli level during OAE 2. The same is true for enrichments pattern of redox-sensitive or sulphide forming trace metals: Sediments deposited under truly anoxic to euxinic conditions such as the Bonarelli level and OAE 2 sediments of ODP Sites 1258 and 1260 are both highly enriched in the oxyanions Mo and U (for Furlo also Sb), while the enrichment patterns for the black

levels of Furlo and for black shales of Wunstorf reveal a preference of chalcophile trace metals (Fe, As, Co, and Ni). From this we conclude that more suboxic-anoxic conditions rather than truly anoxic-euxinic conditions did prevail, although we have to admit, that deposition of Mo and U at Wunstorf might be obscured by higher sedimentation rates and/or the change in water column TM inventory proposed by Hetzel et al. (2009).

Another similarity for the black levels of Furlo and black shales of Wunstorf are the higher amounts of Mn in comparison to the other black shales listed in Table 7.2. In summary, we can state from inorganic-geochemical parameters that the depositional environment of black shales of Wunstorf located in the Central-European shelf sea seems to be less extreme than conditions within deeper ocean basins during OAE 2.

Tyson and Pearson (1991) addressed the factors controlling continental shelf anoxia. The authors could show that ancient epeiric sea black shales rather reflect dysoxia-anoxia at the sediment-water interface than true anoxia and that seasonal stratification is the best model explaining these dysoxia-anoxia. During times of minimal seasonal variations the thermocline establishing during the summer could be stabilized due to less intense winter mixing. Such conditions may be triggered by orbitally induced changes in insolation and thus might be of major importance at lower and mid latitudes. The generally warmer temperature during the mid-Cretaceous might have favoured the occurrence of such thermocline stability and stratification might have become more permanent.

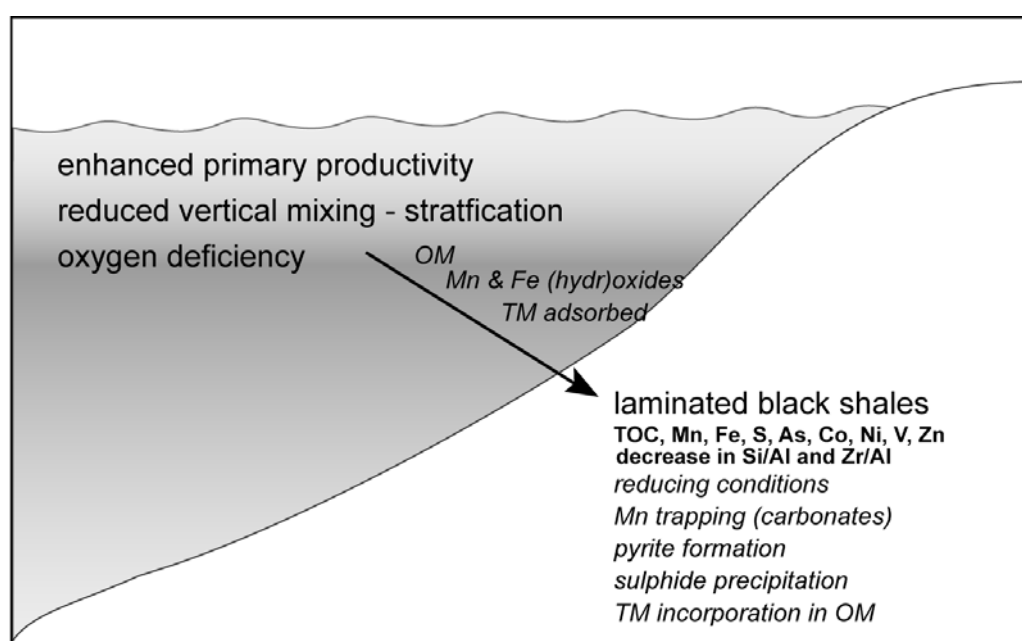


Figure 7.8 Depositional model for black shale layers of the Wunstorf section based on geochemical parameters.

This model is in good agreement with our results: From cyclic minima in Si/Al and Ti/Al ratios we conclude a decrease in vertical mixing during times of black shale deposition. Due to water column stratification water masses below the thermocline become de-oxygenated and dysoxic to anoxic bottom waters established in an OMZ. As we assume moderate to enhanced primary productivity, higher oxygen demand may accelerate the oxygen deficiencies. Extension of the OMZ would lead to the reductive mobilization of Fe from near shore areas explaining the Fe enrichment seen in black shales of Wunstorf.

Summary and palaeoenvironmental implications for black shale deposition

The conclusions from geochemical data regarding the palaeoenvironment during black shale formation at Wunstorf are summarized in a conceptual depositional model (Figure 7.8). Orbitally induced climate changes lead to less vertical mixing during black shale deposition intensifying water column stratification. Assuming moderate to enhanced primary productivity with an OMZ impinging on the continental shelf, the OMZ would be extended and reductive Fe mobilization from near-shore areas would result in elevated Fe/Al ratios. The transgressive system tract above the “Fischschiefer” would support enhanced Fe and nutrient supply, mobilizing so far unavailable nearshore and land-locked nutrients. However, this explanation by eustasy alone would not explain the cyclic distribution patterns of black shales following precession cycles.

Regarding redox conditions at the sediment-water interface, we conclude suboxic rather than euxinic bottom waters allowing deposition of Mn or Fe (oxyhydr)oxides. Burial of organic matter as a result of increased productivity and oxygen deficiency intensified reducing conditions just below the sediment-water interface, leading to formation of Fe sulphides. Since we assume that As and Co were adsorbed on Fe(hydr)oxides, the enrichment of these TM supports our idea of deposition under suboxic conditions and pyritization of the sediment shortly after burial. However, euxinic conditions with free hydrogen-sulphide in the water column leading to precipitation of Fe-sulphide as well as As- and Co-sulphide cannot be completely excluded.

Acknowledgements

We would like to thank the Wunstorf Coring Scientific Drilling Party, especially Jochen Erbacher and Silke Voigt, for their kind support. Thanks also to Bernhard Schnetger for analytical advice, Eleonore Gründken, Carola Lehnert and Martina Wagner for technical assistance and Christian März, Astrid Forster and Christian Linnert for helpful discussions and critical comments.

References

- Algeo, T.J., Lyons, T.W., 2006. Mo-total organic carbon covariation in modern anoxic marine environments: implications for analysis of paleoredox and paleohydrographic conditions. *Paleoceanography* 21, PA1016.
- Arthur, M.A., Dean, W.E., Pratt, L.M., 1988. Geochemical and climatic effects of increased marine organic carbon burial at the Cenomanian/Turonian boundary. *Nature* 335(6192), 714-717.
- Arthur, M.A., Schlanger, S.O., Jenkyns, H.C., 1987. The Cenomanian/Turonian Oceanic Anoxic Event, II. Palaeoceanographic controls on organic-matter production and preservation. In: Brooks, J., Fleet, A.J. (Eds.), *Marine Petroleum Source Rocks*. Geological Society, London. Special Publication 26, 401-420.
- Berner, R.A., 1970. Sedimentary Pyrite Formation. *American Journal of Science* 268, 2-23.
- Berner, R.A., 1984. Sedimentary pyrite formation: an update. *Geochimica et Cosmochimica Acta* 48(4), 605-615.
- Bernstein R.E., Byrne R.H., 2004. Acantharions and marine barite. *Marine Chemistry* 86(1-2), 45-50.
- Bertram, M.A., Cowen, J.P., 1997. Morphological and compositional evidence for biotic precipitation of marine barite. *Journal of Marine Research* 55(3), 577-593.
- Bishop, J.K.B., 1988. The barite-opal-organic carbon association in oceanic particulate matter. *Nature* 332(6162), 341-343.
- Böning, P., Brumsack, H.-J., Böttcher, M.E., Schnetger, B., Kriete, C., Kallmeyer, J., Borchers, S.L., 2004. Geochemistry of Peruvian near-surface sediments. *Geochimica et Cosmochimica Acta* 68(21), 4429-4451.
- Böning, P., Brumsack, H.-J., Schnetger, B., Grunwald, M., 2009. Trace element signatures of Chilean upwelling sediments at ~36°S. *Marine Geology* 259 (1-4), 112-121.
- Breit, G.N., Wanty, R.B., 1991. Vanadium accumulation in carbonaceous rocks. A review of geochemical controls during deposition and diagenesis. *Chemical Geology* 91(1-2), 83-97.
- Broecker, W.S., Peng, T.-H., 1982. *Tracers in the Sea*. Eldigio Press, Palisades, New York.
- Brumsack, H.-J., 1980. Geochemistry of Cretaceous black shales from the Atlantic Ocean (DSDP Legs 11, 14, 36, and 41). *Chemical Geology* 31, 1-25.
- Brumsack, H.-J., 1988. Rezente, Corg-reiche Sedimente als Schlüssel zum Verständnis fossiler Schwarzschiefer. Habilitationsschrift, Georg-August Universität Göttingen, Germany.
- Brumsack, H.-J., 1989. Geochemistry of recent TOC-rich sediments from the Gulf of California and the Black Sea. *Geologische Rundschau* 78(3), 851-882.
- Brumsack, H.-J., 2006. The trace metal content of recent organic carbon-rich sediments: implications for Cretaceous black shale formation. *Palaeogeography, Palaeoceanography, Palaeoecology* 232(2-4), 344-361.

- Brumsack, H.-J., Heydemann, A., Kühn, V., Rachold, V., Usdowski, E., 1995. Geochemistry and mineralogy of Middle Aptian sediments from the Lower Saxony Basin, NW Germany. *Neues Jahrbuch für Geologie und Paläontologie, Abhandlungen* 196(2), 235-255.
- Calvert, S.E., Pedersen, T.F., 1993. Geochemistry of recent oxic and anoxic marine sediments: implications for the geological record. *Marine Geology* 113(1-2), 67-88.
- Canfield, D.E., Raiswell, R., Bottrell, S., 1992. The reactivity of sedimentary iron minerals toward sulfide. *American Journal of Science* 292, 659-683.
- Dean, W.E., Arthur, M.A., 1989. Iron-sulfur-carbon-relationship in organic sequences, I. Cretaceous Western Interior Seaway. *American Journal of Science* 289, 708-743.
- Dehairs, F., Chesselet, R., Jedwab, J., 1980. Discrete suspended particles of barite and the barium cycle in the open ocean. *Earth and Planetary Science Letters* 49(2), 528-550.
- Dehairs, F., Goeyens, L., Stroobants, N., Bernard, P., Goyet, C., Poisson, A., Chesselet, R., 1990. On suspended barite and the oxygen-minimum in the Southern Ocean. *Global Biogeochemical Cycles* 4(1), 85-102.
- Delayne, M.L., 1998. Phosphorus accumulation in marine sediments and the oceanic phosphorus cycle. *Global Biogeochemical cycles* 12(4), 563-572.
- Dellwig, O., Hinrichs, J., Hild, A., Brumsack, H.-J., 2000. Changing sedimentation in tidal flat sediments of the southern North Sea from the Holocene to the present: a geochemical approach. *Journal of Sea Research* 44(3-4), 163-181.
- Dymond, J., Suess, E., Lyle, M., 1992. Barium in deep-sea sediments: A geochemical proxy for paleoproductivity. *Paleoceanography* 7(2), 163-181.
- Erbacher, J., Friedrich, O., Wilson, P.A., Birch, H., Mutterlose, J., 2005. Stable organic carbon isotope stratigraphy across Oceanic Anoxic Event 2 of Demerara Rise, Western Tropical Atlantic. *Geochemistry, Geophysics, Geosystems* 6, Q06010.
- Erbacher, J., Mosher, D.C., Malone, M.J., Shipboard Scientific Party, 2004. Proceedings of the Ocean Drilling Program, Initial Reports, 207. College Station, TX (Ocean Drilling Program), pp. 89.
- Erbacher, J., Mutterlose, J., Wilmsen, M., Wonik, T., Wunstorf Drilling Scientific Party, 2007. The Wunstorf Drilling Project: Coring a global stratigraphic reference section of the Oceanic Anoxic Event 2. *Scientific Drilling* 4, 19-21.
- Ernst, G., Schmid, F., Seibert, E., Wood, C.J., 1983. Event-Stratigraphie im Cenoman und Turon NW-Deutschlands. *Zitteliana* 10, 531-554.
- Föllmi, K.B., 1996. The phosphorus cycle, phosphogenesis and marine phosphate-rich deposits. *Earth-Science Reviews* 40 (1-2), 55-124.
- Forster, A., Schouten, S., Moriya, K., Wilson, P.A., Sinninghe Damsté, J.S., 2007. Tropical warming and intermittent cooling during the Cenomanian/Turonian oceanic anoxic event 2: sea surface temperature records from the equatorial Atlantic. *Paleoceanography* 22, PA1219.
- Friedrich, O., Erbacher, J., Moriya, K., Wilson, P.A., Kuhnert, H., 2008. Warm saline intermediate waters in the Cretaceous tropical Atlantic Ocean. *Nature Geoscience* 1, 453-457.
- Friedrich, O., Erbacher, J., Mutterlose, J., 2006. Paleoenvironmental changes across the Cenomanian/Turonian Boundary Event (Oceanic Anoxic Event 2) as indicated by benthic foraminifera from the Demerara Rise (ODP Leg 207). *Revue de Micropaléontologie* 49(3), 121-139.
- Gale, A.S., Jenkyns, H.C., Kennedy, W.J., Corfield, R.M., 1993. Chemostratigraphy versus biostratigraphy: data from around the Cenomanian-Turonian boundary. *Journal of the Geological Society* 150(1), 29-32.
- Hatch, J.R., Leventhal, J.S., 1992. Relationship between inferred redox potential of the depositional environment and geochemistry of the Upper Pennsylvanian (Missourian)

- Stark Shale Member of the Dennis Limestone, Wabaunsee County, Kansas, USA. In: Meyers, P.A., Pratt, L.M., Nagy, B. (Eds.), *Geochemistry of Metalliferous Black Shales*. *Chemical Geology* 99(1-3), 65-82.
- Heggie D., Lewis T., 1984. Cobalt in pore waters of marine sediments. *Nature* 311(5985), 453-455.
- Hetzel, A., Böttcher, M.E., Wortmann, U.G., Brumsack, H.-J., 2009. Paleo-redox conditions during OAE 2 reflected in Demerara Rise sediment geochemistry (ODP Leg 207). *Palaeogeography, Palaeoceanography, Palaeoecology* 273(3-4), 302-328.
- Huerta-Diaz, M.A., Morse, J.W., 1992. Pyritization of trace metals in anoxic marine sediments. *Geochimica et Cosmochimica Acta* 56(7), 2681-2702.
- Jacobs, L., Emerson, S., Huested, S.S., 1987. Trace metal geochemistry in the Cariaco Trench. *Deep-Sea Research Part A* 34(5-6), 965-981.
- Jacobs, L., Emerson, S., Skei, J., 1985. Partitioning and transport of metals across the O₂/H₂S interface in a permanently anoxic basin: Framvaren Fjord, Norway. *Geochimica et Cosmochimica Acta* 49(6), 1433-1444.
- Jarvis, I., Gale, A.S., Jenkyns, H.C., Pearce, M.A., 2006. Secular variation in Late Cretaceous carbon isotopes: a new $\delta^{13}\text{C}$ carbonate reference curve for the Cenomanian-Campanian (99.6-70.6 Ma). *Geological Magazine* 143 (5), 561-608.
- Jarvis, I., Murphy, A.M., Gale, A.S., 2001. Geochemistry of pelagic and hemipelagic carbonates: criteria for identifying systems tracts and sea-level change. *Journal of the Geological Society* 158(4), 658-696.
- Leckie, R.M., Bralower, T.J., Cashman, R., 2002. Oceanic anoxic events and plankton evolution: Biotic response to tectonic forcing during the mid-Cretaceous. *Paleoceanography* 17(3), 1040.
- Nijenhuis, I.A., Brumsack, H.-J., de Lange, G.J., 1998. The trace element budget of the eastern Mediterranean during Pliocene sapropel formation. In: Robertson, A.H.F., Emeis, K.-C., Richter, C., Camerlenghi, A. (Eds.), *Proceedings of the Ocean Drilling Program, Scientific Results*, 160. College Station, TX (Ocean Drilling Program), 199-206.
- Paytan, A., Kastner, M., Chavez, F.P., 1996. Glacial to interglacial fluctuations in productivity in the equatorial Pacific as indicated by marine barite. *Science* 274(5291), 1355-1357.
- Paytan, A., Mearon, S., Cobb, K., Kastner, M., 2002. Origin of marine barite deposits: Sr and S isotope characterization. *Geology* 30(8), 747-750.
- Piper, D.Z., 1994. Seawater as the source of minor elements in black shales, phosphorites and other sedimentary rocks. *Chemical Geology* 114(1-2), 95-114.
- Prakash Babu, C., Brumsack, H.-J., Schnetger, B., 1999. Distribution of organic carbon in surface sediments along the eastern Arabian Sea: a revisit. *Marine Geology* 162(1), 91-103.
- Pratt, L.M., Force, E.R., Pomeroy, B., 1991. Coupled manganese and carbon isotopic events in marine carbonates at the Cenomanian-Turonian boundary. *Journal of Sedimentary Research* 61(3), 370-383.
- Prauss, M.L., 2006. The Cenomanian/Turonian Boundary Event (CTBE) at Wunstorf, north-west Germany, as reflected by marine palynology, *Cretaceous Research* 27 (6), 872-886.
- Redfield, A.C., 1958. The biological control of chemical factors in the environment. *American Scientist* 46, 205-221.
- Sangiorgi, F., Brumsack, H.-J., Willard, D.A., Schouten, S., Stickley, C.E., O'Regan, M., Reichert, G.-J., Sinninghe Damsté, J.S., Brinkhuis, H., 2008. A 26 million year gap in the central Arctic record at the greenhouse-icehouse transition: Looking for clues. *Paleoceanography* 23, PA1S04.

- Schenau, S.J., Prins, M.A., de Lange, G.J., Monnin, C., 2001. Barium accumulation in the Arabian Sea: Controls on barite preservation in marine sediments. *Geochimica et Cosmochimica Acta* 65(10), 1545-1556.
- Schenau, S.J., Reichart, G.-J., de Lange, G.J., 2005. Phosphorus burial as a function of paleoproductivity and redox conditions in Arabian Sea sediments. *Geochimica et Cosmochimica Acta* 69(4), 919-931.
- Schlanger, S.O., Arthur, M.A., Jenkyns, H.C., Scholle, P.A., 1987. The Cenomanian-Turonian Oceanic Anoxic Event, I. Stratigraphy and distribution of organic carbon-rich beds and the marine $\delta^{13}\text{C}$ excursion. In: Brooks, J., Fleet, A.J. (Eds.), *Marine Petroleum Source Rocks*. Geological Society, London. Special Publication 26, 371-399.
- Schlanger, S.O., Jenkyns, H.C., 1976. Cretaceous oceanic anoxic events: causes and consequences. *Geologie en Mijnbouw* 55, 179-184.
- Schmitz, B., 1987. Barium, equatorial high productivity, and the northward wandering of the Indian continent. *Paleoceanography* 2(1), 63-77.
- Smedley, P.L., Kinniburgh, D.G., 2002. A review of the source, behaviour and distribution of arsenic in natural waters. *Applied Geochemistry* 17(5), 517-568.
- Tribouillard, N., Algeo, T.J., Lyons, T., Riboulleau, A., 2006. Trace metals as paleoredox and paleoproductivity proxies: An update. *Chemical Geology* 232(1-2), 12-32.
- Turgeon, S., Brumsack, H.-J., 2006. Anoxic vs dysoxic events reflected in sediment geochemistry during the Cenomanian-Turonian Boundary Event (Cretaceous) in the Umbria-Marche Basin of central Italy. *Chemical Geology* 234(3-4), 321-339.
- Tyson, R.V., Pearson, T.H., 1991. Modern and ancient continental shelf anoxia: an overview. In: Tyson, R.V., Pearson, T.H. (Eds.), *Modern and ancient continental shelf anoxia*. Geological Society, London. Special Publication 58, 1-24.
- Voigt, S., Aurag, A., Leis, F., Kaplan, U., 2007. Late Cenomanian to Middle Turonian high-resolution carbon isotope stratigraphy: New data from the Münsterland Cretaceous Basin, Germany. *Earth and Planetary Science Letters* 253(1-2), 196-210.
- Voigt, S., Erbacher, J., Mutterlose, J., Weiss, W., Westerhold, T., Wiese, F., Wilmsen, M., Wonik, T., 2008. The Cenomanian – Turonian of the Wunstorf section – (North Germany): global stratigraphic reference section and new orbital time scale for Oceanic Anoxic Event 2. *Newsletters on Stratigraphy* 43(1), 65-89.
- Voigt, S., Gale, A.S., Flögel, S., 2004. Midlatitude shelf seas in the Cenomanian-Turonian greenhouse world: Temperature evolution and North Atlantic circulation. *Paleoceanography* 19, PA4020.
- Voigt, S., Gale, A.S., Voigt, T., 2006. Sea level change, carbon cycling and palaeoclimate during the Late Cenomanian of northwest Europe; an integrated palaeo environmental analysis. *Cretaceous Research* 27(7), 836-858.
- von Breymann, M.T., Emeis, K.C., Suess, E., 1992. Water depth and diagenetic constraints on the use of barium as a paleoproductivity indicator. In: Summerhayes, C.P., Prell, W.L., Emeis, K.C. (Eds.), *Upwelling Systems: Evolution since the Early Miocene*. The Geological Society, London. Special Publication 64, 273-284.
- Wedepohl, K.H., 1971. Environmental influences on the chemical composition of shales and clays. In: Ahrens, L.H., Press, F., Runcorn, S.K., Urey, H.C. (Eds.), *Physics and Chemistry of the Earth* 8. Pergamon, Oxford, 305-333.
- Wedepohl, K.H., 1991. The composition of the upper earth's crust and the natural cycles of selected metals. *Metals in natural raw materials. Natural Resources*. In: Merian, E. (Ed.), *Metals and Their Compounds in the Environment*. VCH, Weinheim, 3-17.
- Wilmsen, M., 2003. Sequence stratigraphy and palaeoceanography of the Cenomanian Stage in northern Germany. *Cretaceous Research* 24(5), 525-568.

Appendix

Appendix A7.1 Quantification limit, precision, and accuracy of analyzed elements.

Element	Method	Quantification limit	Precision SD (1 σ) (rel%)	Accuracy (rel%)
S	IR-analyzer		2.9	-0.1
TC	IR-analyzer		0.7	2.7
TIC	Coulometry		1.1	0.2
Si	XRF	1.40 %	1.3	-1.0
Ti	XRF	0.018 %	1.0	-3.6
Al	XRF	0.26 %	1.8	-0.4
Fe	XRF	0.21 %	1.0	-2.8
Mg	XRF	0.06 %	1.4	-1.3
Ca	XRF	0.14 %	1.1	-0.6
Na	XRF	0.22 %	2.8	-0.3
K	XRF	0.08 %	2.0	2.9
P	XRF	0.004 %	1.0	0.7
As	XRF	2 ppm	2.0	8.4
Ba	XRF	40 ppm	1.6	2.8
Co	XRF	10 ppm	15.7	3.9
Cr	XRF	30 ppm	4.8	-1.0
Cu	XRF	10 ppm	7.1	-21.7
Mn	XRF	155 ppm	5.7	-8.1
Mo	XRF	20 ppm	2.5	-3.5
Ni	XRF	20 ppm	2.3	-6.1
Pb	XRF	5 ppm	14.4	4.8
Rb	XRF	5 ppm	2.9	-1.9
Sr	XRF	20 ppm	1.2	-2.0
U	XRF	3 ppm	7.6	10.0
V	XRF	20 ppm	1.2	-2.6
Y	XRF	10 ppm	4.4	-0.1
Zn	XRF	20 ppm	1.7	1.3
Zr	XRF	10 ppm	6.3	0.9

Note: Procedures and accuracy of all methods were checked with in-house reference materials (IR-Analyzer: PS-S (n=72); coulometry: Loess (n=54); XRF: DR-BS (n=12)). Precision is defined as 100% times the best estimate standard deviation (1 σ) divided by the mean of the repeats. SD = standard deviation. Accuracy is defined as 100% times the difference between the mean of the repeated analyses and the expected value divided by the expected value.

8. Conclusions and Perspectives

This study presents an inorganic geochemical study of two OAE 2 sequences located in different paleogeographical settings which exhibit different lithological expressions of black shale deposition. At Demerara Rise (ODP Leg 207; tropical Atlantic) sediments deposited during OAE 2 form part of a thick black shale succession, while within the Cenomanian-Turonian sediments sequence at Wunstorf (north Germany) OAE 2 is presented by rhythmically bedded laminated black shales, dark organic-rich marls and marly limestones. As changes in water column redox conditions lead to responses in the coupled biogeochemical sulfur-carbon-metal cycles and associated sedimentary signal formation, distribution patterns of redox-sensitive and sulfide forming trace metals are analyzed for paleoenvironmental reconstructions of these two settings.

For sediment cores recovered during ODP Leg 207 it can be shown that squeeze cake material (pore water squeezing residues) is useful for providing a first overview of the lithologic units by applying standard geochemical methods. Major element analysis indicates a common origin of the terrigenous detritus similar to average shale, whereas the clay-dominated Unit I reveals a more weathered terrigenous component. Cross-correlation analysis of elements provides information about different mineral phases suggesting different depositional environmental features. Heavy minerals phases and quartz-bearing sands display a high-energy synrift deposit in Unit V. The Cretaceous black shales of Unit IV are clearly enriched in redox-sensitive and stable sulfide-forming elements indicating high paleoproductivity and severe oxygen depletion in the water column. The complete sulfidization of the black shales and significant excess sulfur denote a sulfidic environment, leading to sulfur incorporation into organic matter.

High-resolution major and minor element data were generated for both black shale sequences from Demerara Rise (ODP Leg 207) and for the Cenomanian-Turonian sedimentary succession at Wunstorf to identify changes in redox-conditions of the depositional environment during OAE 2. Using distribution patterns of trace element enrichment differences between both paleogeographical settings could be demonstrated. From the depletion in Mn and enrichment in sulfide-forming metals (Fe and Co) during OAE 2 it is concluded that OAE 2 at Demerara Rise represents a euxinic environment whereas black shales deposited before and after OAE 2 are much more compatible with a situation encountered in modern coastal upwelling systems within an expanded oxygen-minimum-zone. Euxinic conditions within the water column are confirmed by high ratios of reactive to

total iron as well as specific biomarkers. For the Wunstorf succession the situation is different. Black shale deposition occurs rhythmically both within and above the level of the positive carbon isotope excursion defining OAE 2. Thus, the circumstances favoring organic carbon burial apparently prevailed longer in the Wunstorf basin than globally. Geochemical analysis reveals no significant differences between black shale packages deposited during OAE 2 and thereafter. From variations in element/Al ratios of the terrestrial input, we postulate orbitally induced changes leading to less vertical mixing. Thus black shale deposition was likely caused by intensified water column stratification than by enhanced primary productivity. Enrichment patterns of diagnostic trace metals hint to suboxic to anoxic conditions at the sediment-water interface.

The importance of black shale deposition during OAE's for global trace metal cycles is evidenced in the C/T black shales of Demerara Rise. A decline in seawater derived trace metal enrichment during OAE 2 hints to a change in the trace metal inventory of seawater. Beside these paleoceanographic studies, element distribution patterns in pore waters reveal information about post-depositional and on-going diagenesis in the sediment. A reaction-transport model is used to infer the long-term evolution of anaerobic organic matter degradation in Cretaceous black shales from the distribution of authigenic barite in sediments drilled at Demerara Rise. The inversely determined parameters reveal that the reactivity of the organic matter was already low at the time of its deposition in the Cretaceous. Simulation results thus indicate that the enhanced preservation of organic matter under euxinic conditions presumably was the main cause for the formation of organic-rich Cretaceous black shales at Demerara Rise.

The results of this study show how questions regarding the paleoenvironment of OAE 2 sediments can be addressed using high-resolution major and minor element data. Trace metal distribution patterns are identified to reflect changes in redox conditions. Due to dilution effects by biogenous carbonates some trace metals are only present in concentrations close to the detection limit of the X-ray fluorescence (XRF) analysis used here. Inductively coupled-plasma mass spectrometry (ICP-MS) would make a precise determination possible. Further ICP-MS analyses would extend the spectra of diagnostic trace metals (e.g., Ag, Bi, Cd, Re, Sb) making more paleoproxies available. For example, the Re/Mo ratio may be used to distinguish between suboxic and truly anoxic conditions of bottom waters. When the seawater trace metal draw-down in the proto-North Atlantic is considered, the magnitude of trace metal enrichment during OAE 2 may mirror the trace

metal inventory and obscure redox conditions controlling trace metal burial. For this reason the Re/Mo ratio may not be suitable as a redox-proxy for black shales of Demerara Rise. For these sediments iron and sulfur speciation data are shown to be useful for distinguishing between anoxia at the sediment water interface and truly euxinic conditions in the water column. These analyses may bear important information about euxinic conditions restricted to the pore space within the sediment or prevailing within the water column during black shale deposition at Wunstorf.

The multi-proxy approach bears a high potential for paleoenvironmental reconstructions of sediment cores drilled by ODP. Scientists of different disciplines work on the same cores addressing questions regarding the paleoenvironment such as primary productivity, redox conditions, paleotemperature, water column stratification. As described, the comparison with results of organic-geochemical and paleontological studies confirms the depositional model, which is based on major and minor element data, for reconstructing the paleoenvironmental setting for Cenomanian-Turonian black shales of Demerara Rise. Because the Wunstorf Scientific Party also pursues a multi-proxy approach, the paleoenvironmental reconstruction for OAE 2 at Wunstorf based on inorganic geochemistry will possibly be evaluated as work of other groups is in progress.

Besides the potential of major and minor element data for reconstructing the depositional environment the results presented here reveal certain limitations when only inorganic-geochemical analyses are used when interpreting element distribution concerning the detrital sediment supply. On the one hand, changes in the composition of terrigenous material may indicate changes in superordinate parameters, such as paleoclimate or paleogeography. On the other hand changes in sediment input may override depositional signals or may influence diagenesis leading to post-depositional element migration. Mineralogical studies, e.g. by X-ray diffraction, may provide insights into the origin of the detrital material. In the case of the Cenomanian-Turonian black shales of Demerara Rise mineralogical studies may help to identify the so-called “ash layers”. For the Wunstorf succession mineralogy may provide important information about the origin of the described changes in Si/Al ratios as well as alterations in paleo-currents in relation to the Plenus Cold Event.

Curriculum vitae

Almut Bunte

geb. Hetzel

Dipl. Umweltwiss.

geb. am 23.12.1978 in Marl (Westf.)

verheiratet, ein Sohn (1 Jahr)

08/1985 - 07/1989

Grundschule an der Emslandstraße, Marl

08/1989 - 07/1998

Geschwister-Scholl-Gymnasium, Marl

10/1998 - 12/2003

Studium an der Carl von Ossietzky – Universität Oldenburg

Studiengang: Marine Umweltwissenschaften (Diplom)

Thema der Diplomarbeit „Haupt- und Spurenelementverteilung in Sedimenten des Demerara Rise (ODP Leg 207)“ in der Arbeitsgruppe Mikrobiogeochemie

08/2002 - 12/2002

Auslandsstudium: Besuch des Kurses „From Mountain to Fjord – Geology and Ecology of Western Norway“ an der Høgskulen i Sogn og Fjordane, Sogndal, Norwegen

01/2004 - 12/2006

Anstellung als wissenschaftliche Mitarbeiterin in der Arbeitsgruppe Mikrobiogeochemie, Carl von Ossietzky – Universität Oldenburg im Rahmen des DFG Schwerpunktprogrammes „ODP/IODP“ unter der Leitung von Herrn Prof. Dr. H.-J. Brumsack. Die daraus resultierenden Ergebnisse bilden die Grundlage zur vorliegenden Dissertation.

Conference abstracts

- Böttcher, M.E., Brumsack, H.-J., Arndt, S., Hetzel, A. (2004): Authigenic sulfur phases as recorders for black shale-triggered anaerobic oxidation of methane: Results from ODP Leg 207. Annual Meeting German Mineralogical Society (DMG), 14. – 16. October 2005, Essen, Germany. *Berichte der Deutschen Mineralogischen Gesellschaft, Beiheft zum European Journal of Mineralogy*. 16: 18.
- Böttcher, M.E., Brumsack, H.-J., Arndt, S., Hetzel, A. (2004): Authigenic sulfur phases as recorders for black shale-triggered anaerobic methane oxidation (AMO). Joint Colloquium IODP/ICDP, 17. – 19. March 2004, Bremen, Germany.
- Böttcher, M.E., Brumsack, H.-J., Arndt, S., Hetzel, A. (2004): Authigenic sulfur phases as recorders for black shale-triggered anaerobic methane oxidation (AMO). Annual Meeting Geochemistry, German Mineralogical Society (DMG), 14. – 15. May 2004, Hannover, Germany.
- Böttcher, M.E., Brumsack, H.-J., Hetzel, A., Schipper, A. (2005): Biogeochemistry of diagenesis caused by a black shale-fueled marine biosphere. Annual Meeting of the German Association for Stable Isotope Research (GASIR), 10. – 12. October 2005, Jena, Germany.
- Böttcher, M.E., Brumsack, H.-J., Hetzel, A., Schipper, A., Arndt, S., Wirtz, K.W. (2005): Biogeochemistry of diagenesis caused by a black shale-fueled marine biosphere (ODP Leg 207). Joint Colloquium IODP/ICDP, 14. – 16. March 2005, Potsdam, Germany.
- Böttcher, M.E., Brumsack, H.-J., Hetzel, A., Schipper, A., Arndt, S., Wirtz, K.W. (2005): Biogeochemistry of diagenesis caused by a black shale-fueled marine biosphere (ODP Leg 207). International Symposium on the Cretaceous, 05. – 09. September 2005, Neuchatel, Switzerland.
- Böttcher, M.E., Brumsack, H.-J., Hetzel, A., Schipper, A. (2005): Authigenic sulfur phases as recorders for black shale-triggered anaerobic oxidation of methane: Results from ODP Leg 207. Isotope Workshop of the European Society for Isotope Research (ESIR), 25. – 30. June 2005, Leipzig, Germany. *UFZ-Report* 02/2005:121.
- Böttcher, M.E., Hetzel, A., Brumsack, H.-J., Arndt, S., Wirtz, K.W., Gehre, M., Prieto, M. (2007): Authigenic barite formation caused by black shale fueled AOM in the deep biosphere of ODP Leg 207. Annual Meeting of the Geologische Vereinigung (GV), 01. – 05. October 2007, Bremen, Germany. *Terra Nostra* 2007/1-2, 50.
- Böttcher, M.E., Hetzel, A., Brumsack, H.-J., Arndt, S., Wirtz, K.W., Gehre, M., Prieto, M. (2007): Authigenic barite formation caused by black shale fueled AOM in the deep biosphere of ODP Leg 207. Annual Meeting of the German Association for Stable Isotope Research (GASIR), 08. – 10. October 2007, Bayreuth, Germany.
- Böttcher, M.E., Hetzel, A., Brumsack, H.-J., Schipper, A. (2005): Iron speciation and sulphur isotope biogeochemistry of sediments from the Demerara Rise (ODP Leg 207). EGU General Assembly, 24. – 29. April 2005, Vienna, Austria. *Geophysical Research Abstracts*, Vol. 7, 07384.

- Böttcher, M.E., Hetzel, A., Brumsack, H.-J., Wortmann, U.G., Schipper, A. (2007): Dynamics of redox-sensitive tracers through the C/T in the southern North-Atlantic (ODP Leg 207): A high-resolution study. EGU General Assembly, 15. – 20. April 2007, Vienna, Austria. Geophysical Research Abstracts, Vol. 9, 09211.
- Böttcher, M.E., Hetzel, A., Brumsack, H.-J., Wortmann, U.G., Schipper, A. (2007): Dynamics of redox-sensitive proxies in OAE2 black shales of the southern North-Atlantic (ODP Leg 207) Annual Meeting of the Geologische Vereinigung (GV), 01. – 05. October 2007, Bremen, Germany. Terra Nostra 2007/1-2, 51.
- Hetzel, A., Böttcher, M.E., Arndt, S., Prieto, M., Gehre, M., Brumsack, H.-J. (2006): Authigenic barite formation triggered by black shale-fueled anaerobic methane oxidation in the deep biosphere of ODP Leg 207. Annual Meeting Geochemistry, German Mineralogical Society (DMG), 14.-15. June 2006, Kiel, Germany.
- Hetzel, A., Böttcher, M.E., Arndt, S., Prieto, M., Gehre, M., Brumsack, H.-J. (2006): Authigenic barite formation triggered by black shale-fueled anaerobic methane oxidation in the deep biosphere of ODP Leg 207. Joint Colloquium IODP/ICDP, 27. – 29. March 2006, Greifswald, Germany.
- Hetzel, A., Böttcher, M.E., Arndt, S., Prieto, M., Gehre, M., Brumsack, H.-J. (2006): Authigenic barite formation triggered by black shale-fueled anaerobic methane oxidation in the deep biosphere of ODP Leg 207. EGU General Assembly, 02. – 07. April 2006, Vienna, Austria. Geophysical Research Abstracts, Vol. 8, 09360.
- Hetzel, A., Böttcher, M.E., Brumsack, H.-J., Wortmann, U.G., Schipper, A. (2007): Dynamics of redox-sensitive tracers through the C/T in the southern North-Atlantic (ODP Leg 207): A high-resolution study. Joint Colloquium IODP/ICDP, 19. – 21. March 2007, Potsdam, Germany
- Hetzel, A., Brumsack, H.-J. (2004): Erste anorganisch-geochemische Charakterisierung der Kreide-Schwarzschiefer des Demerara Rise (ODP Leg 207). Annual Meeting Geochemistry, German Mineralogical Society (DMG), 14. – 15. May 2004, Hannover, Germany.
- Hetzel, A., Brumsack, H.-J. (2005): Trace metal patterns in C/T black shales: Paleoenvironmental implications. Annual Meeting Geochemistry, German Mineralogical Society (DMG), 06. – 07. May 2005, Bremen, Germany.
- Hetzel, A., Brumsack, H.-J. (2005): Trace metal patterns in C/T black shales: Paleoenvironmental implications. Joint Colloquium IODP/ICDP, 14. – 16. March 2005, Potsdam, Germany.
- Hetzel, A., Brumsack, H.-J. (2005): Trace metal patterns in C/T black shales: Paleoenvironmental implications. International Symposium on the Cretaceous, 05. – 09. September 2005, Neuchatel, Switzerland.
- Hetzel, A., Brumsack, H.-J., Shipboard Scientific Party ODP Leg 207 (2004): Inorganic geochemistry of Cretaceous black shales from Demerara Rise (ODP Leg 207). Joint Colloquium IODP/ICDP 17. – 19. March 2004, Bremen, Germany.
- Hetzel, A., Forster, A., Brumsack, H.-J. (2006): Black shale deposition during Mid-Cretaceous Anoxic Event OAE2: Reconstructing environmental conditions using trace metal signatures. Annual Meeting Geochemistry, German Mineralogical Society (DMG), 14. – 15. June 2006, Kiel, Germany.
- Hetzel, A., Forster, A., Brumsack, H.-J. (2006): Depositional environment of Cenomanian/Turonian black shales from Demerara Rise (ODP Leg 207) -

Implications from trace metal patterns. Joint Colloquium IODP/ICDP, 27. – 29. March 2006, Greifswald, Germany.

- Hetzel, A., Forster, A., Brumsack, H.-J. (2006): Depositional environment of Cenomanian/Turonian black shales from Demerara Rise (ODP Leg 207) - Implications from trace metal patterns. EGU General Assembly, 02. – 07. April 2006, Vienna, Austria. Geophysical Research Abstracts, Vol. 8, 09382.
- van Bentum, E., Hetzel, A., Forster A., Reichert, G.-J., Brumsack, H.-J., Sinninghe Damsté, J. S. (2007): Reconstructing water column anoxia during the Cenomanian-Turonian boundary event using biomarker and trace metal proxies. EGU General Assembly, 15. – 20. April 2007, Vienna, Austria. Geophysical Research Abstracts, Vol. 9, 07871.

Acknowledgements / Danksagung

Mein besonderer Dank gilt zuerst meinem Doktorvater Prof. Dr. H.-J. Brumsack für die Überlassung „seiner“ Kreide-Schwarzschiefer. Die Bearbeitung dieses interessanten Themas (CTBE) im Rahmen des „großen“ ODP war für mich „kleine“ Doktorandin eine große Herausforderung, die mir aber den Einstieg in den „Wissenschaftszirkus“ erleichterte und viele Kontakte ermöglichte, die meinen Blick über den Tellerrand „Geochemie“ hinaus förderten. Außer für die Betreuung und die interessanten Diskussionen möchte ich Dir, Hans, vor allem für das entgegengebrachte Vertrauen bei der mir frei überlassenen Projekt-Bearbeitung und Präsentation der Ergebnisse danken. Ich hoffe, es war in Ordnung, dass ich in Greifswald unbedingt bis nach den Schnitzeln und dem Kartoffelsalat bleiben wollte...

Prof. Dr. M.E. Böttcher danke ich für die anregende Zusammenarbeit, für interessante Diskussionen, für stets neue Motivation durch wiederholte Anrufe in Hameln und nicht zuletzt für die Übernahme des Zweitgutachtens. Danke auch, Michel, für den Aufenthalt in Warnemünde, wo Du der erste warst, der uns Tipps zum Eltern-Sein gab.

Dr. B. Schnetger möchte ich dafür danken, dass er mir bei allen aufkommenden analytischen Fragen Hilfestellung bot, mich dazu anregte, eigene Ideen umzusetzen - ich weiß jetzt, dass Fe-Spektren quasi mit allem überlappen - und mir einen kleinen Einblick in die universitäre Lehre verschaffte. Danke, Barnie, dafür, dass manchmal dienstags schon Freitag war (TGIT).

Dr. S. Turgeon danke ich für die ersten Erfahrungen mit der Analytik von Schwarzschiefern als studentische Hilfskraft - auch wenn ich da noch nicht ahnte, wie oft mir Gubbio und Tarfaya noch begegnen sollten. Und was ist eigentlich ein „OAE“? Danke für Deine Erklärungen und dass Du immer ruhig und gelassen bliebst, wenn ein „Steeeven!“ aus dem letzten Labor zu hören war.

Carola Lehnert, Michaela Schwarting, Eleonore Gründken, Martina Wagner, Nicole Becker und allen Hiwis ein großes Dankeschön für ihr Engagement und ihre Hilfsbereitschaft im Labor. Ohne Eure Unterstützung wäre diese Probenanzahl nicht zu bewältigen gewesen. Danke auch für die Erfüllung der per Email übermittelten Wünsche aus der Ferne.

Außerdem bedanke ich mich bei allen aktiven und ehemaligen Mitgliedern der AG „Mikrobiogeochemie“: Den frühen Mitstreitern für die nette Aufnahme als Steven's

Hiwi; Philipp für seine Gesellschaft an langen Abenden während der Endphase der Diplom- bzw. Doktorarbeit; Olaf, Maik und Schossi für Asyl im „Zentrum der Arbeit“ während der Laborphasen; Kerstin für die Salzwiesen-Erfahrungen. Außerdem möchte ich mich ganz herzlich bei Melanie für ihre Gastfreundschaft und für motivierende Worte bedanken. Schön zu wissen, dass man immer willkommen ist. Christian als mein Ansprechpartner zur Geochemie jenseits von Pampers und PEKiP-Kursen danke ich für fachliche Diskussionen, Literaturbeschaffung und Durchlesen der Publikations-Entwürfe.

Dann möchte ich mich noch bei meiner Leidensgenossin Astrid Forster bedanken. Astrid, Du weißt, wie schwer es ist, fernab vom Schuss nach erledigtem Wohnungsputz, Bügeln, etc. den Wünschen der Reviewer nachzugehen. Ach ja, was macht die Diss?

Sandra Arndt möchte ich danken, weil sie es solange mit mir in einer WG ausgehalten hat und dann auch noch neben mir den Schreibtisch in der Geochemie bezogen hat. Es freut mich, dass uns nach fünf Jahren und Deinen Umzügen im europäischen Ausland immer noch die Biogeochemie des Demerara Rise verbindet.

Bei meinen Kollegen im „interdisziplinären“ Büro möchte ich mich für die tolle Arbeitsatmosphäre bedanken. Bei wechselnder Besetzung blieb stets Raum für `ne Tasse Kaffee, bei der Fragen zur Geochemie, zu Papierkram, zu Praktikumsprotokollen oder dem Leben an sich (z.B. Fanfreundschaften) diskutiert wurden. Ohne Euch wäre das ganze nur halb so schön gewesen. Bleibt nur die Frage, wo der Schal jetzt eigentlich geblieben ist...

Nicht zuletzt möchte ich mich bei meiner Familie bedanken. Meiner Mutter danke ich für die Unterstützung und den positiven Zuspruch. Durch häufiges Babysitten hast Du die Fertigstellung dieser Arbeit maßgeblich vorangetrieben. Christoph danke ich für das Verständnis, welches er als frisch gebackener Vater und als Ehemann einer „fast-fertigen Frau Doktor“ aufgebracht hat. Sorry für die vielen Stunden am Rechner zu unmöglichen Zeiten. Ganz besonderer Dank gilt Moritz. Danke, dass Du Dich schon so ausdauernd allein mit den Literatur-Ordern H-M beschäftigen konntest und doch um Dein Recht gekämpft hast, indem Du den Aus-Knopf am Computer entdeckt und benutzt hast, noch bevor Du Mama sagen konntest.

Zum Schluss sei noch erwähnt, dass die Arbeit von der Deutschen Forschungsgemeinschaft im Rahmen des Schwerpunktprogramms „ODP“ finanziell gefördert wurde. Dafür sei auch ihr gedankt.

Erklärung

Hiermit versichere ich, dass ich die vorliegende Arbeit selbstständig angefertigt und keine anderen als die angegebenen Quellen und Hilfsmittel verwendet habe. Zusätzlich erkläre ich, dass diese Dissertation weder in ihrer Gesamtheit noch in Teilen einer anderen wissenschaftlichen Hochschule zur Begutachtung in einem Promotionsverfahren vorliegt oder vorgelegen hat.

Hameln, im Juni 2009

Almut Bunte

